Present and Future of Surface Enhanced Raman Scattering

Judith Langer,[1] Dorleta Jimenez de Aberasturi,[1] Javier Aizpurua,[2] Ramon A. Alvarez-Puebla,[3,4] Baptiste Auguié,[5,6,7] Jeremy J. Baumberg,[8] Guillermo C. Bazan,[9] Steven E. J. Bell,[10] Anja Boisen,[11] Alexandre G. Brolo,[12,13] Jaebum Choo,[14] Dana Cialla-May,[15,16] Volker Deckert,[15,16] Laura Fabris,[17] Karen Faulds,[18] F. Javier García de Abajo,[4,19] Royston Goodacre,[20] Duncan Graham,[18] Amanda J. Haes,[21] Christy L. Haynes,[22] Christian Huck,[23] Tamitake Itoh,[24] Mikael Käll,[25] Janina Kneipp,[26] Nicholas A. Kotov,[27] Hua Kuang,[28,29] Eric C. Le Ru,[5,6,7] Hiang Kwee Lee,[30,31] Jian-Feng Li,[32] Xing Yi Ling,[30] Stefan Maier,[33] Thomas Mayerhöfer,[15,16] Martin Moskovits,[34] Kei Murakoshi,[35] Jwa-Min Nam,[36] Shuming Nie,[37] Yukihiro Ozaki,[38] Isabel Pastoriza-Santos,[39] Jorge Perez-Juste,[39] Juergen Popp,[15,16] Annemarie Pucci,[23] Stephanie Reich,[40] Bin Ren,[32] George C. Schatz,[41] Timur Shegai,[25] Sebastian Schlücker,[42] Tay Li-Lin,[43] K. George Thomas,[44] Zhong-Qun Tian,[32] Richard P. Van Duyne,[41] Tuan Vo-Dinh,[45] Yue Wang,[46] Katherine A. Willets,[47] Chuanlai Xu,[28,29] Hongxing Xu,[48] Yikai Xu,[10] Yuko S. Yamamoto,[49] Bing Zhao,[50] Luis M. Liz-Marzán[1,51]

[1] CIC biomaGUNE and CIBER-BBN, Paseo de Miramón 182, 20014 Donostia-San Sebastián, Spain

[2] Materials Physics Center (CSIC-UPV/EHU), and Donostia International Physics Center

(DIPC), Paseo Manuel de Lardizabal 5, 20018 Donostia - San Sebastián, Spain

[3] Departamento de Química Física e Inorgánica and EMaS, Universitat Rovira i Virgili, 43007 Tarragona, Spain

[4] ICREA-Institució Catalana de Recerca i Estudis Avançats, Passeig Lluís Companys 23, 08010 Barcelona, Spain

[5] School of Chemical and Physical Sciences, Victoria University of Wellington, PO Box 600, Wellington 6140, New Zealand

[6] The MacDiarmid Institute for Advanced Materials and Nanotechnology, PO Box 600, Wellington 6140, New Zealand

[7] The Dodd-Walls Centre for Quantum and Photonic Technologies, PO Box 56, Dunedin 9054, New Zealand

[8] NanoPhotonics Centre, Cavendish Laboratory, University of Cambridge, Cambridge CB3 0HE, UK

[9] Department of Materials and Chemistry and Biochemistry, University of California, Santa Barbara, CA 93106-9510, United States

[10] School of Chemistry and Chemical Engineering, Queen's University of Belfast, Belfast BT9 5AG, UK

[11] Department of Micro- and Nanotechnology, The Danish National Research Foundation and Villum Foundation's Center for Intelligent Drug Delivery and Sensing Using Microcontainers and Nanomechanics (IDUN), Technical University of Denmark, 2800 Kongens Lyngby, Denmark

[12] Department of Chemistry, University of Victoria, P.O. Box 3065, Victoria, BC V8W 3V6, Canada

[13] Center for Advanced Materials and Related Technologies (CAMTEC), University of Victoria, Victoria, BC V8W 2Y2, Canada

[14] Department of Chemistry, Chung-Ang University, Seoul 06974, South Korea

[15] Leibniz Institute of Photonic Technology Jena, 07745 Jena, Germany

[16] Institute of Physical Chemistry and Abbe Center of Photonics, Friedrich-Schiller University Jena, 07745 Jena, Germany

[17] Department of Materials Science and Engineering, Rutgers University, 607 Taylor Road, Piscataway NJ 08854, United States

[18] Department of Pure and Applied Chemistry, University of Strathclyde, Technology and Innovation Centre, 99 George Street, Glasgow G1 1RD, UK

[19] ICFO-Institut de Ciencies Fotoniques, The Barcelona Institute of Science and Technology, 08860 Castelldefels (Barcelona), Spain

[20] Department of Biochemistry, Institute of Integrative Biology, University of Liverpool, Biosciences Building, Crown Street, Liverpool L69 7ZB, UK

[21] Department of Chemistry, University of Iowa, Iowa City, Iowa 52242, United States

[22] Department of Chemistry, University of Minnesota, 207 Pleasant Street SE, Minneapolis, Minnesota 55455, United States

[23] Kirchhoff Institute for Physics, University of Heidelberg, Im Neuenheimer Feld 227, 69120 Heidelberg, Germany

[24] Nano-Bioanalysis Research Group, Health Research Institute, National Institute of Advanced Industrial Science and Technology (AIST), Takamatsu, Kagawa 761-0395, Japan

[25] Department of Physics, Chalmers University of Technology, S412 96 Goteborg, Sweden

[26] Department of Chemistry, Humboldt-Universität zu Berlin, Brook-Taylor-Str. 2, 12489 Berlin-Adlershof, Germany

[27] Department of Chemical Engineering, University of Michigan, Ann Arbor, Michigan 48109, United States

[28] Key Lab of Synthetic and Biological Colloids, Ministry of Education, International Joint Research Laboratory for Biointerface and Biodetection, Jiangnan University, Wuxi, Jiangsu, 214122, China

[29] State Key Laboratory of Food Science and Technology, Jiangnan University, JiangSu, China

[30] Division of Chemistry and Biological Chemistry, School of Physical and Mathematical Sciences, Nanyang Technological University, 21 Nanyang Link, 637371 Singapore

[31] Department of Materials Science and Engineering, Stanford University, Stanford, CA 94305, United States

[32] State Key Laboratory of Physical Chemistry of Solid Surfaces, Collaborative Innovation Center of Chemistry for Energy Materials (iChEM), MOE Key Laboratory of Spectrochemical Analysis & Instrumentation, Department of Chemistry, College of Chemistry and Chemical Engineering, Xiamen University, 361005 Xiamen, China

[33] Chair in Hybrid Nanosystems, Nanoinstitute Munich, Faculty of Physics, Ludwig-Maximilians-Universität München, 80539 Munich, Germany

[34] Department of Chemistry & Biochemistry, University of California Santa Barbara, Santa Barbara, California 93106-9510, United States

[35] Department of Chemistry, Faculty of Science, Hokkaido University, North 10 West 8, Kita-ku, Sapporo, Hokkaido 060-0810, Japan

[36] Department of Chemistry, Seoul National University, Seoul 08826, South Korea

[37] Beckman Institute, Micro/Nanotechnology Lab, and Institute for Genomic Biology, University of Illinois at Urbana- Champaign, 1406 W. Green Street, Urbana, IL 61801, United States

[38] Department of Chemistry, School of Science and Technology, Kwansei Gakuin University, Sanda, Hyogo 669-1337, Japan

[39] Departamento de Química Física and CINBIO, University of Vigo, 36310 Vigo, Spain

[40] Department of Physics, Freie Universität Berlin, Berlin 14195, Germany

[41] Department of Chemistry, Northwestern University, Evanston IL 60208-3113, United States

[42] Physical Chemistry I, Department of Chemistry and Center for Nanointegration Duisburg-Essen (CENIDE), University of Duisburg-Essen, 45141 Essen, Germany

[43] National Research Council Canada, Metrology Research Centre, Ottawa K1A0R6, Canada

[44] School of Chemistry, Indian Institute of Science Education and Research Thiruvananthapuram, Vithura Thiruvananthapuram 695 016, India

[45] Fitzpatrick Institute for Photonics, Department of Biomedical Engineering, and Department of Chemistry, Duke University, 101 Science Drive, Box 90281, Durham, North Carolina 27708, United States

[46] Department of Chemistry, College of Sciences, Northeastern University, Shenyang 110819, China

[47] Department of Chemistry, Temple University, Philadelphia, PA 19122, United States

[48] School of Physics and Technology and Institute for Advanced Studies, Wuhan University, Wuhan 430072, China

[49] School of Materials Science, Japan Advanced Institute of Science and Technology (JAIST), Nomi, Ishikawa 923-1292, Japan

[50] State Key Laboratory of Supramolecular Structure and Materials, Jilin University, Changchun 130012, China

[51] Ikerbasque, Basque Foundation for Science, 48013 Bilbao, Spain

Abstract:

The discovery in 1974 of the enhancement of Raman scattering by molecules adsorbed on nanostructured metal surfaces is considered a landmark in the history of spectroscopic and analytical techniques. Much experimental and theoretical effort has been spent toward understanding the surface enhanced Raman scattering (SERS) effect, and demonstrating its potential toward various types of ultrasensitive sensing applications in a wide variety of fields. Forty five years later, SERS has blossomed as an extremely rich area of research and technology, but additional efforts are still needed before it can be routinely used as a commercial product. In this Review, prominent authors from all over the world joined efforts to summarize the current state-of-the-art in understanding and using SERS, as well

as to propose what can be expected in the near future, in terms of research, applications, and technological development.

Table of Contents image:

Contents:

1.   Modeling and new concepts

1.1. SERS Mechanisms: Electromagnetic
1.2. SERS Mechanisms: Chemical
1.3. Modeling of Molecular Species at Surfaces
1.4. Modified Electronic Absorbance of Molecules on Surfaces
1.5. Strong Coupling Regime
1.6. Extreme Interaction Regime (Quantum Effects)
1.7. Outlook for Future SERS Applications

2.   SERS substrates

2.1. Surface Chemistry, Stability, and Solution-Phase Nanoparticles – A Balancing Act
2.2. Anisotropic Nanoparticles: Nanostars
2.3. SERS in Single-Nanoparticle Dimers (Precision SERS)
2.4. Self-Assembled Nanoparticles
2.5. Vertically Aligned Au Nanorod Arrays
2.6. Assembly on Rough, Flexible or Curved Supports
2.7. Hole-Mask Colloidal Lithography
2.8. Nanopillars
2.9. Nanostructured Dielectrics and Hybrids

3.   SERS Tags

3.1. SERS Nanotags: Noble Metal Nanoparticles Coated with Raman Reporter Molecules
3.2. Fluorescent Dyes for SERRS and Multiplexing
3.3. SAM of Small Aromatic Thiols and Spectral Multiplexing
3.4. Protection and Stabilization
3.5. Bioconjugation to SERS Labels
3.6. Brightness of SERS Nanotags

4.   Analytical Techniques and Quantification

4.1. Analytical Techniques
4.2. SERS Chemosensors
4.3. Enantioselective Discrimination of Chiral Molecules by SERS
4.4. Quantitative SERS with Plasmonic Nanogap Particles
4.5. Remote SERS
4.6. Shell-Isolated Nanoparticle-Enhanced Raman Spectroscopy (SHINERS)
4.7. Analytical Quantification

5.   Analytical Methods and Devices in Biomedical Applications

5.1. Basic Techniques in Biomedical applications
5.2. Methods in Biological Applications
5.3. Devices
5.4. Future Outlook

6.   SERS in Biomedicine: From Single-Molecule Detection to *in vivo* Studies

6.1. Detection of Biomarkers
6.2. Detection of Circulating Tumor Cells
6.3. Detection of Pathogens
6.4. Immuno-SERS (iSERS) Microscopy
6.5. Multiplexed Cell Discrimination Using SERS Imaging
6.6. Future Prospects of SERS in Medicine

7.   Environmental Monitoring

7.1. Detection of Toxins
7.2. Water and Food Analytics
7.3. Nonpolar Organic Pollutants

8.   Related Techniques

1.   SESORS and SESORRS
2.   Electrochemical SERS
3.   Surface Enhanced Hyper Raman Scattering (SEHRS)
4.   Tip-Enhanced Raman Scattering (TERS)
5.   Surface Enhanced Infrared Absorption (SEIRA)

9.   Monitoring Chemical Reactions

9.1. Plasmon-Mediated Chemical Reactions (PMCR) and Plasmon-Enhanced Molecular Spectroscopy (PEMS)
9.2. Plasmon-Induced Chemical Reactions - Practical Examples
9.3. Electrochemical Reactions
9.4. Spatial Confinement in Gaps and Hotspots
9.5. Liquid- and Gas-Based Reactions

10.   General Conclusions and Outlook

Surface Enhanced Raman Scattering, or SERS, is a commonly used sensing technique in which inelastic light scattering (**Figure 0.1**) by molecules is greatly enhanced (by factors up to 10^8 or even larger, enabling single molecule SERS in some cases) when the molecules are adsorbed onto silver or gold nanoparticles. Since its original discovery over 40 years ago, it has enjoyed steady growth of interest in the research community, and it has spawned a variety of other spectroscopic techniques that take advantage of enhanced local fields that arise from plasmon excitation in the nanoparticles, for optical phenomena such as fluorescence or nonlinear optics. In addition, the coupling of SERS with AFM or STM tips has led to tip-enhanced Raman scattering (TERS) which is a powerful imaging tool. For analytical applications, SERS can be differentiated from many techniques by the rich vibrational spectroscopic information that it provides, and this has led to applications in many different directions, including electrochemistry, catalysis, biology, medicine, art conservation, materials science and others.
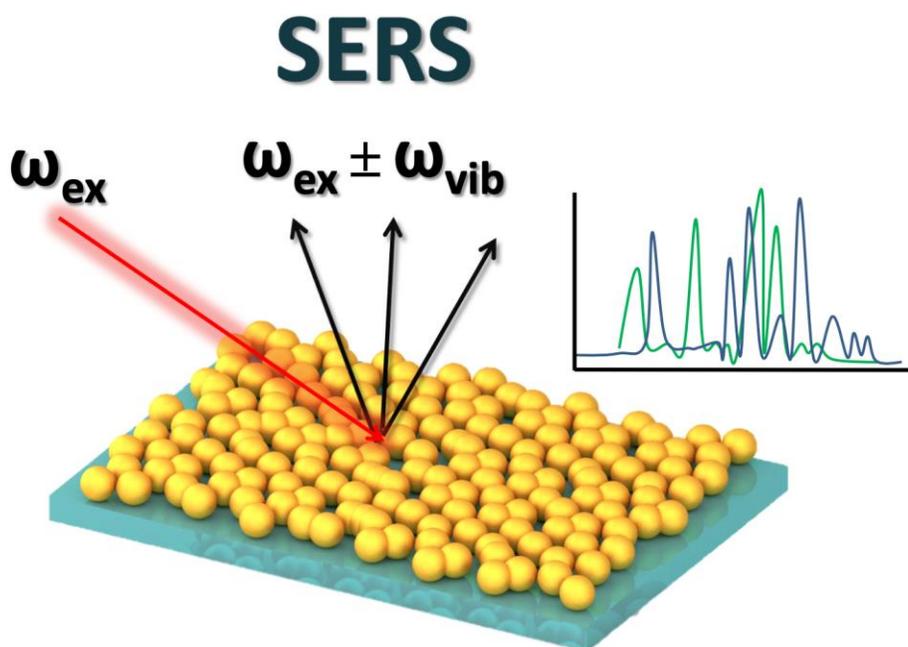
Figure 0.1. SERS involves inelastic light scattering by molecules adsorbed onto silver or gold nanoparticles.

The discovery of SERS has a relatively short history. It was accidentally discovered by Fleischmann and co-workers in 1974 during measurements of the Raman scattering of pyridine on rough silver electrodes,[1] who ascribed the enhancement to a surface area effect. The phenomenon was identified independently by Jeanmaire and Van Duyne,[2] and Albrecht and Creighton[3] in 1977, both of whom suggested enhancement factors of 10^5-10^6. The connection with plasmon excitation was suggested by Albrecht and Creighton as a resonant Raman effect involving plasmon excitation, as proposed earlier by Philpott.[4] Subsequently, the connection of SERS intensities to enhanced fields arising from localized surface plasmons in nanostructured metals was noted by Moskovits.[5] Forty five years later, tens of thousands of research papers have been published on SERS,[6] which discuss in great detail elements of the theory behind it, the design of a wide variety of (mostly metallic but not only) enhancing substrates, and their implementation in a huge variety of applications. Indeed, SERS has become a research field in its own right, as a source of exciting scientific phenomena, as well as one of the most sensitive analytical techniques currently available. Numerous excellent review articles have been published on various aspects of SERS and related topics, and even comprehensive overviews of the technique. There is thus probably no need to carry out an extensive literature review again. However, during the recent 26th *International Conference on Raman Spectroscopy* (XXVI ICORS, Jeju, Korea, August 26 – 31 2018),[7] some of us identified the need to put together a comprehensive perspective to describe the current state of the field and the path that we expect will be followed in the near future. We therefore joined efforts to identify the most active areas of SERS research and development, including basic aspects and emerging phenomena, materials synthesis and major applications. We also decided to include a section devoted to other "surface enhanced" techniques, which have seen a significant development in parallel and often profiting from lessons learnt during the optimization of SERS-related methods and materials.

The different sections include both basic and state-of-the-art concepts and methods, but consistently attempting to present a view forward, what we can expect during the coming years, in a way that we expect can guide and inspire not only currently active researchers but also young generations of scientists from different disciplines who can get excited about this rich field of research and its emerging branches into so many different directions.

1. Modeling and new concepts

The use of modeling and advanced theory have become essential for understanding SERS as a fundamental phenomenon, and to correctly interpret and predict experimental results obtained under various conditions and in varying environments. This holds for SERS at the single-molecule/single-particle level, as well as for ensembles comprising either a few or many molecules/particles. Theoretical modeling of SERS intensities and spectra has a long history, which has been reviewed many times.[8-15] There is now good agreement among researchers in the field that the overall enhancement factor is a combination of an electromagnetic (EM) enhancement associated with plasmon excitation in metal particles serving as the SERS substrate, and a chemical (CHEM) enhancement due to the target molecules being able to transfer electrons to/from the metal particles in both ground and excited states, often in the process of forming the metal-molecule bond.

The Raman signal involves absorption of an incident photon of frequency ω_{in} (see **Figure 0.1**), coupling to an internal degree of freedom of the molecule, typically a molecular vibration of frequency ω_{vib}, and re-emission at the difference frequencies $\omega_{\text{em}} = \omega_{\text{in}} \pm \omega_{vib}$, where the sum/difference results in antiStokes/Stokes Raman scattering, respectively. Three inelastic transitions are therefore involved in the process (absorption, vibrational excitation, and re-emission); the vibrational excitation occurs with a probability that depends on the environment through the chemical interaction discussed above, while the other two processes are controlled by the availability of photonic states in the molecules. In the absence of a structured environment (*e.g.*, in solution), the Raman process has a low probability, quantified in terms of the optical cross section (*i.e.*, the area of the incident beam over which incident photons are effectively converted into emitted Raman photons) $\sim 10^{-11}$-10^{-15} nm^2, which depends on whether the process is resonant or non-resonant Raman (*i.e.*, whether the incoming light is or is not resonant with transitions between ground and excited electronic states of the molecule). The low intensity of Raman scattering is clearly insufficient for many practical applications, and therefore, finding the means of enhancing the Raman process is often beneficial. Such means are provided by the large optical field enhancement produced by suitably resonant structures. In particular, the initial absorption process is directly

proportional to the local electric field intensity at the molecule, which plasmons in noble metal nanostructures can dramatically amplify relative to the incident light intensity. Although SERS can be obtained from the electric field enhancement at single nanoparticles, it is advantageous to involve a more elaborate structure, for example by placing the molecules within nanometer-sized gaps between two metal particles (so-called hotspots), which allow intensity enhancement factors as large as EF~10^5-10^6 to be routinely reached.[16-19]

Hotspots can be produced not only at gaps between nanoparticles, but also within nanoparticle junctions and flat metal surfaces supporting plasmon resonances. The resulting field strength depends strongly on the gap distance and other geometrical details. In particular, the EM field amplitude is inversely proportional to the square of the gap distance. The main characteristics for a typical SERS hotspot, the extension of which lies in the 2-10 nm range, are satisfactorily well described within classical electromagnetism by neglecting nonlocal effects and only resorting to the frequency-dependent dielectric functions of the materials involved in the structure. Reducing the nanoparticle gap distance below 1 nm, nonlocal effects come into play, requiring a more sophisticated treatment of the optical response. Additionally, at such small separations the enhancement of EM fields is so strong that the optical response may become nonlinear (*i.e.*, the threshold for nonlinear effects is correspondingly reduced in inverse proportion to the field enhancement). In this strong coupling regime, the intrinsic properties of the molecule-nanoparticle system might be significantly altered, which in turn affects the SERS intensities. Examples are the creation of hot electrons at the nanoparticle surface that can trigger or catalyze chemical reactions, change the photophysical and/or photochemical properties of the adsorbed molecule and modify the excitation dynamics, and the emergence of molecular optomechanical effects. In the extreme coupling regime (*e.g.*, a single molecule inside a nm-sized cavity, or picocavity), classical models are no longer valid and must be complemented by descriptions based on quantum-mechanical approaches. Therefore, specific and accurate modeling of Raman and competing processes in subnano- to nano-sized hotspots are crucial in supporting and/or interpreting experimental results and to enable the design of substrates with the desired SERS response.

1.1. SERS Mechanisms: Electromagnetic Field Enhancement

The electromagnetic enhancement factor has been the subject of numerous studies, typically using computational electrodynamics calculations to determine the enhanced electric field amplitude $\mathbf{E}(\omega)$ that arises when plasmons are excited in a SERS substrate at frequency ω; $\mathbf{E}(\omega)$ is then evaluated at the molecular positions. The SERS enhancement is normally approximated by averaging $|E(\omega)|^4/|E_0|^4$ over the illuminated molecules, where E_0 is the incident (laser) field amplitude. Actually, this analytical result neglects the Stokes shift, which can be included through a slightly more elaborate expression: $|E(\omega)|^2|E(\omega')|^2/|E_0|^4$ where ω' is the Raman emitted frequency. A slightly more accurate approximation is also obtained by correcting the $|E(\omega')|^2$ factor to properly account for the emission from the inelastic emission dipole (sometimes termed dipole re-radiation[20]). Another important issue is related to the significant field gradients that often exist as a consequence of the strong spatial localization of the plasmon enhanced field;[21,22] these gradients contain nondipolar components that can efficiently produce SERS involving dipole-quadrupole and quadrupole-quadrupole in-out polarizabilities; these effects are obviously stronger for transitions involving more spatially delocalized electronic states in the molecule. Calculations based on dipole re-radiation and field gradient effects have rarely been carried out, as the structures of the nanoparticles involved are not known accurately enough to warrant this level of detail in the analysis. Indeed, for most applications, the $|E(\omega)|^4$ expression produces results that are good to about an order of magnitude. In fact, ten years ago, pioneering work by Schatz and Van Duyne on nanoparticle clusters used this level of theory,[23,24] and showed that the electromagnetic enhancement factor for clusters of nanoparticles is often the highest (experimentally measured as $\sim 10^9$) at wavelengths where the plasmon resonance is "dark" " (*i.e.*, at wavelengths corresponding to a dip rather than a maximum in the extinction spectrum). This arises because dark plasmon modes, which are often quadrupolar in character, can nevertheless produce large electric fields in the electromagnetic hotspots between nanoparticles.[24] In addition, it was found that the dipole re-radiation at wavelengths where the plasmon resonance is dark can sometimes lead to stronger than expected far-field intensities, because the dipole field of the adsorbed molecules can more effectively excite quadrupolar and higher-order multipolar resonances than light plane waves can.

Although most numerical simulations of EM enhacement have been limited to relatively simple geometries, or at most a few particles, ensemble effects can be critical in the performance of actual large-scale SERS samples. In a recent example, state-of-the-art electromagnetic computation techniques were used to simulate nanoparticle-based SERS substrates, comprising hundreds of randomly organized gold nanoparticles. The authors unexpectedly concluded that nanoparticle morphologies that provide large enhancements at the single particle level, such as nanostars, do not necessarily improve when organized in close packed arrays; in contrast, simpler morphologies (*e.g.* spheres or rods) lead to significantly increased SERS enhancement as their surface density approaches full coverage (**Figure 1.1**).[19]
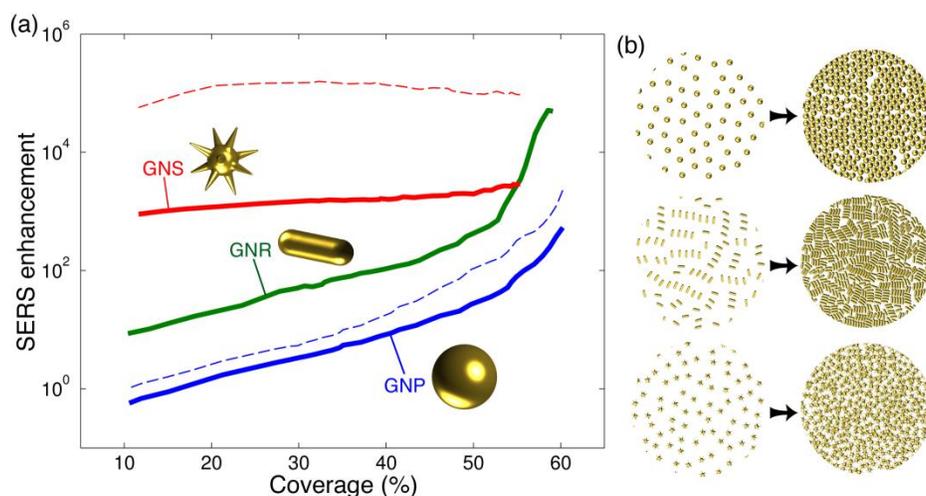
Figure 1.1. Predicted SERS enhancement as a function of surface coverage, for monolayers of gold nanoparticles with different shapes (a). Solid curves obtained for excitation at 785 nm light wavelength (resonant with 65x21 nm nanorods); dashed curves obtained for 633 nm (resonant with 51 nm nanospheres) and 900 nm (resonant with nanostars: 20 nm core, 10 nm branches). Schemes in (b) illustrate low- and hig-density nanoparticle surface coverage. Reproduced with permission from Ref. 19**.** Copyright 2017, American Chemical Society.

In addition to EM enhancements that can be calculated by solving Maxwell's equations for specific nanostructures, more qualitative estimates of enhancement factors based on simple

model structures (such as spheroids) have been developed,[25] and recently used to understand SERS for randomly rough substrates made of aluminum, gold or silver, over a wide range of wavelengths from the UV to the NIR, and in good agreement with experimental data.[26] Prediction of plasmonic properties of nanoparticles with arbitrary morphologies has also been recently simplified by derivation of analytical expressions based on parameters that stem from numerical modeling.[27,28] Nonlocal effects can also play a role in the EM mechanism;[29,30] for example, although gaps between nanoparticles lead to electromagnetic hotspots that often dominate SERS measurements (leading to single-molecule sensitivity[31]), and although classical electromagnetics predicts that enhancements should vary inversely as the square of the gap size,[32] for gaps with dimensions significantly below 1 nm, quantum effects associated with electron tunneling between nanoparticles become important,[21,33,34] changing the dominant plasmon energies significantly, usually resulting in a reduction in the EM enhancement.

1.2. SERS Mechanisms: Chemical

The chemical mechanism of SERS refers to contributions to the Raman scattering that do not rely on the electromagnetic environment (*e.g.*, plasmon excitation), often because they are associated with the transfer of electrons between adsorbed molecules and the nanoparticle substrate. This can arise in two ways corresponding to electron transfer in the ground and excited states of the molecule-metal system. The enhancement factor associated with the former mechanism can be defined in terms of the static polarizability derivatives of the molecule-metal system,[35] which is a property that can be calculated using electronic structure theory using a cluster model for the metal particle, in which the particle is replaced by a small cluster of metal atoms. This type of calculation produces a result that is nominally independent of frequency, which reflects changes in the polarizability derivative due to the transfer of charge by the molecule adsorbed on the metal nanoparticle. Greeneltch *et al.*[36] obtained values from such calculations for several substituted benzene thiolates adsorbed on silver and gold substrates, and compared them to measured enhancement factors. Because the substrates were the same for all of the molecules considered, the variation in enhancement factor for the various molecules was entirely due to changes in the chemical enhancement.

Theory and experiment were in agreement within a factor of 2, and the values which showed a variation of ~10 for the molecules considered corresponded to a chemical enhancement in the 10-100 range.

While the static polarizability derivative provides a simple way to model the chemical effect, including charge transfer (CT) in the optical frequency response is necessary for a complete understanding.[37,38] This, however, is challenging to estimate, as CT states are poorly described with standard density functional theory methods, and strongly mixed with plasmon excitations in models that couple molecules to metal clusters. This means that separating CT effects from plasmon excitations is not rigorously possible. One way to make progress involves the use of semi-empirical molecular orbital methods, such as INDO/S[39] with parameters appropriately chosen to give reasonable plasmonic properties for Ag.[40] Using this approach, it is possible to describe CT effects accurately, and to separate CT and plasmonic contributions to SERS for molecule/cluster models. Such a separation was performed by modifying the INDO/S calculation so that terms in the Hamiltonian responsible for charge transfer between molecule and metal were omitted, thereby yielding an electronic structure that only includes EM effects. The CHEM factor is then generated by comparing results with and without charge transfer for frequencies where plasmon excitation occurs. In a study of the pyridine SERS spectrum on a silver cluster, this analysis generated a CHEM enhancement factor of 10 for excitation near the plasmon resonance.[41] It was also noted that there was a CT excited state about 0.5 eV above the plasmon state, and that this state produced a substantial Raman enhancement (down by a factor less than 10 from the SERS enhancement) when the CT state was excited on resonance. The significant enhancement associated with CT states provides rationalization for recent studies in which large Raman enhancements were observed for systems composed of organic molecules on organic semiconductor substrates, for which plasmon excitation is not present.[42]

Figure 1.2 shows a recent result based on semiempirical INDO/S calculations, for a CO molecule attached to a silver tip, in tip enhanced Raman scattering (TERS).[43] The Ag-CO tip was located near a gold substrate (see inset in **Figure 1.2**) under electrical bias, and the Raman intensity of the CO stretching vibration was measured as the bias was varied, resulting in an increased measured intensity with increasing bias above zero. Results for three different

15

theoretical models of this experiment are plotted, all based on INDO/S with various approaches to defining how the bias induces a static potential between the tip and the substrate. The calculations show that the intensity increase stems from charge-transfer excited states that tune into resonance as the bias becomes more positive. Thus, we directly see how charge transfer excited states can influence SERS intensities. The same theory can also be used to connect SERS measurements to formal potentials for TERS-based single-molecule electrochemical studies.[44,45] We should note that the Ag-CO TERS measurement can also be carried out by monitoring the shift in CO vibrational frequency instead of Raman intensity as a function of potential bias, and exciting developments have also been reported using the Ag-CO system for atomic resolution imaging.[46]
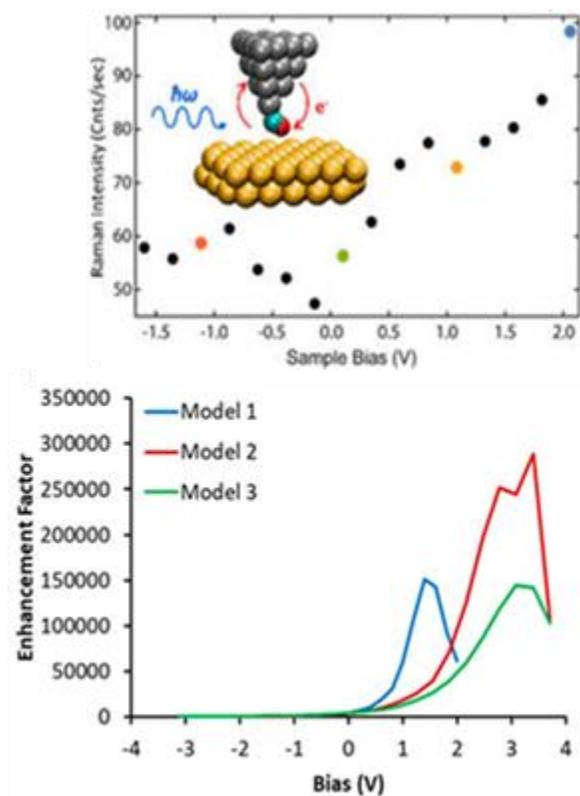
Figure 1.2. Comparison of experiment (top) and theory (bottom) for the CO TERS intensity associated with an Ag-CO tip structure near a gold surface, as a function of potential bias. Inset shows the tip model. Adapted with permission from Ref. 43. Copyright 2018, American Chemical Society.

1.3. Modeling of Molecular Species at the Surface

Another challenge for theory in SERS involves the determination of spectra using computation, which possess sufficient precision to be used to determine the identity of the molecules producing them. This activity is important in almost any study where the identity of the species represented in the SERS spectrum is required, and especially so when SERS is used to study chemical reactions on surfaces. Raman spectra can be generated for isolated molecules using various electronic structure codes; however, much uncertainty exists as to what structural model should be used in the calculations. As noted in the previous example, to properly describe the chemical enhancement factor requires an electronic structure calculation that includes the molecule plus a metal cluster representing the plasmonic metal. The choice of cluster model is important, and, for any model, there are important questions as to which density functional is best,[47] and what level of averaging over molecular orientations on the cluster is needed to generate a meaningful result to be compared with experiment.[48] Ultimately, an exhaustive study requires significant computational resources, and given the level of uncertainty about what molecules are actually present, their protonation and charge state, and possible decomposition pathways, such studies soon become intractable. A greatly simplified approximation which often works well is to calculate the orientation-averaged spectrum associated with the molecule in the absence of any metal atoms and for a simple functional like CAM-B3LYP. **Figure 1.3** shows an example of this type[49] for the molecule bipyridine (BPY), including results for both the H_8 and perdeutero D_8 isomers (where D_8 is used to determine if the spectra arise from single molecules or not). The top panels show waterfall spectra associated with experiments in which initially a relatively intense pulse of 532 nm light is used to irradiate BPY on a gold substrate for a few seconds, followed by SERS spectra measured with 785 nm every few seconds for hundreds of seconds after the pulse. The top spectra in the lower panel are spectra measured for H_8 and D_8, which are in excellent agreement with orientation averaged spectra for BPY calculated using density functional theory (DFT, not shown). The second spectrum shows the presence of additional modes (also seen in the waterfall plots) indicating the presence of another molecule. The bottom spectra in **Figure 1.2** show calculated spectra for anions of the H_8 and D_8 molecules, which are open shell molecules with low lying excited states. It is clear that

the calculated spectra match the extra peaks that show up in the middle panel, which enables the identification of the extra molecules as anions. This recently developed capability for generating resonance Raman spectra of this type using the NWChem program can clearly play an important role.[49] Ultimately, this work and a more recent study of the molecule trans-1,2-bis(4-pyridyl)ethylene (BPE),[50] demonstrate that 532 nm light generates electrons that escape from the nanoparticles, and diffuse on the surface, occasionally converting the molecules to anions, sometimes with other conformational changes that include isomerization, as observed in the SERS spectra. The fact, that the orientation-averaged spectra work well in this application is likely a reflection of the fact that the molecules being observed adopt many orientations on what is a randomly roughened SERS substrate, and that many of the molecules that contribute to the results are not strongly coordinated to the metal surface. The foregoing illustrates how SERS can be used to study molecular surface chemistry using relatively simple modeling.

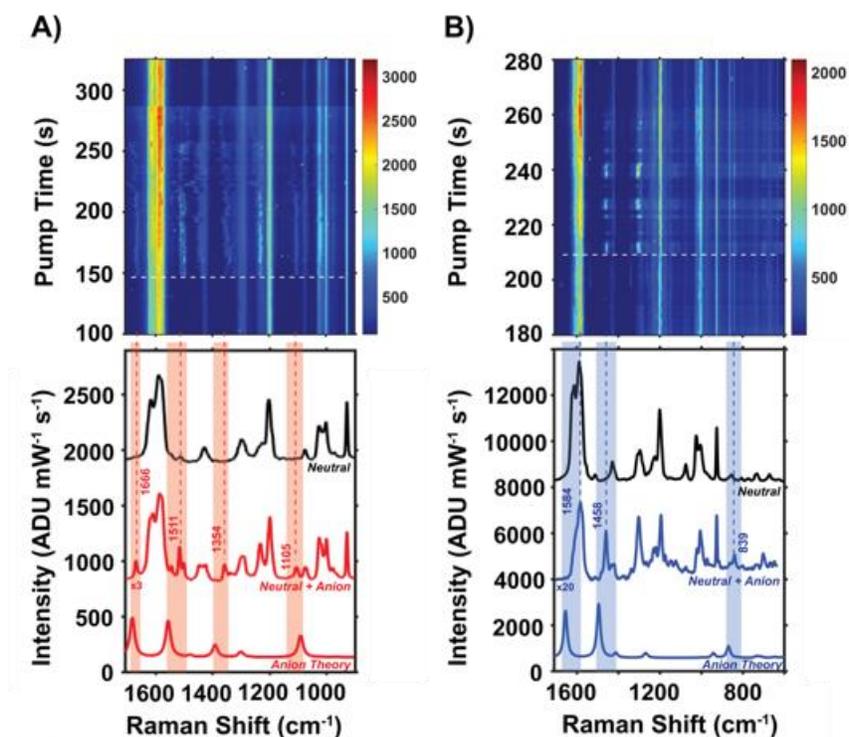Figure 1.3. Representative anion events for both BPY-h_8 and BPY-d_8. (A) Top waterfall plot depicts time-dependent SERS data as a function of optical pump time. Anion modes appear starting at 148 s, indicated by white dotted line. Bottom plot shows the neutral spectrum for

a BPY-h_8 + BPY-d_8 nanosphere assembly (black); The mid-spectrum depicts the contribution from neutral molecules plus BPY-h_8 anion modes that appear (red); The bottom spectrum shows open-shell DFT (CAM-B3LYP) calculation for the radical BPY-h_8 anion. (B) Waterfall plot from a different nanosphere assembly that shows a preference for BPY-d_8 anionic behavior, with anion activity appearing at 209 s of pump time. The top spectrum in the lower plot consists of neutral molecules only (black); the mid-spectrum is neutral plus BPY-d_8 anion modes; the bottom spectrum is DFT (CAM-B3LYP) calculated BPY-d_8 anion modes. Reproduced with permission from Ref. 49. Copyright 2017, American Chemical Society.

1.4. Modified Electronic Absorbance of Molecules on Surfaces

Many SERS studies have been and still are being carried out with analytes under resonant or pre-resonant conditions. The main reason for this choice is practical: Raman cross-sections are much larger (typically by a factor $10^2 - 10^6$) than for non-resonant conditions,[51] yielding stronger signals for a given SERS enhancement factor (EF), facilitating fundamental studies of SERS, notably in the context of single-molecule detection.[52] Other applications also benefit from increased signals, for example the use of SERS tags (see Section 3 below).

   One consequence of using (pre-)resonant analytes is that any change in electronic resonance originating from the molecule's adsorption to the metal can dramatically affect the SERS measurements and their interpretations. In simplified terms, a spectral shift towards the excitation wavelength increases the Raman cross-section of the adsorbed molecule, with respect to its intrinsic cross-section, resulting in an apparent increase in the SERS enhancement factor, which operates in addition to the standard electromagnetic enhancement[53] and surface selection rules.[54,55] And *vice versa* for a spectral shift towards the excitation wavelength. Such a change in Raman polarizability upon adsorption can be classified as an instance of chemical enhancement;[56,57] which, however, has been largely overlooked to date as it could only be indirectly inferred from the SERS EF, which is affected by many factors.

Recent progress in experimental methods has enabled direct access to the modified absorbance spectrum of dye molecules such as Rhodamine 6G and Crystal Violet adsorbed

on metallic nanoparticles[58] (**Figure 1.4**), a first important step toward assessing the effect of adsorption to the metal surface on their SERS response. These experiments have revealed three important points, discussed below in the case of Rhodamine 6G:

- The measured absorption enhancement is somewhat smaller (~ 4 on 60 nm silver nanospheres) than expected from a simple isotropic electromagnetic model (the average surface absorbance enhancement is here predicted to be ~ 15). This can be attributed to orientation effects[59,60] and provides a complementary insight on the importance of preferential orientation in adsorption for quantitative or even semi-quantitative interpretations of SERS experiments.

- The absorbance spectrum of the adsorbed dye is shifted, from about 526 nm to 538 nm in the case of Rhodamine 6G. This relatively small shift could be explained by a chemical interaction,[61] or even by a purely EM interaction (image-dipole effect)[60] with the metal surface. Such a shift in electronic energy is nonetheless likely to affect the (resonance) Raman cross-section by a non-negligible factor: the Raman cross-sections of bare Rhodamine 6G drop by a factor of $10^3 - 10^4$ from 532 nm (resonant) to 633 nm (pre-resonant) excitation[51,62] – a 12 nm red-shift in resonance may therefore result in a measurable increase in cross-section at 633 nm. While these effects have not yet been evidenced directly in the SERS EF, they may explain why Rhodamine 6G has been so extensively used in SERS studies at 633 nm excitation on silver particles, even though its Raman cross-section is relatively small at this wavelength.[51] For molecules such as Crystal Violet, where a dramatic change in the absorption spectrum is observed upon adsorption on silver, with a peak shift from 590 nm down to 500 nm (**Figure 1.4**a), even more substantial changes in SERS EF can be expected.

- The absorbance spectrum varies with dye concentration, with spectral changes observed from a surface coverage as low as 0.1 nm^{-2} for Rhodamine 6G. This may be attributed to electromagnetic dipole-dipole interaction between adsorbed dyes on the surface and is akin to the spectral changes observed in the formation of J- or H-type dimers or aggregates of dyes. This interpretation is further supported by recent theoretical developments in the electromagnetic modeling of anisotropic shells of dyes.[59,60,63] The implications of such dye-dye interactions in SERS have not yet been investigated but could be important. It is generally assumed that SERS enhancements are independent

of analyte concentration, at least in the low-concentration regime where there is no saturation of adsorption. Many studies have therefore used average SERS signals as a proxy for the number of adsorbed molecules, for example to study adsorption isotherms. Dye-dye interactions may affect these interpretations and further work is needed to assess their contribution in concentration-dependent SERS experiments.

These recent results call for additional experiments, complemented by electromagnetic theory and computational chemistry[61,64] (see Section 1.3 above), to refine our understanding of this chemical enhancement contribution to SERS, and how it is affected by the parameters that govern adsorption of specific molecules: their adsorption geometry, relative orientation, (in-)homogeneity in surface coverage, and how much the electronic resonance is affected by adsorption. Pushing experiments to the UV region will be highly desirable in this context, to probe the chemical changes undergone by a wider range of relevant molecules. It will also be instructive to consider different types of nanoparticles (silver, gold, but also dielectric and core-shell particles) with diverse shapes, to explore more comprehensively the full range of molecule-surface interactions. Such studies also have direct relevance to the pursuit of weak and strong coupling (see Sections 1.5 and 1.6 below) between local emitters and nanoparticles that sustain strong plasmonic or Mie resonances, a topic of current interest for applications in quantum optics,[65] spasers,[66] surface-enhanced photochemistry[67] and circular dichroism.[68]
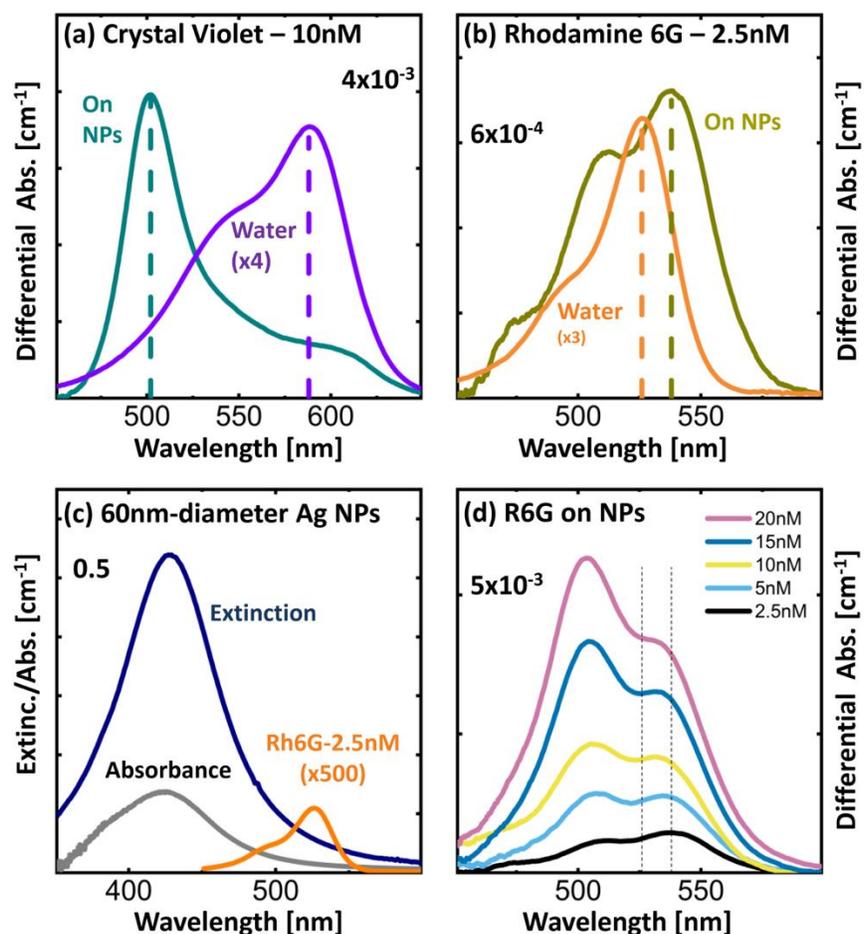
Figure 1.4. (a-b) Measured differential absorbance spectra of Crystal Violet and Rhodamine 6G adsorbed on 60 nm silver nanospheres at low surface-coverage, compared with the reference absorption spectra in water. (c) Extinction and absorbance spectra of the silver nanospheres (at 8pM) compared with the bare Rhodamine 6G spectrum in water. (d) Concentration dependence for the modified absorbance spectra of Rhodamine 6G on 60 nm silver nanospheres. See Ref. 58 for further experimental details.

1.5. Strong Coupling Regime

A recently introduced insight is the strong coupling regime between plasmons and molecular excitons under SERS activity. In 1997, single-molecule (SM) SERS was discovered by enhancement factors of 10^{10} to 10^{14} for dye molecules within plasmonic nanoparticle (NP) aggregates,[69,70] and successfully explained by the EM model, under the condition that NP dimers included SMs at their junctions.[71] It was therefore concluded that the EM model is

the dominant SERS mechanism. The NP dimers generating SM SERS enabled direct examination of various relationships between plasmons and SERS associated with the EM model, because in this strategy one can identify the plasmon "resonance" that is inducing Raman "enhancement" by single-particle spectroscopy.[72] These examinations also highlighted phenomena involving SERS hotspots, as follows: (1) Spectral changes in plasmon resonance by losing SERS activity revealed that SERS hotspots may involve strong coupling, in which EM coupling rates between plasmon and molecular exciton resonances are larger than the dephasing rates of both resonances. (2) The unusual laser energy dependence of broad background emission spectra in SERS was revealed as ultra-fast surface enhanced fluorescence (ultra-fast SEF), in which SEF rates exceed the molecular vibrational decay rates, thus resulting in emission from vibrationally excited states in the electronically excited state. (3) The appearance of forbidden Raman modes in SERS spectra was revealed as the breakdown of the selection rule of Raman excitation by the field-gradient effect. These three insights are related to the strong coupling regime, thus for future perspective the initially proposed EM in SERS model should include these points to more appropriately explain the SERS effect at hotspots.

The main point for considering strong coupling regime in SERS is estimating the size of hotspots which generate SERS. Various efforts toward improving the EM model including strong coupling, revealed that the size of hotspots can be below 1 nm^3 at the junction between NP dimers or NPs on flat metal surfaces.[65] We present below these three topics. First, correlation between strong coupling and ultra-fast SEF has been also investigated as a function of the extremely small hotspot size.[73] Second, in photochemistry, such an extremely small volume of the hotspots indicates that SERS may be useful to analyze the internal structure of SMs.[74] Indeed, SERS spectra usually show spectral changes related to structural changes of SMs located at hotspots.[75] However, the perfect elucidation of such structural changes is quite difficult because reference data for assignment are lacking. Therefore, DFT calculations are helpful to analyze SM structural changes induced by oxidization, local decomposition, *etc*. Third, in photophysics, SM SERS at extremely small hotspots indicates that (ultra- and deep-) strong coupling can directly control the ground-state properties of the molecule, because such changes by $\dfrac{2\hbar g_1}{\sqrt{N}}$ cannot be negligible for a SM condition, where $\hbar g$

is the coupling energy and N is the number of molecules involved in the coupling.[76] Thus, under the SM strong coupling condition, a conventional non-resonant excitation condition can become resonant, thereby resulting in a photochemical reaction by applying energy below the conventional excitation energy threshold and/or in nonlinear optical responses such as the pumping effect and classical Rabi splitting driven by photons. Ultra-fast SEF reveals the control of excited state electron dynamics of SMs at hotspots.[77]

Controlling the size of hotspots is important for the investigation and application of strong coupling in SERS, however, it should be noted that the size of conventional (zero-dimensional) hotspots may be too small for application in practical devices, utilizing the above mentioned photochemical and photophysical phenomena. Thus, we expected that special types of hotspots would be developed which can resolve the size problem. One example is provided by one-dimensional hotspots along the junction in nanowire (NW) dimers or between NWs and flat metal substrates.[78] The two main characteristics of such hotspots are: (1) the volume is considerably larger (at least 10^4 times) than hotspots within NP dimers and (2) hotspots can interact with propagating plasmon modes. The larger volume of hotspots makes SERS phenomena stable by mitigating the effect of molecular fluctuations. Interaction with propagating plasmons may enable transfer of information at hotspots in NW network systems, including zero- and one-dimensional hotspots. We propose that research in this direction, *i.e.*, considering the strong coupling regime and its extentive phenomena including the control over the size of hotspots, will lead to novel photoscience and phototechnology in SERS.

1.6. Extreme Interaction Regime (Quantum Effects)

For many years, the SERS signal from a few or even single molecules has been described as due to the local field produced in the vicinity of the pristine host nanoantenna, and the enhancement factors were obtained from standard electrodynamics methods, within the local dielectric response theory.[32,79] This initial classical description provided the main spectral features of the plasmonic gap,[71,80,81] including its spectral dispersion as the gap closes, as well as the dependencies of the intensity of the corresponding local fields. This approach provided a fundamental understanding of the classical regime of interaction, and served to interpret numerous SERS experiments of molecules in colloidal solution and in TERS

configurations. However, synthesis and fabrication methods have improved their capabilities to build plasmonic nanoantennas, currently being able to reach gaps down to a few nanometers, and below 1 nm, where molecules and material layers can be located.[82] In this extreme regime of interaction, quantum effects due to the dynamics of the electron gas forming the plasmon mode are revealed, and their description requires theoretical approaches beyond classical electrodynamics, as pointed out in the sections above.

An adequate approach to address the optical response, and thus the local fields of plasmonic gaps at this extreme regime relies on solving the time-dependent Schrödinger equation for the dynamics of the electron gas forming the gap. Such an approach turned out to be very valuable to set the limits of classical electrodynamics, and to account for the actual field-enhancements in the cavity. In particular, a quantum mechanical treatment of the optical response, at different levels of accuracy, accounts for (i) dynamical screening effects in the response, the so-called non locality,[83] (ii) the effect of spill-out of the electrons at interfaces which can extend spatially a few Angstroms into the dielectric,[84] (iii) quantum-size effects which are relevant for small clusters and protrusions,[85] (iv) atomistic effects which sculpt the surface charge density at subnanometer dimensions,[86,87] and optical tunneling which sets conduction channels at optical frequencies even before physical contact between the metallic surfaces, thereby quenching and reshaping the distribution of the local fields[34] sensed by the molecules and other sample materials.

This plethora of quantum effects get to their epitome when nm and sub-nm gaps with atomic-scale features are formed within a plasmonic cavity. Theoretical approaches attempted to face these challenges and describe the local fields, and thus the SERS signal, in these extreme situations. A recent example showed how tunneling effects produced charge transfer between metallic interfaces in vacuum at about 4Å gap separation,[34] quenching the local field, as experimentally confirmed.[88,89] However, most of the practical realizations of SERS in plasmonic gaps can still play safe, as most nanogaps used in SERS are larger than half a nm, thereby avoiding the onset of tunneling effects. Nevertheless, some conducting molecules might distort this general rule of thumb,[90,91] and conduction effects between electrodes at optical frequencies might be a matter to be considered more deeply in the future.

In the realm of sub-nm plasmonic gaps, the challenges for accurate modeling are diverse, and in one way or another, many of them have to do with the quantum description of either the plasmonic gap, the material sample, the type of interactions, or all together. A remarkable experimental achievement in a TERS configuration managed to obtain optical Raman maps for selected vibrational modes of a single molecule with sub-nm resolution,[74] thus even competing with the signal obtained in scanning tunneling microscopy (STM). This level of resolution required a previously unthinkable localization of the local fields within the gap, far beyond the typical 5-10 nm lateral plasmonic extent within the gap. Accurate atomistic *ab initio* calculations based on TDDFT, which considered the actual distribution and configuration of atoms within a gap, revealed that atomic-scale localization of the fields was indeed possible,[87] thanks to the varying induced electronic density profile at single atoms acting as an atomic-scale lightning rod.[92] The actual field localization in such a situation is shown in **Figure 1.5**. The simplicity of the concept provides an effective description of this effect by classical means, where atomic protrusions in a cavity can be modeled by corresponding classical interfaces which follow the electronic density profile.[93] Such an extreme localization, as it may happen in many tip apexes, might be responsible, to a large extent, for the sub-nm resolution achieved in an increasing number of experimental TERS realizations.[74,94-96] This extreme localization not only affects resolution but it actually governs a dramatic breaking of Raman selection rules at the single-molecule level, due to the action of the strongly inhomogeneous fields induced at atomic-scale morphologies.[97,98] Activation of unusual vibrational modes of single molecules under stable conditions has been reported both at cryogenic[74,99] and room-temperature conditions.[100,101] Most such features can only be explained in terms of this extreme atomic-scale field localization within the gaps, which have been termed "picocavities" due to the ultrasmall effective mode volume sustained by the atomic features (see **Figure 1.5**).
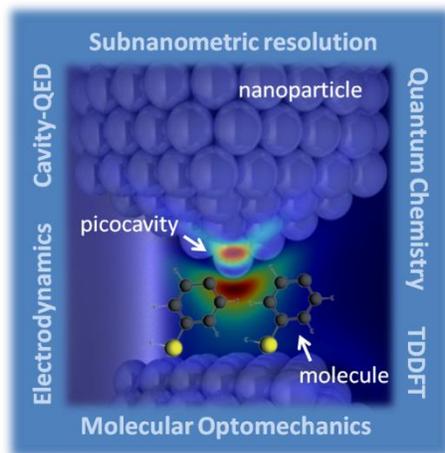
Figure 1.5. Artist's view of a plasmonic gap formed by metallic nanoparticles hosting a set of organic molecules. A picocavity is formed due to the protrusion of a single atom, localizing an electromagnetic field at the atomic scale, thus producing sub-nm resolution and close-to-strong optomechanical coupling. Theoretical methods to address this extreme interaction regime in SERS are outlined on the sides, including electrodynamics, cavity-QED, quantum chemistry, and TDDFT.

Indeed, an additional challenge of the current modeling and understanding of the Raman processes is associated with the possibility to exploit the optomechanical interaction between molecular vibrations and plasmons, beyond the thermal regime. The recently established analogy between non-resonant Raman scattering and an optomechanical process[102] has allowed a description of the dynamics of plasmons and vibrations in SERS, within the framework of cavity-quantum electrodynamics (QED), with the use of a linearized interaction Hamiltonian $\hat{H}_{int}=-\hbar g_o(\hat{a}^{\dagger}\hat{a})\cdot(b^{\dagger}+b)$, where $\hat{a}^{\dagger},\hat{a}$ ($b^{\dagger},b$) are the plasmon (phonon) creation, annihilation operators, and g_o is the vacuum optomechanical coupling, which is inversely proportional to the effective mode volume of the plasmonic cavity, $g_o \propto 1/V_{eff}$. This quantum treatment has predicted a non-linear evolution of the Stokes and anti-Stokes Raman signals, due to the optomechanical interaction.[103] Such an effect has been revealed in molecules in the vicinity of plasmonic "*picocavities*", which boost the optomechanical interaction, g_o, as a result of the extremely reduced effective mode volume.[91] Molecular optomechanical pumping or cooling in plasmonic cavities can overcome thermal effects,[104,105] thereby opening the possibility to control the vibrational dynamics and

reactivity of molecules.[106] Therefore, many unusual trends and variations of vibrational lines in plasmonic SERS might now be reinterpreted in terms of optomechanical interactions. The effort to theoretically describe this rich variety of molecular optomechanical effects in realistic plasmonic cavities results in the cavity-QED framework.[107] Cooling and pumping of vibrational modes, resonant Raman processes, collective effects due to self-assembly of molecules within plasmonic gaps, or the statistics of Stokes and anti-Stokes emissions are theoretical and experimental challenges that the SERS community will need to face sooner or later.

An important issue in the theoretical description of SERS has to do with the assumption of physical interactions between sample (molecule) and cavity (plasmonic gap). In practice, chemisorption of molecules on metallic surfaces often produces a complex redistribution of the molecule-substrate electronic structure and thus of its corresponding polarizability, modifying vibrational modes, and allowing for charge transfer.[108] This effect complicates the modeling and simple description of Raman modes, as well as the dependencies of their intensities, and might require a combined quantum description of the substrate-molecule hybrid, together with the self-consistent action of the induced electromagnetic field at the cavity. In other words, the quantum realm of vibrational spectroscopy in extreme atomic-scale cavities might require the combination of aspects from Condensed Matter Physics, Quantum Chemistry, and Classical or Quantum Nano-optics, which turn SERS into a fascinating arena for theoretical developments, as well as for experimental testing and exploitation of unexpected effects.

1.7. Outlook for Future SERS Applications

Research during the last few years has opened up opportunities for further intriguing SERS science and technology, which in our view has been enabled because of the emerging capability to use bottom-up nano-assembly in a reproducible, robust manner to form nm-sized gap constructs. Let's consider two regimes, with either few or specific numbers of molecules in a fully-defined nanoscale geometry, or a paradigm for simple but robust solution-based SERS sensing.

The first is the nanoparticle-on-mirror (or NPoM) construct, which produces single gaps down to 0.3 nm between two plasmonic metals that can be precisely filled with different

molecular or monolayer systems (for a recent review of this system see Ref. 109). It can be understood as a metal-insulator-metal (MIM) waveguide that confines light, both between the metals and laterally, to give <50 nm^3 mode volumes. This system has opened up improved understanding of the role of molecular conductivity on SERS,[91] as well as identifying the origins of SERS background emission (which sets practical detection limits) as coming (partly) from molecule-metal coupling[110] and partly from the unavoidably enhanced electronic Raman scattering of free electrons in the metal walls.[111,112] Careful kinetic studies of NPoMs show that optically-induced migration of individual metal atoms dominates much of the dynamics.[113] This can even induce metallic nanowires to bridge across the gap, changing both plasmon resonances and SERS.[114,115] This work has been extended to look at memristive electronic memory devices,[116] to study individual charges hopping on and off single redox molecules[117] (which shifts the SERS lines), and to study the influence of electrochemical potentials on SERS.[118] It has also been demonstrated that single emitters can be precisely assembled in NPoMs using DNA origami, thereby allowing SERS of strong coupling systems.[65,119] This and many ongoing experiments reveal much of the nanoworld at interfaces, showing it to be far more subtle, nuanced, and dynamic than previously accepted.

A detailed campaign to study the SERS of NPoMs has revealed the presence of transient sharp vibrational lines which evolve. Using an apparatus devised to automatically drop the laser power as soon as these are detected, and initially at cryogenic temperatures, it was shown that the transient SERS must originate from single molecules in the gap.[99] A variety of evidences proved that single Au atoms move partially out of the close-packed metal surface to yield extra field enhancements of 3-5. Therefore, several-hundred-fold higher SERS enhancements which allow single molecules to emit more than the remaining hundred molecules in the gap.[105,106] These observations also resolve questions from past decades, such as the spatial mapping and irreproducibility of TERS, as well as how single-molecule signals can be observed in SERS – likely emerging from picocavities in the crevices of aggregated metal NPs (though much less controllably). The same Au adatom behavior was also recently shown at room temperature, using several million SERS spectra to prove that the atom prefers to move from the bottom planar Au mirror,[101] at least in some cases. The prospects for intriguing light-matter and catalytic interactions in such atomic-scale regions are fascinating and ongoing.

The second regime of interest has been the use of colloidal metal nanoparticle aggregates when the gaps are set by precise linkers (*e.g.* cucurbit[n]urils, giving 0.9 nm gaps) which can filter classes of small molecules from a heterogeneous soup into SERS active reliable hotspots. This facilitated the detection of neurotransmitters at clinical concentrations in urine,[120] methanol at <1% in ethanol,[121] even using these assays in microdroplets[122,123] and microfluidics.[124] Indeed, they can be used to track chemical reactions routinely[125] and this technology is thus now ripe for exploitation – *e.g.* in the form of the 'Intelligent Toilet' capable of long-term personalized health monitoring. The capability to explore fundamental science at the nanoscale through SERS of individual exquisitely-controlled nano-assembly, as well as developing realistic societal tools for personalized medicine and other challenges, puts SERS in great shape for continuing developments (**Figure 1.6**).
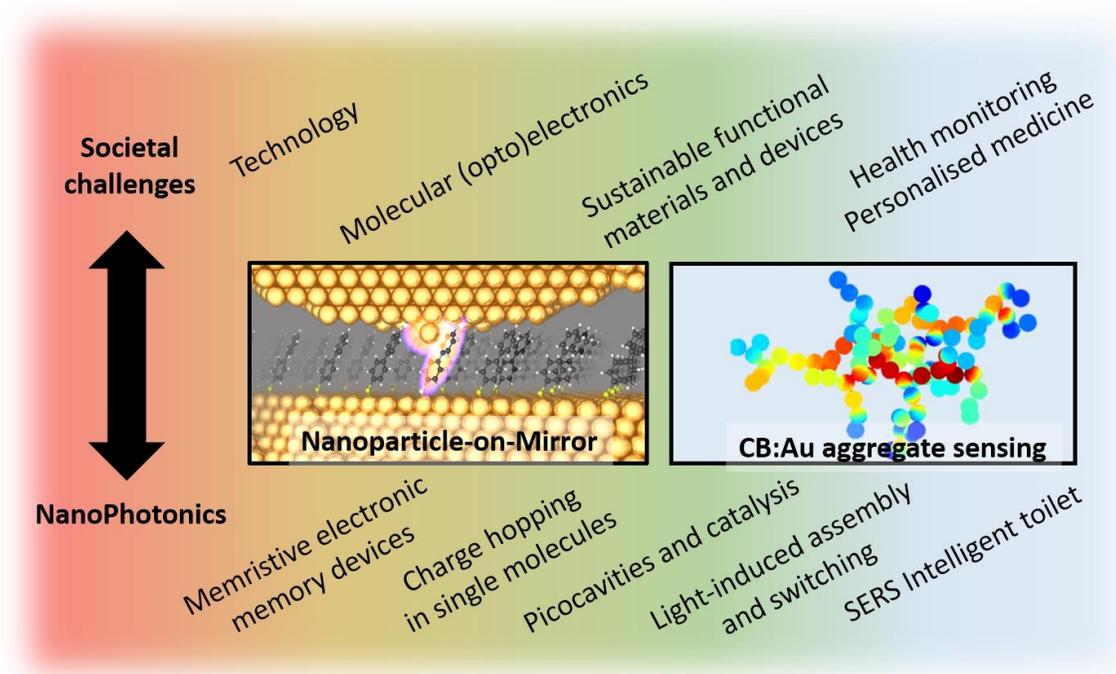
Figure 1.6. Structures ranging from nano-gap geometry (nanoparticle-on-mirror, NPoM) to nanoparticle sensing using CB:AuNP aggregates enable SERS applications from single molecule detection to personalized medicine.

2. SERS Substrates

An important prerequisite for the better understanding of SERS and the application in chemical analysis and single-molecule detection, is the development of highly reproducible, reliable, rational substrates. "Rational" in this case means that the substrate has quasi uniform and predictable optical and near-field properties. The choice of the substrate type, its material and fabrication method depend on the specific application or question to be answered. More fundamentally and academically oriented problems, such as the question of the dependence of SERS enhancement factor on hotspot size/geometry, require fabrication methods to tune the plasmonic structure (at the single particle level), pushing the precision to ultimate limits which are usually time-consuming, costly and hardly possible to produce at large scale. On the other hand, when focusing on (practical) chemical analysis, other aspects rather than high precision are important, *e.g.* large-scale homogeneity and batch-to-batch reproducibility of the substrate, cost-effective and easy fabrication, robust SERS signal intensity, substrate stability, high affinity toward the analyte of interest under given conditions, *etc*.

In this context, the concept of SERS substrates does not only refer to solid substrates but also to colloidal nanoparticles in a dispersion medium (solution). Advantages of using colloidal nanoparticles include highly reproducible and cost-effective synthesis *via* bottom-up strategies, tailored optical properties over a wide wavelength range by tuning particle shape and size, as well as manifold surface functionalization, which render them applicable in different environments and for many analytes. The most widely used nanoparticles display a simple spherical morphology, however at the expense of exhibiting moderate Raman signal enhancement as single particles, because of their high symmetry. Aggregated colloidal nanoparticles still feature low-cost while often exhibiting very strong enhancement due to a three-dimensional (3D) distribution of plasmonic hotspots. However, since colloidal aggregation is a dynamic process, SERS spectra must be recorded within a certain time-window, meaning that the reproducibility of the SERS spectra depends strongly on the precise experimental conditions used. On the other hand, anisotropic plasmonic single-nanoparticles enable substantial Raman signal enhancement, due to the presence of intrinsic hotspots at edges and corners, such as in nanorods and nanocubes, or at sharp protruding features, such as in nanostars. Among all other shapes, gold nanostars have likely attracted the most attention recently: their validity as effective SERS enhancing platforms was proven early on and has been a motivation to further pursue the investigation of their properties over

the last decade.[126-131] Within the general concept of nanostars, we consider a variety geometries and symmetries, and therefore we dedicate a section below to exclusively discuss this particular shape class.

Although colloidal systems pose the potential problem of aggregation in solution, this can be overcome by directing the self-assembly of colloidal nanoparticles into homogeneous and ordered layers and arrays. Multilayered systems and supercrystals offer substrates with three-dimensionally organized hotspot architectures. Alternatively, sophisticated colloidal lithography and chemical etching methods can be also applied. All of these methods allow designing and engineering the hotspot size, geometry and density in a reliable manner, over large areas. Some of the reported assembly strategies allow the fabrication of substrates which are not just restricted to flat supports but can also be applied to flexible, curved or rough supporting materials, thereby leading to sensing applications.

The renewed drive to expand the materials base for plasmonics beyond the coinage metals and aluminum, motivated by both extension of localized plasmon resonances into the infrared, as well as issues around loss, temperature stability and CMOS compatibility,[132] is expected to also have an influence on the development of substrates for SERS.[133] Transition metal nitrides, transparent conductive oxides, metal sulfides, as well as doped oxides, could well be candidate materials for future surface enhanced spectroscopy substrates, and a survey of those materials from this point of view is called for.

2.1. Surface Chemistry, Stability, and Solution-Phase Nanoparticles – A Balancing Act

Nanoparticles synthesized using bottom-up synthetic methods are widely used as SERS substrates. Most often these materials are synthesized *via* metal-reduction routes in the presence of electrostatically-stabilized chemical species, dynamic stabilization using molecules or ions with reversible affinity for an interface, or covalently attached surface ligands. Each of these surface chemistries offers different advantages and disadvantages for subsequent SERS applications, as these surface chemistries simultaneously promote the suspension of the nanostructures in solution, lead to the formation of electromagnetic hot spots for increased SERS signals,[134] and/or can block the metal surface from adsorption of the targeted molecules when used for direct detection.[135] The latter mechanism can limit

direct SERS detection because of signal suppression arising from short range chemical enhancement mechanism routes associated with SERS. Solution-phase nanoparticles are inherently "metastable" because colloidal dynamics induce frequent collisions between nanostructures due to Brownian motion.[136,137] These materials can remain stably suspended in solution for long periods of time, yet can also undergo degradation through dissolution,[138-140] aggregation,[136,137] and/or sedimentation[141] processes, during storage and/or use. While dissolution is dependent of electrical potential differences between the metal nanoparticle composition and other chemical species in solution, both sedimentation and aggregation depend on the dynamic movements of nanostructures in solution. The kinetics of these processes can be modeled using collision theory.[142,143] In so doing and by treating nanostructures as point charges moving in three dimensions in water at room temperature, it is estimated that over ~10^4 particle collisions will occur per second in a 1 mL solution containing ~5 nM nanostructures.[137] The energetics involved with the collisions will dictate whether nanostructures aggregate forming potential hotspots for large SERS enhancement, form relatively larger aggregates in solution which can lead to electromagnetic losses and particle sedimentation if the mass of the aggregates overcomes buoyancy forces, or remain stably suspended in solution thus exhibiting plasmonic properties that are maintained.

Surface chemistry and the local environment surrounding nanostructures in the solution phase, control the energetics and fate of these materials for SERS applications. Both molecule orientation and dwell time at high field strength locations must occur suggesting that adsorption is required.[135] Second, the energetics of nanoparticle collisions must be considered as these influence the underlying plasmonic properties and enhancement associated with SERS substrates.[144] In other words, both chemical and electromagnetic enhancement mechanisms influence the observed spectroscopic signal, and these both depend on the local environment surrounding the nanostructures and their surface chemistry. The probability of observing a SERS signal for a given molecule increases as the analyte exhibits more favorable binding energies and non-zero sticking probabilities to an interface.[145,146] Many parameters including material composition, solvation, and local surface chemistry can either promote the sticking probability of a molecule or prohibit it. In general, SERS signals are detectable for a given molecule if that molecule exhibits a larger attractive potential to the surface *vs.* its incident kinetic energy, thus increasing its residence time at the

interface and thereby exceeding the collection time window for a SERS measurement.[135] It is well established that thiolate-containing molecules are excellent targets for SERS measurements, as residence times are large, thereby promoting adsorption *via* displacement of stabilizing agents and solvent molecules.
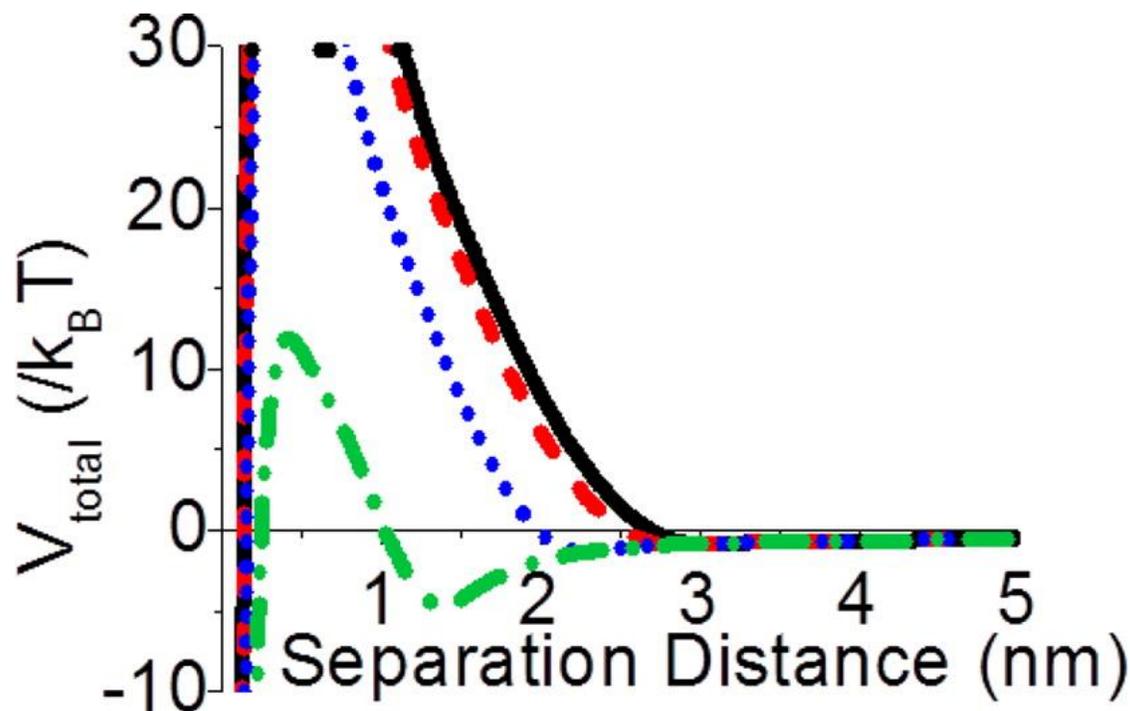
Figure 2.1. The total interaction pair potentials between two (••••) Au@TA, (- - -) Au@MHA, and (——) Au@MUA nanoparticles predicted using xDLVO theory. Reproduced with permission from Ref. 137. Copyright 2015, American Chemical Society.

Not all molecules, though, disrupt the local nanoparticle environment sufficiently so that SERS measurements can be made. In these cases, SERS can still be observed if the molecules are trapped between small nanoparticle clusters. As such, the energetics of nanoparticle interactions also influence the likelihood of observing SERS signals. One model that is commonly used to describe these interactions is the extended Derjaguin, Landau, Verwey, Overbeek (xDLVO) theory.[147-150] The xDLVO theory models the pairwise interaction potential between two objects[148-150] as a function of van der Waals, electrostatic, and steric (osmotic and elastic) potential energies.[148-150] The sum of these separation distance-dependent interaction potentials can accurately predict whether colloidal particles will form aggregates (irreversible clusters), agglomerates (reversible cluster formation), or will remain

in an identical state as the initial primary particles.[137] In most cases, the short-range attractive van der Waals potential is the driving force behind cluster formation. It has been shown for both silver[151] and gold[137,144] particles that, these attractive potentials depend on the size-dependent dielectric constants of the metals and the magnitudes of these interaction potentials increase with decreasing nanoparticle dimensions (for nanoparticles with diameters below ~100 nm). It was recently demonstrated that the smallest dimensions of a nanostructure such as the tips of gold nanostar spikes (*i.e.*, branched nanostructures) drive nanoparticle clustering behavior,[144] as well as the reproducible use of these materials in SERS assays.[152] Clearly, attractive interactions between colloidal nanostructures in solution can shorten the average separation distance, thus increasing the electromagnetic field strength at gaps between nanostructures and increasing SERS signals. For visible light excitation, edge-to-edge nanoparticle separation distances of 0.8-1.5 nm are likely ideal for maximizing the electromagnetic enhancement of SERS chromophores between nanostructures.[134] This range is limited at shorter separation distances *via* quenching mechanisms[153] and by field decay at larger separation distances.[154-157]

Surface functionalization, electrostatic potentials from ions at the particle interface, and solvent ultimately provide opposing forces to attractive potentials induced *via* van der Waals forces.[136,148,149] To understand how these parameters influence interparticle separation distances and, in turn, SERS signals, both electrostatic terms (dependent on ionic composition of the solution) and those that depend on solvent and surface chemistry (*i.e.*, osmotic and elastic potentials) must be considered.[136,148,149] All in all, the sum of these interaction potentials should be considered in a way that balances the likelihood of molecule-interface affinity for SERS detection without yielding uncontrolled aggregates, if quantitative SERS signals are sought. As such, how nanoparticle and medium attributes contribute to these processes should be understood.[137] Increasing ionic strength has been shown to compress the electrostatic repulsive double layer[137] and decrease solution permittivity,[158] thereby reducing electrostatic repulsive interaction potentials between colloidal nanostructures. Similarly, the osmotic potential between nanostructures arises from the competition of solvent molecules to solvate surface bound functional groups on two nanoparticles at short inter-particle spacing. This stabilizing force comes into play when the edge to edge separation distance between nanostructures is less than twice the thickness of

one adsorbate layer.[136,148] When separation distances are shorter than one adsorbate thickness, entropic effects arise from surface ligand compression,[148] resulting in an elastic contribution to the potential. These stabilizing forces can be large, that is exceeding $100/k_BT$ when the separation distance between two SERS-active particles is less than 1 nm. By comparison, the elastic potential is repulsive but smaller in magnitude.

The various mechanisms involved in nanoparticle clustering energetics offer an opportunity in SERS detection, as equilibrium separation distances between nanostructures can be tuned, leading to separation distances ideal for SERS excitation at visible wavelengths (0.8-1.5 nm). As shown in **Figure 2.1**,[4] the addition of a self-assembled monolayer composed of thioctic acid, 6-mercaptohexanoic acid, or 11-mercaptoundecanoic acid on ~13 nm gold nanospheres yielded ideal interparticle separation distances in this critical range, as differences in monolayer thickness and packing density influence contributions to the energetics between nanoparticles upon collision. Moving forward, the metastability or the retention of plasmonic properties by solution-phase SERS substrates will be key toward the reproducible use of these materials. As such, synergistic contributions from attractive van der Waals potentials, electrostatic surface potentials, solvent composition, and surface ligands could be balanced to facilitate the rational design of solution-phase SERS assays while also considering nanoparticle stability, fate, and interparticle interactions.

2.2. Anisotropic Nanoparticles: Nanostars

While nowadays the term *nanostars* is quite pervasive in the literature, owing in particular to the wealth of applications that these particles have found, it identifies in reality a group of nanoparticles with a wide variety of morphologies, whose only common trait is to have a uniform core, often spherical, and several branches of variable sharpness, length, number, and crystallinity, depending on the synthetic method.

The first reports of branched gold nanoparticles appeared in the early 2000s involving the use of CTAB and ascorbic acid, with or without NaOH.[159,160] Hafner then proposed in 2006 the term *nanostar* to describe gold nanoparticles characterized by spherical cores and protruding spikes, which he synthesized from both CTAB-capped seeds and commercial seeds employing ascorbic acid as the reducing agent, in the presence of NaOH.[161] However, only the systematic experimental studies by Liz-Marzán and co-workers,[162-165] and the

theoretical explanation of their plasmonic response by Nordlander and co-workers,[166] established gold nanostars as a very specific nanoparticle morphology, with streamlined and unified synthetic protocols. Nonetheless, these particles can still be found in the literature under a wide variety of names. For instance, they have been defined as branched nanoparticles,[167] nanoflowers,[168] multipods (tetrapods, hexapods, or octapods),[169] nanourchins,[170] highly-branched nanostructures,[171] hedgehog nanoparticles,[172] spiky nanoparticles,[173] wrinkled nanoparticles,[174] nanodendrites,[175] nanopopcorn,[176] nanoflowers,[177] and even nanoechinus.[178] While one can understand that a nanoparticle called nanopopcorn may have shorter and more rounded branches than another termed nanourchin, in certain instances the differentiation has become quite blurry, especially as the field has moved forward during the past ten years and research has focused more on the application, rather than the synthesis and detailed characterization of these particles. There needs to occur therefore, after a decade of research, a clarification of what are the defining parameters that characterize a nanostar, including a neat classification of the synthetic protocols.

The synthesis of gold nanostars was first proposed as a seeded protocol involving the use of CTAB as the surfactant.[161] Later on, a poly(vinylpyrrolidone) (PVP)-mediated protocol was proposed,[162] that produced high yields of reproducible gold nanostars with multiple short spikes when conducted in dimethylformamide (DMF). Interestingly, another seeded approach (mediated by CTAC) was reported roughly at the same time, which involved the use of four growth solutions to produce regular nanostars with short branches,[179] resembling what we currently define as multipods. Such multipod-like nanostars, with ten identical (short) pyramidal arms and twinned morphology, can currently be synthesized with impressive uniformity *via* a different seeding method employing a single growth solution (**Figure 2.2**).[180] Later on, a seeded growth method mediated by HEPES buffer was proposed by Pompa and co-workers,[181] who obtained nanostars with short, rounded spikes, protruding from a large spherical core. Interestingly, HEPES and other kinds of Good's buffers are now regularly employed to produce nanoparticles with only four to five spikes, in the seedless version of the synthesis.[182] The advantage of using HEPES is that its biocompatibility discards toxicity concerns that can be raised when polymers or surfactants are employed instead (*e.g.* CTAB). Eventually, Vo-Dinh proposed a surfactant-free, seed-mediated method that led to the tunable synthesis of biocompatible gold nanostars stabilized only by ascorbic

acid without requiring the use of toxic surfactants (*e.g.* CTAB).[183] This type of nanostars is arguably the one that has so far led to the most intense signal enhancements in direct SERS sensing applications, likely due to the approachable metallic surface, not hindered by the presence of surfactants and perhaps because of the presence of a significant amount of silver used in the synthesis.[184] While the majority of protocols involve the use of seeds, few other seedless methods have been reported, in addition to that mediated by HEPES.[185,186] One protocol involved the use of either glucosamine or glucosaminic acid as the only reagents needed for both reduction and induction of shape anisotropy.[186] Following this method, Feldmann and co-workers proposed another seedless method mediated by CTAB,[187] which enabled the study of SERS properties at the single particle level.[166] Overall, while the seedless methods may appear more advantageous for their simplicity, they afford only limited tunability and lead to higher polydispersity. One question that arises now is however the following: what defines monodispersity in branched nanoparticles? Is it the overall diameter, or the aspect ratio of the spikes? Or is it the number of spikes rather than their sharpness? These questions become even more important when the nanostars are characterized by high shape anisotropy, such as those first proposed by Pallavicini and co-workers,[188] and recently studied more in depth at the Fabris group (**Figure 2.2**).[189]

If we go back chronologically through the literature, on a sort of *journey down memory lane*, we realize that, during their first years of existence, gold nanostars have been thoroughly studied and characterized, with a variety of technical tools, including femtosecond laser spectroscopy,[190] dark field scattering,[191] photoelectron emission microscopy,[192] and two-photon photoluminescence.[183] Their nonlinear response was explored,[193] along with their performance in SERS.[161-166,180,184,193,194] Similarly, their optical response was theoretically modeled, *in primis* by Nordlander and co-workers,[166] but also by García de Abajo and others.[162,183,194,195] Thereafter, the community has been steered away, perhaps lured by the exceptional field enhancements they produce and the possibility of using them for chemical sensing, intracellular imaging, or catalysis. Because of this, fundamental studies on the synthesis and growth mechanisms or on the theoretical and computational understanding of their plasmonic response have substantially decreased in number.

In the last couple of years however, the community has turned back to tackle a better understanding of these intriguing nanoparticles. The growth of symmetric nanostars has been

carried out in microfluidic devices,[196] and followed in real time by liquid cell TEM;[197] their purification *via* density gradient centrifugation was reported,[198] their dark field response was studied in great detail and confirmed computationally,[199] and systematic studies to optimize monodispersity and plasmonic response of surfactant-free nanostars were carried out.[200] Detailed accounts on the growth mechanism of PVP-capped gold nanostars were also reported,[201] and the influence of seed morphology and silver nitrate concentration on the final morphology and stability of nanostars with few, long, high aspect ratio spikes was also studied.[189] Because gold nanostars are generally characterized by limited shelf lives, the parameters affecting their stability were analyzed in detail by Haes and co-workers.[144] Along the same lines, the thermal stability of nanostars was studied in 3D in real time by Bals and co-workers, who showed that faster atomic migration from the tip to the base of the spike occurs as the temperature increases.[202] Finally, three-dimensional finite element method simulations were reported to understand in detail the origin of the plasmonic resonances of gold nanostars with highly elongated spikes, and their 3D coupling behavior was proposed.[203]

In the wake of this renewed interest on the fundamental properties of gold nanostars, we need to ask ourselves as well which are the properties of these particles that are most relevant to SERS. How do we calculate the enhancement factor of substrates produced by such complicated particles? We could simplify their morphology,[189] or find methods to evaluate their extinction coefficient and surface areas.[204,205] But how do we move forward to ensure that each nanostar produces the same enhancement? In many applications this may not be an issue, but if we think about a parallel between SERS tags and fluorescent dyes, how will we make the former competitive if their response is inconsistent? Also, could an improvement on the quality, tunability, monodispersity, and reproducibility of nanostars improve the chance for SERS to become truly quantitative? While artificial intelligence appears to be infiltrating every area of science, there is an opportunity to understand how these tools can be leveraged to first optimize, and then drive, the synthesis of gold nanostars to extend the reach of SERS toward true applicability in medicine, forensics, and catalysis, or even more.
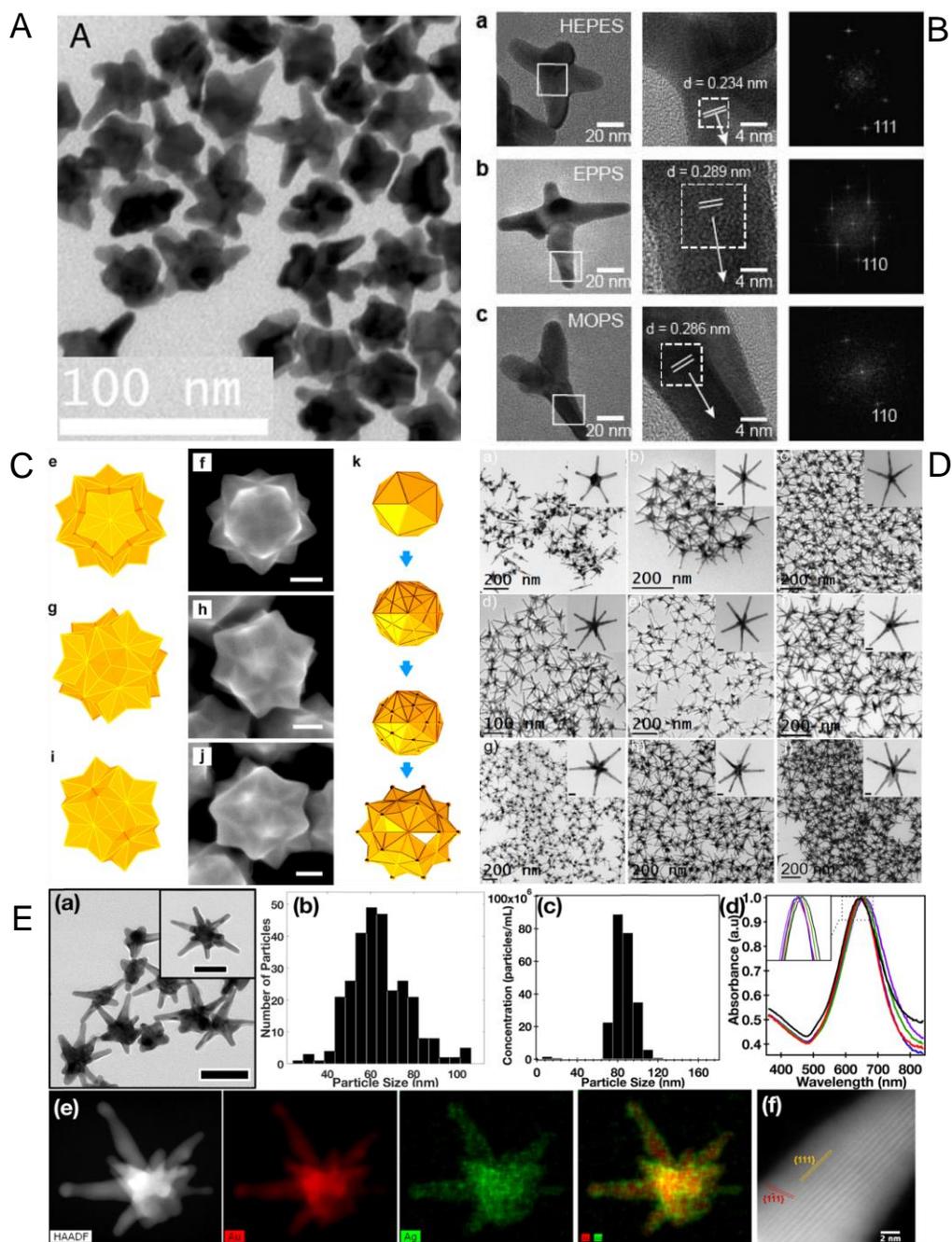
Figure 2.2. Gold nanostar morphologies vary substantially depending on the synthetic protocol used. A) PVP-capped gold nanostars synthesized *via* seed-mediated approach. Adapted with permission from Ref. 190. Copyright 2012, Elsevier B. V. B) A Good's buffer-mediated seedless method yields nanostars with few rounded branches. Adapted with permission from Ref. 182. Copyright 2016, American Chemical Society. C) Multipod

nanostars with pyramidal branches can be synthesized with high control and reproducibility employing PVP in the presence of dimethylamine. Adapted with permission from Ref. 180. Copyright 2015, American Chemical Society. D) Gold nanostars with few, long spikes can be obtained with high reproducibility employing Triton X 100 as surfactant. Adapted with permission from Ref. 189. Copyright 2019, Royal Society of Chemistry. E) Tunable spike length and number can be achieved in gold nanostars employing ascorbic acid as the capping agent. Adapted with permission from Ref. 200. Copyright 2018, American Chemical Society.

2.3. SERS in Single-Nanoparticle Dimers (Precision SERS)

A set of substrates that are particularly interesting for understanding the fundamental mechanism of SERS are lithographically prepared metal nanostructures that have a single or very few hotspots, *i.e.*, lithographic plasmonic oligomers.[89,206,207] They may be fabricated in large quantities with excellent control over their geometry, especially over the gap size between the plasmonic building blocks. Subtle geometrical changes allow tailoring the oligomers, *e.g.* to support Fano resonances between two optical excitations.[208,209] A key advantage of plasmonic oligomers is that their structure is accessible by electron and force microscopies, allowing us to relate their structure to their optical properties and SERS efficiency. The optical properties of plasmonic oligomers have been studied *via* far-field absorption and scattering, as well as by near-field optical mapping.[208,210-214]

Some experimental data obtained from SERS by plasmonic oligomers challenged our theoretical description of SERS. For systematic studies of SERS by a single, well-defined hotspot, Raman probes have been explored and found to be highly beneficial. A super-sharp Si tip was *e.g.* used to correlate the electromagnetic near field with the SERS enhancement. A dual scattering scanning near-field microscope/surface enhanced Raman setup correlated the spatial distribution of the enhanced field with the distribution of the SERS signal produced by the Si tip, finding excellent agreement of the hotspot shape and relative intensity pattern with the electromagnetic enhancement model.[214] Another interesting probe comprises graphene and other two-dimensional materials, which are transferred onto plasmonic oligomers.[215,216] Graphene is a non-resonant Raman scatterer, with a constant cross section

in the IR and visible energy ranges.[217,218] This means that any change in the SERS intensity with respect to polarization, laser energy and so on are caused by the plasmonic hotspot (as opposed to intrinsic variations in the Raman scattering cross section that occur in many other materials).[215,219] Conversely, the extreme localization of SERS hotspots allowed detecting strain in two-dimensional materials with sub-wavelength resolution, using phonon frequencies as a marker for strain.[220] To study how plasmonic enhancement depends on the excitation wavelength, the laser excitation was varied in small steps ($\approx$ 5 nm) in SERS experiments on graphene, coupled to a plasmonic dimer. The SERS resonance profile found a resonance that differed strongly ($\approx$ 200 meV) from the plasmonic resonance obtained by elastic scattering in dark-field spectroscopy.[216] The discrepancy was much larger than the difference to be expected between near- and far-field resonances (<50 meV), which remains yet to be resolved.

Another key feature that requires additional experimental studies is the total SERS enhancement. First sets of quantitative experiments were performed on individual hotspots where the plasmonic nanostructures were imaged with electron and force microscopies, but the position, density, and orientation of the molecular Raman probes were inaccessible experimentally.[23,221-223] The studies reported an experimental SERS enhancement that was 10^2-10^4 stronger than predicted by accompanying simulations. A further refinement of this approach involved Raman reporter molecules (α-sexithiophene) encapsulated in carbon nanotubes (6T@CNT), as shown in **Figure 2.3**.[224] Carbon nanotubes were used as nanocontainers to carry molecules into the plasmonic hotspots, thereby making molecular position and orientation visible by SEM and AFM. 6T@CNT have the added benefit that the large distance between 6T molecules and the gold surface (large on atomic scales, several nm), as well as the presence of a carbon wall between 6T and the gold surface, prevent both enhancement by surface roughness and chemical enhancement. Nevertheless, the experimentally determined enhancement of almost 10^5 was two orders of magnitude higher than that simulated for the configuration in **Figure 2.3**.[224] Our current understanding of SERS thus appears to miss ingredients that can explain the higher experimental intensity, as well as the apparent shift in resonance energy. Recent proposals to describe SERS within the microscopic description of the Raman effect and within the framework of optomechanics may guide us toward a full description of the effect.[102,105,225] Such a description may need to

include more explicitly phenomena related to strong light-matter coupling, such as superradiance and Rabi shifts of plasmonic resonances.[226]
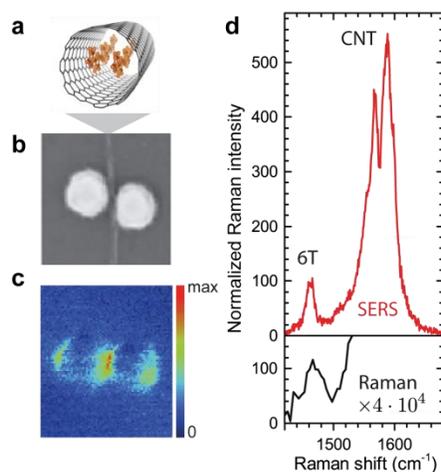
Figure 2.3. Quantitative SERS enhancement using 6T molecules encapsulated in carbon nanotubes. (a) Encapsulation process, adapted with permission from Ref. 227. Copyright 2016, American Chemical Society. (b) SEM image of a gold dimer with 6T@CNT deposited in the gap. (c) SNOM image of the plasmonic hotspot. (d) SERS (red) and Raman (black) spectra of 6T measured under plasmon resonance conditions (638 nm). The total enhancement on several dimers varied between $3 \cdot 10^4 - 9 \cdot 10^5$, corresponding to $1 \cdot 10^6 - 4 \cdot 10^7$ for the enhancement of the Raman cross section. Reproduced with permission from Ref. 224. Copyright 2017, Royal Society of Chemistry.

2.4. Self-Assembled Nanoparticles

- **Monolayers at liquid-liquid interfaces**

The quest for uniform, reproducible and affordable enhancing substrates aimed at realizing the potential analytical applications of SERS, has led to substrates that have generally fallen into two broad classes: aggregated colloidal nanoparticles (NPs) and solid substrates carrying plasmonic nanostructures.[228-231] Solid substrates are generally more stable and convenient to handle, both in use and storage, but the sophisticated fabrication procedures typically

required for their production render them considerably more expensive than aggregated colloidal NPs.

Metal liquid-like films (MeLLFs) combine the advantages of conventional aggregated colloids and solid substrates. Since they consist of a densely packed monolayer of colloidal Ag/Au NPs assembled at the interface of two immiscible liquids, they are easy and inexpensive to prepare but still provide stable hot-spots.[232] The key to inducing self-assembly of colloidal Ag/Au NPs into MeLLFs at liquid-liquid interfaces (LLIs) is to remove the electrostatic repulsion between adjacent particles at the interface. For Ag/Au NPs, this has typically been achieved through surface functionalization using strongly adsorbing charge-neutral organic "modifier" molecules, such as thiols.[233,234] However, these strongly adsorbing modifiers may also block the adsorption of analytes to the surface of the enhancing particles. Bell and co-workers recently reported that charged colloidal Ag/Au NPs can be induced to assemble at LLIs without any surface modification, by using hydrophobic "promoter" ions, such as tetrabutylammonium (TBA$^+$), which carry an opposite charge to the NPs. Such promoter ions act as charge screening agents and thus reduce the electrostatic repulsion between adjacent particles at the oil side of the LLI (**Figure 2.4**),[232,235] so that densely packed interfacial NP films form spontaneously when an aqueous Ag/Au colloid is shaken with an immiscible organic solvent, in the presence of a low concentration of promoter. The particles within these reflective MeLLFs are optically coupled and yield strong SERS enhancement at a level similar to that obtained from aggregation of the parent colloids. However, unlike aggregated colloids, MeLLFs are typically stable for days and have excellent signal uniformity, with a striking relative standard deviation of 1.1% in absolute signal intensity over mm-scale enhancing areas.[232] Moreover, since MeLLFs lie at the water-oil interface, this allows them to directly interact with analytes dissolved in either phase for in-situ detection of both water and non-water soluble analytes, such as dipicolinic acid and 4-mercaptobenzoic acid, down to below ppb levels. The ability to perform dual-phase analysis is extremely important since this facilitates applications of SERS in various fields, ranging from the detection of important analytes with low solubility in water such as hydrocarbons and explosives to the in-situ monitoring of chemical reactions in organic solvents.
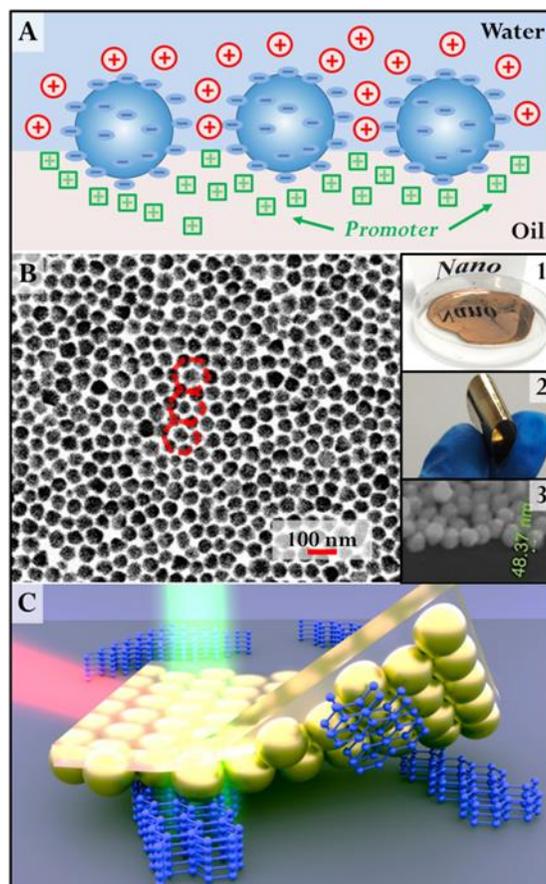
Figure 2.4. A: Schematic illustration of "promoter" induced NP interfacial self-assembly. B: SEM characterization of SENS showing short-range hexagonal particle packing. Insets 1 and 2 show optical images of an Au MeLLF and an Au SENS, respectively. Inset 3 is a tilted SEM image of SENS showing the NPs anchored in the polymer. C: Schematic illustration of SENS used for solvent-free SERS analysis. Adapted with permission from Ref. 235 (Copyright 2016, American Chemical Society), 239 (Copyright 2018, Elsevier B. V.).

Apart from being a versatile enhancing substrate as shown above, MeLLFs can also be used as a simple precursor for constructing bulk-scale solid enhancing substrates with densely packed, uniform hotspots on their surfaces. Stable and robust enhancing substrates carrying a monolayer of densely packed Ag/Au NPs can be created by simply dip-coating various rigid substrate materials in MeLLFs.[232,236] Using MeLLFs-coated transparent quartz plates as the enhancing material allowed continuous *in situ* SERS monitoring of the headspace directly above various bacterial cultures and revealed strong characteristic bands from chemisorbed dimethyl disulfide (DMDS).[236] Since DMDS is a fermentative metabolite

commonly produced by a variety of viable bacteria, it can therefore be used as a general SERS marker compound for the identification of viable bacteria cultures. Using a hand-held Raman system, the sensitivity limit for headspace SERS detection of *E. coli* DH5a was found to be 1.5×10^7 CFU/mL, which corresponded to detection of bacterial infection within 15 min of inoculation of the growth medium. This combination of generality and speed offers a convenient and low-cost bedside detection of bacterial infections, as well as rapid and high-throughput screening of antibiotics against specific bacterial infections.

- **Monolayers at liquid-air interfaces**

The main disadvantages that come with dip coating MeLLFs onto solid substrates are the weak attachment of the NPs to the surface of the substrate material through van der Waals forces, and that the initial particle packing of the MeLLFs at the LLI may be perturbed when the deposited film is dried. Ideally, a method is required to transform the mobile interfacial particle arrays into bulk freestanding films which are strong enough for routine handling while retaining their initial nanostructure. This can be achieved by growing a supportive thin polymer film onto the MeLLFs, at the organic side of the LLI, through *in situ* solvent evaporation-induced deposition of predissolved polymer, as shown in **Figure 2.4**.[237] This approach results in materials with particles anchored onto the surface of the supporting polymer films, with the majority of their surfaces still remaining exposed, rather than being trapped within the polymer layer, which is why they have been named surface-exposed nanoparticle sheets (SENS). Importantly, neither the self-assembly nor the polymer deposition process involve material-specific chemical reactions, which means that this approach can be readily used to generate bulk scale (100's of cm^2), flexible and robust NP/polymer hybrid materials carrying various types of densely packed plasmonic NP surface layers. Since the initial packing of the particles at the LLI is preserved, the optical properties of the SENS resemble those of the parent MeLLFs and they exhibit strong and uniform SERS enhancement. Using monodisperse spherical Au NPs *ca*. 50 nm in diameter as the plasmonic components in SENS and thiophenol (TP) as the probe analyte, the enhancement factor (EF) and average signal uniformity within 1.5×1.5 cm^2 areas were measured to be *ca*. 10^7 and 8%, respectively.[238]

A significant advantage that arises from the combination of flexibility, robustness and exposed plasmonic surface in SENS is that they can be physically pressed into contact with solid analytes, to achieve solvent-free quantitative SERS measurements, as shown in **Figure 2.4**.[239] SERS requires the target molecules to sit in plasmonic hotspots, which are typically only a few nm across. Therefore, in order for solid samples to be able to diffuse into enhancing regions they are normally either dissolved into a solvent or vaporized prior to the analysis. However, it may not be desirable or even possible to dissolve the sample, for example if the structure of the analyte changes in solution or the physical form of the sample needs to be retained. Since the enhancing hotspots in SENS are exposed and physically accessible but also firmly anchored onto a robust and flexible polymer substrate, solid analytes are pressured into the enhancing hotspots in SENS to generate intense SERS signals. Examples of solid dry samples ranging from explosives to pharmaceuticals have been demonstrated using this approach, which allows quantitative SERS analysis down to picogram-levels. Moreover, the excellent signal uniformity in SENS means that the physical distribution of the analytes can be mapped using the SERS signal intensity, which allows non-destructive, solvent-free SERS imaging.

Related studies were carried out by using gold nanoparticles with different morphologies and a variety of surface coatings, providing also various degrees of hydrophobicity. Indeed, deposition and self-assembly at the water-air interface can be facilitated by using nanoparticles covered with hydrophobic surface ligands, as recently shown for Ag and Au nanospheres of different sizes up to 200 nm, as well as anisotropic Au nanorods, nanotriangles and nanostars, using a mixture of thiolated polyethylene glycol (PEG-SH) and 1-dodecanethiol in chloroform, leading to SERS enhancement factors at 785 nm for thiophenol as high as $3x10^6$ for AuNR monolayers.[240] Interestingly, the same study showed that dense monolayers of Au nanostars are not as efficient, in agreement with numerical simulations that demonstrate collective optical effects leading to lower near field enhancements.[19] Liquid-air interfaces were also used to monitor the optical and Raman enhancement properties of gold nanospheres and nanorods, *in situ* and in real time by watching the dynamic response of NP positioning at the interface, the authors identified the need to include X-ray reflectivity and GISAXS measurements to accurately determine interparticle distances at the interface.[241]

- **Multilayers**

Applications of SERS require large-area substrates with reliable and reproducible enhancement at a pre-defined wavelength and scalable production at low cost. Despite the availability of substrates partly meeting such requirements (see previous section), most of them still suffer from expensive fabrication methods (lithography) or display a random distribution of hotspots. Recent efforts have focused on improving the organization of NPs within thin films, toward more intense and uniform distribution of hotspots. A recently introduced substrate comprises self-organized colloidal gold nanoparticles with diameters >30 nm (**Figure 2.5**). The nanoparticles self-organize into hexagonally packed layers that cover up to mm^2 areas.[242] Particularly interesting are the pronounced plasmonic resonances in the near-IR that arise for nanoparticle multilayers, *e.g.* in the peak labeled DM in **Figure 2.5**. Such resonances originate from plasmons with vanishing dipole moment that are normally considered optically forbidden.[243] These excitations are optically active because of the large nanoparticle diameter and the retardation of the incoming light. Their energy and lifetime are tuned by nanoparticle diameter and gap size, but for a given structure the excitations are uniform across the entire sample area.[243,244] The effect of the dark mode on SERS is illustrated in **Figure 2.5** for excitation at 785 nm (1.58 eV). No plasmon gets excited in the gold nanoparticle monolayer (**Figure 2.5**) resulting in the Raman spectrum of polystyrene without SERS enhancement. For the bilayer, an increase is observed in the overall scattering intensity, because the laser is in resonance with the dark plasmon mode; the additional intensity corresponds to 10^4 enhancement. Adding more layers increases the number of plasmon excitations to the gold multilayer spectrum (**Figure 2.5**).[243] For thicker films these modes transform into standing waves, similar to what is observed for disordered three-dimensional NP arrangements.[245] Nanoparticle multilayers and crystals open the route towards tailoring the SERS enhancement to a specific laser excitation and analyte wavenumber for large-area SERS substrates. The plasmon resonances may be matched to the incoming and scattered photon wavelength by controlling the system parameters.
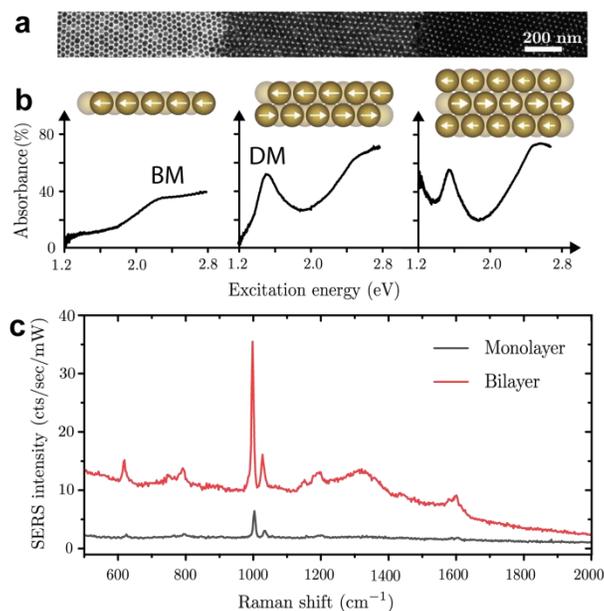
Figure 2.5. Self-organized gold nanoparticle layers as SERS substrates. (a) TEM images of hexagonally packed gold nanoparticles in a monolayer (left), bilayer (middle), and trilayer (right). BM – bright mode, DM – dark mode. (b) Absorption spectra and plasmon eigenmodes of the gold layers shown in (a). (c) Raman spectrum of polystyrene measured on the monolayer (black) and the bilayer (red). The 5-10 increase in total scattering intensity corresponds to $\approx 10^4$ enhancement of the Raman cross section. Adapted with permission from Refs. 243 (Copyright 2018, American Chemical Society) and 244 (Copyright 2019, Royal Society of Chemistry).

In a more elaborate development, Klajn and co-workers applied a liquid-air self-assembly method to obtain binary multilayers comprising Au and Fe_2O_3 nanoparticles, which were then treated to chemically remove the iron oxide, leaving so-called gold "nanoallotropes". The resulting highly ordered hierarchical structure, displayed highly efficient SERS enhancement due to the availability of small interparticle gaps (hotspots) and larger ones that allow the analyte molecules to diffuse through the entire superlattice.[246]

2.5. Vertically Aligned Au Nanorod Arrays

In the search for substrates that provide uniform SERS enhancement, self-assembled arrays of anisotropic plasmonic nanostructures with a regular pattern of hotspots offer additional elements for optimization and light manipulation. Mono- and multi-layered, vertically

aligned gold nanorod (AuNR) arrays have been obtained through self-assembly, by keeping a balance between AuNR concentration and physicochemical parameters of the solvent. For example, Tay and colleagues[247] achieved large vertically aligned AuNR superlattices by adjusting NaCl concentration in a colloid containing 2 nM AuNRs. An experimentally determined critical AuNR concentration of 2.0 nM and 50 mM NaCl produced well-ordered vertically aligned, hexagonally close-packed AuNR array as shown in **Figure 2.6**. The self-assembly and formation of AuNR superlattices occurs while the rods are suspended in the aqueous phase, so that the ionic strength of the solution affects the way AuNR rafts are assembled on the planar substrate. As previously observed in similar systems, the self-assembled vertically aligned AuNRs produce hexagonally packed structures containing a regular pattern of hotspots in the longitudinal interparticle junctions between nanorods, when excited with an electromagnetic radiation polarized parallel to the planar carrier substrate. The elongated rod shape and vertically aligned assembly facilitate trapping of the analyte of interest within the interparticle region with high local field intensity, making it an ideal SERS sensor. As prepared, the surfaces of AuNRs are passivated with CTAB molecules, which provide necessary electrostatic repulsion between AuNR and play a key role in the self-assembly process. For the AuNR array to function as a SERS sensor, it is necessary to remove some of the surface bound CTAB molecules to allow the analyte of interest to reach the highly enhanced interparticle junctions. Exposure to UV-ozone cleaning disrupts the CTAB layer, allowing SERS detection of analyte molecules, which was tested by the detection of a small common SERS reporter molecule thiophenol and subsequently applied to SERS detection of cannabinol (CBN), the metabolite of tetrahydrocannabinol (THC), as shown in **Figure 2.6**.[248]
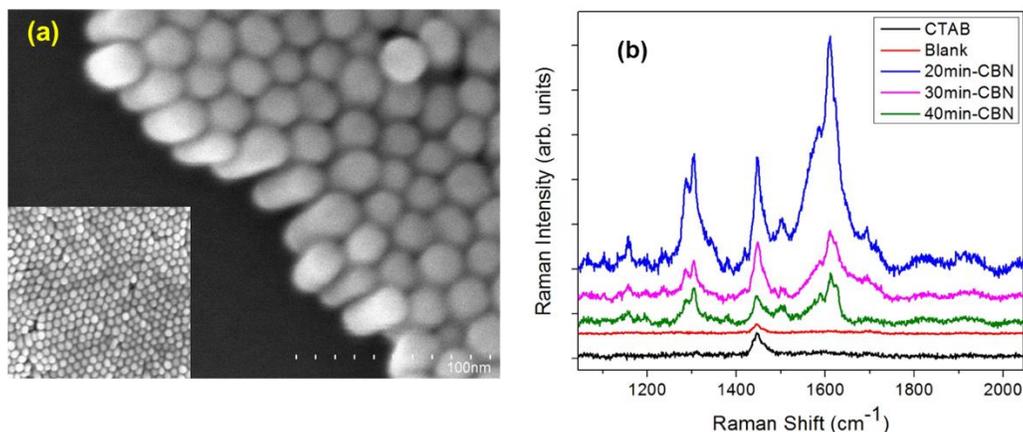
Figure 2.6. (a) SEM image of a vertically aligned AuNR array. (b) SERS spectra of CBN on AuNR arrays. Adapted with permission from Ref. 248. Copyright 2018, Elsevier B. V.

As the SERS intensity is related to the number of hotspots per illumination volume, perfectly and homogeneously packed 3D nanorod supercrystals are expected to be one of the most efficient architectures for robust and reliable SERS substrates. Alvarez-Puebla *et al*. showed that highly monodisperse CTAB-stabilized Au nanorods spontaneously crystallize into regular islands of uniform dimension, comprising *ca*. 15 monolayers of standing nanorods, upon slowly drying the nanorod colloid in a controlled humidity atmosphere. Such nanorod supercrystals were shown to provide ultrasensitive biodetection of scrambled prions (see Section 6 below).[249] In a subsequent work, Liz-Marzán and co-workers investigated systematically (both experimentally and by numerical modeling) the influence of the number of stacked Au nanorod monolayers, on the SERS efficiency of the supercrystals.[250] In order to improve the efficiency of self-assembly, monodisperse Au nanorods were coated with an amphiphilic alkanethiolate (1-mercaptoundec-11-yl)hexa(ethylene glycol), termed MUDOL or MUHEG, and subsequently drop-casted onto glass slides, so that supercrystals comprising standing nanorod multilayers were spontaneously formed upon drying. Depending on the initial nanorod concentration, regular supercrystals comprising 1 up to 20 monolayers could be obtained (in the spontaneously formed coffee ring area). Interestingly, the SERS signal of crystal violet (CV) was found to be almost identical for supercrystals of 1-3 monolayers (EF= 10^7) when excited at 633 nm, but half for the monolayer than for the multilayer when exciting at 785 nm. This result is in agreement with simulations, assuming that the analyte cannot

penetrate within the gaps between nanorod monolayers, and thus only the upper layer contributes to the SERS enhancement.

A strategy to tune the size and morphology of supercrystals over large scales can be achieved by controlled evaporation within a patterned substrate, leading to small supercrystals within a silicon pattern[251] or to large supercrystals within micron-sized pillars, on a transparent glass substrate.[252] By using an elastomeric polydimethylsiloxane (PDMS) template, Hamon *et al*. obtained uniform, stable, reproducible micron-sized Au nanorod supercrystals arrays over mm^2 scale areas.[252] The SERS EF for CV excited at 633 nm was determined to be 3.1 x 10^5. A similar template-assisted self-assembly procedure was used for the fabrication of regular micron-sized pyramidal supercrystal substrates made of highly monodisperse PEGylated Au nanospheres, over mm^2 areas.[253] In these examples, the size and shape of each individual supercrystal, as well as the periodicity of the array, are limited by the dimensions of the cavities in the PDMS template and the dimensions of the nanoparticles. By selecting a suitable lattice parameter - nanoparticle size combination, the strong optical response of the superstructures can be tuned over the visible to the near-infrared (NIR) range, which is appealing for multiple SERS applications. Supported by electromagnetic simulations, Matricardi *et al*. have recently shown that regular square arrays of hexagonally packed supercrystals leads to highest SERS enhancement when the surface lattice plasmon resonance wavelength (lattice parameter L=500 nm) matches the laser excitation wavelength (785 nm).[254] The authors also observed that the absolute SERS enhancement correlates to the numbers of nanoparticle layers (and hotspots) within the supercrystal and that the absolute intensity and its relative standard deviation (RSD) depend on the degree of local order within the array. An extension of this work to gold nanorod superlattices has been reported, where the use of ethanol as co-solvent was shown to significantly improve the superlattice quality.[255]

2.6. Assembly on Rough, Flexible or Curved Supports

Recent efforts have been directed to implementing large-scale, robust and economic production of reproducible SERS substrates. The mechanical properties of the support material can also be a limiting factor, *e.g.*, on curved surfaces or hard to access places, in swab applications *etc*. Paper thus appears as an inexpensive, flexible, lightweight,

biodegradable nanoparticle support that may overcome these problems. Li *et al*. developed SERS substrates impregnated with Au nanorods by dip coating.[256,257] A drawback however was the required dipping time of 2 days. SERS paper substrates have also been fabricated in large scale by inkjet printing and screen printing of highly concentrated nanoparticles.[258-260] The pen-on-paper approach presented by Polavarapu *et al*. is the easy, fast and effective do-it-your-self variation, which does not require any instrumentation.[261] The concentrated nanoparticle ink (3mg/mL) can be filled in a commercially available ink pen and the SERS arrays painted directly onto slightly hydrophobic inkjet paper, in the desired size (limited by the pen orifice). In contrast to commonly used filter paper-based substrates, this method has the advantage that no additional hydrophobizing step of the paper is required to avoid spreading of the ink and analyte of interest. The immobilized nanoparticles are so well adhered at the fibers that they cannot be removed by sticky tape or redissolved into solution. The pen-on-paper approach was demonstrated for different types of nanoparticles, including spherical citrate-stabilized Au and Ag nanoparticles, as well as CTAB-stabilized Au nanorods, reaching a detection limit of 10 aM for malachite green.

Some specific SERS applications may require that the nanoparticle support be not only flexible, but also transparent. This is the case when excitation of the plasmonic nanostructure and detection of the analyte should occur through the backside of the supporting material, *e.g.*, the direct, non-destructive analysis of art works or historic textiles[262] and other curved surfaces. The support material polymethylsiloxane (PDMS) fulfills many such useful requirements, as it allows facile assembly of different types of nanoparticles such as Au and Ag nanospheres,[263,264] as well as Au nanostars,[265-267] lacks toxicity, and the interfering intrinsic Raman signal is not very pronounced.

Analysis of biofluids such as blood and urine using Raman spectroscopy has originated diagnostics which are minimally invasive, readily accessible, and from repeated samplings.[268,269] However, analysis in biofluids additionally requires compatibility in high ionic strength environments, which contain various biomolecules, easily inducing NP aggregation and severely interfering with SERS spectra.[270,271] The development of an omnidispersible SERS probe, capable of rapid biodetection using layer-by-layer (LbL) coated 'hedgehog particles' (HPs) is an example of a generation of colloids with pronounced

surface corrugation and high dispersion stability.[272] Surface corrugation as a dispersion strategy based on surface nanoscale topography, was first demonstrated using spiky colloids referred to as 'hedgehog' particles (HPs) consisting of a micron-sized polystyrene (PS) core surrounded by nanoscale zinc oxide spikes.[273] The HPs' mesoscale geometry resembles that of spiky pollen grains, and of some cells and viruses with highly corrugated surfaces.[274] Surface corrugation from the spikes leads to marked reductions in contact area and van der Waals forces, resulting in the ability to disperse particles in both organic and aqueous solvents. In the case of biological particles of micro-, meso-, and nano-scale dimensions, the HP structural motif enables accurate control over particle agglomeration and adhesion resulting in both greater colloidal stability and specificity of attachment.

The introduction of LbL films on highly corrugated particles allows for high NP loadings and can be used to create dense coatings of plasmonic NPs for SERS applications.[275,276] By introducing gold NPs to the spiky HP geometry, Kotov and co-workers created dense conformal plasmonic nanoparticle films with tunable thickness.[272] Importantly, these modified Hedgehog particles, maintain excellent dispersion stability in high ionic strength environments (**Figure 2.7**). Confocal microscopy shows dispersed single Au NP-modified HPs, while large aggregates are observed for Au NP-modified PS beads. Au NP-modified HPs were also shown to form stable dispersions in heptane, illustrating dispersibility in environments of extreme ionic strength or polarity.[272]
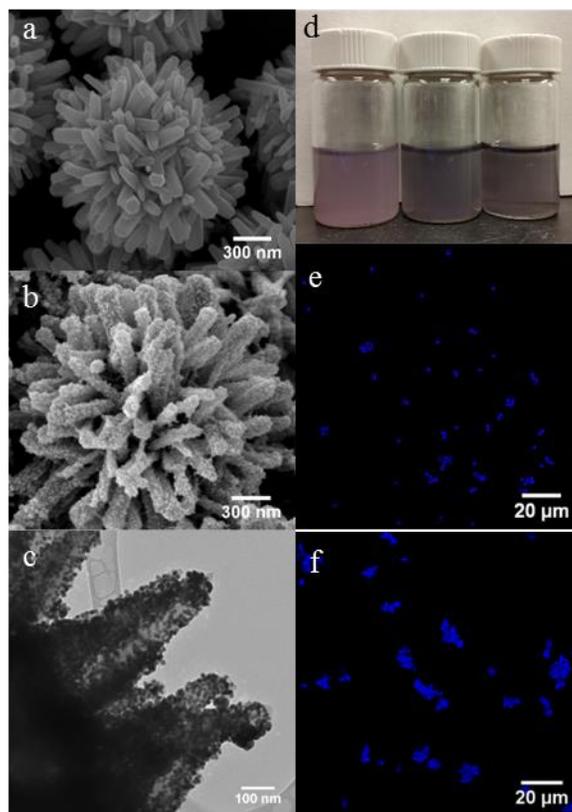
Figure 2.7. SEM (a,b) and TEM (c) images of HP modified with two bilayers of gold nanoparticles. (d) Photographs of dispersions of LBL-modified HPs withgold layer thickness increasing from left to right, in 1 M NaCl. (e,f) Confocal microscopy images of Au-coated HPs (e) and PS Beads (f), in 1 M NaCl. Adapted with permission from Ref. 272. Copyright 2018, American Chemical Society.

The SERS performance of HPs was assessed using two probe molecular dyes: methylene blue (MB) and rhodamine 6G (R6G). As the density of the NPs increased, the SERS signal from MB correspondingly increased due to the proximity of the Au NPs, resulting in hotspots where SERS enhancement occurs.[277] Two model biofluids were used to examine signal stability with other biomolecules present: tryptic soy broth with addition of 1% glucose (TSB), and Dulbecco's modified eagle medium (DMEM) media with 5% fetal bovine serum and 1% penicillin/streptavidin, commonly used as bacteria growth medium and in blood culture, respectively. Au-coated HPs were able to detect both dyes in complex media with over an order of magnitude increase of intensity compared to Au-coated beads, and can detect R6G in the presence of MB in both types of complex biological media (**Figure 2.8**) whereas

Au-coated beads cannot. Au nanostars were also unable to detect the probe molecules in complex media even when equipped with a polyethylene glycol stabilizer layer. This indicates that the greater degree of corrugation observed in HPs is critical for dispersion and for a stable SERS signal to be maintained, and must be accounted for in the design of a corrugated SERS probe.

For future SERS probes, the importance of dispersion stability to allow for a more robust and stable SERS signal is critical for sensing in biofluids. Surface corrugation represents an interesting strategy to engineer dispersion stability in a wide array of environments. The introduction of surface corrugation to create plasmonic structures has the potential to create a family of SERS sensors with stability in a wide range of biofluids and the capability to perform sensitive multiplexed detection.
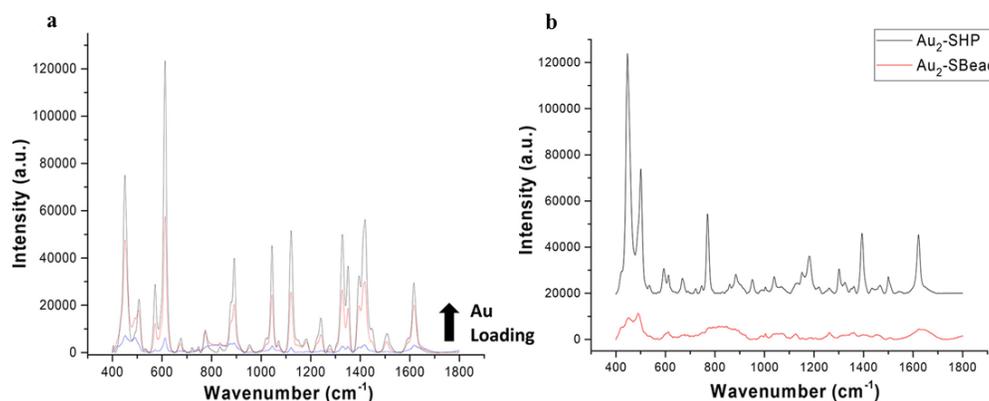
Figure 2.8. (a) Background-corrected Raman scattering intensity of various AuNP-modified HPs for detection of 1 μM methylene blue with increasing loading of AuNPs; 1 bilayer (blue), 1 bilayer with salt (red), 2 bilayers with salt (black). (b) Raman scattering spectra obtained with HP (black) and PS Beads (red) modified with two bilayers of gold nanoparticles of 1 μM MB and 1 μM R6G in TSB. Adapted with permission from reference 272. Copyright 2018, American Chemical Society.

2.7. Hole-Mask Colloidal Lithography

Hole-mask colloidal lithography (HCL) is a cost-effective and versatile nanofabrication method based on colloidal self-assembly lithographic patterning for generating homogeneous macroscopic areas (up to several cm^2) of nanostructures with short-range translational order but well-defined particle shape and orientation.[278] Early versions of the technique were used to fabricate basic nanoplasmonic structures, such as nanorings,[279] while later developments

allowed for fabrication of more advanced structure types, *e.g.* chiral particles.[280] HCL structures are extremely useful for a variety of plasmonics applications, for example nanoplasmonic biosensing,[281] but they have in general turned out to be relatively inefficient SERS substrates because they typically lack the sharp protrusions or nanogaps that have turned out to be crucial ingredients in SERS.[71] The structures shown in **Figure 2.9** are an exception to this. Here, angle resolved deposition was used to generate Au dimers with nanometric gap lengths ($d = 7.1 \pm 4.2$ nm std.) and with an underlying Au mirror surface to amplify field enhancement further.[282] The structures could be used to record SERS signals from attograms of BPE, a common SERS probe molecule. The corresponding enhancement factor was estimated to the order of 10^{11}. This is, in fact, orders of magnitude higher than what can be expected from pure electromagnetic field enhancement in these nanogaps, indicating that additional amplification due to surface induced molecular resonance effects are also at play here.[282]

In a recent development,[283-285] a variant of HCL was used to fabricate metasurfaces and colloids comprising silicon nanoparticles of various shapes and sizes (**Figure 2.9**). Such high refractive index nanoparticles support pronounced geometrical resonances (Mie modes) in the visible to the NIR wavelength range. The Mie resonances are superficially similar to localized surface plasmons in terms of far-field optical behavior, but the associated enhanced near-fields are mostly confined to the nanoparticle interior rather than to the surface. **Figure 2.9**) illustrates this effect for high aspect ratio Si nanodisks that support a particular resonance feature known as an "anapole".[286] The anapole is manifested as a dip in the extinction efficiency and a concomitant amplification of the local field inside the disk for certain disk radii. This in turn generates strongly enhanced Raman scattering from the Si 522 cm^{-1} optical phonon.[286] While not a SERS effect in the classical sense, it is not far-fetched to imagine that Mie resonances in high-index dielectrics can be combined with plasmons in metal nanostructures to generate a huge variety of novel and powerful substrates for SERS and other nanophotonic applications.
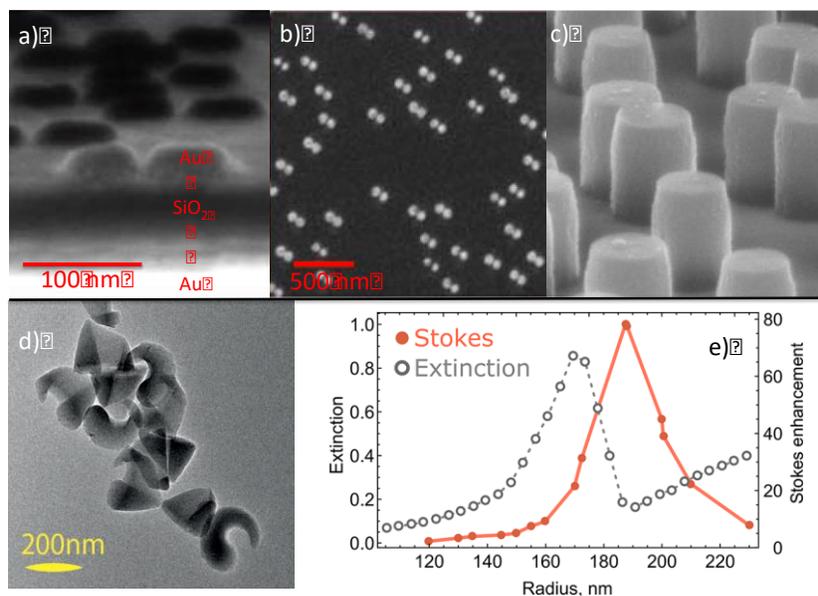
Figure 2.9. Resonant nanostructures fabricated through hole-mask colloidal lithography. a) Side view of SERS substrate consisting of gold nanodisk dimers fabricated on top of a Au mirror with a SiO$_2$ spacer layer in between; b) top view of a Au dimer-on-mirror SERS substrate illustrating the uniform dimensions and orientations of the individual nanostructures. c) Si nanopillars and d) chiral Si colloids fabricated by a variant of HCL; e) illustration of near-field amplification and Raman scattering enhancement in Si nanodisks supporting an anapole resonance. Figure reproduced with permission from Refs. 282 (Copyright 2015, Royal Society of Chemistry), 283 (Copyright 2017, American Chemical Society), 284 (Copyright 2017, Wiley-VCH), 286 (Copyright 2018, American Chemical Society).

2.8. Nanopillars

Densely spaced nanometer sized pillars have been used as SERS substrates for several decades. Vo-Dinh and co-workers fabricated nanopost array substrates for SERS detection using nanoparticle arrays as masks for submicron photolithography.[287] When metallized, these nanopillars (NPs) can offer large enhancement factors (EFs), often in combination with a leaning effect of the NPs.[288-290] Upon exposure to liquid and subsequent evaporation, the NPs can form clusters due to collective leaning of the pillars induced by capillary forces (**Figure 2.10**). The cluster formation ensures that analyte molecules are trapped and positioned in the vicinity of hotspots. The majority of these NP substrates are realized by top-

down fabrication using lithography based techniques, *e.g.* nanosphere lithography,[291] block co-polymer lithography,[292] and phase-shift interference lithography.[293] Different designs with small assemblies ranging from two to seven NPs have been studied, with the pentagonal assembly having the largest enhancement.[294] These substrates have, among other uses, been applied in melamine detection in milk.[295] NP substrates can also be produced by lithography-free techniques, such as mask-less reactive ion etching (RIE).**Error! Bookmark not defined.** Furthermore, these pillars can be replicated by injection moulding to potentially facilitate large scale and cost efficient manufacturing of substrates, also allowing for direct integration of microfluidics for sample handling.[296]
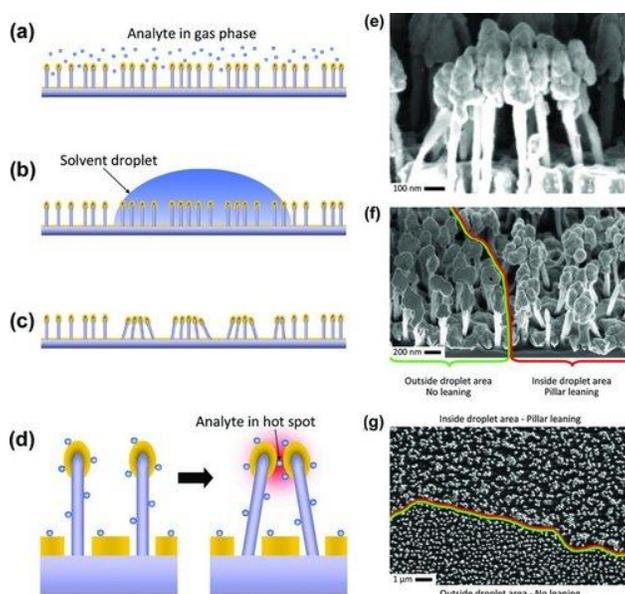
Figure 2.10. Concept of leaning nanopillar substrate. (a–c) Scheme of the leaning mechanism. d) Scheme of the enhancement mechanism. When solvent evaporates, surface tension pulls the silicon nanopillars together, trapping analytes at the hotspot, giving rise to a large Raman signal. e) SEM image of a cluster of leaning silver-coated silicon nanopillars. f) Tilted SEM image of the outer perimeter of the evaporated solvent droplet area. The nanopillars to the right have leaned to form hotspots while the nanopillars to the left remain vertical and free-standing. g) SEM image of a nanopillar substrate, seen perpendicular to the surface. The line indicates the outer perimeter of the evaporated solvent droplet. Bottom: individual free-standing nanopillars. Top: clusters of nanopillars. Reproduced with permission from Ref. 288. Copyright 2012, Wiley-VCH.

Polymer nanopillars have been realized in regular patterns combining lithography and nanoimprint.[297] Here a detailed and inverse NP substrate is first realized and subsequently transferred into polymer *via* nanoimprint. In a different approach, polymer NPs with integrated gold particles have been realized using anodic aluminium oxide as a template.[298] Recently, superhydrophobic polymer NPs have been realised by mask less RIE using Ar plasma.[299] Wafer-scale fabrication of silicon NP substrates have been realised by maskless reactive ion etching. By fine tuning the etching process, it is possible to customize pillar height, density and width.[288] Hotspot engineering has been conducted on these substrates and high SERS EFs and extraordinary signal uniformities over large sampling areas (~50 cm^2) have been achieved.[300-302] These substrates are now being commercialized, enabling a variety of applications and studies.[303-309]

The concept of mask-less etching can be transferred to glass substrates, allowing for realization of NPs as well as more exotic structures such as nanocylinders.[310] Glass NP substrates have been patterned with gold electrode structures and applied for combined electrochemistry and SERS detection.[311] An exceptionally good electrochemical as well as SERS performance were obtained, probably as a result of overall larger nanostructured electrode surface and the presence of isolated metallic caps on the pillars. An applied potential on the NP substrate enabled 20 times increase in signal intensity when detecting melamine.

Large-area, uniform, and robust nanohoodoos (pillars with a 'neck') can be fabricated in wafer-scale using block copolymer lithography, which provides an ordered etch mask with uniform structures with high resolution and high precision.[312] Gold is evaporated onto the nanohoodoos forming gold nanoparticles, thereby creating a SERS substrate that can be used for both gas and liquid sensing. Upon drying of a deposited analyte solution, the gold nanoparticles slide on the nanohoodoos and form particle clusters with strong, dense, and uniform hot spots. Gold can be removed by wet etching and the substrate can be re-metalized. In this way the substrate can be recycled numerous times and other plasmonic materials can be applied.

2.9. Nanostructured Dielectrics and Hybrids

The renewed drive to expand the materials base for plasmonics beyond the coinage metals and aluminum, motivated both by extensions of localized plasmon resonances into the infrared, as well as issues around loss, temperature stability and CMOS compatibility,[132] is expected to also have an influence on the development of substrates for SERS.[133] Transition metal nitrides, transparent conductive oxides, metal sulfides, as well as doped oxides, could well be candidate materials for surface enhanced spectroscopy substrates, and a survey of those materials from this point of view is called for. A completely different route towards extending the materials base for SERS substrates does away with surface plasmon resonances altogether, and instead investigates the use of dielectrics and semiconductors. A pioneering study by Hayashi and co-workers on GaP small particles,[313] dating back to 1988, saw evidence of an electromagnetic enhancement of Raman scattering due to Mie resonances, yet further reports compared to the scale of plasmonic-based SERS research have been scarce. While this might be partially due to often smaller local field enhancements than possible with metals, it must be recognized that dielectric substrates can offer a number of advantages for enhancing light/molecule interactions at surfaces: compatibility with semiconductor device processing, a wide parameter space for electronic structure and bandgap tuning, potential for surface-modification beyond thiol bonds, and crucially less extreme conditions in terms of heat generation and photochemical reactions compared with plasmonic surfaces.

Similar to metal-based substrates, any enhancement of Raman scattering in molecule-semiconductor systems can be conceptually broken down into an electromagnetic and a chemical contribution. The chemical contribution is associated with charge-transfer resonances from the HOMO level of the molecule to the conduction band of the semiconductor, and from the valence band to the LUMO level.[314] Bandgap and exciton formation should hence allow for a wide parameter space, in terms of tuning and optimizing enhancement *via* this route.

For structured dielectric surfaces, the electromagnetic enhancement is due to morphological, Mie-type resonances, which can be either electric or magnetic in nature. For dielectric structures of a few wavelengths size, higher-order Mie modes, also known as whispering gallery modes, provide large quality factors; however the associated sharp resonances are not optimal for SERS, as they cannot overlap with both the excitation laser light and the Stokes-

shifted beam. The substantial advances in nanotechnology now enable the controlled generation of dielectric nanostructures of sizes on the order of the wavelength in the material, and crucially also nanosized gaps between dielectric components in antenna-like configurations. This in turn enables the exploitation of low-order electric and magnetic Mie resonances, with their much broader spectral width and, in gap structures, reduced mode volumes, which has in recent years lead to exciting discoveries in dielectric nanophotonics based on single antennas and metasurfaces.[315] The possibility of thus tailoring nanoscale light fields with dielectrics requires the employment of nanostructured dielectrics and semiconductors for SERS[316] and surface-enhanced spectroscopies more generally. For example, a significantly reduced local heat generation has been demonstrated for silicon dimer nanoantennas, compared to equivalent plasmonic nanoantennas,[317] while recently SERS and surface enhanced fluorescence for monolayer coverage have been observed.[318] Although the absence of fluorescent quenching would allow the use of the same nanostructured dielectric substrate for both enhancement of Raman scattering and fluorescence emission, contrary to metals, in practice the non-suppression of background fluorescence needs to be taken into account when choosing the illumination laser wavelength. Other intriguing developing materials are metal oxides, particularly when doped with oxygen vacancy centers. Large SERS enhancements have been shown for non-stochiometric tungsten oxide[319] and a variety of ion-irradiated metal oxides.[320] In hybrid structures composed of Ag or Au colloids on top of titanium oxide thin films, the chemical enhancement factor in Raman scattering can be increased *via* photoinduced oxygen vacancy creation,[321] opening up additional pathways for substrate-molecule charge transfer.

3. SERS Tags

The selective detection and localization of target molecules requires target-specific ligands for molecular recognition *via* non-covalent interactions. For example, proteins are selectively recognized by antibodies directed against them as antigens, while for nucleic acids the complementary oligonucleotide strands are employed. The optical identification and visualization of the target-specific ligands, and therefore the target molecules, typically require labeling agents, for example, fluorescent dyes/quantum dots[322] (*e.g.*, in

immunofluorescence) or enzymes, which give rise to a colored reaction product upon incubation with a colorless substrate (*e.g.*, horseradish peroxidase in ELISA and immunohistochemistry). SERS nanotags are an emerging class of labeling agents based on molecularly functionalized, Raman-encoded noble metal nanoparticles.[323,324]

Advantages of SERS nanotags over existing labeling approaches include i) multi-color detection: the tremendous spectral multiplexing capacity for parallel detection/localization is due to the narrow FWHM of vibrational Raman bands compared to the broad emission profiles of molecular fluorophores (**Figure 3.1**); ii) quantification: the SERS signal is proportional to the number of SERS nanotags; iii) no or minimal photo-bleaching, *i.e.* high photo-stability of the SERS signal in repeated and/or long-term measurements; iv) single laser wavelength excitation: all SERS spectra of a set of spectrally distinct SERS nanotags can be excited by using a single laser excitation; v) suppression of autofluorescence in biological/biomedical applications: the use of SERS nanotags with plasmon resonances in the red to NIR elegantly circumnavigates the excitation of unwanted and interfering autofluorescence; NIR excitation is also required for biomedical applications *in vivo*.[325-328]

A disadvantage of SERS nanotags is their large size and weight compared with molecular fluorophores, but also with quantum dots.[329] For many bioanalytical applications such as assays (*e.g.*, in microfluidics or lateral-flow assays on membranes), where typically no restrictive spatial constraints are relevant, this steric aspect is typically not a problem. However, the size of SERS nanotags – typically several tens of nm – becomes relevant when confocal high-spatial resolution microscopy on single biological cells is performed.[330] Last but not least, SERS nanotags are colloids and sample purity is an issue which is often overlooked. Obtaining purified colloids is more challenging compared with conventional fluorescent dyes, for which established separation techniques from analytical chemistry are known for decades.[331]
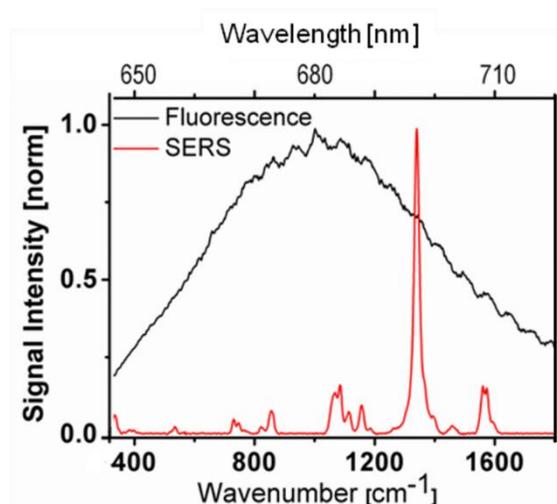
Figure 3.1. Comparison of spectral emission profiles: fluorescence from Cy5 and SERS from 4-NTB on AuNPs excited with 632.8 nm laser. Reproduced with permission from Ref. 332. Copyright 2014, Royal Society of Chemistry.

3.1. SERS Nanotags: Noble Metal Nanoparticles Coated with Raman Reporter Molecules

SERS nanotags typically comprise a noble metal nanoparticle (NP) coated with a Raman reporter molecule for identification *via* its characteristic Raman spectrum. **Figure 3.2** shows a schematic representation of a SERS nanotag, specifically designed for red laser excitation, which is beneficial for bioanalytical and biomedical applications where autofluorescence often occurs: the hollow Au/Ag nanoshell is coated with a self-assembled monolayer (SAM) of an aromatic thiol featuring a high Raman scattering cross section and protected by a silica shell.[333]
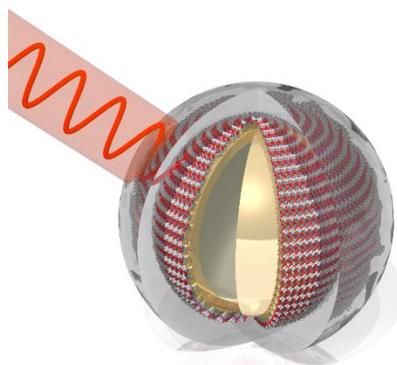
Figure 3.2. Sketch of a SERS nanotag comprising a hollow Au/Ag nanoshell coated with a self-assembled monolayer of an aromatic thiol as the Raman reporter molecule. The particle is protected by a silica shell. Rerproduced with permission from Ref. 333. Copyright 2009, Wiley-VCH.

For bioanalytical and biomedical applications, the SERS nanotag is conjugated to target-specific ligands such as antibodies or oligonucleotides. A wide variety of configurations for SERS nanotags exist and also various options for their bioconjugation are available. **Table 3.1** summarizes the most common types, which are based on the variation of i) the type of metal NP, as well as its size and shape; ii) number of NPs: monomer *versus* assembly; iii) the type of Raman reporter (*e.g.*, fluorescent dyes for SERRS or SAMs of small aromatic thiols); iv) the protective shell (*e.g.*, short ethylene glycol (EG) or long PEG, biopolymers, and silica); v) the type of bioconjugation, depending on available functional groups on the protective shell (carboxylic acids, amines, thiols, *etc*.).

Table 3.1. Components of SERS nanotags with some examples.

Component of SERS nanotag	Examples
Plasmonic NP: metal, size, shape	Au, Ag; spheres, rods, stars
Number of NPs	Monomer *vs*. cluster
Raman reporter molecule	Dyes, aromatic thiols
Protective shell	EG/PEG, BSA, silica
Bioconjugation	*via* COOH, NH$_2$, SH

In the following two subsections we discuss the advantages and disadvantages of using either fluorescent dyes for SERRS or aromatic thiols for SERS.

3.2. Fluorescent Dyes for SERRS and Multiplexing

The fabrication of a SERS nanotag with the highest possible SERS efficiency requires the choice of the best plasmonic nanoparticle that will act as Raman enhancer, as well as the best Raman reporter that, in principle, should have an inherently large Raman cross section.[334]

Chromophores and fluorophores including cyanine dyes, crystal violet, malachite green, nile blue, R6G, *etc*. fulfill this requirement. Additionally, by using an excitation laser line in the Raman measurements that overlaps with the absorption spectrum of the Raman reporter, we are under Resonant Raman conditions (surface enhanced resonance Raman scattering, SERRS). Thus, for cases where the SERRS conditions are fulfilled, an increase in the Raman enhancement of 10-100 fold over conventional SERS experiments have been reported.[335]

Therefore, the fabrication of a library of SERRS tags for multiplexing purposes will depend on either a collection of dyes with a similar absorption band and in resonance with the selected excitation laser line, or the combination of dyes capable of producing a SERRS signal over a wide range of excitation wavelengths (typically from 514 to 1064 nm). Unfortunately, the availability of Raman dyes that satisfy both approximations is somehow limited, which hampers the potential applications of the SERRS tags for multiplexing. Alternatively, different combinations of dyes in the Raman encoding shell would allow an encryption based on either frequency alone or using signal intensity as an additional code element.[336]

3.3. SAM of Small Aromatic Thiols and Spectral Multiplexing

Porter and co-workers have introduced aromatic thiols/disulfides as Raman reporters because they form a SAM on gold surfaces *via* stable Au–S bonds.[337-379] Advantages of using small aromatic thiols as Raman reporters are: i) reproducible SERS signatures due to the dense packing and uniform orientation of Raman reporter molecules within the SAM,[333,340,341] ii) Maximum SERS brightness due to the maximum surface coverage with Raman reporter molecules (**Figure 2**) compared to sub-monolayer coverage;[333] iii) high spectral multiplexing capacity as the number of vibrational bands scales linearly with the number of atoms; iv) no or minimal photobleaching since resonant electronic excitation of the molecule is avoided.

The brightness of SERS nanotags depends on both the Raman scattering cross section of the individual Raman reporter adsorbed on the metal surface and the number of reporters per particle.[325] Fluorescent dyes generally feature larger Raman scattering cross sections, however their packing density on the metal surface is typically much lower, compared to SAMs.[342,343] Aromatic thiols also generate fewer vibrational bands as their molecular size is

typically significantly smaller than those for fluorescent chromophores.[333,344] The latter aspect has been exploited in a quantitative 6-plex SERS experiment. Specifically, various mixtures of 6 SERS nanotags with distinct spectral signatures were employed. The stoichiometry of the mixtures was known *a priori* for comparison with the results from spectral decomposition. By using the known SERS signature of the 6 individual particle types, the SERS spectra of the mixtures could be quantitatively decomposed into the contributions of the individual particles.[345] Overall, a good agreement between experiment (SERS spectrum of the mixture) and simulation (different linear combinations of the 6 individual SERS tag spectra) was obtained.

Finally, it should be noted that, in addition to the use of commercially available Raman reporter molecules, some groups have also designed and synthesized custom-made Raman reporters. Examples include the conjugation of existing dyes to thiol-containing linkers for binding to the metal surface[346-349] and the modification of aromatic thiols with triple bonds and short hydrophilic linkers containing terminal carboxy groups for bioconjugation.[350]

3.4. Protection and Stabilization

Direct hydrophilic stabilization of SAMs (short spacers)

Colloidal stability and solubility in water of SERS nanotags are both largely dominated by the Raman reporters adsorbed on the metal surface.[351,352] The conjugation of ethylene glycol (EG) spacers to the terminus of a Raman reporter molecule, *e.g.* the carboxylic acid of mercaptobenzoic acid or one of its derivatives, can significantly increase both the colloidal stability as well as the solubility in water, since the hydrophilic EG groups point towards the interface with the suspension medium. By using a mixture of a Raman reporter extended with a short hydrophilic monoethylene glycol (MEG) unit comprising a terminal hydrophilic OH group, and the same Raman reporter extended with a longer triethylene glycol (TEG) moiety with terminal COOH moieties for bioconjugation, not only increased the steric accessibility of the SAM for bioconjugation *via* the longer TEG-COOH spacer, but also provided an option for controlled bioconjugation by varying the ratio of the two spacer units (MEG–OH : TEG–COOH).[340,353-355] A further advantage of the hydrophilic EG units is the minimization of non-specific binding.[340] This is a very important aspect in many biological and biomedical

applications: the binding selectivity is determined by the target-specific binding molecule and should not be hindered by non-specific binding of the labeling agent, which might lead to false-positive results.[356] However, although both colloidal stability and water solubility are both guaranteed by this approach, many biomedical applications, in particular those *in vivo*, require the use of significantly longer EG chains.

Stabilization by polymers and biopolymers

Metal nanoparticle stabilization is a critical issue if the SERS tags are to be dispersed in biological fluids, since they will be prone to aggregating in high ionic strength media, which would compromise the stability of the SERS signal. Different polymers have been employed as protective layers to confer stability to SERS encoded particles in biological media and to prevent the release of the Raman reporter or non-specific protein adsorption.[357] Polyethylene glycol (PEG) can be considered as the most versatile polymer, due to its biocompatibility allowing prolonged blood circulation lifetimes. Additionally, PEG synthesis through controlled polymerization can readily incorporate well-defined end-groups. For instance, the presence of an end-thiol functionality allows anchoring onto the metal nanoparticle surface, while preserving enough space to bind the Raman reporter (**Figure 3.3**).[352] Alternative strategies comprise the encapsulation of plasmonic nanoparticles within crosslinked polymers such as poly(N-isopropylacrylamide) (pNIPAM).[358] The encapsulation of single plasmonic nanoparticles within the microgels was based on a grafting through polymerization approximation.[359] The porous nature of the pNIPAM coating allows the incorporation of Raman reporters, even if they do not have a specific affinity towards the metal nanoparticle surface, through diffusion and subsequent trapping by sealing the porous shell by layer-by-layer deposition of an outer polyelectrolyte coating, which eventually facilitates covalent conjugation with antibodies (**Figure 3.3**).[360,361] Raman-encoded SERS tags have also been stabilized by encapsulation with an amphiphilic diblock copolymer such as polystyrene-block-poly(acrylic acid), through a thermodynamically controlled self-assembly process leading to uniform coatings (**Figure 3.3**).[362] A similar process was used for the stabilization of SERS encoded nanostars, using the copolymer dodecylamine-modified polyisobutylene-alt-maleic anhydride (PMA).[363] Phospholipids have also been reported to

provide coatings that render the nanoparticles biologically compatible and highly versatile.[364-367]
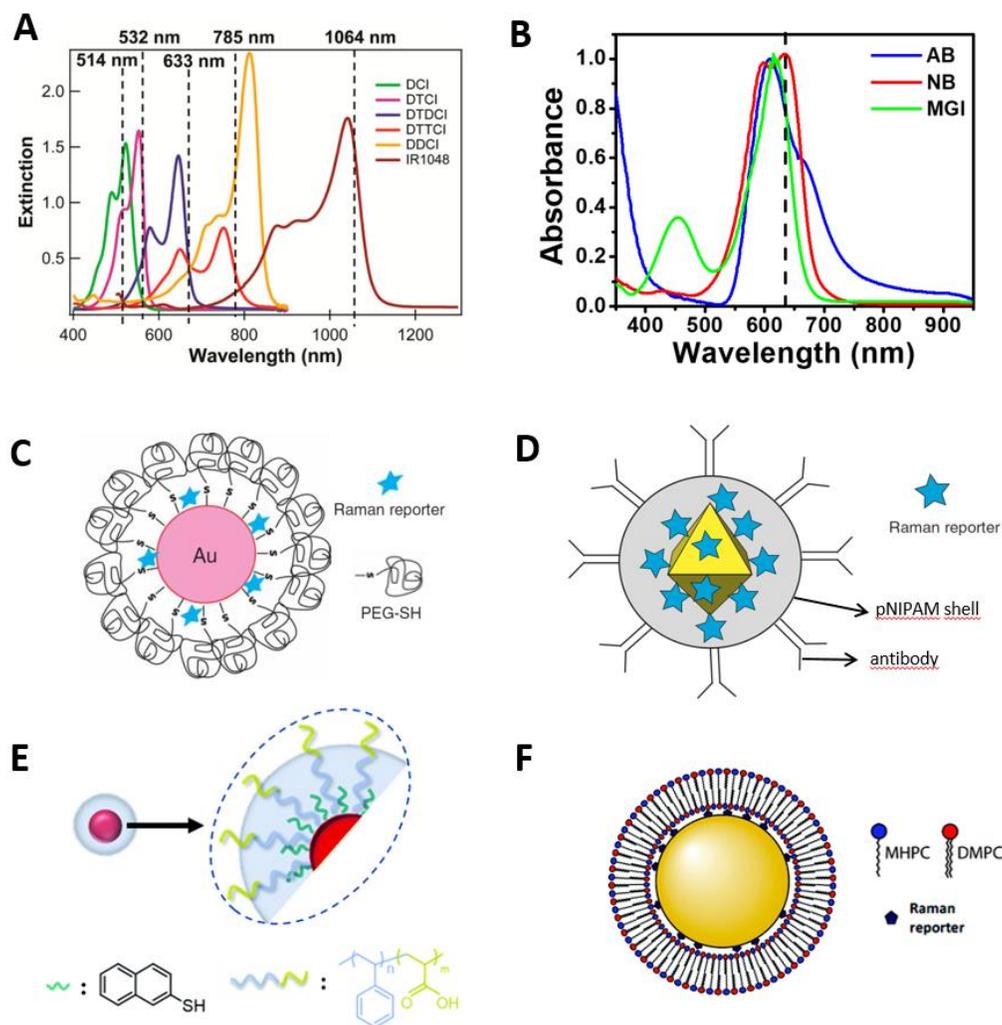
Figure 3.3. (A-B) Resonant Raman configuration; multi-dye conjugates capable of producing signals over a wide range of common excitation wavelengths (A) and dye conjugates with similar optical properties for multiplexing (B). Adapted with permission for Refs. 336 (Copyright 2014, American Chemical Society) and 360 (Copyright 2015, Wiley-VCH), respectively. (C-F) Configuration for protection and stabilization; thiolated polystyrene (C), pNIPAM shell (D), PSS-PAA block copolymer encapsulation (E) and phospholipid coated SERS nanotags (F). Adapted with permission from Refs. 352 (Copyright 2007, Springer-Nature), 360 (Copyright 2015, Wiley-VCH), 368 (Copyright 2018, Royal Society of Chemistry), and 364 (Copyright 2010, American Chemical Society.), respectively.

High molecular weight proteins such as bovine serum albumin (BSA) have also been reported as suitable stabilizing agents for encoded metal nanoparticles, preventing their aggregation as well as the desorption of Raman active molecules.[346,351,369,370] BSA adsorption onto metal surfaces was suggested to occur *via* an electrostatic mechanism, in combination with binding of the single free external thiol group on N-form BSA (associated with a cysteine residue) to the the metal surface.[371,372] Other proteins, such as antibodies, could be similarly used as stabilizing agents after binding the Raman reporter molecules, giving rise to a one-step biconjugation of the SERS tags.[373]

Silica Encapsulation of SERS Nanotags

Natan and co-workers introduced silica-encapsulated SERS nanotags, obtained by co-adsorption of a Raman reporter and mercaptosilane (1:20 stoichiometry for incubation) onto the metal NP surface, followed by silica deposition on the vitreophilized NPs.[374,375] This approach leads to sub-monolayer coverage of Raman reporter molecules (*ca*. 5 % based on the 1:20 stoichiometry) on the metal surface due to competitive surface adsorption with mercaptosilane. Doering and Nie presented a similar approach towards silica-protected SERS nanotags,[376] while Schlücker and co-workers introduced the concept of silica-encapsulated SERS nanotags with 100 % surface coverage of Raman reporters, which leads to significantly brighter particles compared to sub-monolayer coverage.[333,377] The subsequent formation of a silica shell around the SAM of aromatic thiols was initially achieved by preparing vitreophilic NPs using layer-by-layer deposition of polymers such as PAH and PVP onto SAM-coated NPs.[333] Since this route involves several steps in different solvents and multiple centrifugation steps, it becomes labor-intensive and time consuming. A faster route can be achieved by using Raman reporter-SiO$_2$ precursor conjugates, which contain both the actual Raman reporter molecule and a silane covalently attached to it.[341] However, this approach requires an additional step using organic synthesis under protective atmosphere, due to the use of a moisture-sensitive silane.

The deposition of a silica shell around a SERS nanotag is attractive because it provides high mechanical stability and the option for long-term storage.[374] In addition to AuNPs and Au/Ag nanoshells, silica encapsulation has also been demonstrated for a variety of other plasmonic NPs, including gold nanorods,[378] gold nanostars,[379,380] gold NP dimers,[332] and assemblies,[381]

which highlights the potential of this approach. A potential drawback is however, that electrostatic interactions with biological material render silica prone to non-specific binding. Thus, in particular for applications *in vivo*, an additional PEG coating using silane-PEG is recommended.[382]

The plasmonic substrate can however be modified into either positive or negative charge by suitable surface modification, which allows electrostatic binding of various charged analyte molecules. The hydroxyl groups on the surface of silica can also be conveniently functionalized for incorporation of various analyte molecules. Modification of silica using bioreceptors enables potential application in immunoassays.[374,383] On a different direction, the metal-molecule charge transfer contribution to SERS can be eliminated by silica coating, as varying the thickness of the silica shell further allows tuning the electromagnetic field experienced by the analyte molecule. In a recent study, Swathi, George Thomas and co-workers have investigated the Raman signal enhancement by varying silica shell thickness (t = 3 to 25 nm). By using $Ag@SiO_2$ with a negative surface charge (ζ = -33 mV) and a positively charged analyte molecule (1-pyrenyl(methyl)trimethylammonium hexafluorophosphate), an enhanced Raman signal intensity was observed when the probe molecules were placed at t ≤ 10 nm. At larger thickness, probe molecules are at sufficiently large distance from the plasmonic core that they experience negligible enhancement.[384] Silica coating can also be used to tune plasmon hybridization, when brought in close proximity.[385] In a recent study, the gap distance between dimeric $Ag@SiO_2$ nanostructures was varied from 1.5 up to 40 nm, by increasing the silica shell thickness. A dimerization process was achieved by binding the ammonium ion screening the negative charge on the silica surface. An enhancement in Raman signal intensity (10^5-10^6) was observed at hotspots, decaying with gap distance. The SERS enhancement at hotspots was found to follow a $1/d^n$ dependence, with n=1.5, in agreement with theoretical studies by Schatz and co-workers.[32,386]

3.5. Bioconjugation to SERS Labels

Direct conjugation of ligands to unprotected SERS nanotags

The final step in the preparation of SERS tags is the bioconjugation step with a targeting entity, which confers to the encoded particle a high specificity to the molecule of interest.

The bioconjugation approach will strongly depend on the configuration of the SERS tag and, more precisely, on its protection and stabilization. Thus, for unprotected SERS nanotags direct bioconjugation to the plasmonic nanoparticle could be achieved through the adsorption of proteins (*i.e.* antibodies, thiolated DNA) by either electrostatic interactions or covalent binding. Within this direct bioconjugation, different alternatives have been developed, such as the co-adsorption of a thiolated Raman reporter and the antibody leading to a mixed monolayer.[338] An alternative design involves a bifunctional coating, where first a thiolated Raman reporter with a terminal succinimide group is attached and the protein can then be covalently attached through the formation of an amide linkage.[339]

Conjugation of ligands to protected SERS nanotags

The bioconjugation of protected SERS tags relies on the terminal functional group of the stabilizing shell. Typically, most common end groups are either carboxyl groups or primary amines, which facilitate further bioconjugation of the nanoparticles through the formation of an amide bond by carbodiimide activation.[387] The extensive library of different functionalities reported from polymer chemistry readily allows functionalization of nanoparticles with biological molecules through chemical approaches, such as Michael addition, click chemistry or Diels-Alder reaction, among others.[388] Bioconjugation from biopolymer stabilized nanoparticles relies on the availability of terminal amine and carboxyl groups, allowing subsequent functionalization through EDC/NHS chemistry as described above.[389] For example, Knudsen *et al*. described the stabilization of SERS tags by BSA adsorption, but in combination with glutaraldehyde, leading to a cross-linked organic encapsulation.[390] The addition of glutaraldehyde removes most of the surface amino groups from BSA, rendering a SERS tag with a net negative charge from the carboxylic acid groups. For silica-encapsulated SERS nanotags, silanes with amino or thiol groups (*e.g.*, APTMS, MPTMS) can be employed for bioconjugation. Heterobifunctional crosslinkers, such as those with a NHS ester at one terminus and a succinimide at the other, can couple the amino (or thiol)-functionalized SERS tags to target-specific ligands such as antibodies *via* their thiol (or amino) moities (**Figure 3.4**).[333] A similar strategy can be also used to link with sugar head groups such as mannose for lectin targeting, allowing for the specific uptake by macrophages and thereby serving as an *in vitro* model for the detection of atheroslerosis.[391]
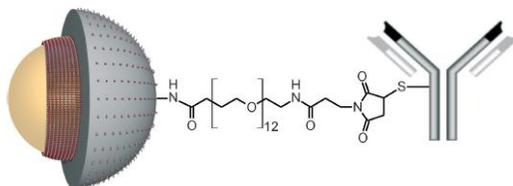
Figure 3.4. SERS nanotag-antibody conjugate with a heterobifunctional linker molecule. Reproduced with permission from Ref. 333. Copyright 2009, Wiley-VCH.

3.6. Brightness of SERS Nanotags

Ensemble experiments

The evaluation of the brightness of a SERS tag relies on measuring the SERS enhancement factor (EF). The EF is a relative measurement of the effect of the plasmonic nanoparticle on the scattering intensity of the Raman reporter. From a qualitative point of view, a relatively simple method to estimate the SERS enhancement efficiency is the measurement of the analytical enhancement factor (AEF),[57] which can be calculated as:

$$AEF = \frac{\frac{I_{SERS}}{c_{SERS}}}{\frac{I_R}{c_R}}$$

where I_{SERS} and I_R are the intensities of the SERS and Raman signals, respectively, and c_{SERS} and c_R are the concentrations of the analyte in the SERS and control Raman experiments respectively. Although ensemble measurements of the SERS intensity can be a useful measure to characterize SERS performance for analytical applications, in particular for SERS in colloidal solutions, uncertainties about SERS tag concentration, size heterogeneity, and a lack of widely accepted external intensity standards for calibrating intensity, represent significant hurdles against this approach.[51]

Alternatively, the variation of the SERS intensity as a function of particle concentration has been proposed as a way to test how quantitative and reproducible the intensities of SERS tags are.[360] Nam *et al*. reported that SERS nanotags (under non-resonant conditions) composed by Au/Ag plasmonic nanosnowmen can be detected at concentrations as low as 1 pM. Interestingly, for the same configuration but under resonance conditions, the lowest

detectable particle concentration was 5 fM, which represents an improvement of two orders of magnitude in the detection limit, additionally showing a linear dependence over 1-100 fM range, which makes them suitable for quantification purposes.[392]

Single-particle experiments

Conventional SERS experiments are performed on colloids in a cuvette. This type of ensemble measurements yield a mean value of the SERS intensity averaged over all particles within the focal volume during the acquisition time. Quasi-spherical AuNP and AgNP are the most commonly metal colloids used in SERS and it has been demonstrated that monomers are not SERS-active, but small clusters of AuNP such as dimers and trimers are.[23,381,393-395] From a pragmatic point of view, one does not necessarily have to care about the monomer/cluster composition of the colloid, as long as there is enough SERS signal for detection. However, this aspect clearly matters when microscopic SERS experiments are performed, in which, due to spatial constraints, only single particles may bind to a given biological target.[396] Computer simulations are very helpful in the theory-guided design of bright SERS nanotags which are detectable at the single-particle level.[199,381] A convincing experimental demonstration of single-particle SERS brightness typically requires correlative experiments either on immobilized tags[70,199,397] or in suspension.[398]

The ideal SERS nanotag would be a highly monodisperse colloid in which each and every single particle gives an equally strong SERS signal. This highly ambitious aim requires synthetic efforts for producing highly uniform SERS nanotags, advanced separation techniques for isolating the highly SERS-active particles, and finally sophisticated single-particle SERS characterization techniques in suspension to determine the distribution function of the SERS intensity for a sufficiently large number of individual tags.

4. Analytical Techniques and Quantification

4.1. Analytical Techniques

The task of analytical techniques dealing with SERS is either identifying or quantifying molecules, or both. To reach this aim many different approaches for many different

molecules/components (or classes of molecules) have been developed during the past decades. In general, the identification of a molecule/component can be performed *via* direct or indirect strategies. Direct measurements are characterized by recording and analyzing the analyte's own fingerprint, whereas indirect strategies use the SERS response of a secondary molecule, stimulated by the presence of the analyte. Normally, direct techniques offer the advantage to reflect the instantaneous situation of the molecule (binding state, orientation, molecular conformation, interaction to the surface and to surrounding molecules) but imply label-free SERS measurements, which are often more challenging due to very low Raman cross sections for most molecules. This problem can be overcome by using a bright molecule as a messenger (label), featuring an extraordinarily high SERS cross section. Analytical detection schemes based on label molecules or SERS tags, belong to indirect techniques. Indirect pathways are also possible without labels in the classical sense, *e.g.* when the SERS response of a secondary molecule changes or depends on the interaction with the analyte. These molecules can be of different nature and in general are selective to a specific analyte. Chemosensors such as molecular beacons, aptamers, or DNA sequences are some of the molecules used in biomedical applications (see Section 5 for some examples). Moreover, the different interaction of chiral molecules with the plasmonic substrate or with the ligand attached to the substrate can be used to discriminate between two enantiomers using SERS.

The large signal enhancements in SERS generate stronger and more stable signals than those from chemical fluorophores, but the lack of precise control over the degree of amplification typically results in poorly reproducible, non-quantifiable SERS signals. Over the years, focus has been on the enhancement of the Raman signal, rather than quantifying the signals, which is of high importance for various analytical aplications. The enhancement factors reported are often overclaimed or misclaimed, thereby limiting practical application, particularly in diagnostics and bioimaging.[399-402] Addressing these issues should be one of the central topics for future advancement in the field of SERS, which aims to build a well-defined analyte-nanogap system with outstanding uniformity for large area scaling. To this end, plasmonic nanogaps should be fabricated in a robust way to ensure a reproducible field enhancement. The highest SERS enhancement would be obtained in the narrowest gap distance (sub-nanometer size) before quantum quenching effects dominate.[89,403,404] Further optimization of SERS detection also demands many aspects of excitation and detection matching, such as

plasmon resonances in wavelength,[405,406] polarization[407-409] and emission direction.[410] Sub-nanogaps can be realized by aggregation, assembly or lithographic methods (see section 2) but also in core-shell nanoparticles having tailored gaps between core and shell (so-called intra-gap). Alternatively, sub-nanogaps can also be generated between nanoparticles and flat metallic surfaces. Such a situation is realized in nanoparticle-over-mirror (NPoM) configuration, with a dielectric and a defined spacer between nanoparticle and mirror. Shell-isolated nanoparticles (SHINs) can also be considered as a specific realization where the dielectric spacer is equivalent to the nanoparticle shell, additionally acting as a protection or coating. SHINs are flexible nanoparticle systems for analytics because, as well as the size, material and shape of the plasmonic core, the material and thickness of the dielectric layer and the support can be tailored for specific application strategies.

4.2. SERS Chemosensors

Chemosensors (also molecular sensors) can be considered as an analytical concept (or device), which is used for sensing of an analyte. They are typically composed of a signaling moiety and a recognition moiety, which in the presence of the analyte generate a detectable signal or a signal change. SERS-based chemosensors comprise plasmonic nanoparticles or nanostructures functionalized with specifically binding ligands (the chemosensors) as receptors, which can selectively recognize the analyte of interest. The analyte-ligand interaction changes the original ligand SERS signal or gives rise to a different SERS signal. Advantages of this method include the generation of highly selective sensors, but also the use of the chemosensor as an analytical standard for quantitative purposes. An advantage of SERS chemosensors is the high sensitivity and the small bandwidth of the molecular fingerprint that permits distinguishing even molecules with similar structures. The same concept can be applied to target biological material, *e.g.*, by functionalization of the nanoparticles with specific antibodies, aptamers, peptides *etc*. (Section 5). This kind, to which also some of the SERS labels described in section 3 belong, works as a SERS biosensor. SERS chemosensors and biosensors have been designed for many different analytes, from single atoms such as metal ions,[411-414] to small ions and molecules,[415-417] biomolecules,[418,419] genes,[420] cells and tissues, both *in vitro* and *in vivo*.[421] A look into the recent literature reveals a heavily rising tendency and interest in the development of SERS

sensors; examples of analytical applications are presented in more detail in other sections below.

4.3. Enantioselective Discrimination of Chiral Molecules by SERS

Molecular chirality is one of the most intriguing fundamental characteristics in various fields such as catalysis, chemical biology, and pharmacology.[422-427] Two kinds of enantiomers in biological process can demonstrate essential differences in terms of physiological responses. Various conventional spectroscopic methods have been used to explore enantiomeric discrimination, such as fluorescence spectroscopy, nuclear magnetic resonance (NMR) spectroscopy, vibrational circular dichroism (VCD), and Raman optical activity (ROA). Most of these approaches require either the synthesis of a specialized chiral entity as a chiral selector or the use of circularly polarized light (chiral light).

Few studies have been reported on achieving chiral discrimination by SERS, which unfortunately lack generality and show poor distinction between enantiomers. As a result, we can say that generic spectroscopic enantioselective detection by SERS has not been realized due to difficulties in the fabrication of a SERS receptor with the specific stereochemical properties required to detect molecular chirality. Ozaki and co-workers proposed a label-free enantioselective discrimination method for chiral molecules based on SERS,[428,429] which does not require either chiral reagents or chiral light. The enantioselective discrimination of various chiral alcohols was achieved by SERS through charge–transfer (CT) contributions.[428,429] The relative peak intensities in the SERS spectra of a chiral selector without chirality rely strongly on the chirality of its surroundings. This marked spectral discrepancy probably arises from the tendency of chiral isomers to form intermolecular hydrogen-bonding complexes with the chiral selector in different molecular orientations, resulting in different CT states and SERS intensities of the adsorbed selector molecules in the system. **Figure 4.1** shows the fabrication process for the chiral discrimination system based on SERS.[429] The Ag-chiral selector molecule complex was fabricated on a glass substrate by a previously reported method.[428,429]
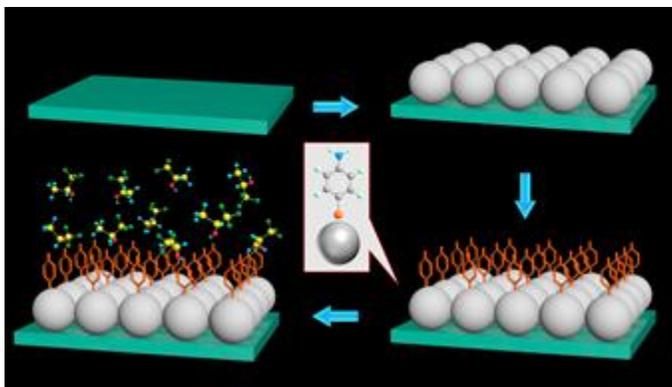
Figure 4.1. Schematic view of the fabrication process of a chiral discrimination system based on SERS. Reprinted with permission from Ref. 429: Copyright 2016, American Chemical Society.

Figure 4.2 shows the SERS spectral features for the enantiomeric separation of *p*-mercaptopyridine (MPY).[428] Of note is a marked intensity decrease of the band at 1578 cm^{-1} (the non-totally symmetric vibration, b$_2$ mode) and a simultaneous intensity increase of the band at 1612 cm^{-1} (the totally symmetric vibration, a$_1$ mode) when the Ag-MPY complex was immersed in a solution of the *S* enantiomer, or even in the racemic mixture (**Figure 4.2**). Additionally, the enantioselective discrimination indicator, *i.e.* the ratio of the intensity of the bands at 1202 and 1220 cm^{-1}, in both 2-butanol and 1-methoxy-2-propanol (MOIP) increased when increasing the *S* enantiomer content (**Figure 4.2**B,E). It was considered that there are some slight differences in the spatial structures of the *S* and *R* enantiomer-MPY complexes *versus* Ag NPs, generating different energy states that could induce differentiated CT processes between the adsorbed MPY and the Ag substrate.[428] In general, changes in the relative Raman intensities of adsorbates in a SERS spectrum could be a visible manifestation of a CT transition and be considered as a propensity rule to estimate the occurrence of a photoinduced CT process. According to the CT mechanism, it can be inferred that the *S*-type enantioselective discrimination process in an assembled system increases the contribution of the Frank–Condon term and simultaneously inhibits the Herzberg–Teller term. Nevertheless, in spite of the hydrogen bonding interaction with the Ag-MPY complex, the *R* enantiomer may have a difference in either orientation or composition, leading to a different CT state being involved in the CT transition. In this case, SERS enhancement of the MPY molecules may still be greatly influenced by the Herzberg–Teller effect. Thus, this enantioselective

phenomenon in SERS spectra is dominated by the CT enhancement mechanism, based on the effect of intermolecular hydrogen bonding in the system. In this label-free enantioselective discrimination method, the selectivity originates from the enantioselectivity of the intermolecular hydrogen bonding interactions. The difference in protonation of the Ag-MPY complex through hydrogen bonding leads to formation of different CT states of the complex, which are further manifested in remarkable differences in the SERS spectra.[428]
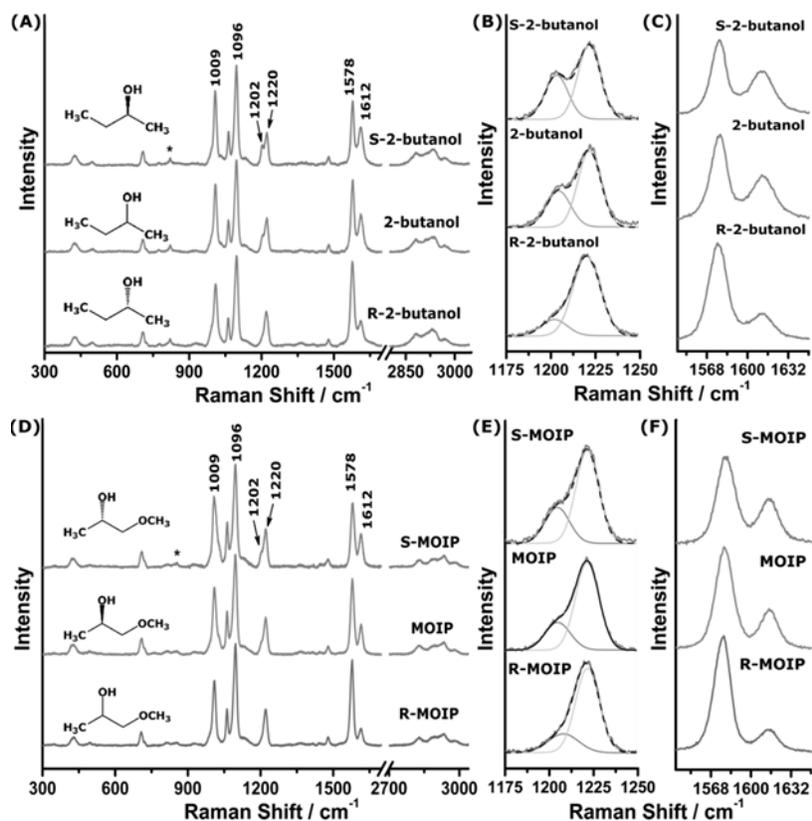
Figure 4.2. A, D) Normalized SERS spectra of the MPY-Ag complex separately immersed in different chiral alcohols (2-butanol and MOP, respectively) in their optical pure and racemic forms. B, E) and C, F) Magnifications of the 1175-1250 cm^{-1} and 1540-1650 cm^{-1} spectral regions of the SERS spectra shown in (A) and (D), respectively. Reproduced with permission from Ref. 428. Copyright 2014, Wiley-VCH.

To further explore the possible mechanism of enantioselective discrimination, a series of SERS experiments were carried out with *p*-aminobenzenethiol (PATP) as the chiral selector molecule.[429] Laser excitation wavelength-dependent and concentration-dependent SERS

experiments revealed that CT-induced chiral discrimination enhanced the differences between both enantiomers of two chiral alcohols (2-butanol and 1,1,1-trifluoro-2-propanol) interacting with PATP, by SERS. It was proposed that the directions of CT from Ag nanoparticles to PATP molecules are different under different enantiomeric conditions, resulting in different CT transitions and significantly different SERS spectra.[429]

The above studies demonstrate discrimination between two enantiomers and break the traditional notion that chiral discrimination requires other chiral entities as chiral selectors or the involvement of chiral light in the system. This approach may thus be of great significance in the field of chiral separation and chiral catalysis. The above studies did not consider the possibility that chirality of plasmonic nanostructures may contribute to enantiomeric discrimination. Investigation of the hotspot-by-hotspot dependence ability of the chiral selector may reveal the local chirality of plasmonic nanostructures, which should be complemented by DFT calculations for CT complexes. Similar studies may also be possible using TERS. It has been reported that the metal tip in TERS has intrinsic chirality.[74,430] even if chirality is averaged out by a collective measurement by SERS. Ozaki and co-workers recently reported the observation of enantiomeric discrimination by TERS, using a chemically modified TERS tip.[431,432] In this case the mechanism of enantiomeric discrimination is probably due to a CT mechanism similar to the SERS case, as well as the chirality by the tip. The contribution of chirality by the tip was confirmed by measuring the tip-by-tip dependence of enantiomeric discrimination. Nurushima and Okamoto[433] reported strong nanoscale optical activity localized in two-dimensional chiral metal nanostructures. As nanostructures with chiral shapes behave like chiral molecules and show optical activity, it is likely that the summation of local optical activities over the entire nanostructure provides optical activity to the chiral nanostructure. Their study indicates that prominent nanoscale local circular dichroism (CD) signals may exist even if only a tiny CD signal is observed as the macroscopic optical activity of the nanostructured sample. In contrast to conventional Raman spectroscopy, where there is no chirality because any chirality would be averaged out, SERS and TERS have intrinsic chiral nature. For example, a hotspot itself is not completely symmetrical and thus may have some chirality. We should probably deepen in our understanding of chirality in the near field.

4.4. Quantitative SERS with Plasmonic Nanogap Particles

Enhancing the SERS signals by many orders of magnitude while uniformly controlling the signal intensities and spectral features from Raman-active molecules on each structure is utterly challenging and complicated, since even one or two nm difference in the position of a Raman dye on a nanostructure can significantly affect SERS signal intensity.[52] Precisely synthesizing plasmonic nanostructures in ultrahigh yield, creating the plasmonically enhanced electromagnetic field on many nanostructures, often assembled, in a reproducible manner, precisely positioning Raman dyes inside a highly localized and enhanced field, controlling the orientation, number and density of dyes, incorporating and tuning resonance effects between laser wavelength, plasmonic structure and dye molecule, measuring and comparing SERS signals from single molecules, single particles and bulk samples in a quantitative manner, and understanding and controlling the interactions between Raman dyes, nanostructures, passivation molecules and target samples, particularly for biomedical and chemical sensing applications, should all be considered for quantitative SERS (**Figure 4.3**). Analytical methods for obtaining the plasmonic gap size, the number and orientation of particle-surface-modified Raman dye molecules and SERS enhancement factors (EFs), significantly influence the outcome of SERS results that vary among different studies by different researchers, with different approaches and setups. Further, the SERS signals from a large number of individual particles should be compared to the SERS signals from bulk samples for quantitative assessment of SERS data. In these regards, from design to applications, many different steps and aspects must be carefully and quantitatively scrutinized to test whether a particular probe or system is actually useful for real applications with SERS (**Figure 4.3**). It should be noted that, although more desired and beneficial, ultrahigh SERS EF values from plasmonically enhanced nanostructures mean that that these structures are likely to generate poorly controllable and heterogeneous SERS signals to a larger degree than the cases with lower EF values.

Important advances have been made for quantitative SERS using plasmonic nanogap structures possessing ~1 nm gaps, either between particles (interparticle gap or intergap) or inside a single particle (intraparticle gap or intragap) (see TEM images in **Figure 4.3**).[89,399,400] Precisely synthesizing the targeted nanostructures in high yield (well over 95%) is the first

step for quantitative SERS,[434,435] and poor controllability of the size and shape of the nanogaps with low structural reproducibility can generate large fluctuations in SERS signal intensity and peak positions (**Figure 4.3**).[436,437] Single-molecule SERS has been shown to be reliable and repeatedly detectable with gold-silver nanodumbells, where a Raman dye is positioned at the center of DNA-tethered gold nanoparticles and interparticle gaps have been engineered by nm-scale tuning of silver shells.[434] It has been theoretically shown that forming ~1 nm or smaller gap is critical toward largely increasing the electromagnetic field within the gap between metal structures, and DNA-tethered nanoparticle dimers with <1 nm interparticle gap can generate a narrow distribution of larger SERS EFs.[435] Intrananogap particles are promising and therefore several methods and strategies have been reported to form nanoparticles with highly uniform and controllable ~1-nm intragaps.[220,438-440] Such particles with robust 1-nm gaps can be used as reliable SERS labels (or SERS tags) with quantitative SERS signals. It should also be noted that quantum tunneling effects may be present for sub-nm (~0.3-0.7 nm or smaller) gaps formed between metal nanostructures,[89,441,442] and this effect should be avoided for stronger SERS signals because tunneling reduces the electromagnetic field inside the nanogap (see Section 1). Therefore, sub-nm accuracy in engineering nanogaps and precisely positioning Raman dyes inside them are needed to obtain maximum and reproducible SERS signals.

If biomedical applications are considered, quantitative aspects and data reliability in SERS become even more important, and surface chemistry of SERS probes is critical in maximizing target binding and minimizing nonspecific binding. Further, large-scale production of targeted SERS probes/substrates with high structural precision and desired functionalities while generating the same detection/imaging results with different batches of probes, particularly as scaling up the synthesized probe amounts, is absolutely necessary for the clinical and commercial use of SERS probes/substrates, but utterly challenging. Although fluorescent probes have been dominantly used in biomedical applications, they suffer from many issues including poor photostability (photobleaching/photoblinking), limited multiplexing capability (broad linewidth), and autofluorescence background signals. In contrast, Raman scattering exhibits sharply and clearly discernible molecular fingerprint peaks with excellent photostability[443] can be free from background signals, and offers richer information on molecules and nanostructures. These features have been recently shown

powerful in biosensing and bioimaging applications with high multiplexing potential, a reliable long-term monitoring capability of biomolecules of interest inside a cell, multimodal bioimaging, and ultrasensitive and quantitative bio-detection.[440,444] Thus, if the quantitative SERS issue can be addressed properly with all the supporting evidences described above, we might now be looking at the emergence of SERS probes/substrates that can finally replace or complement widely used fluorescent probes in the near future and provide opportunities for SERS probes in a wide variety of practical applications.
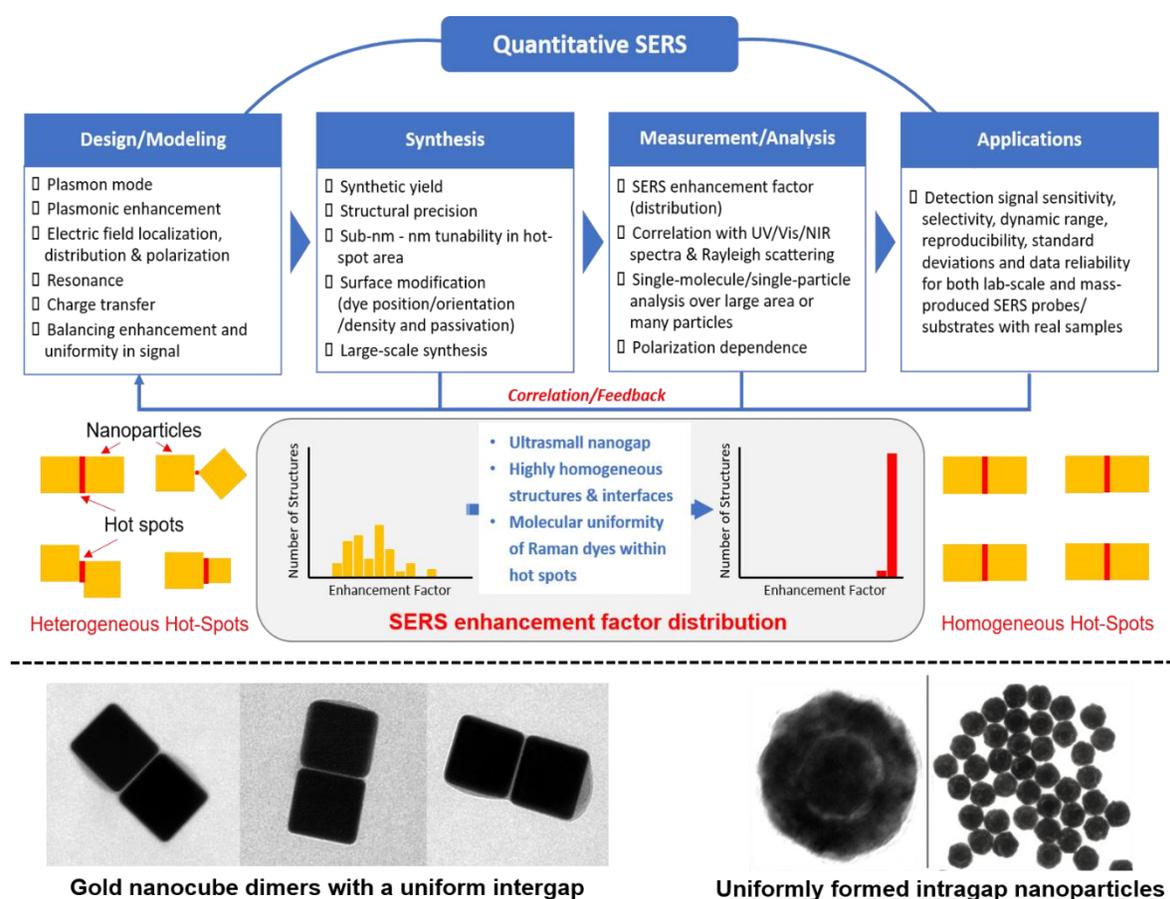
Figure 4.3. Prospects and challenges of quantitative SERS (top) and representative plasmonic nanogap structures for quantiatitve SERS (bottom).

4.5. Remote SERS

For trace-molecule detection and analysis, the SERS sensitivity and reliability critically depend on whether the analyte is stably positioned around the effective hotspot region (**Figure 4.4**), or better yet, the orientation matches the vibration modes and plasmonic fields. To trap analytes inside nanogaps, various techniques have been applied, including plasmon-enhanced optical forces,[445,446] micro-capillarity,[289] DNA assembly,[222,447,448] and host−guest chemistry.[449,450]

Recently, a quantitative SERS study using a MoS_2-spaced metallic nanoparticle-over-mirror (NPoM) system (**Figure 4.4**) by Chen *et al*. tried to meet most of these requirements.[404] By using monolayer MoS_2 to separate the nanoparticle and gold mirror, a robust 0.62 nm-thick gap, which is near the upper limits of field enhancement, was created. To obtain the maximum SERS signal, the optimal resonant excitation was matched by a plasmon-scanning technique. Furthermore, the strict lattice arrangement of MoS_2 filling the gap ensures a precise alignment between the lattice vibrations and the plasmonic field components. As a result, the plasmonic enhancement can be quantitatively probed. These quantitative SERS designs might provide important guidelines for interesting effects under the high gradient plasmonic field, such as quantum plasmonics,[451] plasmon-phonon interactions,[452] selection rule breakdown,[453] and cavity optomechanics.[100,101]
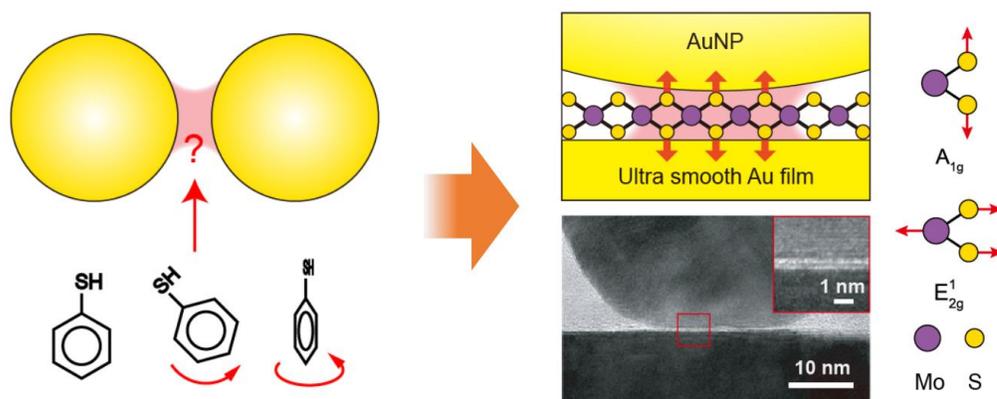
Figure 4.4. While in conventional SERS, the molecules to be probed are hard to trap and control, a Raman probe based on 2D materials can be used to build a robust sub-nanometer gap. It allows a perfect orientation match between the vibrational modes and the local plasmonic fields. Reprinted with permission from Ref. 404. Copyright 2018, Springer Nature.

In conventional local SERS experiments, the samples are directly exposed to a far-field incident beam, to excite a much smaller nanoscopic hotspot region for the desired SERS signal. This local excitation mode not only brings strong background noise from the remaining unenhanced region, but is also unsuitable for some biological studies due to photodamage effects under the strong laser exposure. An effective approach to circumvent these problems is based on using remote SERS, by coupling the hotspots with a plasmonic waveguide. This was first demonstrated in a nanowire-particle system (**Figure 4.5**).[454,455] In this scheme, surface plasmon polaritons (SPPs) are generated at the nanowire end by far-field excitation, and then propagate along the nanowire waveguide,[456] to excite SERS signals of molecules in the nanowire-particle junction (several micrometers away from the laser beam). Owing to the separation between the SERS output region and the excitation beam, this technique allows for high signal-to-noise-ratio (SNR) SERS detection, without losing single-molecule sensitivity. This is especially suitable for applications associated with SERS imaging.

Recently, in an initial stage, the remote SERS technique by virtue of a nanogap-coupled nanowire probe was applied to live-cell SERS endoscopy (**Figure 4.5**).[457] In contrast to the local SERS detection with a laser beam directly illuminating the cell, remotely excited hotspots in the cell show a largely reduced photodamage effect, and much higher SNR SERS signals from the nucleus region. In the future, the sensitivity and specificity of *in vivo* remote SERS detection could be further improved by optimizing the plasmonic nanogaps, using various chemical-linking techniques. Their resonant antenna conditions in complex liquid environments, including resonance and polarization matching, should also be carefully considered. On the other hand, a remote-excitation plasmonic source from a similar nanogap-coupled nanowire probe has been used to suppress the background noise in TERS measurements.[458]
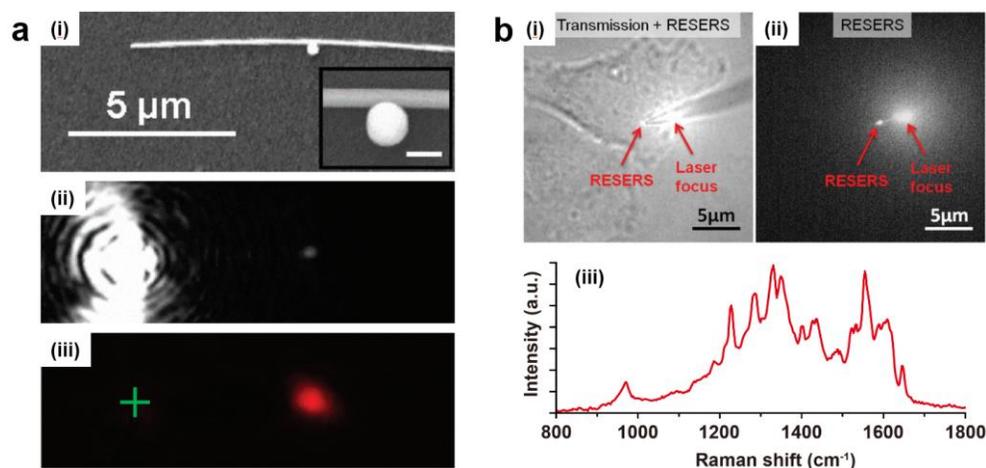
Figure 4.5. (**a**) (**i**) SEM, (**ii**) scattering and (**iii**) Raman images of a nanoparticle-coupled nanowire plasmonic waveguide for remote SERS. The green cross in (**iii**) marks the illumination position. Reprinted with permission from Ref. 454. Copyright 2009, American Chemical Society. (**b**) (**i**) Transmission (**ii**) remote SERS images of a live HeLa cell with the nanoparticle-coupled nanowire endoscopy. (**iii**) the SERS spectrum from the nucleus region of the cell. Reprinted with permission from Ref. 457. Copyright 2014, Wiley-VCH.

The NPoM system is another promising platform for future remote excitation methodology. This is based on the conversion between SPPs propagating along the metal film and localized plasmon modes within the gaps. This can be achieved by momentum matching, through the use of a proper excitation wavelength and control of particle geometry and gap morphology. The propagation of the antenna-mediated SPPs can be flexibly directed by rotating the excitation polarization, or controlling the laser beam position with respect to the gap antenna.[459] By reciprocity, the strongest out-of-plane gap mode can be excited to the maximum by the SPPs due to their vertically-oriented electric field. This facilitates the optimization of SERS detection and studies in a quantitative manner. By further combing specific-targeting techniques[460] in the NPoM system, the remote excitation technique could manifest the potential for future quantitative SERS detection and studies, including bioanalysis and plasmon-driven chemical reactions.[461-463] On the other hand, the remotely-excited gap antenna can be used to avoid damage from the pulsed high power laser for the excitation of plasmon-enhanced nonlinear Raman processes, such as coherent Raman

scattering[464] and molecular optomechanics,[106] making these novel phenomena clearly resolved in a more stable plasmonic analyte-hotspot system.

4.6. Shell-Isolated Nanoparticle-Enhanced Raman Spectroscopy (SHINERS)

Admittedly, SERS is an extremely surface sensitive technique, but it is material limited, requiring nanostructured plasmonic substrates to generate surface plasmon resonances (SPRs) for enhancing the Raman signals. To overcome this limitation, Tian's group developed so-called shell-isolated nanoparticle-enhanced Raman spectroscopy (SHINERS).[465] In SHINERS, inert shell-isolated nanoparticles (SHINs) consisting of plasmonic cores (Au or Ag) and ultrathin but pinhole-free silica shells, work as nano-sized Raman signal amplifiers (**Figure 4.6**). The plasmonic cores generate strong electromagnetic fields, which enhance the Raman signals of nearby molecules, while the silica shells isolate the plasmonic cores preventing physical interactions with the analyte. At the same time, the silica shell can greatly improve the long-term stability of the plasmonic cores, especially when Ag is used.[466] In general, by simply applying SHINs to the probe surface, SHINERS can be used to investigate any type of substrate, with enhancement factors up to 5-8 orders magnitude.[467] SHINERS has now been widely applied in various fields, including electrochemistry (EC), analytical chemistry, catalysis, energy, life sciences, and even people's daily lives.[468]
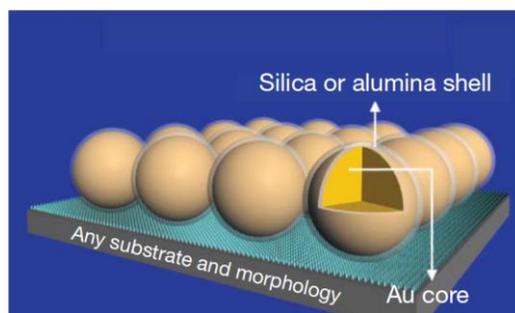
Figure 4.6. Schematic diagram of the principle of SHINERS. Reprinted with permission from ref. 465. Copyright 2010, Springer Nature.

A major application of SHINERS is probing interfacial processes at single crystal surfaces with well-defined surface atomic structures and electromagnetic fields,[468] which is of significance in surface science but can hardly be studied by traditional SERS due to the well-

known material limitation of SERS. Combining SHINERS with electrochemistry (EC), Li and co-workers successfully studied *in situ* the potential dependent adsorption behavior of molecules, such as hydrogen, CO and pyridine, at Au(*hkl*), Pt(*hkl*) and Rh(*hkl*) surfaces, respectively, and observed their different potential dependent adsorption mechanisms.[465,467,470,471] Next, they used *in situ* SHINERS to study catalytic reaction mechanisms at Au(*hkl*) and Pt(*hkl*) single crystal electrodes. For example, during electrooxidation at the Au(*hkl*) single crystal surface, direct Raman spectroscopy evidence of the OH intermediate was observed.[472] Recently, *in situ* electrochemical-SHINERS has been used to monitor the oxygen reduction reaction (ORR) at Pt(*hkl*) surfaces, the most important cathode reaction in fuel cells.[473] When ORR was performed under acidic conditions, OOH intermediates were observed at Pt(111), whereas OH species were observed at Pt(110) and Pt(100) surfaces. However, ORR in alkaline conditions led to observing O_2^- at all three low-index Pt(*hkl*) single crystal electrode surfaces. Therefore, different key intermediate species, generated at distinct Pt(*hkl*) facets, can induce different ORR catalytic pathways.

In contrast with catalysis on well-defined surfaces, nanocatalysts are used throughout industrial processes to greatly enhance their efficiencies. However, nanocatalysts feature more complicated surface structures and are usually dispersed on supports, such as oxides or carbon black, with high surface areas. Therefore, due to the lack of coupling effects between the catalysts and SHINs, it is difficult to directly employ SHINERS to study surface catalysis processes on nanocatalysts. To that end, a general SHINERS-satellite strategy was developed to track nanocatalytic processes *in situ*.[474] Nanocatalysts were deposited on SHINs *via* charge-induced self-assembly, to form SHINERS-satellite (Au core@silica shell@nanocatalyst satellite) nanocomposites, so that the Raman signals of species adsorbed on the nanocatalysts can be effectively enhanced. Using the SHINERS-satellite strategy, the reaction mechanisms and structure-activity relationships for CO oxidation on Pt- and Pd-based nanocatalysts were successfully identified. Additionally, *in situ* SHINERS demonstrated that O_2 is efficiently activated on PtFe bimetallic catalysts, into superoxide and peroxide, even at room temperature, with higher activities than those achieved with a pure Pt catalyst. Conversely, at Pd nanocatalysts CO oxidation only occurs at high temperatures when PdO_x is formed and O_2 is activated to superoxide and peroxide, indicating that O_2 activation is essential for CO oxidation and that surface PdO_x may be the active site.

SHINERS has also been used on numerous substrate surfaces in various fields, to obtain enhanced Raman signals. One example is the application of SHINERS to study the atomically smooth Si single crystal surface, widely used in the semiconductor industry, which successfully provided the Raman signal of the Si-H bond during surface cleaning processes.[465] In addition to metallic and non-metallic substrates, SHINERS can also be used to probe complex biological systems. For instance, membrane structures of living cells were obtained using SHINERS with Raman signals detecting mannoprotein and other bioactive substances related to protein secretion and movement in living cells.[465] In combination with portable Raman spectrometers, SHINERS has also been used in the areas of food safety and rapid detection, to successfully detect pesticide residues on the surface of fruit or vegetables.

SHINERS, therefore, provides the opportunity to overcome the long-standing material and morphological limitations of traditional SERS, while significantly improving the trace analysis capabilities of Raman spectroscopy. The SHIN enhancement concept has been expanded to other surface enhanced spectroscopies. For instance, due to the quenching effect resulting from nonradiative energy transfer between metal substrates and fluorophores, surface enhanced fluorescence displays only around one order of magnitude enhancement. Both the Aroca and Li groups developed shell-isolated nanoparticle-enhanced fluorescence (SHINEF), reporting a 10^3 enhancement factor with general application to different fluorophores, quantum dots, and even phosphorescent molecules.[466,475-478] Li and co-workers also established shell-isolated tip-enhanced Raman and fluorescence spectroscopy by employing shell-isolated tips, which can exclude interference by contaminants and allows acquisition of tip-enhanced Raman and fluorescence signals simultaneously.[479] Thus, it shows promising applications for the Raman and fluorescence dual mode analysis of solutions, such as biological systems. More remarkably, shell-isolated tip-enhanced ablation and ionization mass spectrometry has also been realized, which greatly improved the spatial detection resolution from the micrometer to the nanometer scale.[480] These shell-isolated nanostructure-enhanced spectroscopic techniques with ultrahigh sensitivity and spatial resolution will make it possible to monitor biological and energy conversion processes at a single-molecule or even a single-atom in real-time, thereby providing profound fundamental insights into reaction processes.

4.7. Analytical Quantification

The most fundamental goal of an analytical chemist is answering two questions about an analyte in a sample: 1) what is it? 2) what is its concentration? SERS answers the qualitative question better than several other analytical tools. The SERS pattern is a vibrational fingerprint of the species being analyzed, leading to direct identification.[52] Advanced chemometric methods can be applied to extract the spectral signature for each component in a complex mixture[481] The high sensitivity inherent to SERS allows identification of particular analytes, even at very low solution concentrations. The ability of SERS to answer the quantitative question is regularly challenged by analytical chemists outside the SERS research field. This skepticism is justified by the reputation of SERS being an irreproducible technique. The source of irreproducibility has been assigned to the nature of the SERS substrate (metallic nanostructured surface that supports the effect). As extensively discussed above, the plasmonic SERS effect requires molecules to be adsorbed on surface regions of strong localized fields, *i.e.* hotspots. The electric field distribution around a hotspot is not homogeneous and it is highly dependent of the local geometric characteristics of the metallic nanofeatures. In principle, this causes a high degree of variability in SERS intensities, since nanometric changes in molecular position, orientation and nanoparticle geometry should result in very large changes of the scattering response. This "limitation" of the SERS technique has arguably precluded the widespread application of the method in industrial settings. However, the last 20 years have been marked by an accelerated development in nanotechnology, including methods for design, fabrication and synthesis of nanostructures.[482,483] Motivated by trying to find solutions to the "substrate reproducibility problem", SERS researchers played a pivotal role in those advances and reported several approaches, with different degrees of sophistication, for substrate preparation (some of these approaches are described in this perspective). In fact, hundreds of papers have been published over the years on how to produce SERS substrates with different characteristics, including large-area, low-cost, high efficiency and "good reproducibility". The state-of-the-art in the field offers a variety of technologies to prepare substrates (from either top-down or bottom-up approaches) that present reasonable (less than 20% RSD) variations in SERS intensities.[482] Even commercial substrates that provide a good degree of reproducibility are now available.[484] These substrates allow the construction of robust calibration curves from

SERS data that can be used for quantification in real-world analytical applications. Beside the control of substrate reproducibility, the processing and analysis of spectral features for quantification is another significant challenge, in particular in complex mixtures and environments, multicomponent samples (of known or unknown composition) and at low concentrations down to the single-molecule level.

Development of chemometrics for quantitative SERS

Whilst many would consider analytical techniques within SERS limited to nanoparticle production, different types of sample processing and analysis, an important aspect that has been developed over the last decade is the use of chemometrics. These computational approaches are based on multivariate data analyses and use the whole SERS spectra rather than specific bands for quantification. A recent review of mathematical approaches for quantifying analytes from SERS data,[485] details two general approaches, which are summarized and exemplified here.

The first approach uses a readily identifiable unique peak that is specific to the substance being quantified. In this case, one can generate a simple calibration model by plotting the intensity or area of the band against analyte concentration. In order to overcome any extraction efficiencies from complex samples or any unavoidable analytical challenges (*viz.*, number and arrangement of nanoparticles in the collection voxel, or laser power fluctuations) recent developments have involved the use of isotopologues (also referred to as isotope dilution surface enhanced Raman scattering (ID-SERS)) where isotope substitution is used in an internal standard, with the same molecular formula and structure as the determinand.[486] This method leads to different but recognizable vibrations (*e.g.*, a CH at ~2800 cm^{-1} is shifted to ~2100 cm^{-1} in CD) which can then be used for ratio-based correction. However for ^{12}C to ^{13}C and ^{15}N to ^{14}N, the shifts are generally more modest and peak overlap is observed, especially within the fingerprint region of the SERS spectra; therefore, these ratio corrections involve the use of chemometrics. Examples of the use of isotopologues, often with chemometrics, for absolute quantification include assessing nicotine levels within electronic cigarettes,[487] as well as drugs and biomarkers in human biofluids: measuring codeine in plasma[488] and uric acid in serum.[489] Other analytical approaches for absolute quantification involved the standard addition method (SAM) with the incorporation multivariate analyses.

Recent examples include the quantification of various drugs and metabolites in urine including the antibiotic nitroxoline,[490] nicotine[491] and uric acid, as this metabolite is a potential marker for preeclampsia during pregnancy.[492]

Chemometrics, which has been central to the above studies, uses multivariate calibrations such as partial least squares regression (PLSR), although there are many other versions of supervised, or even unsupervised, learning methods.[493] In PLSR a set of standards are prepared where one knows the level of the substance to be quantified. SERS spectra are obtained (directly, with isotope additions, or *via* SAM) and a PLSR model generated that associates the spectra with the level of the determined target. This process needs to be validated carefully, which can be achieved by generating more samples containing known levels of target molecules, and then testing the model's predictive power.[493] One of the advantages of using multivariate PLSR calibration is that structured outputs (*i.e.*, the Y variables) can be used,[494] which contain multiple analytes to be quantified, thus allowing quantitative multiplexed analysis with SERS.[495]

Analytical Quantification from Single-Molecule Measurements

Although the substrate reproducibility problem has been tamed, there are still challenges related to SERS quantification, particularly for a non-specialist. Some of them are experimental pitfalls, such as sampling[496] and acquisition conditions (time or laser power, for instance), that need to be tailored for a particular analysis. However, there are also fundamental characteristics of SERS that need to be considered, particularly when attempting SERS quantification at ultralow concentrations (generally, less than 1 nM). One of these characteristics are SERS intensity fluctuations (SIFs),[100,497] which are observed at low concentrations and constitute a challenge for a robust analytical calibration. The origin of these intrinsic fluctuations can be rationalized considering a simple Langmuir model for the analyte adsorption onto the SERS-active surface. In this case, the concentration in solution (the quantity of interest for an analytical chemist) is related to the amount of adsorbed analyte (surface coverage or concentration) by an adsorption equilibrium constant (K_a). For a typical adsorbate (K_a around 10^7, for instance), the surface coverage would be around 1% for a 1 nM solution. Below 1 nM, the surface coverage would decrease linearly with the solution concentration (Langmuir model). In these conditions, variations in Raman intensities arise

due to the number and nature of the SERS hotspots. The electric fields in SERS hotspots are tightly localized and occupy a relatively small fraction of the surface area illuminated by the excitation laser.[498,499] When the surface concentration is also small, then the probability of molecules to be found in a hotspot becomes low. This leads to strong variations (spatial and temporal) of the SERS signal, which, at the limit, can be assigned to single molecules visiting the SERS hotspot. **Figure 4.7** shows an example of an experimental time-dependent trajectory of SIFs for rhodamine 6G (R6G) adsorbed on a nanostructured silver surface. The inset in **Figure 4.7** shows 5000 spectra acquired at every second. The "SERS intensity" from each spectrum was used to generate the temporal trajectory. Note that although intensity is plotted in **Figure 4.7**, more sophisticated approaches to analyze this type of data, involving principal component analysis (PCA) or other data reduction methods, are preferred. In that case, the whole spectral pattern is considered and photodecomposition products can be readily identified and removed from the dataset.[500,501]
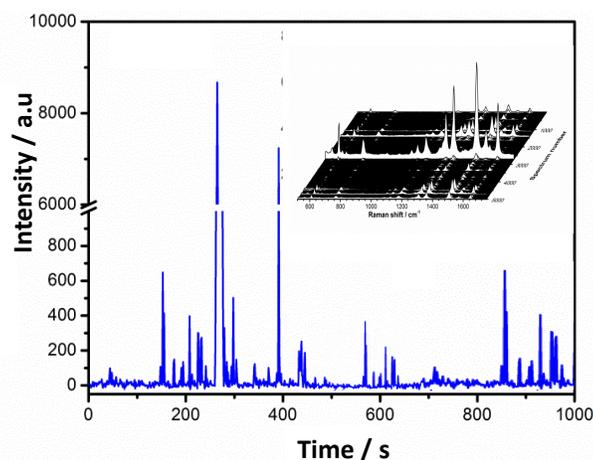
Figure 4.7. SERS Intensity of 10 nM R6G adsorbed on silver colloids recorded *versus* time. The spectral dataset is shown in the inset. Excitation was at 633 nm and acquisition time was 1 second. Adapted with permission from Ref. 501. Copyright 2013 D.P. dos Santos.

The wild intensity fluctuations shown in **Figure 4.7** provide a challenge for the generation of a proper calibration curve. The distribution of intensities in this case is not Gaussian and simply measuring an average is not appropriate. Moreover, the large fluctuations lead to large error bars. These issues can be somehow tackled by increasing the sample size; however, for a long-time trace, the laser excitation fixed in a spot at the nanostructured surface would

increase the probability for photodecomposition products and other artifacts. A methodology has been suggested for SERS quantification at ultra-low concentration conditions, particularly when the strong SIFs can be related to single-molecule SERS events.[502] The substrate was a thin film of immobilized gold nanoparticles on a glass slide. Enrofloxacin (ENRO) and ciprofloxacin (CIPRO), two fluoroquinolone antibiotics which are emerging contaminants found in surface waters[481] were analyzed by SERS at ultra-low concentrations (less than 1 nM). The analytes were drop casted on the nanostructured surface and several areas of the slide were spatially mapped[503] using a Raman microscope. Spatial mapping was preferred to avoid photodecomposition, because, in this case, the diffraction-limited laser illumination was moved from a particular spot right after the 1 second spectral acquisition. It is assumed that, as the concentration decreases into the pM regime, the Raman signal generated from a particular illuminated spot (pixel) will originate from single molecule events.
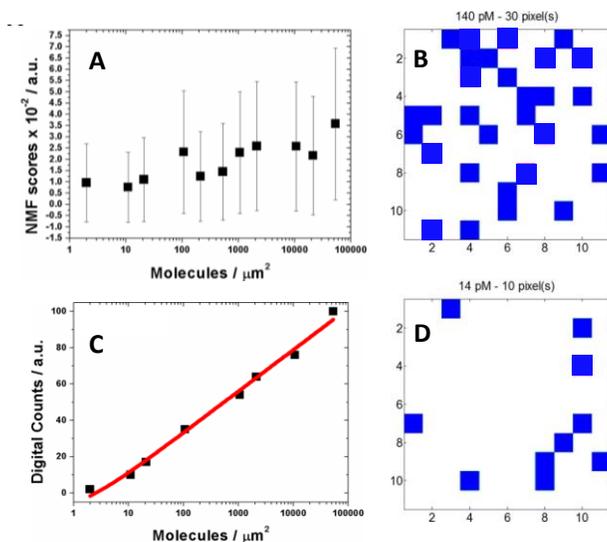
Figure 4.8. A) Analytical calibration curve using the average value of the SERS intensities (represented as NMF scores). The error bars are related to the magnitude of the fluctuations; B) digital SERS mapping for CIPRO (100 molecules/μm^2) adsorbed on immobilized gold nanoparticles; C) revised calibration curve obtained using the digital SERS procedure; D) digital SERS mapping for CIPRO (10 molecules/μm^2) adsorbed on immobilized gold nanoparticles. Adapted with permission from Ref. 502. Copyright 2018, American Chemical Society.

Figure 4.8A shows a typical analytical calibration curve obtained by plotting the average scores from the non-negative matrix factorization resolution method (NMF - equivalent to SERS intensities, but the whole spectrum is considered instead of just one band) against the number of molecules being illuminated (the concentration ranged from 3 pM to 14 nM). The large variations in SERS intensities, as depicted in **Figure 4.8**, lead to very large "error bars" and preclude proper quantification. **Figure 4.8**A nicely illustrates a fundamental problem for SERS quantification that is related to the nature of the phenomenon, rather than to substrate variability. In order to circumvent this problem, a methodology was suggested, based on the digitization of the SERS signal. The technique is based on the assumption that the SERS signal from each pixel of a SERS map is from a single molecule event. In that case, quantification can be achieved by counting the number of single-molecule events (defined by establishing an intensity threshold above the background) observed in the map for a particular concentration. **Figure 4.8**B,D shows two digitized SERS maps at different concentrations. The number of single-molecule events in the 50 x 50 μm^2 maps, represented by blue squares, scales with the concentration, as shown in **Figure 4.8**C. The digital procedure described here is general and could be implemented for any type of analyte, as long as the SIFs are due to single-molecule events.**Error! Bookmark not defined.** In terms of substrates, this method is suitable for nanostructured surfaces with "immobilized" hotspots. In the case of suspensions, other factors, such as aggregation process (that traps molecules in certain regions of the surface) and the even the dynamics of the movement of the nanoparticle clusters within the suspension might also play a role.[504]

The methodology described here provides a robust alternative for SERS quantification in conditions of extreme fluctuations (ultralow concentrations). As in any procedure based on counting statistics, the error in the determination will scale with the number of (single-molecule) events (counts). Therefore, this digital SERS procedure should provide reliable results as long as a large area SERS map is considered. SERS quantification has been dubbed as the Achilles' heel of the technique. However, with the advent of substrates with a high level of reproducibility, methods are being devised to tackle fundamental sources of Raman intensity variations, particularly at ultralow concentrations.[505-507] Pre-concentration procedures have also been described,[508,509] and they can be incorporated into devices for an integrated approach for SERS quantification from highly diluted solutions. The further

development of methods capable of transforming SERS intensity variations into useful analytical signal might constitute the next step towards a wider application of the SERS technique in industrial, commercial and clinical settings.

5. Analytical Methods and Devices in Biomedical Applications

SERS has attracted increasing interest in the development of novel methods and devices for biomedical applications. Practical and sensitive diagnostics and cost-effective techniques, capable of simultaneously detecting the presence of several biomarkers (*i.e.* multiplex detection) associated with specific diseases at the point-of-care (POC), are highly desirable. SERS has provided solutions for many diverse medical applications due to its versatility. Different analytical techniques, methods and devices have been developed to overcome the different needs. Before delving into the details of the different applications, we mention here the most common and some novel techniques used in biomedical applications.

5.1. Basic Techniques in Biomedical Applications

Label-free SERS measurements in biofluids

As mentioned in Section 4 above, direct determination of analytes can be performed by recording the characteristic signal of the analytes in close contact with plasmonic nanoparticles. If we focus on biomedical applications such as the analysis of biofluids, we need to consider that the readout of the signal and therefore the result of the analysis is always associated to three parameters: the nature of the analyte, the nature of the fluid, and the nature of the optical enhancing material. Additionally, the desired output about the analyte, either ultrasensitive detection or/and quantification, should also be considered. Notably, although in some cases, the mere presence of a given chemical species in a biofluid is indicative of disease, in modern medicine it is essential to achieve quantification of the levels of certain parameters, to provide an adequate diagnosis, but also to understand the effect of a given treatment after diagnosis. For example, although SERS can be successfully applied to the diagnosis of degenerative disorders (*e.g.*, presence of amyloid proteins in Creutzfeldt-Jakob[249] or Alzheimer's[510] diseases), infectious (*e.g.* the presence of virus,[511] bacteria[512] or fungi,[513] or genetic diseases (presence of mutations in DNA),[514] indicators of other

malignancies are not so obvious and depend on the excess or shortage of a given molecule in the biofluid.

SERS direct detection in the biomedical field has proven useful in the demonstration of the analytical capabilities of technique (*i.e.*, single-molecule detection and ultrasensitive qualitative analysis) however the inherent complexities of the biofluids (*i.e.*, blood, saliva, urine, *etc*.) hinder its direct applicability. Notwithstanding, the direct addition of the biofluid to the plasmonic substrate may yield good results in two situations. First, when the analyte to be determined has a very strong affinity for the plasmonic surfaces. In such a case, the retention of the analyte on the plasmonic surfaces is preferred to the other components of the sample, giving rise to the possibility of quantitative/semiquantitative detection in well-designed plasmonic platforms. A clear illustration of this is for example the determination of scrambled Creutzfeldt-Jakob prions in blood samples by using Au nanorod supercrystals (**Figure 5.1A**). In this case, the prionic protein presents an amino acid sequence of -Met-Lys-His-Met-, known to have and extraordinary affinity for gold surfaces. This high affinity, together with the exceptional enhancing properties of nanorod supercrystals, allowed the SERS quantification of the prion at low (pM) levels.[249] Second, direct approaches are also useful when the target analyte can be easily purified from the main components of the biofluid. A typical example is the detection of single point mutations in nucleic acids (**Figure 5.1**B). These macromolecules can be easily extracted from cells, purified and cut into the desired fragments by using commercial kits and endonucleases. Subsequent addition of the samples to the appropriate plasmonic surfaces (in this case positively charged spermine derivatized silver nanoparticles) allows classification of the samples, by using statistical protocols, into their respective groups, wild type or mutated, which is of paramount importance in the treatment of several neoplasm such as colorectal cancer.[515]

Indirect strategies in biofluids: SERS chemobiosensors

The indirect detection of analytes in biological media based on the SERS response of a secondary molecule - a chemosensor - that changes in the presence of the analyte, is very useful for analysis in complex media. In particularly complex systems, such as biofluids, when the study of analyte levels (quantification) is required, indirect strategies are commonly used, and SERS biosensors are excellent systems. The complexity of biofluids, which

includes millions of substances different to the target analytes, requires the external functionalization of the plasmonic materials with chemical species capable of imparting selectivity toward those analytes (*i.e.* chemosensors).[506] The target analyte is determined here through a structural or electronic change in the selective molecule (reflected in its SERS spectrum) upon combination with the analyte. Advantages of this method include the generation of highly selective sensors but also the use of the chemosensor as an analytical standard for quantitative purposes. These biological chemosensors can be employed for the analysis of small and large molecules and can themselves be small or large molecules. For example, small chemosensor molecules have been used to monitor chloride[516] or nitric oxide[517] inside living cells but also amyloid proteins.[518] The most common chemosensor used in biological systems relies on the use of biomolecules with high affinity and specificity against their analytical targets; especially aptamers, peptides and proteins (antibodies). Again, these macromolecules have been used for detecting both small metabolites, such as benzoylecgonine,[519] and large proteins such as ovoalbumin[520] or thrombin.[521] Unfortunately, the low SERS cross-section of polymers (including biopolymers) is well known,[522] resulting in the limited availability of aptamers, peptides or proteins that may gather specificity, selectivity and high SERS signals all together. Possible solutions include the use of internal and external molecular labeling of the chemosensor. In the internal labeling, a molecule with high cross-section for SERS is introduced as a bridge between the plasmonic surface and the chemosensor itself. Detection is based on orientation changes of this molecule (also known as molecular spring) upon conjugation of the chemosensor with its target, in agreement with surface selection rules (**Figure 5.1**C).[523] This approach results very efficient for analysis of bulky analytes. For example, it has been demonstrated in the quantitative determination of oncoproteins in cell lysates[524] or even whole blood.[525]

Molecular beacons: Small analytes do not promote great orientation changes and, thus, the use of external labels, such as molecular beacons, may result of good interest. Classically, molecular beacons are fragments of nucleic acids with a stem-and-loop structure doubly labeled with a fluorophore and a quencher group on each end. In the absence of targets, the molecular beacons act as switches that are normally closed by the stem part (in the "off" position) without observed fluorescence background because of quenching. However, upon binding to their targets, conformational changes in the MB open the hairpin, and fluorescence

is turned "on". MBs are characterized by simple operation and high sensitivity and specificity. By replacing one of the fluorophores with a plasmonic surface, the SERS signal of the other fluorophore can be monitored as a function of MB interaction with the target.[526,527]
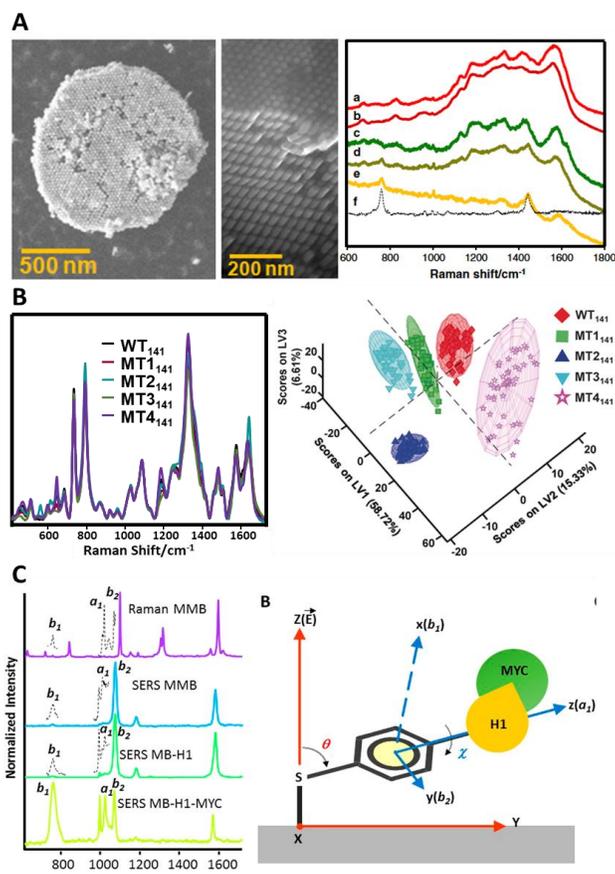
Figure 5.1. (A) SEM images of a typical nanorod supercrystal island film and SERS spectra of (*a*) natural and (*b*) spiked human blood; (*c*) natural and (*d*) spiked human plasma. (*e*) SERS spectra spiked human plasma after spectral subtraction of the matrix (human plasma). (*f*) SERS spectra of the scrambled prion. Adapted with permission from Ref. 249. Copyright 2011, National Academy of Sciences. (B) SERS of 141-nucleobase ssDNA fragment of the wild type K-Ras gene and with different single point mutations and its classification by using partial least-squares discriminant analysis (PLS-DA). Adapted with permission from Ref. 515. Copyright 2017, Wiley-VCH. (C) SERS detection of the oncoprotein c-MYC. The sensor includes a specific peptide (H1) for c-MYC chemically attached to an optical molecular spring (mercapto-*N*-methylbenzamide, MMB) which is bound to a silver nanoparticle. Theoretical

and experimental Raman spectrum of MMB and SERS spectra of MMB, MB-H1, and MB-H1 in the presence of c-MYC, on $SiO_2@Ag$. Magnification of the spectral windows between 730−800 and 990−1050 cm^{-1} are also shown. (C-B) Model used in the estimation of the molecular orientation. Absolute orientation of the molecule on the surface and relative orientation of the ring over the surface are represented by *XYZ* and *xyz* axes, respectively. Adapted with permission from Ref. 525. Copyright 2016, American Chemical Society.

A related technique (see Section 8 for details) with direct bioaplication, is surface-enhanced spatially offset Raman spectroscopy (SESORS), which allows the detection of SERS-labeled nanostar probes beneath thick material and bone, such as a monkey skull,[528] thus opening the possibility of noninvasive remote sensing of SERS nanoprobes for biomedical imaging. The possibility of combining the spectral selectivity and high sensitivity of the SERS process, with the inherent molecular specificity of bioreceptor-based nanoprobes provides a multiplex selective diagnostic modality, as well as efficient and versatile multimodal therapy.[529]

5.2. Methods in Biological Applications

The revolution of the currently known as modern medicine has driven the evolution of existing techniques and the appearance of others. The development of microscopic and spectroscopic techniques combined with the preparation of nanomaterials with a high degree of control has been a crucial step that resulted in important findings. When technology advances, measurement methods, devices, *etc.* appear, which are adjusted to the upcoming requirements. SERS is a technique that has evolved considerably and found a variety of applications which recently focused toward biological and medical ones.[530] In medicine, practical and sensitive diagnostic and cost-effective techniques, capable of simultaneously detecting the presence of several biomarkers (*i.e.*, multiplex detection) associated with specific diseases at the point-of-care (POC), are highly desirable. In addition to rapid diagnostic solutions, extremely precise methods, including advanced imaging techniques, are also required for accurate diagnostics and follow up care.[531] SERS imaging has revealed itself as a promising technique that covers several of these characteristics and requirements. However, each system is different from another and therefore different measuring methods should be considered. The most common and simple methods, well-known in the SERS

community, consist in general of a SERS active substrate and a detector which registers the Raman signal generated when the target molecule is combined with the substrate, while irradiating with a laser (direct method). The indirect method makes use of receptors, disposed in the substrate forming a receptor/target signal. A wide variety of advanced methods have been developed to cover such a diversity of biosamples.

SERS based DNA detection methods

Nucleic acid biomarkers, such as DNA, mRNA, and microRNA (miRNA), have long been considered valuable diagnostic indicators to monitor the presence and progression of various diseases. For *in vitro* nucleic acid detection, a label-free SERS-based technology called "Inverse Molecular Sentinel" (iMS) can be used as a homogenous bioassay in solution or on a chip platform (**Figure 5.2A**). The sensing mechanism is based on hybridization of target sequences and DNA probes, resulting in a distance change between SERS reporters and the nanoplatform's plasmonic active surface. As the field intensity of the surface plasmon decays exponentially as a function of distance, a change in the distance in turn modulates the SERS signal intensity, thus indicating the presence and capture of target sequences. The iMS technique is a single-step detection method, with simple delivery of sample solutions onto DNA probe-functionalized nanoplatforms, followed by measurement of the SERS signal after probe incubation. Target sequence labeling and sample washing to remove unreacted components are not required, rendering the technique simple, easy-to-use, and cost-effective. The iMS methodology can be used in solution format for multiplexed detection of miRNA biomarkers of cancer.[532] Alternatively, the iMS approach can also be adapted to a nanochip platform (see Section 5.3 below), which is based on a metal film on nanoparticle (MFON) array substrate, developed for the arguably first analytical application of SERS.[533,534] The MFON type substrate was further developed and referred to as a "Nanowave" chip (**Figure 5.2**B).[535-537] The Nanowave chip has been used for multiplex detection and diagnosis of host genetic biomarkers of respiratory viral infection and infectious diseases such as the dengue virus (**Figure 5.2**C).[538]

Another sensitive yet simple DNA detection method involves a nanoplatform using ultrabright SERS core–shell probes called "nanorattles" (**Figure 5.2**D-H).[539] In this sensitive sandwich assay, the presence of nucleic acid targets is detected by sandwich hybridization of magnetic beads having capture probes and ultrabright SERS-encoded nanorattles having

reporter probes. Upon hybridization, a magnet is applied to concentrate the hybridized sandwiches at a detection spot for SERS measurements. Using this method, a specific DNA sequence of the malaria parasite *Plasmodium falciparum* could be detected with a detection limit of approximately 100 attomoles. Single nucleotide polymorphism (SNP) discrimination of wild type malaria DNA and mutant malaria DNA, which confers resistance to artemisinin drugs, was also demonstrated.[540] The simplicity of the method renders it a suitable tool for molecular diagnostics at the point-of-care (POC) and in resource-limited settings.

A SERS-based bioassay using plasmonic nanorattles was also developed for rapid diagnosis of head and neck squamous cell carcinoma (HNSCC), which is a critical challenge, particularly in low and middle income countries. In a blinded HHSCC trial, the SERS nanorattle-based technique demonstrated a sensitivity of 100% and specificity of 89%, supporting its use as a useful alternative to histopathological diagnosis.[541] In comparison to histopathology, which can take several months in remote limited-resources regions, the SERS nanorattle method can provide a diagnosis within only a few hours, allowing for earlier treatment before the onset of distant metastases.
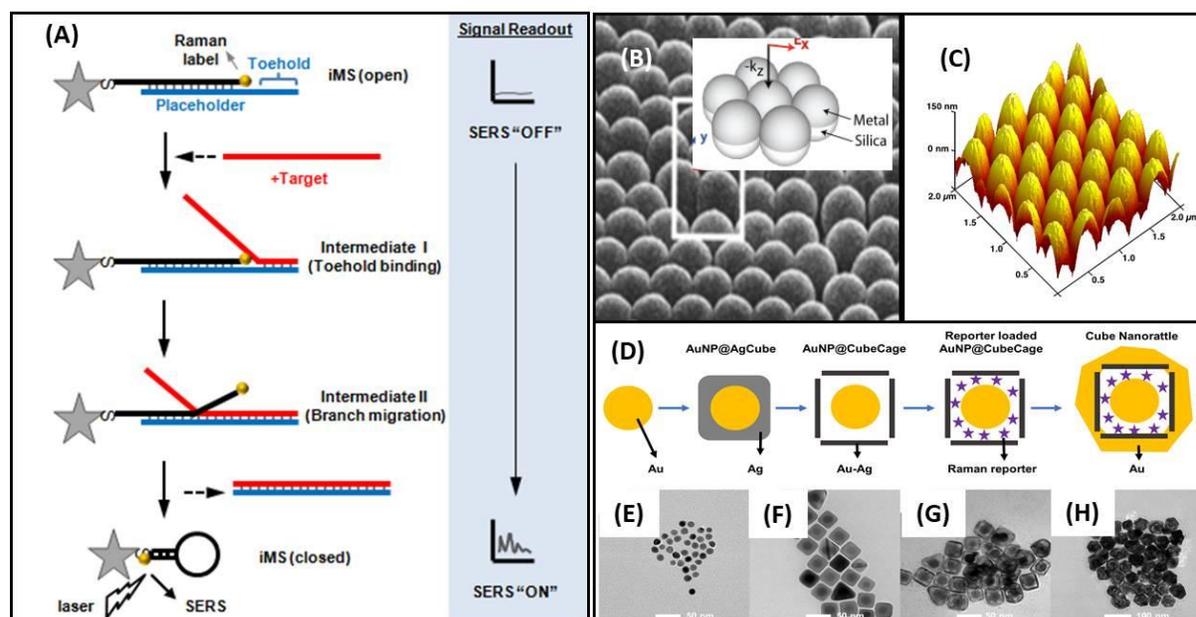
Figure 5.2. A). Operating principle of the iMS detection approach ("Off-to-On" scheme). The "stem-loop" DNA probe of the iMS, having a Raman label at one end of the stem, is immobilized onto a metallic nanoparticle or nanostar *via* a metal-thiol bond. In the absence of the target, the probe is "open" with very low SERS signal ('Off' state). Upon exposure to

a target sequence, the target first binds to the toehold region (intermediate I) and starts displacing the DNA probe from the placeholder *via* branch migration (intermediate II), finally releasing the placeholder from the nanoparticle system. This allows the stem-loop to "close" and brings the Raman label closer to the plasmonic metal surface, producing a strong SERS signal ('On' state). Adapted with permission from Ref. 532. Copyright 2016, American Chemical Society. (B) Nanowave platform consisting of nanosphere arrays coated with a silver film. Adapted with permission from Ref. 533. The inset represents the unit cell used as a 3D model for Finite Element Modeling (FEM) calculations. Adapted with permission from Ref. 535. Copyright 2012, American Chemical Society. (C) AFM image of a bimetallic Nanowave chip used for detection of Dengue nucleic acid biotargets. Adapted with permission from Ref. 538. Copyright 2014, Royal Society of Chemistry. (D) Synthesis of cubic nanorattles to be used in an integrated "Lab-in-a-Stick" device. TEM images of: (E) AuNP; (F) AuNP@AgCube; (G) Reporter-loaded AuNP@CubeCage; (H) Cube nanorattles. Adapted with permission from Ref. 539. Copyright 2018, Springer Nature.

Another promising method for SERS biosensing is based on anisoptropic gold nanoparticles such as gold nanostars (GNS). For *in vivo* monitoring, implanted SERS nanosensors based on GNS have been developed as "smart tattoos" for the detection of nucleic acid targets. *In vivo* detection of nucleic acid targets was demonstrated using implanted GNS nanoprobes in the skin of a large animal model (pig).[542] The *in vivo* nanosensor involved the iMS detection scheme using GNS with plasmon bands in the NIR tissue optical window, rendering them an efficient platform for *in vivo* optical detection. Nanorattles with Raman reporters trapped between the core and the shell were used as an internal standard system for sensor self-calibration. These results illustrate the usefulness and translational potential of implanted SERS nanosensors for *in vivo* biosensing.

GNS also provide an excellent multi-modality theranostics platform that combines SERS detection with other modalities including two-photon luminescence (TPL), photodynamic therapy (PDT), photothermal therapy (PTT) or photoimmunotherapy, to treat metastatic cancer and produce an anti-cancer 'vaccine' effect.[543] A method to synthesize biocompatible GNS was developed without using a non-toxic surfactant, suitable for *in vivo* applications and future clinical applications.[183] Plasmon-enhanced and optically modulated delivery of nanostars into brain tumors in live animals has been demonstrated. A quintuple-modality

nanoreporter based on gold nanostars for theranostic applications using SERS, TPL, magnetic resonance imaging (MRI), computed tomography (CT), and PTT has also been reported,[544] which overcomes the limitations of conventional optical methods, typically limited to SERS from superficial levels, due to the attenuation caused by highly scattering and absorbing tissue.

Immunoassays

Immunoassays are well-established biochemical tests that measure the presence or concentration of a specific target molecule in solution, through the interaction between antibodies and antigens. To date, enzyme-linked immunosorbent assays (ELISA) using well plates, or chemiluminescence using magnetic beads, have been extensively employed as immunoassays for diagnostic applications. However, such methods have drawbacks, including tedious washing steps, long assay times, the need for large sample volumes, and poor limits of detection (LOD). The LOD is a particularly important parameter, as it is directly related to the capability of using such platforms for early stage diagnosis of the disease. Apart from high analytical sensitivities and low LOD, SERS features other intrinsic benefits, such as facile molecular fingerprinting, operation over a wide range of excitation wavelengths, reduced photo-bleaching and the ability to extract highly resolved spectroscopic signatures. Accordingly, SERS-based assays are well suited for the simultaneous detection of multiple bio-targets within complex analytical samples, such as blood and plasma.[545] Nonetheless, the application of SERS in quantitative analysis of biomolecules is problematic due to the difficulties associated with reproducing SERS enhancement levels. Such variability stems from a lack of control over factors including the degree of particle aggregation, particle size and analyte distributions on particle surfaces. To address some of these critical issues, integration of SERS with microfluidics has revealed several useful advantages over conventional macroscale SERS platforms.[546] For instance, the ability to operate within a continuous flow regime and to generate homogeneous mixing conditions within microfluidic networks, has been shown to afford quantitative SERS-based analysis. The combination of SERS and microfluidics appears to provide an ideal means for ensuring sensitive detection with reproducible measurement conditions and well-defined detection zones. Additional benefits of such an integrated system for bio-analytics includes

the ability to make measurements using minimal sample volumes and low analyte concentrations.

5.3. Devices

The point-of-care (POC) concept, which is directly related to lab-in-a-stick" portable devices and microfluidic systems coupled with immunoassay methods, has already been mentioned several times in this Perspective. Such devices rely on the idea of achieving easy, fast but accurate medical diagnostic tools, which can be used everywhere, available for everyone, with no need for an expensive technology. This idea goes hand in hand with the concept of reaching a more personalized medicine. For that purpose, nanotechnology has provided the possibility of reducing device size and producing such point-of-care tools. Several devices have been reported and many more are under development.[547]

Microfluidics-based devices

Chon *et al*.[548] reported a SERS-based on-chip immunoassay, using magnetic beads in a continuous flow regime. Magnetic immunocomplexes were trapped by solenoids embedded in microfluidic channels. Whilst successful in application, memory effects caused by the deposition of nanoparticles on channel walls affect both measurement reproducibility and sensitivity. To address these issues, the same group[549] developed a two-phase liquid/liquid segmented flow system for SERS measurements (**Figure 5.3**). This system allows the generation and manipulation of monodisperse, nanoliter-sized liquid droplets in an immiscible carrier fluid, with high throughput. Compared to single phase flow, the localization of reagents within discrete and encapsulated droplets enhances mixing, minimizes residence time distributions, and affords ultrahigh analytical throughput. An integrated microfluidic system, including droplet generation, transport, mixing, merging and splitting modules, has been developed for both efficient immunoreactions and wash-free assays, where immunoreactions could be efficiently performed by transport through multiple winding channels. Subsequently, large droplets including magnetic immunocomplexes were split into daughter droplets for the wash-free immunoassay. It should be noted that the integration of SERS with such a microfluidic platform can be used to perform rapid, sensitive and safe immunoassays of hazardous materials, since all immunoreaction and detection processes are carried out within isolated nanoliter volumes, in an automated manner.

More recently, SERS studies have been combined with microfluidics to perform immuno- and cellular assays. SERS-based microfluidic technology can also be applied to DNA analysis. Current DNA detection techniques typically require DNA amplification using PCR and detection of amplified signals by fluorescence. It is thus possible to detect very low concentrations of DNA without amplification using SERS-based microfluidics, due to enhanced detection sensitivity. It is also possible to detect multiple analytes simultaneously, since SERS target signals are much narrower than fluorescence bands. For use in medical diagnostics, an important aspect would be in the miniaturization of the optical sensing device. Although typical dimensions of microfluidic channels are very small, most Raman spectrometric systems comprise bulky optical components, including lasers, microscopes, monochromator and detector, which are external to the microfluidic channel. A fully integrated and portable Raman system would be required for real-time, in-the-field analysis. Such integrated systems are likely to become a powerful next-generation biomedical diagnostic tool. In conclusion, the use of microfluidic platforms allows an exquisite degree of control over mixing times, scattering geometries, localized heating and photo-dissociation. Consequently, their marriage with SERS-based detection schemes affords reproducible and quantitative analysis. We propose that SERS-based microfluidic platforms will have a substantial impact on biomedical diagnostics in the near future. In this respect, it is also important to realize that a closer collaboration between medical and scientific communities will be critical in creating such robust platforms for a wide range of diagnostic applications.
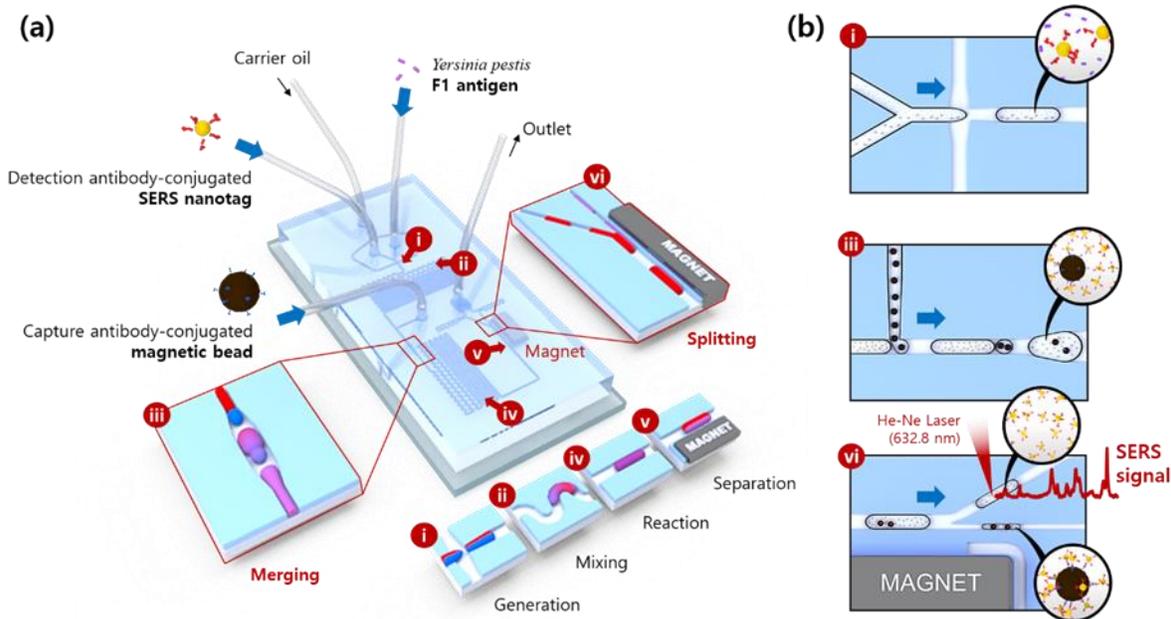
Figure 5.3. (a) Schematic illustration of an integrated SERS-based microfluidic channel composed of six microdroplet compartments: (i) droplet generation from the shear force at the interface between the aqueous and oil phases, (ii) droplet mixing for the first immunoreaction, (iii) droplet merging for the formation of magnetic immunocomplexes, (iv) droplet mixing for the second immunoreaction, (v) droplet splitting for the wash-free immunoassay, and (vi) Raman detection of unbound SERS nanotags in supernatant solution droplets. **(b)** Extended images for (i) droplet generation, (iii) droplet merging, and (vi) droplet splitting. Adapted with permission from Ref. 546. Copyright 2017, American Chemical Society.

In relation with infectious disease detection, Vo-Dinh *et al.*[539] developed a method for the direct detection of pathogen RNA in blood lysate, which uses a SERS-based bioassay integrated in a "lab-in-a-stick" portable device. This device could detect RNA from *plasmodium falciparum* malaria parasite, directly from an infected red blood cell lysate. This was the first report of SERS-based direct detection of pathogen nucleic acid in blood lysate without nucleic acid extraction or target amplification, underlining the potential of this integrated bioassay for field use and point-of-care diagnostics. Direct detection of genetic biomarkers in body fluid lysates without target amplification is likely to revolutionize nucleic acid-based diagnostics.

Another alternative lab-on a chip (LOC) device combined with SERS that allows high-throughput SERS measurements under reproducible measurement conditions, has been developed by Popp and co-workers.[490,550,551] Here, the walls of a glass microfluidic channel system were silanized to induce the formation of aqueous droplets in a stream of mineral oil. *Via* various ports, aqueous solutions of the target analytes, the silver colloid and the aggregation agent, as well as water to dilute the sample, were pumped into the channel system. As a consequence, droplets were formed and guided through a meandric channel to guarantee complete mixing of the droplet content. Finally, SERS spectra were recorded by focusing the laser beam into the channel with 1 s integration time. As the recorded spectra were measured within the droplet as well as within the mineral oil phase, all spectra with contributions from the oil were subsequently separated from the dataset. Thus, a powerful LOC-SERS system was developed allowing for the recording of large databases in a short time. In the case of the antibiotic levofloxacin, the potential of the LOC-SERS detection scheme in bioanalytics was illustrated by employing artificial as well as human patient urine as matrix.[490] Interestingly, the SERS signal of the analyte molecule was increased upon dilution of the spiked artificial urine matrix with water, which has been attributed to a lower competition for free binding sites on the metallic surface. Moreover, patient urine samples were applied as a matrix and the target analyte levofloxacin was spiked within these samples. For all investigated urine samples, the root mean square error of prediction (RMSEP), which was interpreted as the limit of detection, was between 0.057 mM and 0.16 mM. In a second example, the standard addition method was applied to detect nitroxoline in spiked human urine samples using LOC-SERS as analytical tool.[550] Here, urine samples from a healthy volunteer were spiked with the target analyte and the detection parameters were estimated by means of LOC-SERS, *i.e.* the limit of detection was ~3 μM (0.57 mg/L), the limit of quantification was ~ 6.5 μM (1.23 mg/L) and the linear range was between 4.28 and 42.8 μM (0.81−8.13 mg/L). As the minimum inhibitor concentration (MIC) value of the most common uropathogens is within this range, the LOC-SERS technique illustrated its great potential in biomedical detection. Moreover, seven clinical urine samples were spiked with nitroxoline to simulate real samples with unknown concentrations. The standard addition method was applied and SERS spectra were analyzed employing the multicurve resolution alternating least-squares algorithm to predict the initial concentration of the target analyte.

Thus, LOC-SERS was proven as an excellent tool in biomedical application fields, thereby opening the path toward precision medicine, to control and adjust the drug level and avoid toxicity effects. In order to identify mycobacteria, the cells were first disrupted with a bead-beating system and in a second step, SERS spectra were recorded by employing a LOC-SERS system.[551] Thus, in general all molecules within cells were allowed to interact with the metallic surface and could contribute to the overall SERS spectra. Within this study, six species of mycobacteria were applied and it was found that the SERS spectra were dominated by the cell wall component mycolic acid, which features a structure that is specific for different mycobacteria species. Due to the LOC-SERS technique, a large dataset was established for all investigated species in a short time, *i.e.* more than 2100 single SERS spectra of one species could be recorded in 1 h. To discriminate the bacteria, a hierarchical chemometric model was developed. Thus, the potential for future applications to provide reliable information to physicians was clearly illustrated. In the future, SERS in microfluidics should play an important role for automated sample feeding and sensing operation for online monitoring, such as drug monitoring in intensive care units.

Cartridge SERS

As an alternative to LOC-SERS and for application in scenarios where no monitoring of a target analyte concentration over a time period is required, *e.g.* estimating the contamination of surface water with drug molecules to initiate measures against pollution, a SERS-based cartridge system was developed.[552] Here, the SERS substrate was embedded within a cartridge and after incubation with the analyte solutions, SERS spectra were recorded. For each measurement a different SERS-active surface was required and the cartridge system was recycled. In future applications such as food analytics or environmental monitoring, the development of disposable cartridges with an implemented SERS substrate, fabricated cost-efficiently, will be of high importance.

5.4. Future Outlook

SERS nanosensors and nanoreporters are effective and versatile platforms for biochemical sensing, imaging and medical theranostics. SERS detection techniques, which have high multiplexing capability, will be critical toward future personalized and genomic medicine. The ability to simultaneously detect multiple biomarkers, such as nucleic acids (DNA,

mRNA, miRNA, *etc.*) is important for many applications and for the future medicine based on point-of-care diagnostics, high-throughput screening systems, biology research and early medical diagnostics, at the gene and molecular level. Novel methods therefore should be found to explore and exploit at maximum the possibilities offered by SERS. Novel substrates such as gold nanostars also provide useful tools for *in vivo* SERS sensing and theranostics applications. Due to their well-established features, including the lack of photobleaching and photodegradation, the ability to perform multiplexed bioanalysis, and narrow spectral fingerprints, SERS nanosensors and nanoprobes coupled with advanced POC devices, may lead to important theranostic applications for the medicine of the future.

6. SERS in Biomedicine: From Single-Molecule Detection to *in vivo* Studies

SERS has been proved extremely useful toward a large number of analytical issues related with biomedical applications. After describing in the previous section, the main techniques, methods and devices that have emerged as a consequence of technological advances, we now focus on the improvement of diagnostic tools that may lead to applying selective treatments for various diseases. All of these examples are based on the properties of SERS as an analytical technique. There is thus a current need to develop rapid, sensitive, simple, and reliable devices for the identification of ions (*e.g.* calcium for bone regeneration), cancer biomarkers or pathogens such as different kinds of bacteria. Additionally, improvements in imaging modalities have been inspired by the development of more complex study systems, which are more realistic with respect to human bodies, typically based on 3D cell cultures, animal models or *in vivo* experiments. To image such systems, high penetration depth, no photobleaching and minimum overlap between signals is desired. In the NIR biological transparency windows (650-950 nm (NIR-I); 1 to 1.35 µm (NIR-II); 1.5 to ~1.8 µm (NIR-III)),[553,554] we find optimal light transmission through tissue, with maximum penetration and minimized autofluorescence. Thus, thanks to the accessibility to NIR-responsive SERS substrates and to its non-invasive character that avoids the need for fixing cells, confocal SERS imaging has also found a niche as a promising bioimaging technique.

From single-molecule detection through *in vivo* studies, we can find an huge variety of examples which profit from SERS detection. We start this section by dealing with the

simplest systems based on biomarker detection and detection of pathogens, either directly or indirectly, measuring their internal signaling. We will then focus on single cell imaging, continue with complex cell cultures, tissues and finally with a perspective toward using SERS for *in vivo* studies that may allow image-guided surgery of tumor margins and development of endoscopy-SERS coupled systems to identify and localize internal tumors.

6.1. Detection of Biomarkers

SERS-based biomedical diagnostics is vital for early biomedical monitoring. Various targets have been reported for small molecules (dopamine,[555,556] folic acid,[557] toxin,[558] *etc*.), macromolecules (vascular endothelial growth factor,[559] prostate-specific antigens,[560] alpha fetoprotein,[561] DNA,[562] *etc*.).

One of the most fascinating and -in terms of spectroscopic interpretation- most challenging aspects of biomedical applications in SERS are the spectra produced by the biomolecular species directly, in the absence of a tag, reporter, or indicator molecule. Such label-free, intrinsic SERS spectra have been reported from all kinds of cells, ranging from bacteria and other microorganisms[563,564] through plant and animal cells, including body fluids, tissue sections, and cell or tissue extracts. SERS spectra from bacterial and eukaryotic cells in cell cultures add significantly to our understanding of the interaction of plasmonic nanostructures with the intracellular and extracellular environments. Therefore, by controlling or defining the interaction of the SERS substrate with the biological system, intrinsic SERS signals can be used to detect specific biomarkers[565] or physiologically relevant biomolecular species inside or near individual cells, such as AMP,[566,567] important metabolites in normal[568] and tumor cells,[569] neurotransmitters,[567,570] or trehalose.[571] SERS microscopy always indicates the presence of an interaction of the substrate with the samples and allows, *e.g.*, mapping the position of plasmonic nanoparticles.[572-574] An important aspect in SERS experiments of live cells, and when gold or silver nanoparticles are used as plasmonic substrates, rather than when cells are attached to solid sensors[575,576] or nanoelectrodes,[577] or when substrates are inserted into cells in needle-type approaches,[568,578-581] is the control of the plasmonic properties, which are critical for SERS enhancement. Different from labeled SERS tags, the sensitivity of the SERS experiment cannot be modified by changing the type or number of reporter molecules, *e.g.*, by exploiting molecular resonance of a dye molecule, but only by

optimizing the SERS enhancement of the plasmonic nanostructure, and by maintaining it inside the biological environment. If nanoparticles enter cells, they are processed depending on their uptake mode and their constantly changing bio-functionalization, which occurs before, during, and after uptake, *i.e.* in the cellular exterior and inside different cellular compartments. Gold nanoparticles are very efficient SERS substrates for label-free cellular probing due to tunable size and shape, which influence both their enhancement, aggregate formation, and transport inside cells and tissues. As examples, spheres,[566,574] shells,[582] as well as flowers,[583] nanorods[584] and nanostars[575] have been used to record intrinsic SERS spectra from cells. Metal nanoparticles for intracellular SERS can be stabilized by silica coating with varying porosity, so that analyte molecules can reach the plasmonic surface while aggregation in the endosomal system is controlled.[567,573]

Experiments quantifying the amount and distribution of nanoparticles in cells by mass spectrometry,[585] together with high-resolution ultrastructural imaging of the cells and the nanoparticles help understanding the changes in plasmonic properties and SERS enhancement of a particular type of SERS nanoprobe. Such experiments clearly show that the microscopic distribution and SERS spectral signatures are correlated, rather than the number of nanoparticles that are located in a cell,[586] yet the morphology and interparticle distances within nanoaggregates are crucial. The interaction with different kinds of biomolecules in the cellular environment results in aggregates with high variation in SERS enhancement. Specifically, the combination of non-ideally spherical nanoparticles was recently shown to have a strong influence on the local field enhancement of gold nanostructures for NIR excitation,[587] and is expected to play a major role in the different overall enhancement observed inside cells. Modeling the electromagnetic field distributions of highly SERS-active particles[588] and their arrangements that are representative of typical specific biomolecule-nanoparticle in the complex biosystem,[589] including the characterization of dark modes, which are expected to play a major role in the SERS enhancement,[590] will help optimize SERS signals *in vitro* and *in vivo*. Improvements in elucidating nanoaggregate geometries in the biological environment are expected from ultrastructural imaging and tomography.[573,591]

Understanding the formation of the biomolecular corona, *i.e.* the modification the surface of a nanoparticle undergoes inside a biological system, is a main prerequisite for all applications

of nanoparticles in theranostics and biotechnology, including SERS. In fact, SERS itself is one of the few tools that can be used to understand the composition, structure and dynamics of the biomolecular corona, not only in cells but also in the related biofluids and cell culture media. As an example, the protein corona of silver nanoparticles largely differs under identical incubation conditions from that of gold nanoparticles,[592] and of their silica-coated versions,[573] while the specific ring-shaped morphology along endosomal membranes that was observed for silver nanoparticles can be related to their particular surface composition.[592] The endosomal system of eukaryotic cells is easy to target, yet highly complex and of varying molecular composition and pH. The very dynamic nature of this organelle makes it ideal for assessment of optical and multifunctional nanoprobes for drug delivery[593-595] and theranostics.[596,597] Plasmonic structures, as key components of SERS probes, can offer high local optical fields for both sensitive diagnostic probing with SERS and efficient therapeutic tools. Particularly attractive are those multifunctional probes combining photothermal capabilities with the potential to monitor localization and therapeutic efficiency by SERS, and to better understand their action.[598-603] Among them are also materials with SERS properties that do not rely on the plasmonic properties of gold or silver, such as molybdenum oxide,[604] or 2D nanomaterials in chemo-photothermal therapy such as black phosphorous[605] or graphene.[606,607] Of course, such non-plasmonic nanoparticles, *e.g.* from ZnO, are also very attractive tools for cancer detection, and apart from their role in novel SERS tags[608] might serve for intrinsic SERS detection in the future.

From the endosomal system, nanoprobes can be targeted to other organelles, for example the nucleus, where processes related to drug and/or nanoparticle induced apoptosis and DNA structure[609] can be monitored by SERS. Considering the therapeutic possibilities of the nanoparticles and all reporter-based sensing enabled by SERS, for example monitoring of pH,[610,611] presence of ROS,[612,613] NO signaling,[614] or even temperature,[615,616] a whole SERS-based toolbox for monitoring cellular physiology is at hand. Apart form the nucleus, also mitochondria have been targeted and can be observed by SERS,[617,618] in particular due to their important role in apoptosis.[619]

Nevertheless, a major challenge posed by the strong variations in Raman cross-sections of the different molecular groups renders some classes of molecules in the cells undetected, in particular cellular membranes and their lipids, even if probes are known to reside in close

proximity to cell membranes, in the many examples of endocytotic delivery. Outside cells, SERS spectra of pure lipids and lipid vesicles have been reported, efficient interaction of molecules and SERS substrates being obtained by functionalization of nanoparticles,[620-622] by using lipid-alkanethiol bilayers,[623] or the *in situ* synthesis of gold nanoparticle-liposome composite structures that mimic the composition of the cellular outer membrane.[591] However, reports of *in situ* and *in vivo* lipid SERS spectra are relatively rare.[624,625] In complex biosystems, where other molecules are also present, contributions to SERS spectra by lipids have been found mainly when the interaction with the SERS substrates was enhanced, *e.g.* by using plasmonic substrates that directly connect to the outer cell membranes, such as nanoelectrodes.[577] Lipid signals are also detected when the abundance of lipids in a biological system is particularly high.[626,627] As recently evidenced in a macrophage model of Leishmania infection, SERS microscopy can show the distinct distribution of cholesterol and its ester ergosterol, as well as of glycoinositol-phospholipids, all of which are secreted by the parasite in vacuoles inside the cells and are highly specific for the infection.[627] Lipid spectral contributions have also been discussed in a SERS analysis of exosomes,[628] although most SERS characterizations of these important organelles in cancer diagnostics rely on protein biomarkers.[565,629,630]

From the mere perspective of accurate detection, the controllable selectivity of plasmonic substrates that are used to obtain fingerprint-like SERS spectra from complex bioorganic samples will always compete with the selectivity of a targeting chemosensor used for functionalization of a labeled SERS tag of controlled enhancement and its reproducible spectral information due to a specific 'flavor'. From the perspective of compositional and structural information that is gained from the biological cell, the spectroscopic information is of completely different quality, and, even though it relies on the interaction with a plasmonic nanostructure provides enormous insight into cellular biochemistry.

Biomarker detection using SERS tags

Although various SERS active plasmonic substrates can be used for biomolecule sensing, with great potential in biodetection, often matrix effects disturb detection sensitivity and accuracy. A potential strategy to address this issue would be based on developing ultrasensitive SERS detection based on signal amplification.[631] SERS tags have been used

for DNA amplification in biomedical detection, *e.g.* applying PCR as an amplification strategy for highly sensitive detection of DNA with femtomolar sensitivity.[632] NP assemblies additionally exhibit high signal to noise SERS signals which can be used to distinguish different targets.[633-635] An interesting strategy has been developed based on SERS-encoded discrete silver pyramids (**Figure 6.1A**).[634] Three silver NPs assembled in DNA-directed pyramids were labeled with three different Raman tags. Through a specific bioreaction between the aptamers and their corresponding targets, the reconfigurable structured pyramids switched into a smaller gap state, which induced stronger SERS. LOD in the attomolar range were obtained for the multiplex detection of mucin-1, thrombin, and PSA. In these systems, other signals such as circular dichroism and fluorescence are used next to SERS as screening signals.[636]

SERS signals have also been developed for quantitative detection of specific classes of biomolecules *in situ* in living cells (miR-21, telomerase).[637,638] Combination of two signals (SERS, CD) which can operate independently, detection of two types of targets (nucleic acids or proteins) was achieved, using two independent graphene oxide–Au NP assemblies (**Figure 6.1**B).[633] Hybridization of the molecular probe with the micro-RNA miR-21 leads to the separation of the Raman tag from GO reducing the Raman signal, while EpCAM recognition decreases the CD signal in parallel. Also based on the multiple signal sensing principle, assemblies of Au nanorod dimers with upconverting nanoparticles (UCNP) in a core-satellite structure, successfully induced two independent signals (SERS and luminescence) (**Figure 6.1**C).[635] The miR-21 target triggered the disassembly of Au NR dimers, leading to decreased Raman signal, while the target telomerase induced release of upconverting nanoparticles from Au NRs, resulting in increased luminescence, leading to LOD for miRNA of 0.011 amol/ng$_{RNA}$, and LOD by luminescence of 3.2×10^{-13} IU (**Figure 6.1**C). Other structures such as Au-Au-UCNP trimers, encoded with SERS and luminescence also enabled ultrasensitive monitoring of dual cancer biomarkers (mucin-1 and Alpha-fetoprotein).[639] Detection of multiple targets is crucial for early stage diagnosis, so that false positive or negative signals can be eliminated in biomedical samples. Future work toward optimizing stability in real samples could improve further point-of-care applications. Single-molecule SERS and real-time SERS imaging of live cells provide useful tools for monitoring intracellular compartments and targets.[640]
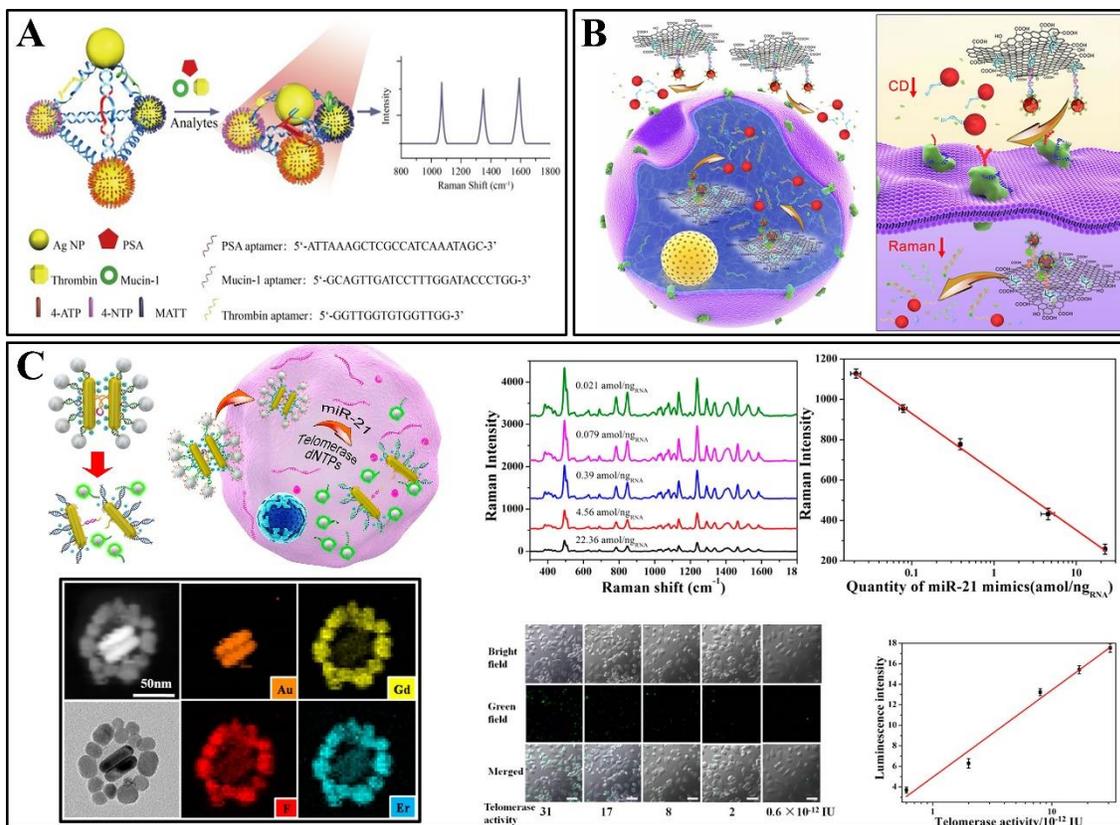
Figure 6.1. (A) Multiple detection of biomarkers (PSA, thrombin, and mucin-1), using SERS encoded Ag-pyramids based on three Ag NPs modified by different Raman reporters. Adapted with permission from Ref. 634. Copyright 2015, Wiley-VCH. (B) GO–Au structures used for simultaneous detection of epithelial cell adhesion molecule (EpCAM) and miR-21 using CD and SERS signals. Adapted with permission from Ref. 633. (C) Au NR Dimer-UCNP Core−Satellite nanostructures for miR-21 SERS detection and telomerase detection by luminescence. Adapted with permission from Ref.635. Copyright 2017, American Chemical Society.

6.2. Detection of Circulating Tumor Cells

The fast and accurate optical analysis of cells in biofluids for cancer diagnosis is a current matter of intense research. Such determinations face a major challenge related with the usually small content of the cells of interest in the biofluid. Circulating tumor cells (CTCs) in blood are characterized by extremely low CTC concentration, ranging from units to tens in 8 mL of blood (standard volume for analysis) in stage IV cancer. Because of such extremely low CTC concentrations in blood, many methods use an enrichment process prior

to the quantification step, some of them based on physical properties such as size, density or deformability, and others resting on biological properties such as protein expression. By far, the most common protocol makes use of magnetic particles, usually comprising iron oxide, functionalized with antibodies against the epithelial cell adhesion molecule (EpCAM). The rationale for this choice lies on the idea that epithelial linage is not common in blood and thus, epithelial cells in blood are most likely related to cancer. EpCAM-magnetic particles are thus exposed to the blood sample and, after an appropriate time for conjugate binding to the targeted cells, they are extracted by means of a permanent magnetic field. These systems typically use more than one antibody. For example Cell Search® (Jansen Technologies) use also anti-CD45, attached to a dye, as a negative control to detect false positives due to the partial retention of anti-EpCAM by the mononuclear cell fraction of blood.[641] Approaches have recently emerged to address these issues, mainly based on encoded plasmonic nanoparticles and SERS, which enable the multiplex quantification of different CTCs.[642,643] Advantages of this methodology include ultrahigh analytical resolution combined with a virtually unlimited number of available codes and thus markers, that can be studied simultaneously. Unfortunately, state-of-the art SERS acquisition times are longer than 10 ms, hindering the use of this technique for real samples, where a single CTC is diluted among billions of other cells. Thus, a viable solution could be achieved by combining the acquisition speed of fluorescence (down to ns) for rapid screening and sorting,[644] with the analytical resolution of SERS applied to the smaller cell fraction, previously separated by physical or molecular techniques.

6.3. Detection of Pathogens

The detection of the causing agent of given infectious diseases has also gained much interest. The specificity and detection limit that SERS allows are suitable for the detection of low abundance but dangerous pathogens, which pose risk for human health. The most common infections are produced by bacteria such as *E. coli*, *S. aureus* or *S. typhimurium* that can commonly be transmitted *via* food and water. Therefore, effective detection tools are necessary to avoid spreading of bacteria colonies and to rapidly identify infection by different pathogens in humans. It is also of high importance finding fast and inexpensive methods that

can be used in underdeveloped countries, where drinking water accessibility is reduced and contamination is very common.

As recently reviewed,[563] the first report that SERS directly on bacteria was reproducible enough to allow bacterial discrimination and identification to the species and sub-species levels was reported by Jarvis and Goodacre.[645] In this study bacteria were mixed with colloids, dried and after SERS detection multivariate discriminant analysis was used for identification. Following this work, Ziegler and colleagues reported a similar analytical approach but introduced a novel and robust identification procedure incorporating SERS barcodes.[646] However at the time these studies did not attempt to identify the biochemical origin of the SERS signal. By contrast, recent studies have employed the use of isotope substrates, such as glucose uniformly labeled with ^{13}C or ^{15}N ammonium hydroxide, during bacterial growth – a process called stable isotope probing (SIP).[647] In this process heavier isotopes are incorporated into bacterial biomass, resulting in changes of vibrational frequencies (due to reduced mass in the vibrations) and thus leads to Raman/SERS shifts toward lower wavenumbers. This process allows the origin of vibrations to be elucidated and, with reference SERS spectra of natural and isotope standards of key molecules, enables unequivocal chemical identification. The first study by Premasiri *et al.*[648] showed that purine-related molecules were predominantly measured by SERS of intact bacteria, while other studies using SERS-SIP have also used this principle for the same purpose.[649,650] This approach has also been used to image single bacterial cells and identify phenotypic function in mixed communities.[651] SERS is becoming a powerful tool for characterizing bacterial pathogens, where this method can be used to assess antibiotic susceptibility or resistance, both by probing the bacteria directly[652] or from measuring the volatile organic compounds from the headspace of bacteria cultures.[653]

Rather than detecting bacteria directly, Liz-Marzán and co-workers aimed at measuring their intercellular signaling processes, *i.e.* quorum sensing (QS). Most bacteria exist in nature as biofilms, which support their QS, a cell-to-cell communication mechanism that allows bacteria to monitor and respond to cell density and changes in the environment. Because QS and biofilms are involved in the ability of bacteria to cause disease, it is important to find methods for the noninvasive analysis of QS in natural bacterial populations. Bodelón *et al*.

reported the preparation of nanostructured plasmonic substrates to monitor, using label-free SERRS, the presence of pyocyanin, a QS signaling metabolite in growing *Pseudomonas aeruginosa* biofilms and microcolonies.[654] Pyocyanin, a heterocyclic nitrogen-containing compound of the phenazine family produced by *P. aeruginosa*, and excreted into the environment, plays important roles in biofilm morphogenesis in this microorganism. The strategy was based on the use of hybrid materials comprising a plasmonic component within a porous matrix that allows diffusion of small molecules only.[655] Although different combinations were tested, the use of mesoporous silica-coated micropatterned supercrystal Au nanorod arrays enabled SERRS detection of QS-behavior (*i.e.* pyocyanin expression) at early stages of biofilm formation and allowed imaging the phenazine produced by small clusters of bacteria colonizing micron-sized plasmonic features (25 μm^2 on average), as shown in **Figure 6.2**. Subsequent work demonstrated the application of this method to study interspecies bacterial interactions, both for separated bacterial colonies[656] and for mixed colonies.[657]
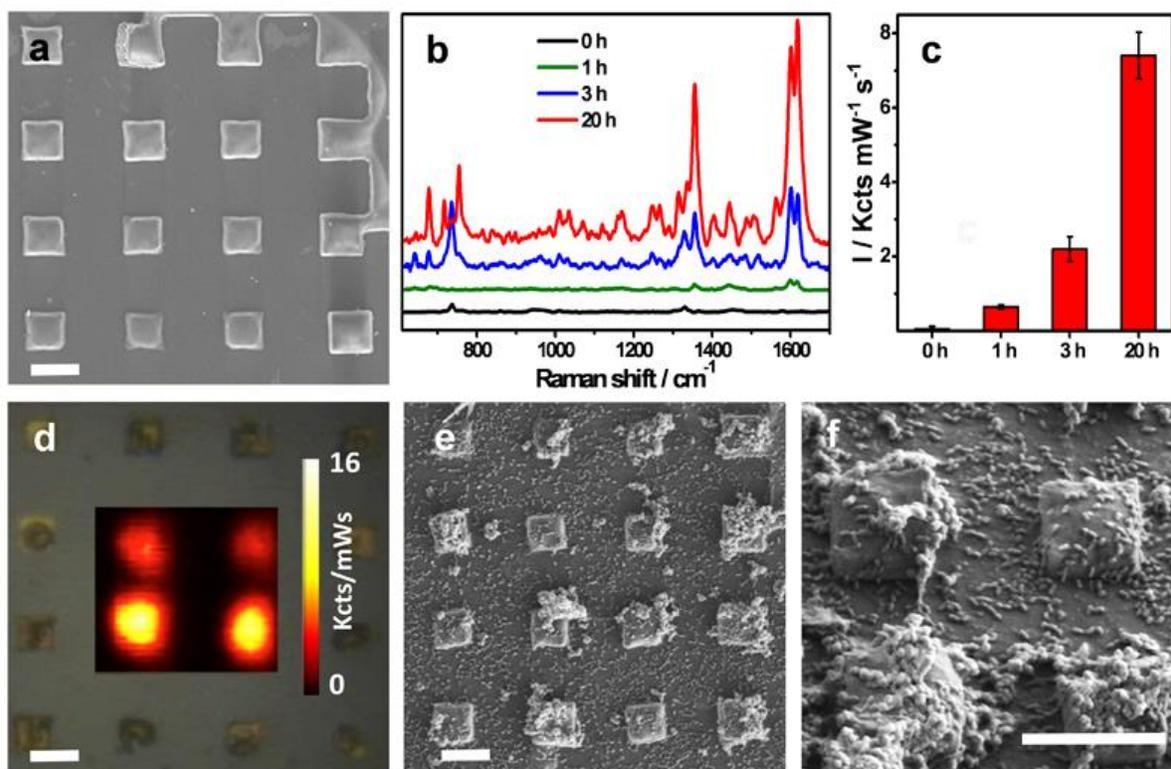
Figure 6.2. *In situ* detection and imaging of pyocyanin produced by *P. aeruginosa* PA14 grown on micropatterned SiO$_2$-coated Au nanorod supercrystal substrates. a) SEM images;

scale bar: 5 μm. b) Representative SERRS spectra measured at 0, 1, 3 and 20 hours of bacteria growth. c) Relative SERRS intensities (1600 cm^{-1}), recorded at 0, 1, 3 and 20 hours. d) Optical image of the substrate and SERRS mapping of pyocyanin (1600 cm^{-1}) at 20 hours of growth. Scale bar: 5 μm. e,f) SEM images of supercrystals colonized by P. aeruginosa (20 h) at different magnifications. Scale bar: 5 μm. Reproduced with permission from Ref. 654. Copyright 2016, Springer Nature.

In some cases localized infections may give rise to septicemia or blood infection. This systemic disease, defined as the presence of one or less colony forming bacterial unit (CFU) per 1 mL of blood, may produce death in hours. Therefore, the direct detection of bacteria is not a trifling measurement. Despite all recent improvements in sample manipulation and concentration, the standard approach to direct SERS analysis of bacteria, dried on a solid substrate, still retains major issues in terms of spectral fluctuations, long measurement time to acquire statistically reliable datasets, and lack of quantitative response. These limitations can be potentially addressed by combining SERS with microfluidic devices. As explained in Section 5 above, such approaches drastically reduce the acquisition time, while improving the spectral reproducibility by analyzing the sample in suspension.[658]

As the ultimate goal for bacterial identification is completely bypassing the culture step, which takes from 24 hours to several days, concentration procedures have been implemented into SERS-microfluidics biosensors. For example, by applying non-uniform electric fields on dielectric particles, including cells and microorganisms, it is possible to control their location.[659] Combining short-range dielectrophoresis and long-range electroosmosis flows, it is possible to rapidly and selectively concentrate pathogens in a diluted human blood sample, at the stagnation area on a SERS-active roughened electrode.[660]

Unfortunately, while the sensitivity issue has been addressed by some methods, only small volumes (~microliters) of samples, which are often not relevant for clinical diagnosis, can actually be investigated. Mixing of bacteria-containing biofluids with antibody-functionalized SERS-encoded silver nanoparticles induced the accumulation of the particles at the bacteria membrane. By designing SERS-encoded particles to yield, upon adhesion onto the bacteria walls, a dense array of inter-particle gaps in which the Raman signal is exponentially amplified by several orders of magnitude relative to the dispersed particles

(**Figure 6.3**). Under this scenario, the sample can be directly pumped through a millifluidic channel where a backscattered detecting laser continuously monitors the liquid stream, therefore removing the need for time-consuming centrifugation/washing cycles prior to the SERS analysis. In fact, positive events associated with nanoparticle-coated CFUs traversing the laser focus generate SERS intensities well above the background of dispersed encoded nanoparticles. For a demonstration of bacteria detection, three different types of bacteria (*S. aureus*, *E. coli*, and *S. agalactiae*) were successfully and simultaneously quantified, at a pace of 13 min per mL of blood or serum (**Figure 6.3**) and at concentrations ranging from units to tens of CFU/mL.[661]
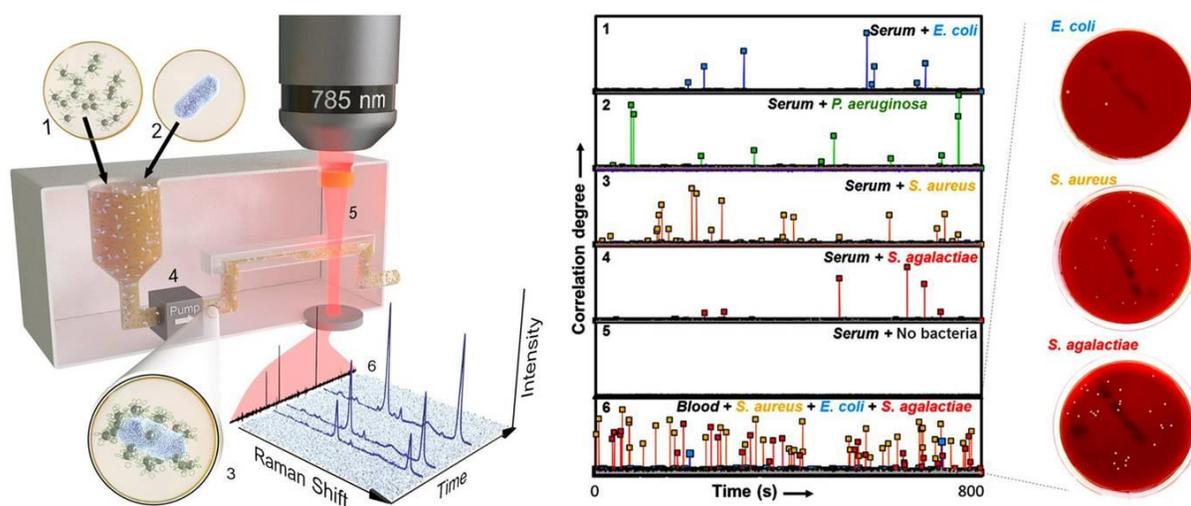
Figure 6.3. Conceptual view of a microorganism optical detection system and its relevant components. Silver nanoparticles (NPs) are separately labeled with different Raman-active molecules and functionalized with bacteria-selective antibodies (**1**). A nanoparticle dispersion is mixed in a vessel (3 mL) with the possibly infected sample fluid (**2**). Several types of bacteria are targeted using NPs prepared with specific combinations of Raman molecules and antibodies. The presence of one of these microorganisms induces aggregation of antibody-matching NPs on its membrane, rapidly evolving toward full random coverage (**3**). The mixture circulates through a millifluidic channel (**4**) and passes through the focus of a 785 nm laser (**5**), which is in turn spectrally analyzed to record the SERS signal generated by the Raman-active molecules (**6**). Targeted bacteria produce a large increase in the SERS signal, whose spectral fingerprints allow the identification of the pathogen. Correlation

between a time series of spectra and the SERS reference of labeled NPs. The analyzed serum samples contain either one pathogen (1–4, see labels) or no pathogen (5, blank). Series 6 shows the result for a blood sample spiked with a combination of three different bacteria (*S. aureus*, *E. coli*, and *S. agalactiae*). Large correlation values reveal the passage of an individual bacteria or CFU. Bacterial cultures (24–48 hours) for the microorganism inoculated in the blood samples (series 6). White spots correspond to the colony forming units. Adapted with permission from Ref. 661. Copyright 2016, Springer Nature.

6.4. Immuno-SERS (iSERS) Microscopy

SERS is not only applied for sensing purposes but can also be used as an accurate imaging tool for *ex vivo* and *in vivo* samples, as we describe below. Immuno-SERS (iSERS) microscopy exploits the benefits of SERS nanotags described in Section 3. Central advantages of this emerging nanobiophotonic technique are the parallel localization of multiple proteins on cells and tissues, protein quantification, and high image contrast.[325,662] The following paragraphs are intended as a brief introduction to iSERS microscopy and its application *ex vivo* to single cells and tissues.

iSERS microscopy employs SERS nanotags conjugated to antibodies for selective protein recognition.[663] Protein localization is based on the characteristic SERS spectrum of the corresponding Raman reporter molecule. False-color images, which visualize the protein distribution in the cell or tissue, are typically generated from a hyperspectral data set of spatially resolved Raman spectra, obtained by point or line focus mapping.[664] The false color encodes the SERS intensity of the corresponding nanotags and thereby, as the SERS signal response scales linearly with the amount of SERS nanotags, it quantitatively reflects the amount of the target protein.[323] Since its first report in 2006, iSERS microscopy, which at that time was termed immuno-Raman microspectroscopy,[665] advances have been largely due to the development of brighter SERS nanotags. As time is a very important experimental parameter, it soon become evident that acquisition times as long as 1 second per pixel in the initial report using hollow Au/Ag nanoshells should be reduced to the millisecond regime by brighter tags such as small silica-encapsulated clusters of Au NPs with single-particle

brightness.[396] In 2011 also the nonlinear variant of iSERS, immuno-SECARS microscopy, was demonstrated.[666] Convincing iSERS results require negative control experiments to unambiguously demonstrate the binding specificity of the SERS nanotag-labeled antibodies. This is achieved by using isotope controls, as the most important and required negative control in which only the corresponding antibody is exchanged, but SERS nanotags and cell/tissue specimens are both the same as in the positive control.[667]

Single cells are the simplest biological system to which iSERS microscopy can be applied and therefore ideally suited for testing its performance and evaluating relevant technical parameters. A critical acquisition parameter in SERS microscopy is the laser power density at the sample, since SERS nanotags can be damaged due to significant heating as a result of absorption. A recent systematic study on single breast cancer cells demonstrated that ca. 1-2 mW/pixel is a suitable upper limit.[668] This value resulted from repeated measurements on the same single cell and the comparison of the corresponding false-color SERS images and spectra. In situations where an electron multiplying (EM) CCD is used for detection, the EM gain can be exploited for faster acquisition. Although the multiplexing advantage of iSERS microscopy is clearly evident in the context of single cell studies, experimental work demonstrating this aspect with a substantial number of SERS nanotags (N > 3 colors) is still missing.[343,348,380,669] In the future, such multi-color studies are urgently needed to unambiguously demonstrate the propagated superiority of iSERS microscopy compared to its optical competitors.

Formalin-fixed and paraffin-embedded (FFPE) tissue is the most commonly employed material in histopathology. Compared to single cells, tissue is a significantly more complex system containing many cells including different cell types. This situation is further complicated by the process of tissue treatment prior to analysis. For maintaining the morphology in subsequent histopathological studies, the native tissue from biopsies is usually fixed in formalin and then embedded in paraffin for finally obtaining µm-thick tissue sections using a microtome. Antigen retrieval techniques are required to make the target protein accessible for antibody recognition in immunostaining. A direct comparison of immunofluorescence and iSERS revealed that the type of antigen retrieval directly affects the iSERS staining results.[670] Several iSERS studies on tissue were performed on prostate-

specific antigen (PSA), an organ-specific but non cancer-specific target protein; PSA is a good test system since it is broadly expressed at high levels in epithelium of the prostate gland.[332,350,356,390,665,670] Again, as for single cells, convincing multi-color iSERS studies on tissue (N > 3 colors) are missing and should be demonstrated in the future for promoting the acceptance of this technique in the biomedical community.[671] Finally, also instrumental challenges such as the fast and automated examination of entire tissue slides with dimensions of ca. 2.5 cm x 1 cm must be solved prior to implementation in routine diagnostics.

6.5. Multiplexed Cell Discrimination Using SERS Imaging

Bright SERS tags can also be applied to monitor complex cell cultures. A recent example of SERS-based imaging demonstrated multiplexed cell discrimination.[363] Instead of measuring the proteins that are present in the cells, SERS-encoded particles were used to label different kinds of cells, which can readily take them up, thereby providing the possibility to monitor live cells over long periods of time. Cell migration and differentiation is of high relevance to understanding tumor cell behavior and, importantly, this study proved the long term stability of such SERS tags. Specific imaging of breast cancer cells from five different cell lines, within a quintuple co-culture over time periods over 24 h were successfully performed, which could be extended into 3D cell culture models.

6.6. Future Prospects of SERS in Medicine

While the number of applications of SERS in biosensing has rapidly increased during the past decade,[327,672,673] its progress toward becoming a widespread clinical diagnostic technology has lagged behind.[674] A specific bottleneck problem is the limited tissue penetration depth achievable, which severely hinders the implementation in full-body, deep tissue, or intracranial applications (the maximum tissue penetration depths for simple SERS setups are on the order of several mm,[675,676] if we do not consider SESOR implementations[677]). In fact, although SERS imaging *via* SERS tags has been carried out in murine models,[676,678] it may be unlikely that this approach will become applicable to molecular imaging of organs in human patients. One should however not discount other (including *niche*) clinical research areas in which SERS has shown or has the potential to demonstrate superiority. Compared to other optical and non-optical techniques, such as fluorescence imaging, magnetic resonance imaging (MRI), or photoacoustic imaging, SERS

may in fact have distinct advantages. For instance, its well-known high sensitivity, and brightness, together with the lack of photobleaching of SERS tags, have proven advantageous with respect to fluorescence techniques for single cell imaging, even at a low concentration of contrast agent.[679] Furthermore, the micrometer-range resolution of SERS is far superior to that of MRI, which ranges in the order of 1 to few mm. To put this value in perspective, if one assumes the diameter of a cancer cell to be of the order of 20 μm, 100,000 cancer cells would need to be present in a tumor tissue for it to be detectable *via* MRI, which may render the analysis too late for certain types of aggressive tumors.[680] Finally, photoacoustic imaging suffers from the lack of targeted imaging agents, compared to the case of SERS,[681] for which there is a large number of available tags.[674] We need, therefore, to ingenuously leverage these advantages for SERS to become a diagnostic technique with true clinical reach.

There are three main clinical implementations of SERS that could find applicability in the near future (**Figure 6.4**): 1) During surgery, for the detection of tumor margins,[682] 2) *via* endoscopy, colonoscopy, or other optical fiber-guided imaging procedure to visualize and detect superficial diseased tissues within the interior of the body,[683] or 3) *via liquid biopsy*, a term that broadly comprises the identification of disease biomarkers in blood or other bodily fluids.[684] Biomarkers that have been the focus of most research efforts include small molecules,[685] proteins,[686,687] DNA and RNA,[688-690] circulating tumor cells,[691] and exosomes.[692]

With respect to the detection of tumor margins or microinfiltrated tumor tissues, a breakthrough demonstration was reported by Kircher and co-workers,[682] who showed that the use of SERS tags, to intraoperatively target glioblastoma tissues in genetically engineered mouse animal models, led to an improved identification of tumor margins compared to the surgeon's eye alone. The approach demonstrated that tags were sufficient to improve tracking of tumor margins employing a portable Raman microscope instead of a benchtop instrument. The same authors also showed that the use of nanostars, instead of silica coated gold nanospheres, improved their ability to image, with high precision, pancreatic cancer, breast cancer, prostate cancer, and sarcoma in animal models,[693] further extending the approach to ovarian cancer *via* use of folate targeting,[694] and to liver cancer *via* intravenous injection of nanoparticles.[695] With no need for surgical dissection, Vo-Dinh and co-workers demonstrated

in vivo SERS detection of gold nanostars accumulated in tumor in a genetically engineering mouse animal model.[599] While these reports have been key to solidifying the relevance of SERS in clinical practice, further considerations need to made for it to be extensive to patients. First of all, the systematic intravenous delivery of imaging tags to the targeted organ would be more complex in humans than in murine counterparts, requiring stabilities of over 24-48 hours, resistance to fouling and protein corona formation,[696] and extremely high biocompatibility. In fact, if one takes into account that, on average, only <5% of the systemically injected nanoparticles reach the target organ, issues related to nanoparticle aggregation, shape reconstruction, accumulation, and toxicity become important. Furthermore, it is unlikely that SERS tags, because of the size of their plasmonic component, will ever be able to cross the blood brain barrier (BBB), unless its functionality has already been altered by damages to its integrity due to disease or impact.[697] On the other hand, to bypass the BBB, one could design biocompatible liquids or gels, containing SERS tags, to be sprayed during open brain surgery onto the brain tissues that need to be excised, at a sufficient concentration to make them detectable *via* a portable Raman spectrometer, in sufficient amounts to cover the area under examination, without affecting its viability and without infiltrating surrounding healthy tissues. Another approach was proposed to bypass the BBB by using lasers to photothermally heat plasmonic nanoprobes (gold nanostars) and optically modulate their delivery into the brain tumor parenchyma with minimal off-target distribution in a murine model.[698] For these issues to be solved productively, there will need to be, if we want to be successful, a collaborative approach among chemists, physicists, materials scientists, and clinicians.

SERS detection of mainly cancerous tissues in animal models has been carried out *via* endoscopy, by adapting the optics of Raman microscopes to available endoscopes. For instance, Zavaleta *et al.*[699] developed a flexible, non-contact, fiber optic-based device with a diameter of 5 mm and inserted it into an existing endoscope to obtain a device with variable working distance (from 1 to 10 mm), which accommodates imperfect centering during endoscopy and nonuniform surface topology in human (and animal) tissues. With IRB approval they were then able to topically administer SERS tags to patients and employ their device during colonoscopy. With a similar approach, Liu *et al.* topically administered a multiplexed cocktail of SERS tags to murine models of esophageal cancer and were able to

visualize tumor tissues in the lumen of the esophagus and to quantify biomarker expression levels by employing a miniature spectral endoscope featuring rotational scanning and axial pull-back.[683] Other implementations of endoscopy include the use of plasmonic nanowire waveguides to limit hotspot light concentration and photodamage by providing remote excitation,[457] and the assessment of gastric and colon disease individually and in multiplex.[700,701] Currently, the main limitation to this approach is the minimum optical fiber diameter (and therefore endoscope) that can be employed, due to constraints in the design and implementation of the excitation and detection optics. Once this issue will be overcome, additional applications, not limited to cancer detection, may become feasible, such as the screening of the upper respiratory system for the presence of viral particles.

As previously mentioned, liquid biopsy holds the promise to render early disease detection and monitoring much simpler to carry out and less painful for the patient. In particular, the possibility to evaluate the presence of disease biomarkers in bodily fluids instead of tissues would allow monitoring disease progression and response to therapy, in principle on a daily basis, rather than having to rely on imaging approaches that may or may not detect changes in tumor size. Furthermore, the opportunity to monitor the presence of biomarkers in healthy individuals that may however have genetically inherited the disease from their parents, would open the opportunity to true personalized medicine. In this area, SERS offers many opportunities.[684] Its selectivity and sensitivity, along with the variety of SERS platforms and tags that have been developed over the years, are likely to render it a key player in the medical field. Recently, Li *et al.* designed and implemented a SERS immunoassay to analyze exosomes in 2 μL of clinical serum and discriminate not only pancreatic tumor patients from healthy individuals, but also to distinguish between metastasized and non-metastasized disease.[702] Alvarez-Puebla and co-workers instead implemented a SERS platform to monitor the biomarker c-MYC, a transcription factor de-regulated in 70% of cancers, by leveraging changes in Raman reporter orientation upon binding of the target. They validated the sensor in cell lines, healthy donors, and one cancer patient.[525] One of the main hurdles to overcome in the application of SERS in liquid biopsy will be understanding how to process the specimens of bodily fluids to minimize matrix interference in the resulting spectra. When targeting circulating tumor cells, it will be necessary to design simpler enrichment methods than those developed in recent years, based on complex microfluidic devices. One promise

lays in the use of aptamers, which, based on their ability to capture cells by recognizing cell surface biomarkers, have recently shown to achieve capture efficiencies of 50-60%, with values of 40% for cell numbers as low as 10, which is realistic in the case of circulating tumor cells.[686] Importantly, the use of truncated aptamers produced an increase in capture efficiency, promising with respect to clinical implementations of SERS in liquid biopsy.

Looking ahead, one of the hurdles to increase applicability of SERS in medicine will be its implementation alongside clinical trials to address questions that are important to clinicians. A recent study by Bhamidipati *et al.* has shown that SERS may aid the oncologist in the stratification of prostate cancer patients, compared to immunofluorescence alone, by quantifying the expression of the prostate specific membrane antigen (PSMA) in tissue microarrays obtained from 34 patients with varying stage of prostate cancer.[686] What the study showed was that some patients who had been clinically staged at low risk showed instead high PSMA expression, while other patients who had been staged at high risk, showed only low PSMA expression. While this was a retrospective study, if these patients had been on an ongoing clinical trial, the SERS data would have definitely called for further investigation. To proceed along these lines, pairing SERS studies to clinical trials with consenting patients (*i.e.* prospective study) will be necessary to make it possible for SERS to penetrate the clinic and become a diagnostic tool available to the clinicians.
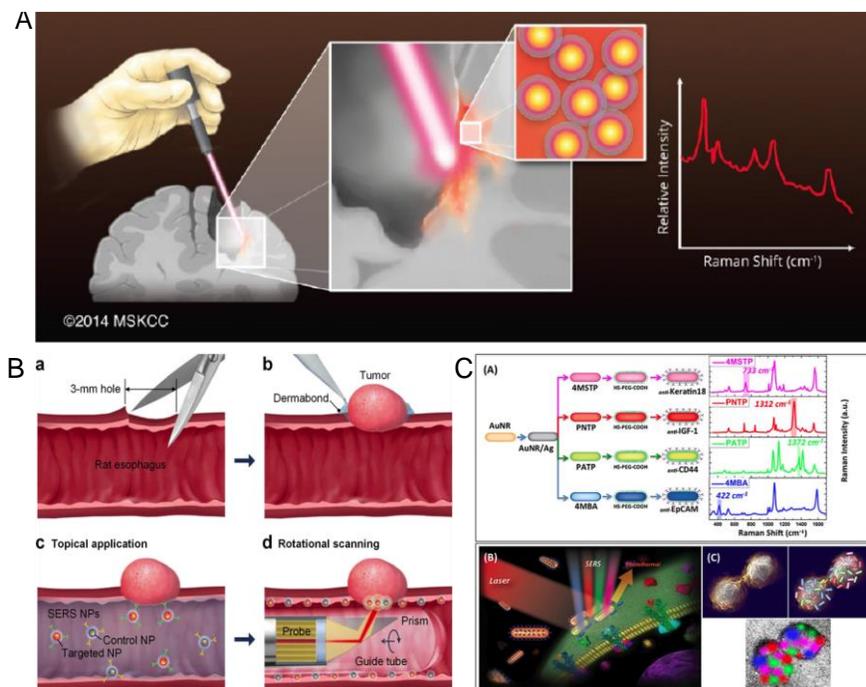
Figure 6.4. SERS tags can be employed to: A) aid in the identification of tumor margins intraoperatively. Adapted with permission from Ref. 682. Copyright 2014, American Chemical Society. B) identify and localize tumor tissues endoscopically. Adapted with permission from Ref. 683. Copyright 2015, Optical Society of America. and C) multiplex detection of circulating tumor cells, by identifying overexpressed membrane biomarkers. Adapted with permission from Ref. 691. Copyright 2014, Springer Nature.

7. Environmental Monitoring

SERS has been widely used for monitoring and quantification of environmental toxins and chemicals,[558,703-705] heavy metals,[706-708] bacteria signaling metabolites,[654] *etc*. Different nanostructures, including NP dimers and oligomers (**Figure 7.1A**),[448,703,708] Au NRs or NP chains (**Figure 7.1**B),[558,706] Au NRs ladders,[707] heterostructures (**Figure 7.1**C),[709] as well as Au NP arrays[710] and nanopillars[711] film structures, among others,[654,712] have been exploited to provide SERS enhancement for environmental detection. Additionally, the application of novel nanomaterials has been explored, including semiconductors,[713] transition metal chalcogenides[714] and metal-organic frameworks,[715] which may further improve the performance of SERS substrates.

Compared to absorption spectroscopy or hydrodynamic size-based sensing technologies, SERS-based detection has achieved better sensitivity, even reaching the picomolar level.[704,707] It has been reported that the use more extensive NP assemblies, such as NP chains *versus* Au nanostar dimers, the sensitivity was further improved (0.45 pg mL^{-1} *vs.* 0.8 pg mL^{-1}).[708] Compared to Au NR oligomers and Au NP chains which have similar sensitivity, sharp tips on the NPs can help improving the detection performance.[707,708] For the detection of environmental toxins or chemicals, the sensitivities provided by end to end Au NR chains or NP-NR-NP trimer structures were however of the same order, indicating a similar SERS enhancement.[558,703] An interesting structure was built by applying the polymerase chain reaction to create alternating plasmonic nanoparticle heterochains, which displayed stronger SERS intensity as the number of NPs was increased (**Figure 7.1**C).[709] Strategies based on NP assemblies for SERS ultrasensitive detection thus provide alternative routes to overcome sensitivity limitations, but require reproducibility and stability optimization for real sample detection. In general, small gaps, larger assemblies (multi-gaps), roughness (sharp tips) and type of NP building blocks, all contribute to the overall SERS enhancement. On the basis of Raman fingerprint spectra, SERS is capable of simultaneously detecting multiple pollutants of varying molecular weight, even distinguishing organic chemicals with similar structures.[634] Although simultaneous monitoring of multiple targets can be possible, the optimal SERS configuration for different molecules with a similar structure, polarity, or molecular weight may be different. Challenges thus remain for SERS detection technology, such as unspecific aggregation of NPs, variation of surface chemistry, and sample matrix effects, which affect the detection performance (sensitivity, selectivity and accuracy). Single-molecule SERS will be important for probing complex chemical and biological environments, which could be realized by means of a dual-function linker that can localize and secure a single target within a plasmonic nanogap, *e.g.* a nanojunction of Ag NP (60 nm) on Ag substrate.[450] Even though the dimensions of the NPs can be tailored to increase the sensor signals,[716] the presence of impurities or the orientation of target molecules can induce fluctuations in single-molecule SERS spectra. SERS provides a great potential to establish a rapid, reliable practical detection platform, in which the targets should be matched to a suitable SERS substrate, optimal laser light, and controlled speed and automation for vast sample monitoring.
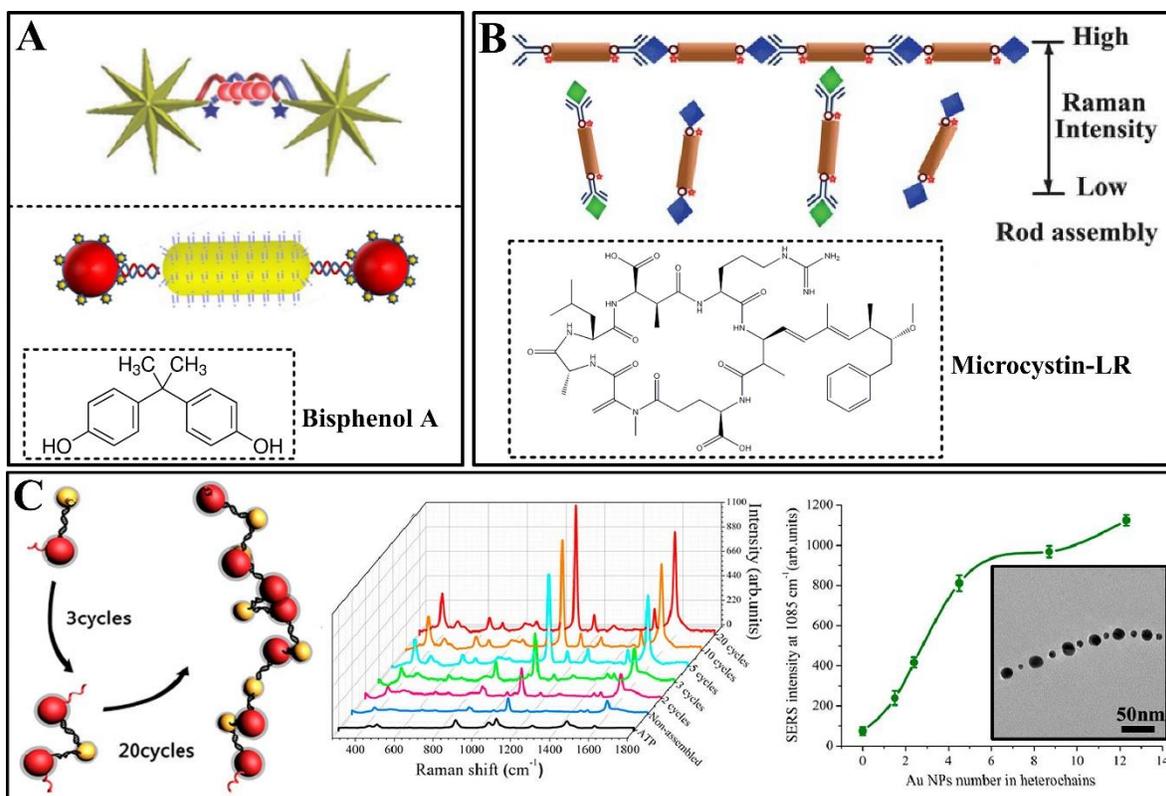
Figure 7.1. (A) SERS active gold nanostar dimer for mercury ion detection (top) and gold nanoparticle-nanorod heteroassemblies for Bisphenol A detection (bottom). Adapted with permission from Refs. 708 (Copyright 2013, Royal Society of Chemistry) and 703 (Copyright 2016, Elsevier B. V.), respectively. (B) SERS active gold nanorod assembly for toxin detection. Adapted with permission from Ref. 558. Copyright 2012, Royal Society of Chemistry. (C) Plasmonic nanoparticle heterochains and SERS enhancement properties. Adapted with permission from Ref. 709. Copyright 2013, American Chemical Society.

7.1. Detection of Toxins

Based on the characteristic vibrational fingerprints, displayed even by very similar molecular species, and the ability to measure Raman spectra in aqueous matrices, intrinsic SERS has a great potential to detect toxins that could compromise our food supply. Several recent publications demonstrate SERS detection of toxic bacteria (*e.g. Salmonella typhimurium*[717] and *Yersinia pestis*[549]), proteins (*e.g.* ricin[718]), and small molecules (*e.g.* mycotoxins[719] and dipicolinic acid[720]). Perhaps the most significant challenge toward exploiting this great potential lies in the requirement that, to achieve a high signal-to-noise ratio in the SERS

spectrum of the toxin itself, the scattering molecule must dwell within a few nanometers of the plasmonic substrate. Thus, the most important design element for an intrinsic SERS sensor lies in the nature of the affinity agent, coating, or capture mechanism that will draw and/or hold the target analyte near the plasmonic surface. In some cases, based on the molecular features of the toxin, the toxin itself will have an affinity for the plasmonic surface and can be directly detected using SERS. An excellent example of this circumstance was reported by Van Duyne and co-workers, comprising the direct SERS detection of dipicolinic acid, a biomarker for *Bacillus anthracis*, quickly and at levels relevant for detection of infectious doses.[721]

In most cases, however, the target molecules do not display a natural affinity for the plasmonic substrates that enable SERS detection. As such, a wide range of affinity agents have been used for SERS detection of toxins (**Figure 7.2**).[722] Among the most important factors to keep in mind when selecting affinity agents are (1) the length of the affinity agent (since this determines how far the analyte will be from the enhancing substrate) and (2) the Raman scattering properties of the affinity agent itself (since these vibrational bands will interfere with new signals from the target).
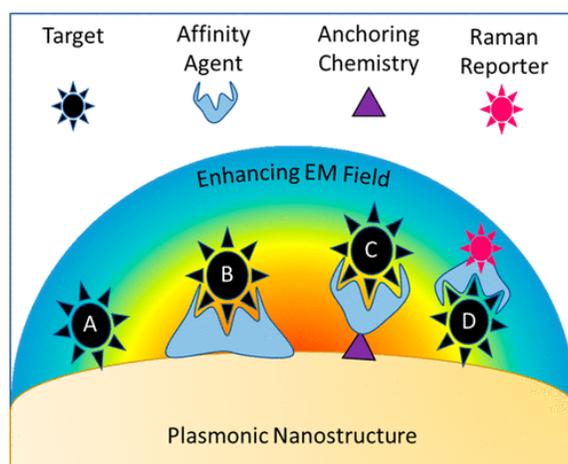
Figure 7.2. Schematic view of various approaches used to localize a Raman target within the enhancing electromagnetic field. Reproduced with permission from Ref. 722. Copyright 2018, American Chemical Society.

Based on the widespread use of antibody affinity agents in traditional assays such as ELISAs, there are many examples of antibody-based detection of toxins. In general, antibodies

themselves are not great Raman scatterers, so their spectral features are not a great source of interference. For example, Porter demonstrated an antibody-enabled sandwich assay SERS detection of two antigenic protein markers of *Bacillus anthracis*.[723] A similar antibody-enabled SERS immunoassay was also successfully used to detect the neurotoxin *Clostridium botulinum*,[724] and a lateral flow assay format was used with antibody-enabled SERS detection of staphylococcal enterotoxin B.[725] In some cases, the antibody is used to capture the target toxin, but an additional capture step is needed to concentrate and probe the captured target. For example, Choo and co-workers concentrated antibody-captured *Yersinia pestis* into microdroplets ahead of SERS interrogation,[549] while Faulds and co-workers used a combination of antibody-modified nanoparticles and lectin-modified nanoparticles to facilitate SERS detection of *Escherichia coli*, *Salmonella typhimurium*, and methicillin-resistant *Staphylococcus aureus*.[717] Keeping affinity agent size in mind, intact antibodies are quite large compared to the exponentially decaying electromagnetic fields at the plasmonic surface, so high affinity antibody fragments, if available, would likely improve the performance of all of these antibody-based detection schemes. In analogy to the three-dimensional structure critical for antibody/antigen interaction, some groups have employed molecularly imprinted polymers (MIPs), a polymer cast around a target-of-interest to create a specific binding pocket, in SERS sensors. To date, there have only been a few applications of MIPs for foodborne toxin detection, including the detection of chloramphenicol in milk and honey[726] and carcinogenic Sudan I in paprika.[727]

Aptamers are another type of affinity agents with significant potential for SERS-based detection of toxins. These DNA or RNA structures do display some Raman scattering features that could interfere with the spectrum from the target analyte, but these bands are well-known and relatively few in number. In the context of detecting toxins using SERS, aptamers have been used most commonly to sense the protein ricin (or components of the protein). This focus on aptamer-enabled detection of ricin is due, in part, to the importance of ricin as a sensing target, but also because an effective aptamer for ricin was generated.[728] With this aptamer in hand, detection of relevant concentrations of ricin has been demonstrated in food matrices and blood.[729-731]

While the specificity of antibodies and aptamers can be advantageous, some toxin sensing applications would benefit from a less specific capture method so that more than one target toxin can be detected simultaneously. One system to consider for this application is self-assembled partition layers like those successfully used by Van Duyne and co-workers to concentrate and detect glucose;[732,733] however, the approach has not been used yet for small molecule toxin detection. An alternative low-specificity capture layer comprises covalently attached linear polymers. This approach has a significant potential because, based on the polymer repeat unit functional groups, particular classes of molecules can be targeted, and if controlled polymerization methods are used, the thickness of the capture layer can also be controlled. In two recent examples, Haynes, Reineke, and co-workers demonstrated that linear polymers can be used to capture the protein ricin[718] or the small molecule aflatoxin B1[719] for intrinsic SERS-based detection.

Finally, in some cases, researchers have avoided using an affinity agent altogether, even if the target toxin does not have a natural affinity for plasmonic substrates, by using physical means to bring the target within the electromagnetically enhancing fields. For example, He and co-workers dried both plasmonic nanoparticles and ricin-containing solution on paper, and demonstrated SERS detection of ricin within 10 minutes.[734] Bell, Goodacre, and co-workers localized mesoscale droplets containing dipicolinic acid (a biomarker for Anthrax) onto SERS substrates by manipulating hydrophobic interactions, yielding detection far below the equivalent infectious dose of *Bacillus anthracis*.[720]

Overall, while there has been some exciting recent progress using SERS to directly detect foodborne toxins, many analyte systems are yet to be explored. We should definitely take advantage of all that we have learnt in the more advanced area of SERS applications in biomedicine, as well as using the best of SERS substrates and measurement platforms.

7.2. Water and Food Analytics

To provide clean drinking water for all humans is one of the major challenges in the 21st century. As a consequence, monitoring water quality is of tremendous importance. A cartridge system with an implemented SERS substrate was applied by Popp and co-workers to detect sulfamethoxazole, a drug molecule, in real water matrices.[552] The required

sensitivity of the SERS-based detection scheme is associated with the maximum allowed concentration of $2 \cdot 10^{-7}$ M. Concentration-dependent SERS measurements were performed and, using this approach, the target analyte could be monitored down to $2.2 \cdot 10^{-9}$ M, in various surface water samples. This example illustrates the potential of SERS-based cartridge systems in future environmental monitoring. Indeed, the future of SERS in environmental science might be related to the implementation of powerful and reproducible SERS substrates with an easy and cost-efficient fabrication protocol, into cartridge systems allowing for fast and cost-efficient one-point measurements in regions with less-developed infrastructure, outside of specialized labs.

On the other hand, establishing a healthy life style to prevent diseases *via* balanced nutrition is of great importance. To illustrate one example where SERS gives insight into nutritional elements of food, the lycopene and β-carotene content in tomatoes was estimated by SERS.[735] Here, SERS substrates prepared by electron beam lithography were applied to build up a database from SERS spectra of lycopene/β-carotene mixtures with different percentages. Principal component analysis with partial least squares regression (PCA-PLSR) was employed for the prediction of the correct content ratio. To prove the robustness of the database in the determination of lycopene and β-carotene percentages in real samples, tomatoes were collected at different ripening states and extraction of the carotenoids was performed. The extracts were investigated by means of SERS and a good agreement with the gold standard HPLC was obtained. Since SERS has the potential to be applied outside of specialized labs, the future of SERS in food analytics might be the pre-testing, *i.e.* all food samples are tested by SERS and when a concentration value with high accuracy is needed, HPLC is applied for selected samples, *e.g.* to confirm the compliance of limiting values (such as food dyes) or minimal required concentration (such as vitamins).

Within the described detection scheme, a label free approach has been applied, *i.e.* all molecules present in the extracts were allowed to interact with the metallic surface. In order to increase the specificity, recognition elements bound to the metallic surface need to be applied. In doing so, the structure and/or orientation of the recognition element are changed upon the specific interaction with the target analyte and thus, the SERS spectrum of the recognition element undergoes detectable variations. This chemosensor concept was applied

during the detection of Cu^{2+} ions in white wine.[414] In this study, gold nanoparticles were modified with a dipicolylamine-based ligand and due to the interaction with Cu^{2+}, the structure of the ligand was changed leading to spectral changes within the SERS response. The detection limit in water was measured to be $5 \cdot 10^{-8}$ M using this method. To illustrate the potential of this detection platform in real application scenarios, such as controlling wine production, Cu^{2+} was spiked into white wine and concentrations below the recommended maximum amount of $7.87 \cdot 10^{-6}$ M could be readily monitored in such a complex matrix.

7.3. Nonpolar Organic Pollutants

In spite of the relatively high polarizability exhibited by the most common nonpolar organic pollutants, like polycyclic aromatic hydrocarbons (PAHs), polychlorinated biphenyls (PCBs) or pesticides, their direct detection by SERS is challenging. The lack of functional groups having any affinity for a metal surface, such as thiols, amines, or carboxylic acids, makes it necessary to design strategies that promote the interaction between pollutants and the plasmonic sensing platform, which is crucial for their SERS detection. The high toxicity of these persistent organic pollutants (POPs) poses adverse health effects in humans and animal exposed to them even at extremely low concentrations, which has promoted the development of ultrasensitive SERS sensors with the ability to capture and detect these molecules. One of the first reported approaches for detecting PAHs and PCBs was based on the functionalization of a plasmonic surface with alkyl thiols to create a self-assembled monolayer, which would interact with hydrophobic molecules through van der Waals forces.[155,736-740] Haynes *et al.*[737,738] demonstrated that the modification of silver film over nanospheres (AgFON) substrates with alkanethiols allowed the detection of PAHs or PCBs with an expected pM limit of detection. These hydrophobic AgFON substrates were used to distinguish two different PAHs/PCBs pollutants from one another in mixtures and could be reused after rinsing with octanol. Interestingly, when investigating the alkyl chain effect on the AgFON SERS performance, it was found that decanethiol monolayers worked better than other alkanethiols, due to the key role of layer thickness (chain length) and crystallinity of the monolayer.[739]

Another strategy to mechanically trap small molecules on or close to the metal surface is based on the combination of plasmonic nanoparticles with poly-(N-isopropylacryamide)

(pNIPAM) (**Figure 7.3**).[741-743] The encapsulation of Au nanoparticles within this thermosensitive polymer creates a core-shell nanostructure where 1-naphtol (1-NOH) can be captured. By shrinking the pNIPAM shell above 32 ºC, 1-NOH gets closer to the Au core surface, allowing SERS detection.[741] As the pNIPAM shell around the Au nanoparticles is usually thick, it can prevent the formation of hot spots, thereby limiting the enhancing ability. The limit of detection can be improved by using wrinkle assisted assembly of pNIPAM-coated Au nanoparticles into parallel linear arrays, for SERS sensing of pyrene traces (a well-known PAH) in the gas phase.[743] The detection limit of pNIPAM based sensors has also been improved by incorporation of magnetic Fe_2O_3 nanoparticles within the pNIPAM matrix, so that the plasmonic composites can be concentrated after the capture of the pollutant, into a small spot, by applying an external magnetic field. This method allowed the first SERS analysis of pentachlorophenol (PCP), a highly toxic contaminant, reaching a detection limit of 1ppb (as mandated by EPA).[742]

Several reports show the use of macrocycles, such as calixarenes, cyclodextrins, or pillarenes, to enhance the ability of plasmonic substrates to capture and detect POPs.[744-750] These macrocycles feature a hydrophobic cavity that can favor the size-selective inclusion and trapping of small hydrophobic pollutants, forming host-guest inclusion complexes. Importantly, the chemical properties of these macrocycles or the shape of the cavity can be tailored by changing the groups on the upper and lower rims. The modification of Ag nanoparticles with dithiolcarbamate functionalized calix[4]arene as host molecules allowed the detection of four different PAHs (pyrene, benzo[*c*]phenanthrene, coronene, and triphenylene) in water, with a limit of detection ranging between 10 nM and 100 pM.[746] By implementing a silica film doped with Ag nanoparticles within a flow cell, 12 different PAHs could be detected *in situ*, in the Baltic Sea.[751] The ammonium pillar[5]arene (AP[5]A) has been used for SERS detection,[748,749] *via* electrostatic layer-by-layer assembly of Au nanospheres, yielding a plasmonic hybrid nanostructure with uniform hot spots across large areas, with remarkable size-selective capture capability for different PAHs (pyrene, nitropyrene, and anthracene) (**Figure 7.3**b).

Another interesting strategy toward improving selective molecular sensing is based on the combination of metal organic frameworks (MOFs) and metal nanoparticles.[752-757] MOFs

exhibit a well-defined, porous structure, tunable pore size, large specific surface area and tailored chemical functionality, which confer them with a high capacity for selective molecular trapping and sensing. Regarding pollutants, the deposition of a MOF film on an AgFON allowed the selective detection of benzene, toluene, nitrobenzene, or 2,6-di-*tert*-butylpyridine from the gas phase. These pollutants did not adsorb onto a bare AgFON surface (**Figure 7.3**c).[756] In a related work, Au nanoparticles embedded within MIL-101 demonstrated good sensing capabilities for quantitative analysis of p-phenylenediamine in environmental water and the tumor marker alpha fetoprotein in human serum.[757] Interestingly, it has been recently demonstrated that certain MOFs (such as ZIF67) can act as SERS-active substrates for specific analytes, achieving enhancement factors up to 10^6 and limits of detection of $\sim 10^{-8}$ M.[758] In spite of the absence of a plasmonic material, the coupling of different contributions, like charge transfer, interband transitions and molecular resonances, resulted in the enhancement of the Raman signals. While ZIF-67 showed excellent SERS performance for R6G detection under 532 nm laser line, it could not be used to detect methyl orange even at high concentrations. The field of MOFs thus facilitates the development of highly selective SERS sensors though there is still much to be learnt about designing optimal systems and generalizability of performance.
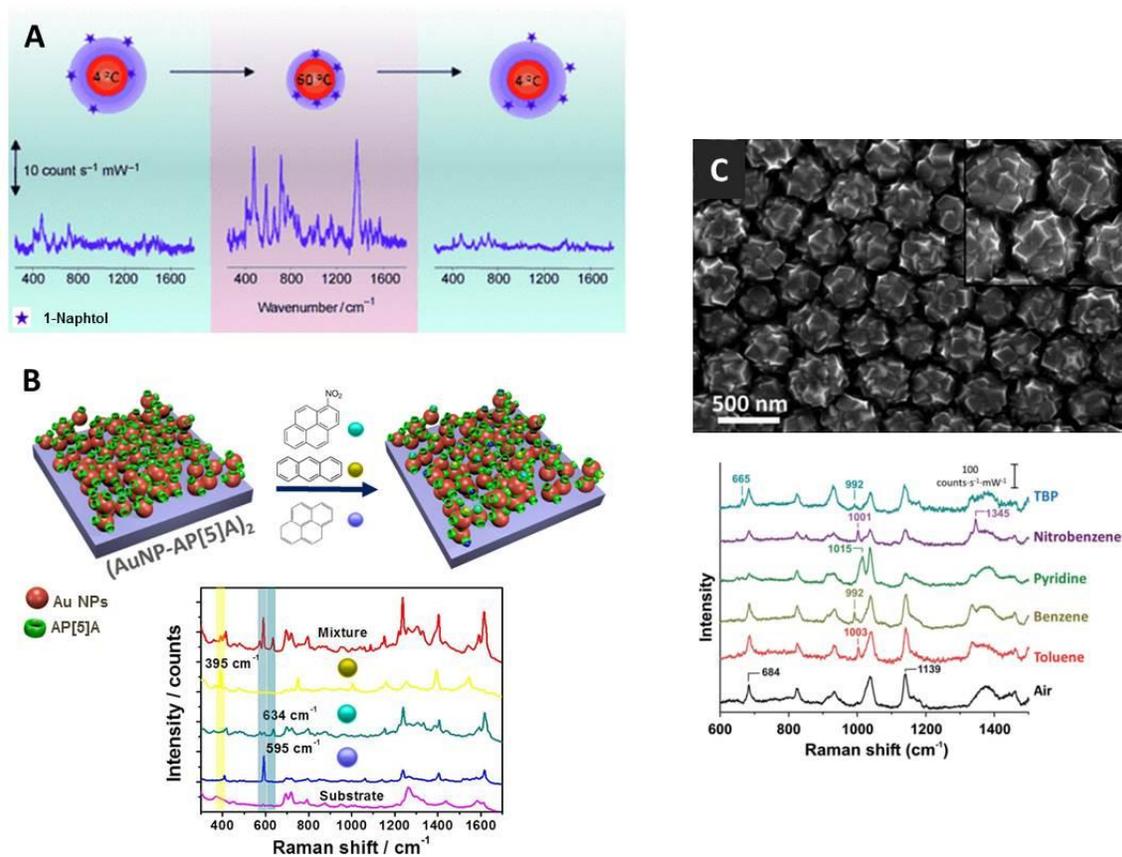
Figure 7.3. a) SERS detection of 1-Naphtol using core-shell Au@pNIPAM colloids. Reproduced with permission from Ref. 741. Copyright 2009, Wiley-VCH. b) Plasmonic thin films fabricated through layer-by-layer (LbL) assemby of Au nanoparticles and ammonium pillar[5]arene (AP[5]A) for (multiplexed) SERS sensing of PAHs in gas or liquid phase. Reproduced with permission from Ref. 749. Copyright 2017, American Chemical Society. c) ZIF8-coated AgFON for the detection of benzene, toluene, nitrobenzene, or 2,6-di-*tert*-butylpyridine in gas phase. Reproduced with permission from Ref. 756. Copyright 2014, Royal Society of Chemistry.

8. Related Techniques

Over the years, several SERS-related experimental technologies and techniques that benefit from high EM field enhancement in plasmonic structures and in nanogaps have been developed for a wide range of applications. Surface enhanced offset Raman scattering

(SESORS) has been advanced in improving signal detection from deeper sites. With electrochemical SERS (EC-SERS) molecular resonances can be tuned to the excitation wavelength, providing information about the electronic states involved in SERS. Surface enhanced hyper Raman scattering (SEHRS) provides complementary vibrational information, due to changed selection rules in multiphoton excitation processes. ip-enhanced Raman scattering (TERS) is able to push the limits of spatial resolution to a few nm with intramolecular chemical resolution. Surface enhanced infrared absorption (SEIRA) offers infrared absorption enhancement factors typically ranging between one and seven orders of magnitude, depending on the measurement and sample details.

8.1. SESORS and SESORRS

Recent work has focused on the creation and development of approaches based on surface enhanced spatially offset Raman scattering (SESORS). This technique makes use of functionalized nanoparticles which contain a strong Raman signal and can be combined with spatially offset Raman (SORS) to give measurements at depth, *e.g.* through tissue. A homemade SORS system initially demonstrated detection of functionalized nanoparticles at depths up to 8 mm through tissue analogues,[677] but a subsequent study already compared a handheld Raman spectrometer with a handheld SORS instrument for the detection of ethanol through plastic barriers.[759] The results showed that the depth achievable for detection was 21 mm through plastic. The work progressed into surface enhanced spatially offset resonance Raman scattering (SESORRS) imaging of a breast cancer tumor model consisting of 3D multicellular tumor spheroids (MTS), using handheld spatially offset measurements and functionalized 100 nm gold nanoparticles.[760] To obtain the maximum depth penetration, a red shifted chalcogenpyrilium dye (λ_{max} = 823 nm) was used to provide resonance enhancement with the Raman excitation wavelength (830 nm), as well as surface enhancement from the gold NPs. This enabled detection of nanoparticles inside the MTS tumor model, through 15 mm of tissue, and 2D heat maps of nanoparticle localization were constructed. The maximum depth of tissue through which it was possible to detect signals from the nanoparticles alone was 25 mm, by using the red shifted chalcogenpyrilium based Raman reporters. A subsequent study demonstrated that a handheld conventional back scattered Raman spectrometer could achieve depths of analysis up to 20 mm through plastic

and 10 mm of tissue sections, indicating that it was not always necessary to use a spatially offset Raman (SORS) instrument, unless depths beyond 5-10 mm were required.[761] Multiplexed detection of nanoparticles in breast cancer tumor models was also demonstrated where a 3-plex was analyzed at depths of 10 mm, using 3 different flavors of resonant nanoparticles that could be differentiated using chemometrics (**Figure 8.1**).[762] To assess the sensitivity of the technique, a minimum concentration of nanoparticles for use with SESORRS was investigated, with the outcome being that femtomolar concentrations of nanotags could be detected at depths of up to 5 mm of tissue accurately.[763] Inverse surface enhanced spatially offset Raman spectroscopy (SESORS) offers the possibility of recovering the SERS signals of gold nanostars through a monkey skull.[764]
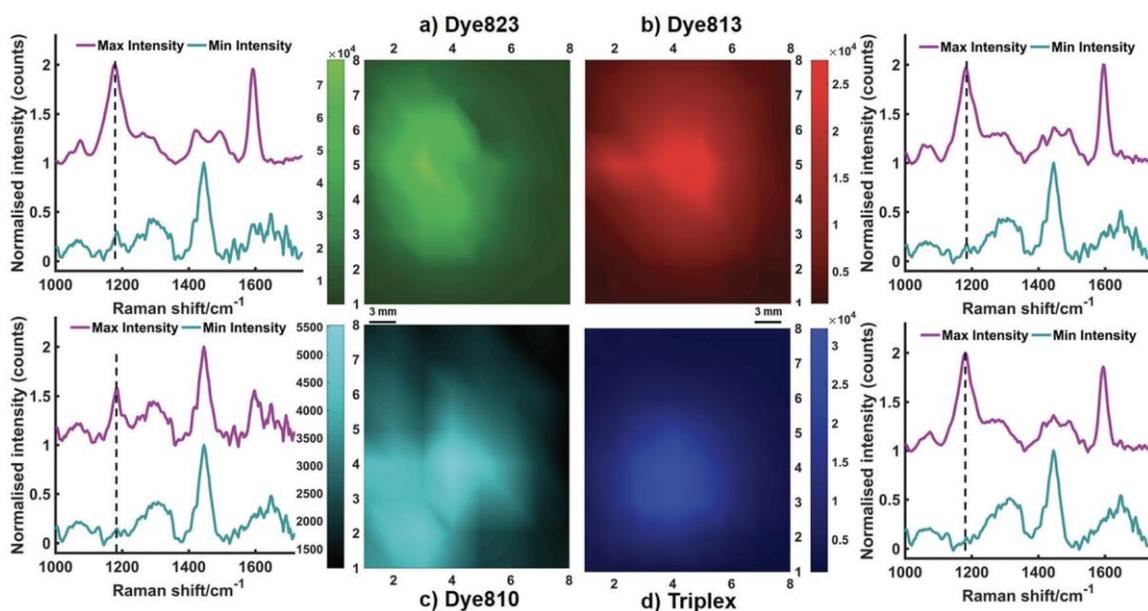
Figure 8.1. SESORRS false color 2D heat maps of the peak intensity at (a) 1178 cm^{-1} (dye 823), (b) 1181 cm^{-1} (dye 813), (c) 1185 cm^{-1} (dye 810) and (d) 1181 cm^{-1} (triplex). Measurements were carried out using an xy translational stage in step sizes of 3 mm to create an image of 8 x 8 pixels. 2D heat maps were generated and show the tracking of each of the four MTS models through 10 mm of tissue. Clear discrimination is seen between spectra collected at the point of maximum intensity where the nanotags were spotted and that collected where the nanotags were not present. The corresponding maximum and minimum collected 8 mm offset spectra also confirm the presence of the nanotags in regions where the

MTS were spotted (a–d). Reproduced from Ref. 762 with permission. Copyright 2018, Royal Society of Chemistry

In order to make all of the measurements previously described biomolecularly specific, an approach using targeted nanoparticles for use in assessing the risk of atherosclerosis *in vivo* was devised. Four different antibodies were attached to gold nanoparticles in a mixed monolayer with specific Raman tags to target ICAM-1, VCAM-1 and p-selectin with an IgG control nanoparticle conjugate.[765] Tail vein injection into inflamed mice showed detection of different nanoparticles in a human saphenous vein grafted onto the back of the mouse. Compared to a control, differences in the levels of the biomarkers were identified, indicating the ability to perform semi-quantitative measurements *in vivo* by means of functionalized nanoparticles and SERS. The next step will be to combine the targeting ability of the nanoparticles with SESORRS, to perform these measurements *in vivo* and at clinically relevant depths.

8.2. Electrochemical SERS

The ultra-high sensitivity of SERS is based on the resonance of the electronic excitation at target molecules and materials excited by plasmons. Not only the localization of the electromagnetic (EM) field at plasmonic nanostructures, but also the additional resonance effect induces vibronic coupling, increasing SERS intensity drastically.[766-770] The effect has been recognized especially at single-molecule observation in aqueous environments, where only the SERS-active target molecule is selectively observed without the SERS contribution from water molecules, which have comparable Raman cross section to that of the target.[771] On the other hand, if one can electrochemically polarize SERS metal substrates to very negative potentials, the evolution of SERS from water molecules is clearly observed.[772,773] The interesting effect of molecular selectivity of SERS depending on the electrochemical potential of the systems implies that the apparent SERS intensity can be used as a probe of the electronic excitation of target molecules and nanomaterials on SERS substrates.

The effect of electrochemical potential on SERS intensity has been regarded as the proof of the charge transfer (CT) process to enhance SERS.[767-770] This contribution is also considered as a chemical (CHEM) enhancement.[36-38] A resonant excitation that induces charge transfer between metal substrates and adsorbed molecules contributes to enhance the SERS intensity.

The enhancement occurs when the excitation energy of light matches the transition between the Fermi level in the metal substrate and an unoccupied molecular orbital, or from an occupied orbital of the molecules to an unoccupied level of the metal. The potential energy of the Fermi level is defined by electrochemical potential. Thus, experimental observations showed a resonant shape in the plot of SERS intensity as a function of electrochemical potential (**Figure 8.2a**),[768] indicating the validity of the CT mechanism. A fitting parameter of the line width Γ reflects the inverse of the characteristic damping time of the excitation. The dependence of the excitation energy on the electrochemical potential showing the SERS intensity maximum has also been used as a measure of the degree of CT. A linear relationship of the electrochemical potential maximum to the excitation energy of light indicates that the CT contribution dominates the enhancement (**Figure 8.2**b).[769] Control of the electrochemical potential for SERS observation varying the excitation light energy, provides information on the electronic structures at molecule-metal substrate interfaces contributing to SERS enhancement.

As additional interesting characteristics of the CT effect, relatively intense non-totally symmetric modes of molecules, which are normally described by relatively small nondiagonal terms in the polarizability tensor, were observed. The contribution of the CT effect on the selectivity of this mode has also been estimated from the slope of the linear plot of the electrochemical potential maximum to the excitation energy of light.[768] The degree of CT contribution to the non-totally symmetric modes is generally higher than that to totally symmetric modes, which are observed at normal Raman spectroscopy. This effect could be understood as the electronic excitation that accompanies CT for the resonance inducing anisotropic polarization of the molecules. A single-molecule observation by SERS is characterized by the observation of very intense non-totally symmetric modes compared with those of totally symmetric modes. The SERS intensity of a non-totally symmetric mode enhanced by the CT effect is typically stronger by one order of magnitude than normal Raman modes enhanced by the EM effect.[771] This characteristic behavior may also provide us with further information on the electronic excitation at CT process, induced by a highly confined plasmonic field. It should be noted that the spatially confined EM field also contributes to the change in the selectivity of the vibrational modes. The dipole-quadupole polarizabilities in SERS become also apparent due to the EM field-gradient effects.[774-777] The

electrochemical potential may also contribute to this effect, because the change in the resonance often results in the energy and localization of plasmons.[778-780] At present, precise tuning of the localization has not yet been achieved.

One should also pay attention to the effects of EM field-gradient on the electronic excitation. The selection rule for the electronic excitation is modified in the plasmonic EM field. The selection rule for the optical transitions between electronic levels is defined by the electronic wave functions, under the assumption of the long wavelength approximation. Thus, the normal selection rules for electronic excitations could be broken at the excitation of LSPR where a huge field intensity gradient exists.[781-783] The effect is experimentally observed as SERS from an isolated single-walled carbon nanotube (SWCNT) located at the gap of the Au dimer structure, as resonant Raman *via* a normally forbidden electronic transition.[453] The transition is characterized as a non-zero wavevector electronic excitation beyond the normal selection rule, leading to the formation of distinct excited electrons and holes with higher and deeper potential energies, compared to those generated by illumination with normal light. This characteristic electronic excitation could also be verified by electrochemical SERS measurements, to obtain detailed information on the potential energy distribution of excited electrons and holes.

An additional effect of the resonance on SERS is also apparent under the condition of the strong coupling states between plasmons and excitons in materials. When the energy of plasmons and that of excitons are close to each other, the spontaneous emission rate and the energy transfer rate are drastically changed compared to the normal case.[784-786] The Raman scattering of the dye molecules has been reported to be strongly coupled to the plasmon of Ag dimer structures.[787] Polarized Raman measurements showed that the maximum enhancement of Raman scattering from the strong coupling regime was achieved at the resonant energy between the hybridized state and the excitation. Active tuning of the coupling strength between dye molecules and metal array structures could be controlled by the electrochemical potential of metal nanostructures (**Figure 8.2**c).[788] The electrochemical potential can vary the number of molecules with controlled distances from metal surface and the direction to the EM filed, which are required for coupling.[789] The possibility of tuning the localization of plasmons for coupling by electrochemical potential control was also suggested by this observation.

SERS provides useful information on light-matter interactions, especially photoabsorption properties at the nanoscale. Considering the effect of resonance enhancement on the Raman process, SERS spectral intensity as well as selectivity of vibrational bands contain details on the electronic excitation of the materials strongly interacting with the plasmon. Significant changes in the selection rules for the electronic excitation could be characterized by the observation of a dependence with the electrochemical potential. Recent theoretical analysis on the localized excitation of materials predicts novel characteristics on not only the excitation of electrons, but also on phonons and spins.[790] Further electrochemical SERS studies could open the possibility for the utilization of the unexpected excitation process in highly confined electromagnetic fields, to control the energy state of molecules and nanomaterials.
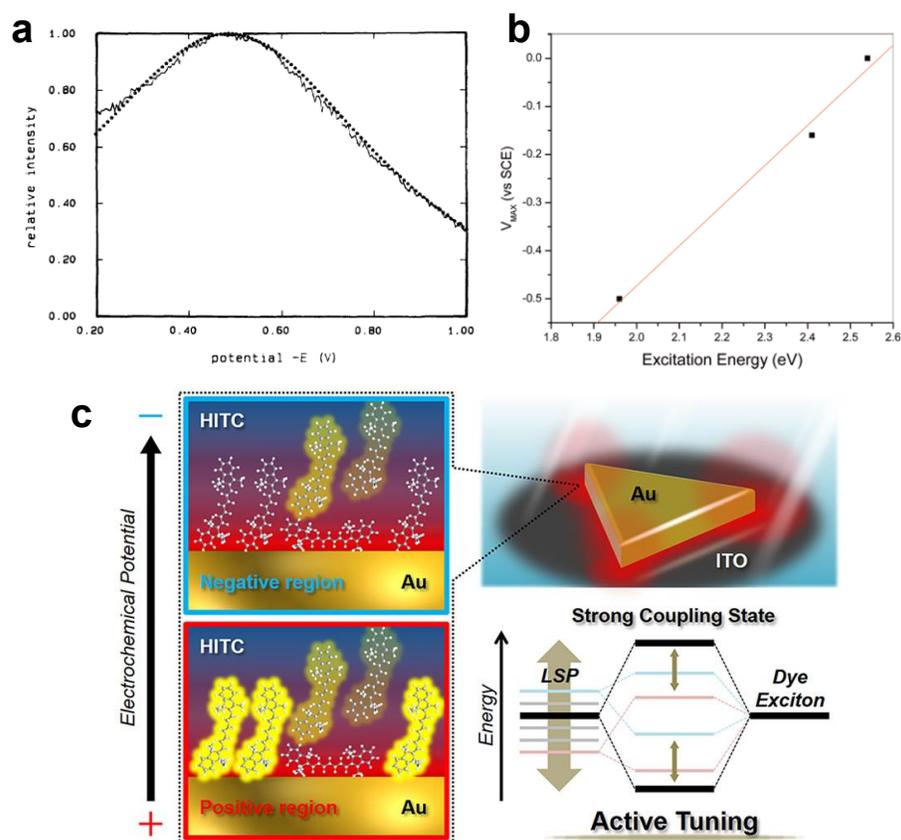
Figure 8.2. (a) Intensity-electrochemical potential profile for the 1020 cm^{-1} line of piperidine on a silver electrode. The dots show the fit of theoretical analysis with $\Gamma = 0.3$ eV ^{3}. (b) Electrochemical potential maximum of the SERS of p-amiothiophenol (PATP) signal as a function of excitation light energy. Reproduced with permission from Ref. 769. Copyright

1986, American Institute of Physics; (c) Schematic presentation of the electrochemical tuning of the strong coupling strength between dye excitons and plasmons. Reproduced with permission from Refs. 788 (Copyright 2008, American Chemical Society), and 789 (Copyright 2018, American Chemical Society).

8.3. Surface Enhanced Hyper Raman Scattering (SEHRS)

Non-linear incoherent optical effects can also utilize enhanced local optical fields of plasmonic nanostructures, in particular hyper Raman scattering (HRS),[791,792] and also second hyper Raman scattering.[793] Two-photon excited, spontaneous Raman scattering that is obtained in the local fields of plasmonic nanostructures, *i.e.* surface enhanced hyper Raman scattering (SEHRS), has been discussed since the 1980s. In SEHRS, the scattered photons are shifted relative to the second harmonic of the excitation wavelength, and the excitation with light in the near infrared is combined with the desirable detection in the visible spectral range (**Figure 8.3**). Although the cross-sections of non-enhanced HRS are extremely low,[794] the HRS signal depends on the square of the incident radiation intensity. The electromagnetic enhancement in SEHRS is the product of the enhancement of the incident field $|A(\nu_0)|^4$ and of the scattered field $|A(\nu_{HRS})|^2$, whereas in SERS it is the product of $|A(\nu_0)|^2$ and $|A(\nu_{RS})|^2$.[795] This shows that HRS benefits enormously from the enhancement by local fields. The total enhancement factor for SEHRS has been reported to be on the order of 10^{20}.[796,797] Cross sections that are comparable to good two-photon fluorophores in SEHRS[797] enable two-photon excited vibrational spectra down to the limit of single molecules[796,798,799] and to collect hyper Raman anti-Stokes spectra.[797,800] Theoretical studies show that the chemical contribution to the overall enhancement in SEHRS can be larger than the corresponding chemical enhancement for SERS.[801-804]

The fact that the HRS process relies on the change in hyperpolarizability of a molecule implies different selection rules, which provide complementary spectroscopic information. Depending on the molecular symmetry, HRS may probe IR active modes or, in addition, so-called silent modes, which are seen neither in Raman nor in IR spectra,[805] thereby SEHRS adds spectral information beyond Raman scattering and in this way, it can improve structural characterization, *e.g.* of molecule-metal interaction,[806] sensing,[807-809] and imaging.[810,811]

The selection rules for non-resonantly excited SEHRS have been discussed by comparing SERS and SEHRS spectra from small organic molecules,[610,812-814] including nucleobases,[815,816] amino acids,[817] drugs,[806] or crystal violet.[64] In the case of centrosymmetric molecules, SERS and SEHRS spectra are complementary to a great extent.[812-814] When the symmetry is lowered during adsorption to the metal, Raman-active modes become visible in the SEHRS spectrum as well. As an example, the non-surface enhanced, resonant HRS and the Raman spectra of beta-carotene are very different from each other,[818,819] but very high similarity of the resonant SEHRS and SERRS spectra is found, because the interaction with the silver surface lowers the symmetry of the adsorbed molecules.[819] The SEHRS and SERS spectra from non-centrosymmetric molecules display bands mostly at the same positions, although with quite different relative intensities,[801,809,815,817] which can be very useful for studying their interactions with the surfaces or for detection. As becomes clear in recent discussions of two-photon resonant SEHRS spectra, it can serve in the characterization of electronic states that are not allowed in one-photon absorption.[820,821]

The high sensitivity of SEHRS with respect to the interaction and orientation of the molecules at surfaces enables probing a very local surface environment using vibrational information that is inaccessible by SERS.[806,814] This will help improve our understanding of molecule-nanostructure interactions, including those utilized in SERS probing. SEHRS spectra of dyes and biological molecules under resonant and non-resonant conditions are typically collected using photon flux densities of 10^{26}-10^{29} photons cm^{-2} s^{-1}, respectively, both from pulsed[797,808,810,816,817,819,822] and tightly focused cw lasers.[823] Many SEHRS experiments have been done using silver nanostructures.[801,823,824] More recently, gold nanorods and their aggregates were also shown to provide optical properties that are specifically suited to support enhancement of SEHRS.[587]

In current developments, the concept of SERS is shown to extend to two-photon excitation in several analytical applications already, and SEHRS signals of both reporters or tags and biological molecules can be used for sensing and imaging. This includes more efficient pH sensors[610,808,825] and the ability of trace detection[809] by reporter species. The advantages of two-photon excitation, together with the strong confinement of SEHRS as plasmonic effect to nanoscopic volumes, led to the development of SEHRS for vibrational imaging and

microscopy.[810,810] SEHRS signals from cultured cells can be obtained[797,811] and used for imaging, and constitute a tool to characterize their microscopic heterogeneity, in particular in combination with SERS. Two-photon excitation allows the use of NIR excitation wavelengths. Biological samples such as live cells will profit from better propagation of the NIR photons through tissues and low phototoxicity. The high enhancement obtained with the gold nanostructures[587] renders them a useful tool in future analytical applications of SEHRS in biological samples, due to low nanotoxicity. As a first example, characterization of gold-based multifunctional drug carriers for tricyclic antidepressants has been achieved by a combination of SEHRS and SERS.[806] In summary, as two-photon excited SERS, SEHRS will provide additional vibrational information and better characterization of molecules and materials, in combination with the advantages of NIR excitation and the high lateral resolution of plasmonics-based spectroscopy.
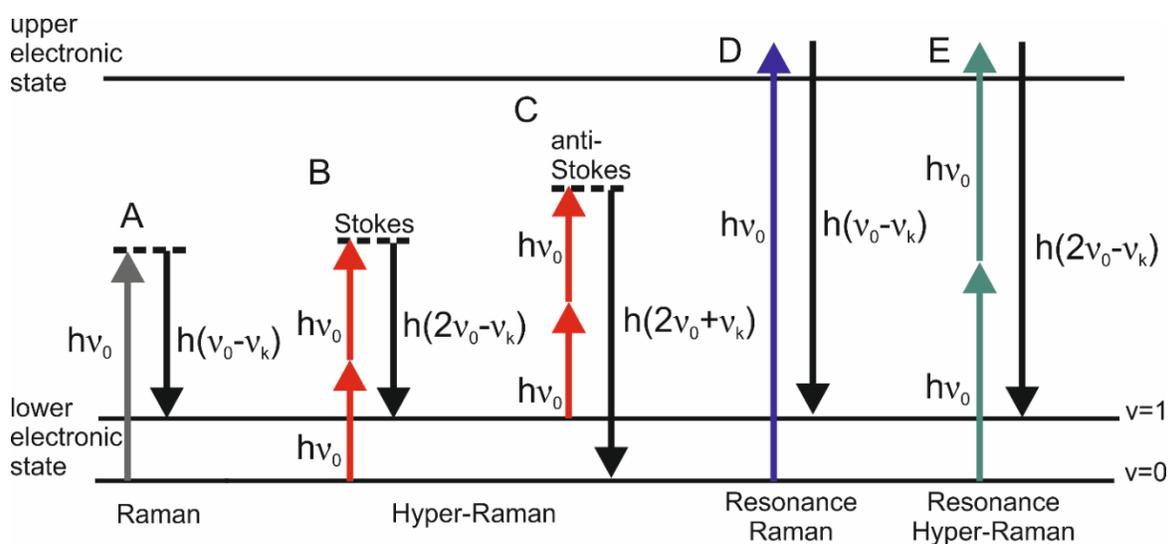
Figure 8.3. Schematic representation of vibrational transitions: linear Stokes Raman scattering (A), Stokes hyper Raman scattering (B), anti-Stokes hyper Raman scattering (C), Stokes resonant Raman scattering (D), and Stokes resonant hyper Raman scattering (E). Molecular systems undergo vibrational transitions from the initial state ($v = 0$ for Stokes, $v = 1$ for anti-Stokes) to the final state ($v = 1$ for Stokes, $v = 0$ for anti-Stokes), linked to a normal mode k with frequency nk. One possible resonance condition is depicted in (E) Reproduced with permission from Ref. 795. Copyright 2017, Royal Society of Chemistry.

8.4. Tip Enhanced Raman Scattering (TERS)

As a sister technique to SERS, tip enhanced Raman scattering (TERS) spectroscopy uses Ag or Au tips with tip apex diameters smaller than 20 nm, to produce strongly enhanced electromagnetic fields at the tip apex (**Figure 8.4.**).[826-828] The highly confined electromagnetic field at the tip apex not only enhances the Raman signal of species in the vicinity of the tip (usually less than 5 nm) but also provides a high spatial resolution below 5 nm by scanning the tip over the sample[95, 829-832], which endows it with the capability to ultimately resolve submolecular features inside one molecule.[74, 833] Indeed, it has been nearly 20 years since the first discovery of TERS in 2000, and the technique has found wide applications in various fields including chemistry, physics, materials science and biology.[829-833]
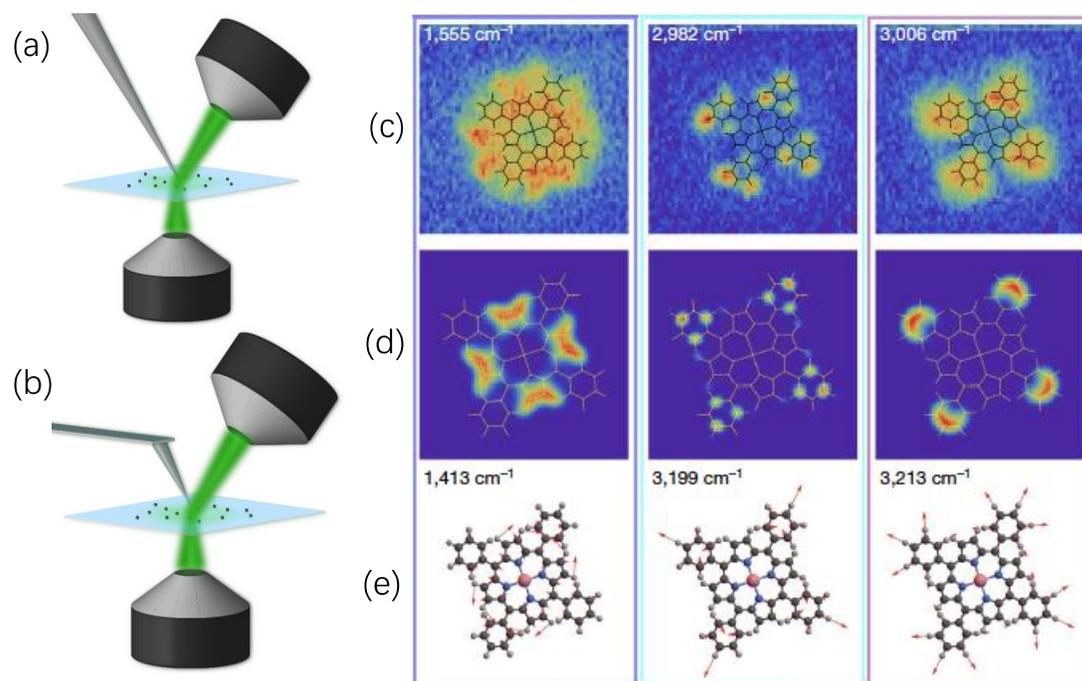
Figure 8.4. Schematic illustration of STM (a) and AFM-based (b) TERS setups. (c) Experimental TERS images obtained with UHV-TERS, which allows visualization of different normal modes of a single molecule. (d) Simulation results. (e) Assigned vibrational normal modes. Reproduced with permission from Ref. 833. Copyright 2019, Springer Nature.

Different from SERS, TERS relies on the enhancement provided by a single tip and from a single hotspot. Therefore, sensitivity is the key issue for TERS, which can be improved by either optimizing the tip structure or the throughput of instruments. Up to now, most TERS works were executed on home-built TERS instruments, including ambient condition STM or AFM based TERS,[826-828] UHV-based TERS (UHV-TERS),[74,833-835] liquid[836] or electrochemical TERS (EC-TERS) systems.[837-839] Some companies are now providing commercial instruments by closely collaborating with TERS researchers, while others provide key components such as AFM/STM systems or Raman spectrometers.

The tip is the core component in TERS, because it should not only be sharp enough to obtain high resolution topological images of the sample, but also supports the LSPR at the desired wavelength, to significantly enhance the near-field Raman signal of the sample.[830,840] Numerous physical and chemical methods have been reported to fabricate tips with a high TERS activity. Different TERS working modes (STM tunneling, AFM cantilever feedback, AFM tuning fork feedback, *etc*.) will require different tip fabrication methods. Electrochemical etching is the most frequently used method to etch silver or gold wires to conveniently obtain TERS tips for STM-TERS.[841-842] Vacuum deposition methods are most widely used to deposit Ag or Au coating on commercial AFM tips for AFM-TERS, and it was found that the formation of island-like structures is advantageous for a large enhancement.[843, 844] This method has also been used to produce commercial TERS tips. More recently, the electrochemical deposition method has also been developed to fabricate Ag and Au AFM-TERS tips with controlled size.[845-846] To improve the stability and prolong the lifetime of TERS tips, especially Ag tips, they can be coated with an ultrathin silica layer to prevent Ag oxidation, adsorption of impurities, and the movement of surface atoms. If a material with a high dielectric constant is used, the TERS signal may not be sacrificed while still maintaining the high stability of the tip.[479] There are reports on TERS imaging with ultra-high spatial resolution, without using a metallic substrate to support gap mode TERS.[847-848] Such a large enhancement and confinement of the EM field from a single tip has not yet been explicitly understood and requires both high spatial resolution characterization of such peculiar tips and theoretical efforts, which may help to rationally engineer tips with ultrahigh enhancement and confinement of the EM field.

The first demonstration of TERS was on the detection of molecular film deposited on a glass slide.[826, 849,850] Thereafter, the studied molecules have been expanded from dye molecules with resonance Raman signal to small aromatic molecules with strong binding affinity to the surface. The employed substrates range from simple glass slides, Au or Ag films to Au or Ag single crystals. TERS has already passed the stage of simply showing its capability of achieving a near-field signal. Instead, the high spatial resolution of TERS has been fully exploited to tackle some important problems in surface science and electrochemistry, as well as to identify biomolecules.[829-832] Specifically, TERS has been used to monitor chemical reactions like simple protonations,[851] but also more complex reactions like dimerization of p-aminothiophenol (PATP) or p-nitrothiophenol (PNTP) to form p,p′-dimercaptoazobenzene (DMAB) and isomerization of azobenzene on the surface or under the influence of plasmon excitation, among others.[852,853] The high spatial resolution of TERS has been fully applied to investigate, with a spatial resolution of 2.5 nm, the electronic properties of bimetallic systems (*e.g.* monoatomic islands of Pd and multilayer Pt islands on Au(111) surfaces), using isocyanidebenzene, sensitive to the substrate electronic properties, as probe molecules.[854, 855] This study revealed interesting properties, including bonding interaction, surface coordination and strain effects, of bimetallic surfaces.

TERS measurements in air are often accompanied by sample degradation, as a result of several effects after plasmon excitation, including plasmon-induced hot carriers, heating, and oxygen activation. There are increasing efforts in developing environmental TERS, *e.g.* in electrochemistry or UHV, to properly control surface states. Electrochemical TERS (EC-TERS), which involves measurements in an electrolyte and under potential control. In this way, the surface states and the interactions and reactions of molecules with the substrate can be controlled in a flexible manner. In EC-TERS, the molecular system to be probed is under complex interaction with its environment close to the operando condition. After the first demonstration of TERS in liquid in 2009,[836] EC-TERS was successfully demonstrated on an STM-TERS system in 2015, by revealing the potential dependent protonation and deprotonation of thiol molecules adsorbed on an Au(111) surface.[837] Almost at the same time, AFM-based EC-TERS was developed to monitor the electrochemical redox behavior of nile blue (NB) molecules on a transparent ITO surface.[838] A step-like feature in TERS voltammograms was observed at low surface coverage, corresponding to the reduction and

oxidation of single or few molecules. There are increasing efforts in employing STM-TERS due to the flexibility of making TERS tips for working under electrochemical conditions.[839, 856] Although EC-TERS is still at an early stage, it shows promising potential in addressing more interesting and challenging issues at the electrochemical interface, including electro(photo)catalysis, corrosion, plasmon-driven electron transfer, and energy storage. With an extremely high spatial resolution down to several nm, it is possible to achieve nanoscale spectral imaging and reveal the structure–function correlation for electrochemical interfaces by correlating the sub-nanometer resolution SPM image with a simultaneous nm resolution TERS image.

Different from EC-TERS, when TERS is working in a UHV chamber (UHV-TERS), it is free of oxygen and other impurities, which can considerably reduce photo-induced reactions. Most importantly, UHV-TERS is generally much more stable than environmental TERS. The first room temperature UHV-TERS demonstrated the TERS signal from a single BCB molecule.[834] Recently, the different adsorption configurations of oxygen on CoPc supported on the Ag(111) surface were probed by UHV-TERS and the vibrational mode coupling of the O−O and Co−O vibrations with the Pc ring was observed.[857] When the temperature was lowered to cryogenic conditions, the mobility of the molecules on the surface and the thermal drift of the instrument can be significantly reduced, which will allow TERS imaging at an extremely high spatial resolution. A milestone work in TERS was the demonstration of sub-molecular (0.5 nm) TERS imaging of a single porphyrin molecule on the Ag(111) surface at a temperature of 80 K and under UHV conditions.[74] The high resolution allows the spatial distinction of two adjacent molecules within van der Waals interactions.[858] When the temperature was lowered to the liquid helium regime (6 K), the Ångström-scale resolution TERS images of different normal modes within a molecule were clearly obtained.[833] Such a spatial resolution challenges our understanding in the framework of traditional electromagnetic theory, but may reveal interesting physics of vibrational spectroscopy and inhomogeneously distributed electromagnetic field under confined picocavity conditions.

All of the above high-resolution studies relied on the use of gap mode TERS, which means Ag or Au substrates were used to couple with the LSPR of Ag or Au tip, to significantly increase the enhancement and spatial resolution. However, more and more studies have

shown a spatial resolution of ~3 nm on carbon nanotubes, allowing the visualization of local defects and strain,[859] and better than 2 nm (and even single amino acid resolution) on amyloid protein crystals,[860] without using the gap mode on an AFM-TERS under ambient conditions. Such high enhancement and resolution cannot be readily explained by a standard electromagnetic model, but may be understood by the following two possibilities: (1) the atomic roughness features on the TERS tips that generate an additional highly confined electromagnetic field sufficient to allow single molecule sensitivity,[87,93] and (2) the special chemical interaction by approaching the tip to a special site on a molecule, which may not be favorable in SERS. In the latter case, even minute position changes (a few Ångstöms) of the tip with respect to the molecule will result in a conformational change and consequently in a change of the Raman pattern.[108]

Increasing efforts are being made toward applying TERS to study novel materials, from carbon nanotubes to various types of 2D materials, including graphene, silicene and various types of transition metal dichalcogenides (TMDC). More recently, TERS was used to image 2D silicene on Ag(111) and achieve a spatial resolution of 0.5 nm benefited from enhancement factors as high as 10^9. The ZO, LO, and TO phonon modes at high frequencies not observable in normal Raman were observed.[861] There is a surging interest on using TERS to characterize TMDCs, including MoS_2, $MoSe_2$, WS_2, and WSe_2, regarding their peculiar properties including special chemical activity, optical properties, and valley related effects, as a result of structural heterogeneities, including doping, defects, and strain in TMDCs.[862] A spatial resolution of 2.3 nm was achieved from monolayer MoS_2 because of giant enhancements up to 5×10^8, as result of the coupling between the Au-coated AFM tip and Au nanocluster arrays. The plasmonic hot electron doping of monolayer MoS_2 was estimated to be in the order of 1.8×10^{13} cm^{-2}, leading to a transient structural shift from the 2H to 1T phase. Such information might not have been achieved without the super-high spatial resolution of TERS.[863]

A remarkably large number of investigations using TERS have been done on bio-related compounds despite the complexity of such samples. TERS has been applied to a wide range of biological samples ranging from biofilms,[864] bacterial[865] and cell surfaces,[866] to single protein and RNA/DNA crystals, molecules and strands.[867-872] The common goal is to

investigate structures that cannot be revealed by standard microscopy techniques. While sequencing has become almost a routine technique and TERS will not be able to compete directly with traditional methods, TERS spectra along the DNA strands, modified DNA and ageing DNA still showed a strong indication of direct sequencing.[873,874] Similar approaches could be foreseen for an analytical application regarding single virus detection and discrimination as no culture step is necessary.[875,876] By scanning over the surface of a virus particle, a spectral fingerprint could be generated to distinguish different viruses.

With the development of nanoscience and experimental techniques, intriguing results are reported, *e.g.* the observation of localized or forbidden vibrational modes and ultrahigh spatial resolution. As mentioned above, these novel phenomena cannot be fully understood by the classical EM theory and thus stimulate a surge of work toward alternative ways to understand the TERS mechanism under well-defined conditions, so that the proposed mechanisms can be strictly verified by experiments.[93,95-98,102,877] Although it has been demonstrated that TERS is able to obtain signals from adsorbed species and reaction products on metal surfaces, great efforts are yet to be devoted to its development into an *operando* technique, so that the dynamic changes of surface structures at active sites and quantification of products at such sites can be monitored with nanometer spatial resolution and at the molecular level. Although EC-TERS has enabled *in situ* characterization of electrochemical processes at solid-liquid interfaces, TERS systems that can work under water and air-free conditions, such as in a glovebox, are highly welcome. Such a facility can be used for studying more practical systems, such as lithium ion batteries and photoelectrochemical systems. All of these important and potential applications require TERS with significantly improved sensitivity and imaging rates. It is also necessary to establish a solid protocol to guide the selection of the tip and optical configuration, as well as excitation wavelength to achieve the optimized sensitivity and spatial resolution. The directional TERS detection scheme is another important approach that may help reducing the background and improving the collection efficiency, but requires a rational design of the tip and sample configuration.[878] By combining non-linear Raman techniques (CARS[879] or SRS[880]) with plasmonic tip enhancement, sufficient Raman signal can be obtained fast enough to achieve (sub-)Ångström resolution under ambient conditions, or even in an aqueous solution. It should also be considered that most TERS systems are optimized to a particular wavelength as they

operate with single-line laser excitation. Recently, an excitation-tunable TERS (eTERS) setup was reported by coupling a commercial TERS system with a tunable laser.[881] The advantage of eTERS is two-fold: first, the combined resonant enhancement and tip enhancement results in much higher enhancement factors than those in conventional TERS; second, eTERS is able to map optical transition energies and specific resonant vibrations at nanometer spatial resolution. It can thus be used to measure, *e.g.*, an optically active component in large biomolecules or optical trap states in two-dimensional materials.[881] Although chemometric methods have been widely used in standard Raman and SERS studies, it would be advantageous if they could also be integrated into TERS software, so as to improve signal quality and TERS imaging speed. The existing challenges in the field also indicate that there is still potential and room to further improve the enhancement and accelerate the development of TERS, which requires the synergistic collaboration between experimentalists and theoreticians.

8.5. Surface Enhanced Infrared Absorption (SEIRA)

Just like SERS, surface enhanced infrared absorption (SEIRA) of molecular vibrations extraordinarily benefits from resonant plasmonic enhancements.[882-886] There is however an important difference: the molecules do not inelastically scatter light, they absorb light at the frequencies of their vibrational resonances which are in the infrared (IR) range. This difference has two consequences for the measured vibrational signal size. On the one hand, the benefit from the near field enhancement is lower than in SERS. For weak vibrational oscillators, the SEIRA enhancement is clearly proportional to the squared near field amplitude enhancement[887,888] and not to its fourth power as in SERS. On the other hand, molecular absorption is a direct process with a much higher cross section than in Raman scattering.

Similar to Raman scattering and SERS, chemical interface processes might modify measured SEIRA signals further.[884,889,890] These chemical interaction processes can be avoided with inert interlayers between the metal surface and the molecules. Then only electromagnetic enhancement occurs, which simplifies the quantitative chemical analysis. The coupling of IR vibrational dipoles with plasmonic resonances is mostly strong enough to lead to a Fano-type vibrational line shape, the asymmetry of which depends on the detuning between the

plasmonic resonance and the vibrational resonance. [882-891] Even Rabi splitting has been observed for strong vibrational dipoles, from optical phonon polaritons of thin layers within the spatial range of the enhanced plasmonic near field.[892] Therefore, the line shape as well as the vibrational signal enhancement depend on the amount of near field enhancement. For the spectral analysis, the Fano lines due to electromagnetic coupling are not really a problem because the right molecular frequencies and vibrational damping can be obtained by spectral fits to Fano lines instead of Lorentzians.[891]

The maximum value of the near field enhancement for a given nanostructure is reached at its plasmonic resonance, see for example Ref. 883 and references therein. This maximum enhancement is the highest possible if the absorption cross section of the plasmonic structure is equal to the cross section for radiation scattering.[893] Such a situation can be reached with geometrically optimized structures and low electronic damping (perfect crystallinity) of the metal, as shown by measurements[894] and simulations[888] for linear nanoantennas (**Figure 8.5**). Then, in SEIRA based on IR extinction measurements, extraordinarily enhanced vibrational signals show up because the vibrational absorption strongly modulates the IR light scattering of the plasmonic system.[888]
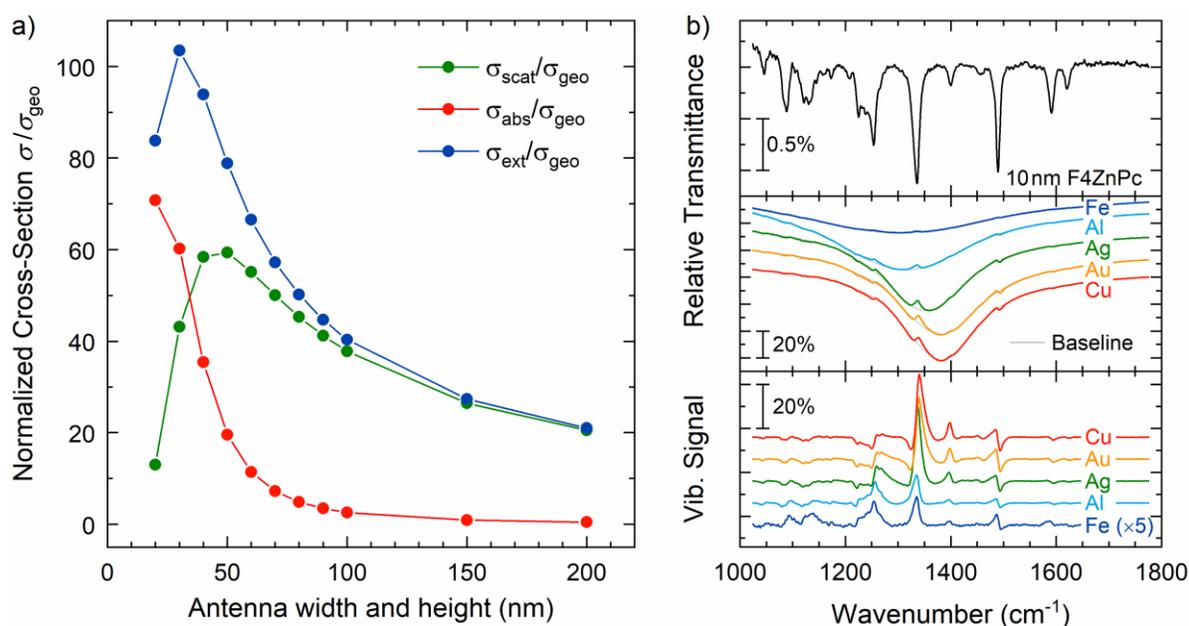
Figure 8.5. (a) Cross sections: σ_{ext} for extinction, σ_{abs} for absorption, and σ_{sca} for scattering of light. These cross sections have been calculated for gold antennas at the fundamental resonance by FDTD simulations and are shown as quantities normalized to the geometric

cross section. Reproduced with permission from Ref. 888. Copyright 2015, American Chemical Society. The maximum near-field enhancement is expected when $\sigma_{abs} = \sigma_{sca}$ at the plasmon resonance. In (b) the relative transmittance (at normal incidence of light) of a 10 nm thick layer of a tetrafluorinated zinc phthalocyanine complex ($C_{32}H_{12}F_4N_8Zn$, short name: F4ZnPc) on a CaF_2 wafer is shown on top. Spectra of 10 nm F4ZnPc on 50 nm high nanoantennas produced on CaF_2 substrates, from various metals are shown in the middle (as transmittance at normal incidence of light with polarization along the antennas divided by the bare substrate's transmittance) and in the bottom panel as baseline corrected vibrational spectra. The width of the nanoantennas has been adjusted to the maximum SEIRA enhancement which is achieved if $\sigma_{abs} = \sigma_{sca}$. SEIRA is directly obvious and, furthermore, it should be noticed that the SEIRA enhancement comes only from the small sample regions with near field enhancement. Bigger enhancement with Cu, Ag, and Au antennas is attained because of the lower electronic damping. Reproduced with permission from Ref. 894. Copyright 2018, American Chemical Society.

SEIRA with metallic nanostructures for which light scattering is marginal is a weaker coupling effect, which is based on the modulation of the light absorption of the nanostructure by the vibrational absorption.[884,888] Examples are metal particles much smaller than a certain wavelength at which they then mainly absorb light but almost do not scatter it.[895] Thus, metal particle layers with particle diameters of less than about 100 nm only absorb IR light. There are many studies on the development of the IR absorption spectrum with particle geometry and density,[890,896,897] and many related SEIRA studies have been published.[884,898,899] The SEIRA signal intensity in such studies benefits from near field hotspots and also from the multitude of adsorption sites for the molecules. The hotspots are, for example, located between particles in a close neighborhood and thus, for a metal island layer as an ensemble of tiny plasmonic particles, the highest SEIRA signals are observed near the percolation threshold.[884,899,900]

Nanostructures consisting of geometrically optimized nanoapertures in metallic layers combine the advantages of concentrated hotspots and notable light scattering, and thus are perfectly suited for huge SEIRA enhancement.[901-904] For chemical sensing of vibrational

signals of clusters (for example, ultrafine dust), bowtie-like apertures are beneficial because they feature a particularly high near field concentration and offer a further advantage that is the trapping of the clusters (**Figure 8.6**).[904]
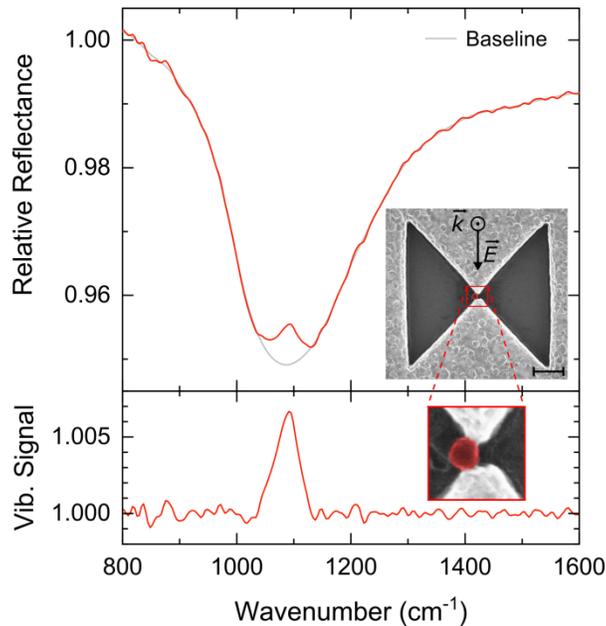
Figure 8.6. (a) Near normal relative reflectance (normalized to the reflectance of the flat gold layer, polarization as indicated in the inset) of one bowtie aperture in a 50 nm thick gold layer (on 2.5 nm Cr as adhesion layer) on CaF_2. The SiO_2 nanosphere (85 nm in diameter) in the gap of the bowtie aperture gives rise to an anti-absorption-like feature on the broader plasmonic resonance spectrum. The geometry of the nanostructure can be recognized in the SEM image shown as inset. (b) Baseline corrected spectrum of the nanosphere. The peak is related to a localized phonon-polariton excitation of the sphere in the Si-O-Si stretching vibration band, and thus material specific. The inset shows a SEM image from (a) as a zoom to the gap region with the sphere colored in red (scale bar: 400 nm). Reproduced with permission from Ref. 904. Copyright 2019, American Physical Society.

Recently, Popp and co-workers succeeded in designing and fabricating slit-based substrates, in which both substrate and electric field are concentrated in the same location. These substrates consist of a periodic array of slits in a gold surface above a dielectric layer and a

continuous gold layer (metal-dielectric-metal structure). For completely filled slits, FDTD calculations predict a signal in reflection as large as 25%, which is even exceeded in the experiment.[905] Without the continuous layer and placed on a thin Si_3N_4-substrate, such substrates can also be employed in transmission mode. Using two slits that cross each other but are not perpendicularly aligned, a gigantic circular dichroism signal is generated.[906] Based on this effect, the first working plasmonic substrates were demonstrated which allow the discrimination of enantiomers based on infrared circular dichroism.[907] For very thin films (thickness < 2 nm) structured substrates are less suited. Here, interference rather than plasmonic enhancement is of particular advantage. In this respect, it was recently shown that working in the internal reflection configuration, interference enhancement should give signals of more than 5% for the CH_2-stretching vibrational bands of a monolayer of octadecane.[908] The same technique should also be able to strongly enhance Raman signals without changing the selection rules, something which is known from ordinary interference-enhanced Raman spectroscopy.[909]

IR and SEIRA measurements are usually done with far field IR microscopes[910] coupled to Fourier-transform spectrometers. A lateral resolution much better than the Abbé limit can be obtained with spectroscopic IR near-field microscopy, for which the detection of the vibrational signal of one molecule was predicted if it sits in a hot spot of the fundamental plasmon resonance of a noble metal nanoantenna, see the Supporting Information of Ref. 882. This experimental result has not been published yet but recent SEIRA experiments have detected the vibrational signal of less than 1000 molecules, still with far field techniques.[911]

9.   Monitoring chemical reactions

Surface plasmons can redistribute not only the electromagnetic field, but also the excited carriers (electron and hole) and heat energy in time and space, which can power chemical reactions. The expansion from plasmon physics (*e.g.* plasmon enhanced molecular spectroscopies (PEMS) and waveguides, *etc.*) to plasmon chemistry has recently attracted a great deal of attention.[912-917] The term plasmon-mediated (also -enhanced, -assisted, -promoted or -induced) chemical reactions (PMCR) is used to describe how nanostructure-based surface plasmons act as mediators to convert the photon energy in time, space and at

various energy scales effectively, thereby driving chemical reactions by localizing photon, electronic and/or thermal energies. The idea of using SPs to enhance chemical reactions was first proposed in 1981 then experimentally realized two years later.[918,919] In recent years, numerous elegant studies demonstrated that plasmonic nanostructures can mediate/catalyze chemical reactions under low-intensity visible light illumination, *e.g.* reactions at the solid-gas interface or at the solid-liquid interface and even electrochemical processes, as a promising approach to facilitate chemical reaction under mild conditions.[920-924] For example, it has been demonstrated that the SP excited electrons can transfer into oxygen molecules to promote oxygen activation by forming transient negative-ion states, which can greatly improve the catalytic oxidation reactions, such as ethylene epoxidation, CO oxidation, and NH_3 oxidation.[921] Furthermore, overall water splitting was carried out by SP excited electrons and holes from Au nanorod arrays in contact with TiO_2 upon visible light irradiation.[920] Most recently, it was found that SPs can be used to reduce the thermal activation barrier by excited carriers.[923]

9.1. Plasmon Mediated Chemical Reactions (PMCR) and Plasmon Enhanced Molecular Spectroscopy (PEMS)

In general, both PEMS and PMCR are three body interactions, including photons, molecules and nanostructures (**Figure 9.1**), and their interface is not sharp. In 2010, Tian and co-workers discovered that SPs could mediate the transformation of p-aminothiophenol (PATP) into p,p'-dimercaptoazobenzene (DMAB) during plasmon enhanced Raman spectroscopy (PERS).[925] In such experiments, surface plasmons were exploited in two ways: mediating the photochemical reaction and allowing *in situ* reliable measurements of the reaction process. Nevertheless, it should be pointed out that PEMS and PMCR are different in some key aspects. For example, the strong bonding between the probe molecule and the metal surface can ensure a satisfactory detection sensitivity for PERS, but it usually blocks the active sites for chemical reactions.
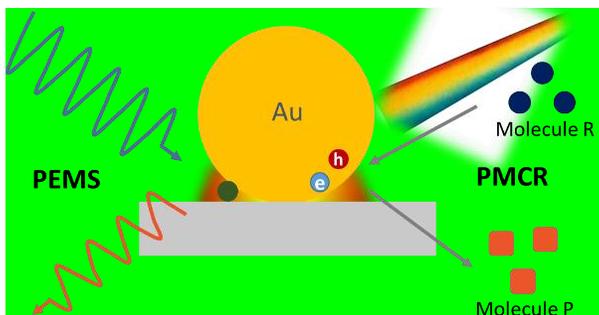
Figure 9.1. Schematic representation of PEMS and PMCR.

The growth and future of PMCR critically depend on the fundamental understanding of SP properties and how they enable chemical reactions. Based on existing reports, it is found that PMCR has its own advantages, distinct from existing photo- and thermal reaction systems.[917] For example, the EM field and/or the thermal field in PMCR systems are usually nano-confined with sharp gradients (sub-nm ~ nm for EM fields, and nm ~ μm for thermal fields) which can drive chemical reactions at an extreme level of spatial selectivity. Moreover, in such systems, both the nano-optics and nano-thermodynamics are special, thereby providing opportunities for mediating reactions with increased efficiencies and/or regulating the product selectivity. Additionally, the lifetime (< ps) and the energy distribution of the excited carriers in PMCR systems are largely different from those in traditional photocatalysts because of the lack of band gap for most plasmon active materials. Based on these characteristics, one should find out the functions that PMCR can do but traditional photo- and thermal reactions cannot.

The field of PMCR is still in an embryonic stage and two main challenges have risen to the forefront: its complex operating mechanism and its limited efficiency. More specifically, one is how to distinguish the influence of multi-effects of surface plasmons on the chemical reaction, especially the photoelectronic and photothermal effects; the other is how to power the chemical reaction more effectively, especially to regulate the product selectivity, which are two key factors for the chemical industry. Predictably, by understanding the mechanism of PMCR in depth, thus rationally designing plasmonic nanostructures, surface plasmons can expand the possibilities for chemistry.

9.2. Plasmon Induced Chemical Reactions - Practical Examples

161

SERS has proven particularly powerful for monitoring reactions on the surface of plasmonic nanoparticles *in situ* and with sensitivity down to the single-molecule level.[499,926] In one class of reactions, excitation of surface plasmons facilitates light-driven photochemistry,[913,927-929] which can be monitored by tracking the evolution of SERS spectra over time. Perhaps the most widely studied example of this is the formation of DMAB on plasmonic nanoparticle surfaces, from either the oxidation of PATP or the reduction of nitrothiophenol (NTP).[925,930-932] SERS is particularly well-suited to study this reaction because the spectra show a clear emergence of vibrational signatures from the newly formed azo bond, allowing the reaction kinetics to be monitored in real time and reaction reversibility under varying conditions to be followed. The mechanism for DMAB formation is believed to be plasmonic in origin, with hot charge carriers produced upon plasmon decay promoting the reaction at the nanoparticle surface,[933-935] although questions about the role of local heating and how other species affect reactivity remain active avenues of exploration.[936-939] Beyond this canonical set of reactions, SERS has also been used to study other plasmon-driven photochemical reactions. For example, Moskovits and co-workers used a combination of SERS and electron microscopy to follow plasmon-driven photochemistry of Pt(II) ions in solution.[940] While electron microscopy revealed deposition of solid material at the surface of gold nanoparticles upon plasmon excitation, suggesting reduction of Pt(II) to Pt(0), subsequent SERS analysis revealed the presence of PtO_2, indicating that both oxidation and reduction products were present. Shin and co-workers used SERS to track the hot carrier induced reduction of Fe^{3+} to Fe^{2+} at the surface of silver nanoparticles, using CN-terminated molecules bound to the silver surface to capture the cation and report subsequent reduction through a shift in the frequency of the CN stretch.[941] A key to each of these examples is that, while light drives the reactions at the plasmonic nanoparticle surface, it also provides an analytical tool for real-time characterization of the products through SERS, highlighting the ability of these materials to serve as both catalysts and probes. Thus, as interest in plasmon-assisted photocatalysis continues to grow, we envision SERS will be a key characterization strategy to monitor these types of reactions *in situ* and in real time. However, the use of SERS for characterizing plasmon-driven reactions must also be accompanied by an appreciation of how hot carrier and thermal effects can impact the observed results, requiring careful analysis of the spectra to untangle potentially complex reaction mechanisms.[929,942]

9.3. Electrochemical Reactions

A second class of reactions that can be interrogated with SERS involves electrochemical conversion of reactants to products under an applied potential, using a variety of nanoparticle and tip enhanced geometries to provide signal enhancement.[118,944-945] As molecules undergo electrochemical oxidation/reduction, changes in the SERS spectra are followed in real time, allowing reactions to be monitored *in situ* as well as providing hidden mechanistic insight.[946,947] For example, Van Duyne and co-workers used SERS with 532 nm excitation to monitor the electrochemical behavior of Rhodamine 6G (R6G) under an applied potential, tracking the loss and gain in the resonantly-enhanced SERS signal from the molecule as it underwent reduction and oxidation, respectively.[948,949] To probe the reduced form of the molecule, the authors switched to 405 nm excitation and found new vibrational modes that were associated with R6G radical formation, as supported by theoretical calculations.[949] Willets and co-workers used SERS to understand a change in the electrochemical behavior of Nile Blue (NB) upon covalent attachment to the surface of gold nanoparticles.[950,951] In this work, the cyclic voltammogram of the molecule shifted from being single peaked to dual peaked upon covalent attachment to the surface of the gold. By monitoring the SERS spectrum as the potential was swept, the authors were able to distinguish two electron transfer events associated with each of the two peaks in the voltammogram: one to the terminal amine and the second to the phenoxazine core. While these examples highlight the power of using SERS in electrochemical environments, it is also important to consider the possibility that plasmon excitation can lead to unexpected changes in the electrochemical behavior, either through local heating or charge carrier production.[943] As SERS continues to be used across a wide range of applications in electrochemical studies, we encourage all results to be carefully analyzed, so as to ensure that no plasmon driven side reactions have occurred.

9.4. Spatial Confinement in Gaps and Hotspots

Beyond using SERS as a spectroscopic tool to follow reactions in real time, SERS imaging has emerged as a powerful strategy for following the spatial dependence of reactions on plasmonic nanoparticles.[952,953] Here, SERS scattered photons are not spectrally dispersed, but are rather imaged directly onto a CCD camera, usually as diffraction-limited spots. By applying techniques from super-resolution imaging, the SERS scattering from molecules

on/near the nanoparticle surface can be spatially localized, often with a precision better than 20 nm.[954] For example, Willets and co-workers used super-resolution SERS imaging to study the electrochemical behavior of Nile Blue on the surface of gold nanoparticles.[953] Nile Blue has a strong SERS signal in its oxidized form, but the signal drops near zero upon reduction. Localizing the SERS signal as different populations of molecules are reduced, provides a window into how the spatial distribution of molecules on the nanoparticle surface affects their electrochemical performance. **Figure 9.2** shows an example of how the spatial origin of the Nile Blue SERS on the surface of an aggregated gold nanoparticle structure changes under different applied potentials. Under oxidizing potentials, when all molecules are expected to generate strong SERS signals, the spatial origin of SERS collapses near the geometric center of the aggregate, indicating the average position of the molecules on the surface. However, as the potential is stepped towards increasingly negative values, such that few molecules remain in the SERS-active oxidized form, the spatial origin of the SERS signal localizes near junction regions (or hotspots), suggesting that these regions have a distinct electrochemical environment that makes the molecules more difficult to reduce (or, conversely, easier to oxidize). This is consistent with the picture that plasmon-generated hot carriers may be associated with regions of strong electromagnetic field enhancement,[940,955] generating local potential differences across the surface of plasmonic nanoparticles.[952] Importantly, this example highlights the power of using SERS imaging to spatially track reactions in real time and to understand how the structure of the plasmonic catalyst affects local reactivity, representing an important future direction as interest in plasmon-assisted photocatalysis continues to grow.
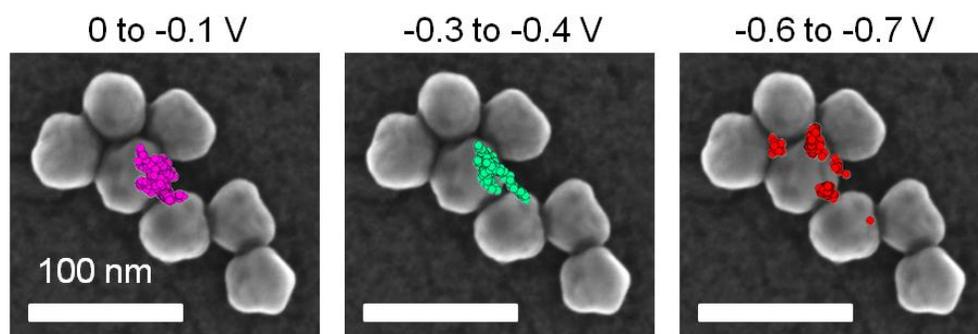
Figure 9.2. Potential-dependent spatial origin of SERS from surface-tethered Nile Blue molecules (colored points) overlaid on an SEM image of the underlying gold nanoparticle aggregate. The applied potential range is indicated at the top of each panel. The data show that molecules located near junction regions are the most difficult to reduce/easiest to oxidize. Potentials are reported relative to a Ag|AgCl electrode. Reproduced with permission from Ref. 953. Copyright 2015, American Chemical Society.

9.5. Liquid- and Gas-Based Reactions

We have seen that SERS is promising for molecular-level reaction tracking owing to its ability to rapidly read-out the identity and composition of reaction species (*e.g.* reactants, intermediates and products), using their characteristic vibrational fingerprints. These attributes allow concurrent elucidation of representative reaction mechanisms and associated kinetic models, even in a multi-step reaction, which were previously not possible using non-molecular-specific techniques such as fluorescence spectroscopy and gravimetric analysis.[956] In this section, we discuss recent efforts to incorporate SERS platforms for *in situ* monitoring of (1) liquid-based reactions and (2) gas-based reactions (**Figure 9.3**).
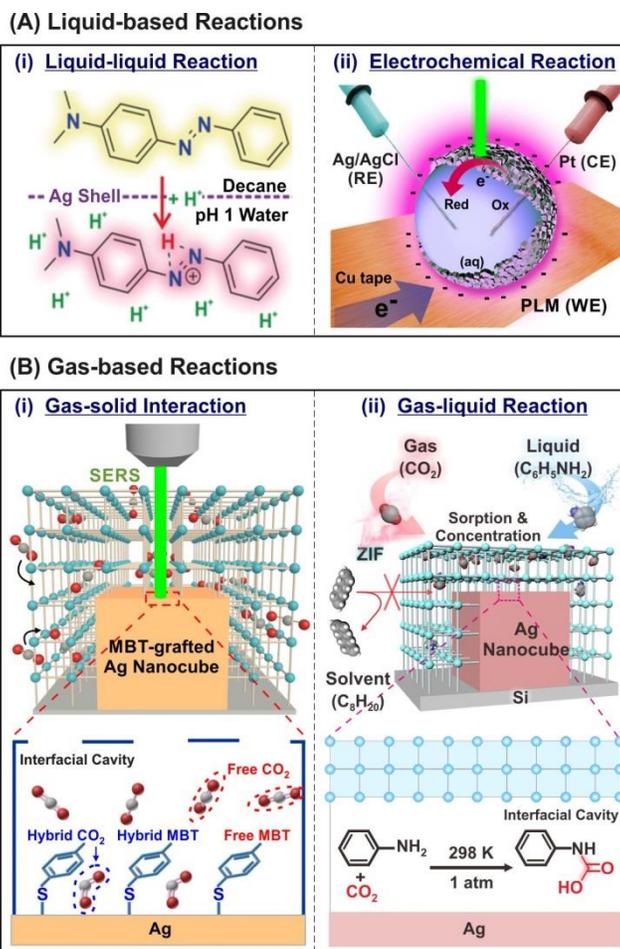
Figure 9.3. Emerging strategies to monitor liquid-based (A) and gas-based (B) reactions using SERS. (A) Particle-assembled microdroplets, such as plasmonic liquid marble and plasmonic colloidosome, have been designed to track (i) immiscible liquid-liquid reactions. Adapted with permission from Ref. 957 (Copyright 2017, American Chemical Society); and (ii) electrochemical reactions. Adapted with permission from Ref. 958 (Copyright 2016, Wiley-VCH). (B) Integrating MOF with SERS to read-out molecular events during (i) gas-solid interaction. Adapted with permission from Ref. 960 (Copyright 2017, American Chemical Society); (ii) gas-liquid reaction. Adapted with permission from Ref. 961 (Copyright 2018, Wiley-VCH).

Liquid-based reactions

In liquid-based reactions, all reaction species are present in one or more liquid phases and it is probably the most common process set-up in research and industrial settings. This

class of reactions undergo reactant-to-product transformations, usually in bulk liquid phase and are hard to track because evolving species may not be present within the electromagnetic hotspot, needed for SERS measurements. It is thus necessary to create 3D plasmonic structures with dense electromagnetic hotspots for efficient interaction and read-out of reaction species. Ling *et al*. demonstrated the use of plasmonic particle-assembled microdroplets, such as plasmonic liquid marbles (PLM; millimeter-sized) and plasmonic colloidosomes (PC; micron-sized), which function as both miniaturized reactors and ultrasensitive SERS platforms for *in situ* reaction monitoring (**Figure 9.3**A-i).[957-959] These microdroplets possess a 3D plasmonic shell to drastically boost the Raman signal by $>10^8$-fold, thereby allowing temporal reaction tracking in a single liquid phase reaction.[957] Beyond single liquid phase detection, PC also offers a powerful approach for swift and stable SERS measurements of dynamic events at a liquid-liquid interface, due to the strategic positioning of a 3D SERS-active ensemble, directly at the interfacial boundary.[958] More importantly, the recorded molecular vibrational signatures allow univocal differentiation of isomeric products during the interfacial protonation of dimethyl yellow. This advantage again highlights the importance of SERS to accurately index reaction species that are otherwise undistinguishable using conventional analytical methods such as HPLC.

Recently, PLM was demonstrated as an isolated spectroelectrochemical microreactor, capable of complementing electrochemistry with *in situ* molecular-level reaction tracking (**Figure 9.3**A-ii).[959] The key strategy lies on the use of an electrically conductive Ag shell as both a 3D working electrode and a SERS-active platform. Using the electro-degradation of an environmental toxin as a model, the Ag shell is capable of resolving multistep electron transfer processes by providing molecule-specific identification and quantification of transient species throughout the electrochemical reaction. It is noteworthy that these insights cannot be obtained *via* electrochemistry alone. Interestingly, the 3D electrode configuration exhibits 2-fold and 10-fold superior electrochemical and SERS performance compared to a conventional 2D microplatform. This work opens an attractive perspective toward the design of next-generation spectroelectrochemical cells for efficient elucidation of electrochemical events in energy and environment related applications, such as batteries, fuel cells or toxin removal.

Gas-based reactions

Among all reactions, it is most challenging to monitor processes involving gaseous species in real time, due to the poor detection sensitivity arising from low molecular concentration in gases. Moreover, the low density and poor gas solubility in liquids inevitably lead to its rapid escape from the reaction mixture, thereby preventing effective interactions between gas molecules and plasmonic surfaces, as required for SERS readout.

To realize gas-based process monitoring, Ling *et al.* integrated metal-organic frameworks (MOF) with plasmonic nanostructures/particles to create a MOF-SERS system (**Figure 9.3**B).[960,961] MOFs are 3D crystalline scaffolds containing an extensive network of nanopores with large specific surface areas up to 7000 $m^2.g^{-1}$. The most critical attribute of MOFs to allow SERS-based gas detection revolves around their excellent gas absorptivity, to accumulate gas molecules directly onto the plasmonic surfaces. This phenomenon improves detection sensitivity by several orders of magnitude, as compared to bare plasmonic particles. For instance, MOF-encapsulated Ag nanocube arrays (Ag@MOF) were reported as ultrasensitive SERS platforms to directly observe the concentration of CO_2 molecules at a nanoscale interface created between a MOF and metal nanoparticle surface (**Figure 9.3**B-i).[959] Quantitative reconstruction of the 3D molecular footprint near the MOF-encapsulated solid surface unraveled the transition of sparsely-distributed and randomly-oriented CO_2 molecules into a quasi-condensed CO_2 liquid state, remarkably at ambient operation of 1 bar and 298 K. It is noteworthy that such dynamic molecular-level details cannot be teased out using conventional monitoring techniques that typically focus on bulk MOFs instead. These valuable insights represent a significant leap forward in the understanding of solid@MOF systems, whereby it is traditionally perceived that gas molecules are merely confined near the solid surface *via* the intrinsic MOF nanopores.

The Ag@MOF system also functions as an excellent analytical platform to follow liquid-gas reactions (**Figure 9.3**B-ii).[961] In this case, the interfacial nanocavities in solid@MOF were exploited to selectively and simultaneously concentrate immiscible gas and liquid reactants within the electromagnetic hotspots. Corroborating SERS measurements and simulations, Ling *et al.* uncovered reaction events at the interfacial cavities and provided the first molecular-level validation to the formation of phenylcarbamic acid from liquid aniline and

CO_2 gas. Notably, phenylcarbamic acid can only be identified *in situ* because it is unstable towards post-reaction treatments required in common characterization techniques, such as NMR spectroscopy or mass spectrometry. By overcoming core challenges in the realm of gas-phase detection, this MOF-SERS approach lays a strong foundation for future investigations into various important fields, including heterogeneous catalysis, removal of greenhouse gases and gas-to-fuel conversions. Additional efforts could also be directed to the optimization of MOF-SERS platforms towards facile, real-time monitoring of homogeneous all-gas reactions.

10. General Conclusions and Outlook

SERS has been confirmed a powerful method to probe simple as well as complex molecules, in contact or close to a plasmonic substrate, usually a metal surface but more recently also generalized to semiconductor or hybrid materials. A broad spectrum of physical, chemical and analytical applications have been proposed, ranging from materials and environmental science through biology and medicine. Such a huge potential, combined with extraordinary technological progress in the development of related instrumentation, has resulted in an explosion of research which pushed SERS forward in many different directions (sometimes even leading to conflicting answers).

Improvement of established classical EM and CHEM mechanisms, implementation of relevant secondary processes and consideration of quantum effects have provided a more precise description and prediction of SERS enhancement (factors), with further demonstration of particularly high values within nano- and subnano-scale gaps between NPs or between NPs and flat metal substrates. One of the major driving forces behind recent progress of SERS has been the practical achievement of nanostructures with excellent quality and tailored morphologies, in some cases featuring smaller and more precisely designed 2D and 3D nanogaps. Such fabrication strategies and techniques have also allowed rapid, fast, cost-effective, reproducible, large-scale production of substrates and nanotags with robust SERS response, for general as well as target-oriented sensing applications.

For analytical purposes, high sensitivity, efficiency and reproducibility of SERS substrates are recurrently discussed as key factors. In this context, specific platforms have been devised and synthesized, toward a variety of sensing strategies based on SERS nanotags, chemosensors, chiral-selective systems, SHINERS, intra-gap core-shell particles and remote SERS, often achieving single-molecule detection. The development and implementation of statistical data analysis currently offers quantification and identification of multiple molecules/components within complex mixtures, which are crucial advancements for biomedical and environmental applications. However, optimization of the optical and chemical properties of SERS platforms, including coupling of the analytes to the plasmonic surface, ideally within hotspots/gaps, as well as an even closer collaboration between theoretical modeling and experimental realization, will be indispensable to obtain a deeper understanding of all relevant aspects and to realize the effective transfer of SERS as a standard analytical method in the near future.

The ability to simultaneously detect multiple biomarkers (multiplexing), such as aptamers or antibodies, is crucial to many applications involving biological samples, toxin-contaminated environments, and for personalized medicine, based on point-of-care early diagnostics, high-throughput screening systems, at the gene and molecule level. Label-free SERS biosensors offer DNA detection through a single hybridization step, with no need for secondary hybridization or post-hybridization washing, thus resulting in shorter assay time and less reagent usage. SERS bioimaging has also revealed itself as an alternative long-term imaging technique providing high selectivity and multiplexing, while avoiding photobleaching, often encountered in fluorescence detection schemes. Additionally, it can be combined with other tradidionally used bioimaging tools (multimodality). Immunoassay platforms coupled with advanced POC devices are important for the fast analysis of biological samples. Such improvements in SERS detection will be critical toward future personalized and genomic medicine.

Applications of SERS in biosensing have seen a rapid increase during the past decade, related to detection of cancer biomarkers, circulating tumor cells or pathogens. However, progress toward becoming a wide-spread clinical diagnostics technology has lagged behind, *e.g.* due to the use of highly diluted samples in complex matrixes and the need for sophisticated

instrumentation. Some of these issues could be solved by using brighter probes, such as SERS tags combined with microfluidic systems, using portable devices. In the case of *in vivo* applications, limited tissue penetration depth has hindered so far implementation in full-body or deep tissues, and therefore applications where the laser beam can access the diseased area are those with a better chance to succeed. It has been predicted that three are the main clinical implementations of SERS that could find applicability in the near future; (a) During surgery, for the detection of tumor margins; (b) *via* endoscopy, colonoscopy, or other optical fiber-guided imaging procedures to visualize and detect superficial diseased tissues within the interior of the body (c) *via* liquid biopsy, a term that broadly comprises the identification of disease biomarkers in blood or other bodily fluids. Efficient and timely disease diagnosis is a critical challenge, particularly in low and middle income countries. These regions are ill-prepared to handle the diagnostic burden due to limited resources, resulting in delayed diagnosis and treatment. SERS biosensors may become a low-cost, resource-efficient alternative to histopathological analysis.

SERS has also been demonstrated as a useful tool to monitor bacterial contamination, as well as inorganic and highly toxic organic pollutants within our ecosystem, which relied on the application of hydrogel- and MOF-based NP platforms, with detection thresholds in the ppb range. Quality control and nutrient quantification in food analytics have been achieved, with detection limits down to the nM range. For the near the future, the implementation of robust, reliable and predictable SERS substrates into cartridge devices could become a promising strategy toward commercial SERS sensors. In the area of renewable energy, there is a strong need to monitor nucleic acid targets, such as microRNAs (miRNAs) involved in molecular regulatory pathways controlling plant growth and development. Such pathways are complex and require tight control of gene expression for various applications, ranging from gene therapy to biofuel development.

A recent but promising research direction has been the use of plasmonic substrates to facilitate catalytic reactions under mild conditions, including liquid-based and gas-based reactions, which can be monitored *in situ* with sensitivities down to the single-molecule level, by tracking the evolution of SERS spectra over time. Electrochemical conversion of reactants to products under an applied potential has been demonstrated. Time-dependent SERS appears

especially appealing to rapidly read out the identity and composition of reaction species (*i.e.* reactants, intermediates and products) and to understand reaction mechanisms which were not accessible by means of non-molecule-specific techniques.

The broad interest in the phenomenon of surface-enhanced signal amplification, the consistently improved control over substrate fabrication, and the plethora of applications under manifold conditions, has resulted in the development of other SERS–related techniques, which promise significant improvements in the spatial resolution, while providing complementary spectroscopic information. With SERS as a mature spectroscopic technique and the tremendous progress in its implementation as an analytical tool, we expect rapid development of commercial products, including tailored enhancing substrates, compact setups and efficient imaging methods that can compete or complement existing goods in a wide variety of technologies.

We close with our list of top 10 items that should be accomplished, to make SERS a fully successful technique, both in research and in the market.

1. Development of standardization protocols for the characterization of plasmonic substrates and evaluation of SERS performance.
2. Reliable methods for the synthesis/fabrication of uniform, highly reproducible and efficient enhancing substrates, with a high degree of structural precision and robust and quantitative SERS response within specification limits (to be established).
3. Design and modeling of the optical and electronic properties, electromagnetic field enhancement, distribution/localization of hotspots and polarization dependence of plasmonic substrates for desired/available/appropriate excitation wavelengths.
4. Generally available modeling/simulation tools for realistic SERS substrate configurations and for the accurate determination of Raman spectra of molecules possibly present in observations.
5. Proof of SERS performance, preferentially using non-resonant molecules (established reporters) and in the absence of charge-transfer resonances.
6. Development of a methodology to determine the density and localization of molecules (including target molecules, surfactants, ions, eventual contaminations etc.) on the plasmonic surface.

7. Characterization, tailoring and modeling of optical and electronic properties of plasmonic substrates in the presence of target molecules.

8. Careful characterization and simulation of substrate-target interactions, stability and reactivity.

9. Rational design, careful characterization and modeling of (functionalized) SERS substrates or tags in real environments/ under real conditions

10. Development of standardized protocols and data processing for (multiple) analyte quantification for different application strategies (with labels, label-free as well as using complex statistical models for unknown compositions).

AUTHOR INFORMATION

Corresponding Author

*E-mail: llizmarzan@cicbiomagune.es.

Conflict of Interest. The authors declare no competing financial interest.

ACKNOWLEDGEMENTS

VOCABULARY

Raman scattering, the inelastic scattering of a photon by molecules which reveals vibrational transitions; **SERS tags**, plasmonic nanoparticles carrying Raman-active molecules which act as spectroscopic barcodes; **quantification**, a method to convert observations into numbers; **biomarker**, a molecule or quantifiable signal revealing a biological condition; **hot electrons,** electrons with high kinetic energy upon acceleration by a strong electric field

References

1. Fleischmann, M.; Hendra, P. J.; McQuillan, A. J. Raman Spectra of Pyridine Adsorbed at a Silver Electrode. *Chem. Phys. Lett.* **1974**, *26*, 163-166.

2. Jeanmaire, D. L.; Van Duyne, R. P., Surface Raman Spectroelectrochemistry Part I. Heterocyclic, Aromatic, and Aliphatic Amines Adsorbed on the Anodized Silver Electrode *J. Electroanal. Chem.* **1977**, *84*, 1-20.

3. Albrecht, M. G.; Creighton, J. A. Anomalously Intense Raman Spectra of Pyridine at a Silver Electrode. *J. Am. Chem. Soc.* **1977**, *99*, 5215–5217.

4. Philpott, M. R. Effect of Surface Plasmons on Transitions in Molecules. *J. Chem. Phys.* **1975**, *62*, 1812-

5. Moskovits, M. Surface Roughness and the Enhanced Intensity of Raman Scattering by Molecules Adsorbed on Metals. *J. Chem. Phys.* **1978**, *69*, 4159.

6. A search in Web of Science, as "TOPIC: (surface enhanced raman) OR TOPIC: (sers)" yields over 37,000 records as of May 2019.

7. http://www.icors2018.org

8. Birke, R. L.; Lu, T.; Lombardi, J. R. In *Surface-enhanced Raman spectroscopy*, Wiley: 1991; pp 211-77.

9. Schatz, G. C.; Young, M. A.; Van Duyne, R. P., Electromagnetic Mechanism of SERS. *Top. Appl. Phys.* **2006,** *103* (Surface-Enhanced Raman Scattering), 19-46.

10. Jensen, L.; Aikens, C. M.; Schatz, G. C., Electronic Structure Methods for Studying Surface-Enhanced Raman Scattering. *Chem. Soc. Rev.* **2008,** *37*, 1061-1073.

11. Payton, J. L.; Morton, S. M.; Moore, J. E.; Jensen, L., A Hybrid Atomistic Electrodynamics-Quantum Mechanical Approach for Simulating Surface-Enhanced Raman Scattering. *Acc. Chem. Res.* **2014,** *47*, 88-99.

12. Tong, L.; Zhu, T.; Liu, Z., Approaching the Electromagnetic Mechanism of Surface-Enhanced Raman Scattering: From Self-Assembled Arrays to Individual Gold Nanoparticles. *Chem. Soc. Rev.* **2011,** *40*, 1296-1304.

13. Wu, D.-Y.; Li, J.-F.; Ren, B.; Tian, Z.-Q., Electrochemical Surface-Enhanced Raman Spectroscopy of Nanostructures. *Chem. Soc. Rev.* **2008,** *37*, 1025-1041.

14. Schatz, G. C., Theoretical Studies of Surface Enhanced Raman Scattering. *Acc. Chem. Res.* **1984,** *17*, 370-376.

15. Harris, N.; Ausman, L. K.; McMahon, J. M.; Masiello, D. J.; Schatz, G. C., Computational Electrodynamics Methods. *RSC Theor. Comput. Chem. Ser.* **2011,** *4*, 147-178.

16. Xu, H.; Bjerneld, E. J.; Käll, M.; Börjesson, L. Spectroscopy of Single Hemoglobin Molecules by Surface Enhanced Raman Scattering. *Phys. Rev. Lett*. **1999**, *83*, 4357-4360.

17. Li, K. R.; Stockman, M. I.; Bergman, D. J. Self-Similar Chain of Metal Nanospheres as an Efficient Nanolens. *Phys. Rev. Lett*. **2003**, *91*, 227402.

18. Alvarez-Puebla, R. A.; Liz-Marzán, L. M.; García de Abajo, F. J. Light Concentration at the Nanometer Scale. *J. Phys. Chem. Lett*. **2010**, *1*, 2428-2434.

19. Solis, S. M.; Taboada, J. M.; Obelleiro, F.; Liz-Marzán, L. M.; García de Abajo, F. J. Optimization of Nanoparticle-Based SERS Substrates through Large-Scale Realistic Simulations. *ACS Photonics* **2017**, *4*, 329-337.

20. Ausman, L. K.; Schatz, G. C. On the Importance of Incorporating Dipole Reradiation in the Modeling of Surface Enhanced Raman Scattering from Spheres. *J. Chem. Phys.* **2009,** *131*, 084708 (1-10).

21. Chen, X.; Jensen, L. Morphology Dependent Near-Field Response in Atomistic Plasmonic Nanocavities. *Nanoscale* **2018,** *10*, 11410-11417.

22. Chulhai, D. V.; Chen, X.; Jensen, L. Simulating Ensemble-Averaged Surface-Enhanced Raman Scattering. *J. Phys. Chem. C* **2016,** *120*, 20833-20842.

23. Wustholz, K. L.; Henry, A.-I.; McMahon, J. M.; Freeman, R. G.; Valley, N.; Piotti, M. E.; Natan, M. J.; Schatz, G. C.; Van Duyne, R. P. Structure-Activity Relationships in Gold Nanoparticle Dimers and Trimers for Surface-Enhanced Raman Spectroscopy. *J. Am. Chem. Soc.* **2010,** *132*, 10903-10910.

24. Kleinman, S. L.; Sharma, B.; Blaber, M. G.; Henry, A.-I.; Valley, N.; Freeman, R. G.; Natan, M. J.; Schatz, G. C.; Van Duyne, R. P. Structure Enhancement Factor Relationships in Single Gold Nanoantennas by Surface-Enhanced Raman Excitation Spectroscopy. *J. Am. Chem. Soc.* **2013,** *135*, 301-308.

25. Greeneltch, N. G.; Blaber, M. G.; Schatz, G. C.; Van Duyne, R. P.,Plasmon-Sampled Surface-Enhanced Raman Excitation Spectroscopy on Silver Immobilized Nanorod Assemblies and Optimization for Near Infrared (λex = 1064 nm) Studies. *J. Phys. Chem. C* **2013,** *117*, 2554-2558.

26. Sharma, B.; Cardinal, M. F.; Ross, M. B.; Zrimsek, A. B.; Bykov, S. V.; Punihaole, D.; Asher, S. A.; Schatz, G. C.; Van Duyne, R. P. Aluminum Film-Over-Nanosphere Substrates for Deep-UV Surface-Enhanced Resonance Raman Spectroscopy. *Nano Lett.* **2016,** *16*, 7968-7973.

27. Yu, R.; Liz-Marzán, L. M.; García de Abajo, F. J.; Universal Analytical Modeling of Plasmonic Nanoparticles, *Chem. Soc. Rev.* **2017**, *46*, 6710-6724.

28. http://www.nanophotonics.es/widgets

29. Ford, G. W.; Weber, W. H. Electromagnetic Interactions of Molecules with Metal Surfaces. *Phys. Rep*. **1984**, *113*, 195-287

30. García de Abajo, F. J. Nonlocal Effects in the Plasmons of Strongly Interacting Nanoparticles, Dimers, and Waveguides. *J. Phys. Chem. C* **2008**, *112*, 17983-17987.

31. Camden, J. P.; Dieringer, J. A.; Wang, Y.; Masiello, D. J.; Marks, L. D.; Schatz, G. C.; Van Duyne, R. P. Probing the Structure of Single-Molecule Surface-Enhanced Raman Scattering Hot Spots. *J. Am. Chem. Soc.* **2008,** *130*, 12616-12617.

32. McMahon, J. M.; Li, S.; Ausman, L. K.; Schatz, G. C. Modeling the Effect of Small Gaps in Surface-Enhanced Raman Spectroscopy. *J. Phys. Chem. C* **2012,** *116*, 1627-1637.

33. Yoon, J. H.; Zhou, Y.; Blaber, M. G.; Schatz, G. C.; Yoon, S. Surface Plasmon Coupling of Compositionally Heterogeneous Core-Satellite Nanoassemblies. *J. Phys. Chem. Lett.* **2013,** *4*, 1371-1378.

34. Esteban, R.; Borisov, A. G.; Nordlander, P.; Aizpurua, J. Bridging Quantum and Classical Plasmonics with a Quantum-Corrected Model. *Nat. Commun.* **2012,** *3*, 1806 (1-9).

35. Morton, S. M.; Jensen, L. Understanding the Molecule-Surface Chemical Coupling in SERS. *J. Am. Chem. Soc.* **2009,** *131*, 4090-4098.

36. Valley, N.; Greeneltch, N.; Van Duyne, R. P.; Schatz, G. C. A Look at the Origin and Magnitude of the Chemical Contribution to the Enhancement Mechanism of Surface-Enhanced Raman Spectroscopy (SERS): Theory and Experiment. *J. Phys. Chem. Lett.* **2013,** *4*, 2599-2604.

37. Birke, R. L.; Lombardi, J. R.; Saidi, W. A.; Norman, P. Surface-Enhanced Raman Scattering Due to Charge-Transfer Resonances: A Time-Dependent Density Functional Theory Study of Ag13-4-Mercaptopyridine. *J. Phys. Chem. C* **2016,** *120*, 20721-20735.

38. Lombardi, J. R.; Birke, R. L. The Theory of Surface-Enhanced Raman Scattering. *J. Chem. Phys.* **2012,** *136*, 144704 (1-11).

39. Gorelsky, S. I. In *Semiempirical SCF MO Methods, Electronic Spectra, and Configurational Interaction*, Elsevier Ltd.: 2004; pp 467-489.

40. Gieseking, R. L.; Ratner, M. A.; Schatz, G. C. Semiempirical Modeling of Ag Nanoclusters: New Parameters for Optical Property Studies Enable Determination of Double Excitation Contributions to Plasmonic Excitation. *J. Phys. Chem. A* **2016,** *120*, 4542-4549.

41. Gieseking, R. L.; Ratner, M. A.; Schatz, G. C. Theoretical Modeling of Voltage Effects and the Chemical Mechanism in Surface-Enhanced Raman Scattering. *Faraday Discuss.* **2017,** *205*, 149-171.

42. Yilmaz, M.; Babur, E.; Ozdemir, M.; Gieseking, R. L.; Dede, Y.; Tamer, U.; Schatz, G. C.; Facchetti, A.; Usta, H.; Demirel, G. Nanostructured Organic Semiconductor Films for Molecular Detection with Surface-Enhanced Raman Spectroscopy. *Nat. Mater.* **2017,** *16*, 918-924.

43. Gieseking, R. L. M.; Lee, J.; Tallarida, N.; Apkarian, V. A.; Schatz, G. C. Bias-Dependent Chemical Enhancement and Nonclassical Stark Effect in Tip-Enhanced Raman Spectromicroscopy of CO-Terminated Ag Tips. *J. Phys. Chem. Lett.* **2018,** *9*, 3074-3080.

44. Gieseking, R. L.; Ratner, M. A.; Schatz, G. C. Semiempirical Modeling of Electrochemical Charge Transfer. *Faraday Discuss.* **2017,** *199*, 547-563.

45. Gieseking, R. L. M.; Ratner, M. A.; Schatz, G. C. Benchmarking Semiempirical Methods To Compute Electrochemical Formal Potentials. *J. Phys. Chem. A* **2018,** *122*, 6809-6818.

46. Tallarida, N.; Lee, J.; Apkarian, V. A. Tip-Enhanced Raman Spectromicroscopy on the Angstrom Scale: Bare and CO-Terminated Ag Tips. *ACS Nano* **2017,** *11*, 11393-11401.

47. Mullin, J. M.; Autschbach, J.; Schatz, G. C., Time-Dependent Density Functional Methods for Surface Enhanced Raman Scattering (SERS) Studies. *Comput. Theor. Chem.* **2012,** *987*, 32-41.

48. Mullin, J.; Schatz, G. C. Combined Linear Response Quantum Mechanics and Classical Electrodynamics (QM/ED) Method for the Calculation of Surface-Enhanced Raman Spectra. *J. Phys. Chem. A* **2012,** *116*, 1931-1938.

49. Sprague-Klein, E. A.; McAnally, M. O.; Zhdanov, D. V.; Zrimsek, A. B.; Apkarian, V. A.; Seideman, T.; Schatz, G. C.; Van Duyne, R. P. Observation of Single Molecule Plasmon-Driven Electron Transfer in Isotopically Edited 4,4'-Bipyridine Gold Nanosphere Oligomers. *J. Am. Chem. Soc.* **2017,** *139*, 15212-15221.

50. Sprague-Klein, E. A.; Negru, B.; Madison, L. R.; Coste, S. C.; Rugg, B. K.; Felts, A. M.; McAnally, M. O.; Banik, M.; Apkarian, V. A.; Wasielewski, M. R.; Ratner, M. A.; Seideman, T.; Schatz, G. C.; Van Duyne, R. P. Photoinduced Plasmon-Driven Chemistry in trans-1,2-Bis(4-pyridyl)ethylene Gold Nanosphere Oligomers. *J. Am. Chem. Soc.* **2018,** *140*, 10583-10592.

51. Le Ru, E. C.; Blackie, E.; Meyer, M.; Etchegoin, P. G. Surface Enhanced Raman Scattering Enhancement Factors: A Comprehensive Study. *J. Phys. Chem. C* **2007**, *111*, 13794–13803.

52. Le Ru, E. C.; Etchegoin, P. G. Single Molecule Surfaced-Enhanced Raman Scattering. *Annu. Rev. Phys. Chem.* **2012**, *63*, 65-87.

53. Le Ru, E. C.; Etchegoin, P. G. Rigorous Justification of the $|E|^4$ Enhancement Factor in Surface Enhanced Raman Spectroscopy. *Chem. Phys. Lett.* **2006**, *413*, 63–66.

54. Moskovits, M. Surface Selection Rules. *J. Chem. Phys.* **1982**, *77*, 4408–4416.

55. Le Ru, E. C.; Meyer, S. A.; Artur, C.; Etchegoin, P. G.; Grand, J.; Lang, P.; Maurel, F. Experimental Demonstration of Surface Selection Rules for SERS on Flat Metallic Surfaces. *Chem. Commun.* **2011**, *47*, 3903–3905.

56. Dieringer, J. A.; McFarland, A. D.; Shah, N. C.; Stuart, D. A.; Whitney, A. V.; Yonzon, C. R.; Young, M. A.; Zhang, X.; Duyne, R. P. V. Surface Enhanced Raman Spectroscopy: New Materials, Concepts, Characterization Tools, and Applications. *Faraday Discuss.* **2006**, *132*, 9–26.

57. Le Ru, E. C.; Etchegoin, P. G. Quantifying SERS Enhancements. *MRS Bull.* **2013**, *38*, 631–640.

58. Darby, B. L.; Auguié, B.; Meyer, M.; Pantoja, A. E.; Le Ru, E. C. Modified Optical Absorption of Molecules on Metallic Nanoparticles at Sub-Monolayer Coverage. *Nat. Photonics* **2015**, *10*, 40–45.

59. Tang, C.; Auguié, B.; Le Ru, E. C. Modeling Molecular Orientation Effects in Dye-Coated Nanostructures Using a Thin-Shell Approximation of Mie Theory for Radially Anisotropic Media. *ACS Photonics* **2018**, *5*, 5002–5009.

60. Auguié, B.; L., D. B.; Le Ru, E. C. Electromagnetic Interactions of Dye Molecules Surrounding a Nanosphere. *ACS Photonics* **2019**, *submitted*.

61. Morton, S. M.; Jensen, L. A Discrete Interaction Model/Quantum Mechanical Method for Describing Response Properties of Molecules Adsorbed on Metal Nanoparticles. *J. Chem. Phys.* **2010**, *133*, 074103.

62. Shim, S.; Stuart, C. M.; Mathies, R. A. Resonance Raman Cross-Sections and Vibronic Analysis of Rhodamine 6G from Broadband Stimulated Raman Spectroscopy. *ChemPhysChem.* **2008**, *9*, 697–699.

63. Auguié, B.; Le Ru, E. C. Optical Absorption of Dye Molecules in a Spherical Shell Geometry. *J. Phys. Chem. C* **2018**, *122*, 19110–19115.

64. Turley, H. K.; Hu, Z.; Silverstein, D. W.; Cooper, D. A.; Jensen, L.; Camden, J. P. Probing Two-Photon Molecular Properties with Surface-Enhanced Hyper-Raman Scattering: A Combined Experimental and Theoretical Study of Crystal Violet. *J. Phys. Chem. C* **2016**, *120*, 20936–20942.

65. Chikkaraddy, R.; de Nijs, B.; Benz, F.; Barrow, S. J.; Scherman, O. A.; Rosta, E.; Demetriadou, A.; Fox, P.; Hess, O.; Baumberg, J. J. Single-Molecule Strong Coupling at Room Temperature in Plasmonic Nanocavities. *Nature* **2016**, *535*, 127–130.

66. Stockman, M. I. Spasers Explained. *Nat. Photonics* **2008**, *2*, 327–329.

67. Cortés, E.; Xie, W.; Cambiasso, J.; Jermyn, A. S.; Sundararaman, R.; Narang, P.; Schlücker, S.; Maier, S. A. Plasmonic Hot Electron Transport Drives Nano-Localized Chemistry. *Nat. Commun.* **2017**, *8*, 14880.

68. Kneer, L. M.; Roller, E.-M.; Besteiro, L. V.; Schreiber, R.; Govorov, A. O.; Liedl, T. Circular Dichroism of Chiral Molecules in DNA-Assembled Plasmonic Hotspots. *ACS Nano* **2018**, *12*, 9110–9115.

69. Kneipp, K.; Wang, Y.; Kneipp, H.; Perelman, L. T.; Itzkan, I.; Dasari, R. R.; Feld, M. S. Single Molecule Detection Using Surface-Enhanced Raman Scattering (SERS), *Phys. Rev. Lett.* **1997**, *78*, 1667-1670.

70. Nie, S.; Emory, S. R. Probing Single Molecules and Single Nanoparticles by Surface-Enhanced Raman Scattering, *Science* **1997**, *275* 1102-1106.

71. Xu, H.; Aizpurua, J.; Käll, M.; Apell, P. Electromagnetic Contributions to Single-Molecule Sensitivity in Surface-Enhanced Raman Scattering, *Phys. Rev. E* **2000**, *62*, 4318-4324.

72. Yamamoto, Y. S.; Ozaki, Y.; Itoh, T. Recent Progress and Frontiers in the Electromagnetic Mechanism of Surface-Enhanced Raman Scattering, *J. Photochem. Photobiol. C* **2014**, *21*, 81-104.

73. Itoh, T.; Yamamoto, Y. S. Reproduction of Surface-Enhanced Resonant Raman Scattering and Fluorescence Spectra of a Strong Coupling System Composed of a Single Silver Nanoparticle Dimer and a Few Dye Molecules, *J. Chem. Phys.* **2018**, *149*, 244701.

74. Zhang, R.; Zhang, Y.; Dong, Z. C.; Jiang, S.; Zhang, C.; Chen, L. G.; Zhang, L.; Liao, Y.; Aizpurua, J.; Luo, Y.; Yang, J. L.; Hou, J. G. Chemical Mapping of a Single Molecule by Plasmon-Enhanced Raman Scattering, *Nature* **2013**, *498*, 82-86.

75. Itoh, T.; Yamamoto, Y. S.; Biju, V.; Tamaru, H.; Wakida, S. Fluctuating Single sp^2 Carbon Clusters at Single Hotspots of Silver Nanoparticle Dimers Investigated by Surface-Enhanced Resonance Raman Scattering, *AIP Adv.* **2015**, *5*, 127113.

76. Ebbesen, T. W. Hybrid Light–Matter States in a Molecular and Material Science Perspective, *Acc. Chem. Res.* **2016**, *49*, 2403-2413.

77. Itoh, T.; Yamamoto, Y. S.; Ozaki, Y. Plasmon-Enhanced Spectroscopy of Absorption And Spontaneous Emissions Explained Using Cavity Quantum Optics, *Chem. Soc. Rev.* **2017**, *46*, 3904-3921.

78. Itoh, T.; Yamamoto, Y. S.; Kitahama, Y.; Balachandran, J. One-Dimensional Plasmonic Hotspots Located Between Silver Nanowire Dimers Evaluated by Surface-Enhanced Resonance Raman Scattering, *Phys. Rev. B* **2017**, *95*, 115441.

79. Ward, D. R.; Grady, N. K.; Levin, C. S.; Halas, N. J.; Wu, Y.; Nordlander, P.; Natelson, D. Electromigrated Nanoscale Gaps for Surface-Enhanced Raman Spectroscopy. *Nano Lett.* **2007**, *7*, 1396-1400.

80. Nordlander, P.; Oubre, C.; Prodan, E.; Li, K.; Stockman, M. Plasmon Hybridization in Nanoparticle Dimers. *Nano Lett*. **2004**, *4*, 899-903.

81. Romero, I.; Aizpurua, J.; Bryant, G. W.; de Abajo, F. J. G. Plasmons in Nearly Touching Metallic Nanoparticles: Singular Response in the Limit of Touching Dimers. *Opt. Express* **2006**, *14*, 9988-9999.

82. Mertens, J.; Eiden, A. L.; Sigle, D. O.; Huang, F.; Lombardo, A.; Sun, Z.; Sundaram, R. S.; Colli, A.; Tserkezis, C.; Aizpurua, J.; Milana, S.; Ferrari, A. C.; Baumberg, J. J. Controlling Subnanometer Gaps in Plasmonic Dimers Using Graphene. *Nano Lett.* **2013**, *13*, 5033-5038.

83. Teperik, T. V.; Nordlander, P.; Aizpurua, J.; Borisov, A. G. Robust Subnanometric Plasmon Ruler by Rescaling of the Nonlocal Optical Response. *Phys. Rev. Lett.* **2013**, *110*, 263901.

84. Giuseppe, T.; Straubel, J.; Kwiatkowski, A.; Rockstuhl, C.; Evers, F.; Xu, H.; Mortensen, N.; Wubs, M. Resonance Shifts and Spill-Out Effects in Self-Consistent Hydrodynamic Nanoplasmonics. *Nat. Commun.* **2015**, *6*, 7132.

85. Fraire, J. C.; Pérez, L. A.; Coronado, E. A. Cluster Size Effects in the Surface-Enhanced Raman Scattering Response of Ag and Au Nanoparticle Aggregates: Experimental and Theoretical Insight. *J. Phys. Chem. C* **2013**, *117*, 23090-23107.

86. Zhang, P.; Feist, J.; Rubio, A.; García-González, P.; García-Vidal, F. J. *Ab initio* Nanoplasmonics: The Impact of Atomic Structure. *Phys. Rev. B* **2014**, *90*, 161407.

87. Barbry, M.; Koval, P.; Marchesin, F.; Esteban, R.; Borisov, A. G.; Aizpurua, J.; Sánchez-Portal, D. Atomistic Near-Field Nanoplasmonics: Reaching Atomic-Scale Resolution in Nanooptics. *Nano Lett.* **2015**, *15*, 3410-3419.

88. Savage, K.; Hawkeye, M.; Esteban, R.; Borisov, A.; Aizpurua, J.; Baumberg, J. Revealing the Quantum Regime in Tunnelling Plasmonics. *Nature* **2013**, *491*, 574-577.

89. Zhu, W.; Crozier, K. Quantum Mechanical Limit to Plasmonic Enhancement as Observed by Surface-Enhanced Raman Scattering. *Nat. Commun.* **2014**, *5*, 5228.

90. Pérez-González, O.; Zabala, N.; Borisov, A. G.; Halas, N. J.; Nordlander, P.; Aizpurua, J. Optical Spectroscopy of Conductive Junctions in Plasmonic Cavities. *Nano Lett*. **2010**, *10*, 3090-3095,

91. Benz, F.; Tserkezis, C.; Herrmann, L. O.; de Nijs, B.; Sanders, A.; Sigle, D. O.; Pukenas, L.; Evans, S. D.; Aizpurua, J.; Baumberg, J. J. Nanooptics of Molecular-Shunted Plasmonic Nanojunctions. *Nano Lett*. **2015**, *15*, 669-674.

92. Urbieta, M.; Barbry, M.; Zhang, Y.; Koval, P.; Sánchez-Portal, D.; Zabala, N.; Aizpurua, J. Atomic-Scale Lightning Rod Effect in Plasmonic Picocavities: A Classical View to a Quantum Effect. *ACS Nano* **2018**, *12*, 585-595.

93. Trautmann, S.; Aizpurua, J.; Götz, I.; Undisz, A.; Dellith, J.; Schneidewind, H.; Rettenmayr, M.; Deckert, V. A classical Description of Subnanometer Resolution by Atomic Features in Metallic Structures. *Nanoscale* **2017**, *9*, 391-401.

94. Xie, W.; Walkenfort, B.; Schlücker, S. A 1.7 nm Resolution Chemical Analysis of Carbon Nanotubes by Tip-Enhanced Raman Imaging in The Ambient. *Nat. Commun*. **2014**, *5*, 3312.

95. Richard-Lacroix, M.; Zhang, Y.; Dong, Z.; Deckert, V. Mastering High Resolution Tip-Enhanced Raman Spectroscopy: Towards a Shift of Perception. *Chem. Soc. Rev.* **2017**, *46*, 3922-3944.

96. Chiang, N.; Chen, X.; Goubert, G.; Chulhai, D. V.; Chen, X.; Pozzi, E. A.; Jiang, N.; Hersam, M. C.; Seideman, T.; Jensen, L.; Van Duyne, R. P. Conformational Contrast of Surface-Mediated Molecular Switches Yields Angstrom-Scale Spatial Resolution in Ultrahigh Vacuum Tip-Enhanced Raman Spectroscopy. *Nano Lett*. **2016**, *16*, 7774-7778.

97. Duan, S.; Tian, G.; Luo, Y. Theory for Modeling of High Resolution Resonant and Nonresonant Raman Images. *J. Chem. Theor. Comput.* **2016**, *12*, 4986-4995.

98. Liu, P.; Chulhai, D. V.; Jensen, L. Single-Molecule Imaging Using Atomistic Near-Field Tip-Enhanced Raman Spectroscopy. *ACS Nano* **2017**, *11*, 5094-5102.

99. Benz, F.; Schmidt, M. K.; Dreismann, A.; Chikkaraddy, R.; Zhang, Y.; Demetriadou, A.; Carnegie, C.; Ohadi, H.; de Nijs, B.; Esteban, R.; Aizpurua, J.; Baumberg, J. J. Single-Molecule Optomechanics in Picocavities. *Science* **2016**, *354*, 726-729.

100. Shin, H.-H.; Yeon, G. J.; Choi, H.-K.; Park, S.-M.; Lee, K. S.; Kim, Z. H. Frequency-Domain Proof of the Existence of Atomic-Scale SERS Hot-Spots. *Nano Lett*. **2018**, *18*, 262-271.

101. Carnegie, C.; Griffiths, J.; de Nijs, B.; Readman, C.; Chikkaraddy, R.; Deacon, W. M.; Zhang, Y.; Szabö, I.; Rosta, E.; Aizpurua, J.; Baumberg, J. J. Room-Temperature Optical Picocavities below 1 nm^3 Accessing Single-Atom Geometries. *J. Phys. Chem. Lett*. **2018**, *9*, 7146-7151.

102.   Roelli, P.; Galland, C.; Piro, N.; Kippenberg, T. J. Molecular Cavity Optomechanics as A Theory of Plasmon-Enhanced Raman Scattering. *Nat. Nanotechnol*. **2015**, *11*, 164-169.

103.   Schmidt, M. K.; Esteban, R.; González-Tudela, A.; Giedke, G.; Aizpurua, J. Quantum Mechanical Description of Raman Scattering from Molecules in Plasmonic Cavities. *ACS Nano* **2016**, *10*, 6291-6298.

104.   Maher, R.; Galloway, C.; Le Ru, E.; Cohen, L.; Etchegoin, P. Vibrational Pumping in Surface Enhanced Raman Scattering (SERS). *Chem. Soc. Rev.* **2008**, *37*, 965-979.

105.   Schmidt, M. K.; Esteban, R.; Benz, F.; Baumberg, J. J.; Aizpurua, J. Linking Classical and Molecular Optomechanics Descriptions of SERS. *Faraday Discuss.* **2017**, *205*, 31-65.

106.   Lombardi, A.; Schmidt, M. K.; Weller, L.; Deacon, W. M.; Benz, F.; de Nijs, B.; Aizpurua, J.; Baumberg, J. J. Pulsed Molecular Optomechanics in Plasmonic Nanocavities: From Nonlinear Vibrational Instabilities to Bond-Breaking. *Phys. Rev. X* **2018**, *8*, 011016.

107.   Kamandar Dezfouli, M.; Hughes, S. Quantum Optics Model of Surface-Enhanced Raman Spectroscopy for Arbitrarily Shaped Plasmonic Resonators. *ACS Photonics* **2017**, *4*, 1245-1256.

108.   Latorre, F.; Kupfer, S.; Bocklitz, T.; Kinzel, D.; Trautmann, S.; Gräfe, S.; Deckert, V. Spatial Resolution of Tip-Enhanced Raman Spectroscopy - DFT Assessment of the Chemical Effect. *Nanoscale* **2016**, *8*, 10229.

109.   Baumberg, J. J.; Aizpurua, J.; Mikkelsen, M. H.; Smith, D. R. Extreme Nanophotonics from Ultrathin Metallic Gaps. *Nat. Mater.* **2019**. DOI: 10.1038/s41563-019-0290-y.

110.   Barnett, S. M.; Harris, N.; Baumberg, J. J. Molecules in the Mirror: How SERS Backgrounds Arise from the Quantum Method of Images. *Phys. Chem. Chem. Phys.* **2014**, *16*, 6544-6549.

111.   Hugall, J. T.; Baumberg, J. J. Demonstrating Photoluminescence from Au is Electronic Inelastic Light Scattering of a Plasmonic Metal: The Origin of SERS Backgrounds. *Nano Lett.* **2015**, *15*, 2600-2604.

112.   Mertens, J.; Kleemann, M.-E.; Chikkaraddy, R.; Narang, P.; Baumberg, J. J. How Light Is Emitted by Plasmonic Metals. *Nano Lett*. **2017**, *17*, 2568-2574.

113.   Sigle, D. O.; Mertens, J.; Herrmann, L. O.; Bowman, R. W.; Ithurria, S.; Dubertret, B.; Shi, Y.; Yang, H. Y.; Tserkezis, C.; Aizpurua, J.; Baumberg, J. J. Monitoring Morphological Changes in 2D Monolayer Semiconductors Using Atom-Thick Plasmonic Nanocavities. *ACS Nano* **2015**, *9*, 825-830.

114.   Mertens, J.; Demetriadou, A.; Bowman, R. W.; Benz, F.; Kleemann, M.-E.; Tserkezis, C.; Shi, Y.; Yang, H. Y.; Hess, O.; Aizpurua, J.; Baumberg, J. J. Tracking Optical Welding through Groove Modes in Plasmonic Nanocavities. *Nano Lett*. **2016**, *16*, 5605-5611.

115.   Herrmann, L. O.; Valev, V. K.; Tserkezis, C.; Barnard, J. S.; Kasera, S.; Scherman, O. A.; Aizpurua, J.; Baumberg, J. J. Threading Plasmonic Nanoparticle Strings with Light. *Nat. Commun.* **2014**, *5*, 4568.

116.   Di Martino, G.; Tappertzhofen, S.; Hofmann, S.; Baumberg, J. J. Nanoscale Plasmon-Enhanced Spectroscopy in Memristive Switches. *Small* **2016**, *12*, 1334-1341.

117.   De Nijs, B.; Benz, F.; Barrow, S. J.; Sigle, D. O.; Chikkaraddy, R.; Palma, A.; Carnegie, C.; Kamp, M.; Sundararaman, R.; Narang, P.; Scherman, O. A.; Baumberg, J. J. Plasmonic Tunnel Junctions for Single-Molecule Redox Chemistry. *Nat. Commun.* **2017**, *8*, 994.

118.   Di Martino, G.; Turek, V. A.; Lombardi, A.; Szabó, I.; de Nijs, B.; Kuhn, A.; Rosta, E.; Baumberg, J. J. Tracking Nanoelectrochemistry Using Individual Plasmonic Nanocavities. *Nano Lett*. **2017**, *17*, 4840-4845.

119.   Chikkaraddy, R.; Turek, V. A.; Kongsuwan, N.; Benz, F.; Carnegie, C.; van de Goor, T.; de Nijs, B.; Demetriadou, A.; Hess, O.; Keyser, U. F.; Baumberg, J. J. Mapping Nanoscale Hotspots with Single-Molecule Emitters Assembled into Plasmonic Nanocavities Using DNA Origami. *Nano Lett*. **2018**, *18*, 405-411.

120.   Kasera, S.; Herrmann, L. O.; del Barrio, J.; Baumberg, J. J.; Scherman, O. A. Quantitative Multiplexing with Nano-Self-Assemblies in SERS. *Sci. Rep*. **2015**, *4*, 6785.

121.   de Nijs, B.; Kamp, M.; Szabó, I.; Barrow, S. J.; Benz, F.; Wu, G.; Carnegie, C.; Chikkaraddy, R.; Wang, W.; Deacon, W. M.; Rosta, E.; Baumberg, J. J.; Scherman, O. A. Smart Supramolecular Sensing with Cucurbit[n]urils: Probing Hydrogen Bonding with SERS. *Faraday Discuss*. **2017**, *205*, 505-515.

122.   Salmon, A. R.; Esteban, R.; Taylor, R. W.; Hugall, J. T.; Smith, C. A.; Whyte, G.; Scherman, O. A.; Aizpurua, J.; Abell, C.; Baumberg, J. J. Monitoring Early-Stage Nanoparticle Assembly in Microdroplets by Optical Spectroscopy and SERS. *Small* **2016**, *12*, 1788-1796.

123.   Taylor, R. W.; Esteban, R.; Mahajan, S.; Aizpurua, J.; Baumberg, J. J.; Optimizing SERS from Gold Nanoparticle Clusters: Addressing the Near Field by an Embedded Chain Plasmon Model. *J. Phys. Chem. C* **2016**, *120*, 10512-10522.

124.   Carnegie, C.; Chikkaraddy, R.; Benz, F.; de Nijs, B.; Deacon, W. M.; Horton, M.; Wang, W.; Readman, C.; Barrow, S. J.; Scherman, O. A.; Baumberg, J. J. Mapping SERS in CB:Au Plasmonic Nanoaggregates. *ACS Photonics* **2017**, *4*, 2681-2687.

125.   Huang, J.; de Nijs, B.; Cormier, S.; Sokolowski, K.; Grys, D.-B.; Readman, C. A.; Barrow, S. J.; Scherman, O. A.; Baumberg, J. J. Plasmon-Induced Optical Control over Dithionite-Mediated Chemical Redox Reactions. *Faraday Discuss.* **2019**. DOI: 10.1039/C8FD00155C.

126.   Xie, J.; Zhang, Z. Q.; Lee, J. Y.; Wang, D. I. C. The Synthesis of SERS-Active Gold Nanoflower Tags for *In Vivo* Applications. *ACS Nano* **2008**, *2*, 2473-2480.

127.   Khoury, C. G.; Vo-Dinh, T. Gold Nanostars For Surface-Enhanced Raman Scattering: Synthesis, Characterization and Optimization. *J. Phys. Chem. C* **2008**, *112*, 18849-18859.

128.   Rodríguez-Lorenzo, L.; Alvarez-Puebla, R. A.; Pastoriza-Santos, I.; Mazzucco, S.; Stephan, O.; Kociak, M.; Liz-Marzán, L. M.; García de Abajo, F. J. Zeptomol Detection Through Controlled Ultrasensitive Surface-Enhanced Raman Scattering *J. Am. Chem. Soc.* **2009**, *131*, 4616-4618.

129.   Pazos-Pérez, N.; Barbosa, S.; Rodríguez-Lorenzo, L.; Aldeanueva-Potel, P.; Pérez-Juste, J.; Pastoriza-Santos, I.; Alvarez-Puebla, R. A.; Liz-Marzán, L. M. Growth of Sharp Tips on Gold Nanowires Leads to Increased Surface-Enhanced Raman Scattering Activity. *J. Phys. Chem. Lett.* **2010**, *1*, 24-27.

130.   Nalbant Esenturk, E.; Hight Walker, A. R. Surface-Enhanced Raman Scattering Spectroscopy *via* Gold Nanostars. *J. Raman Spectrosc.* **2009**, *40*, 86–91.

131.   Hrelescu, C.; Sau, T. K.; Rogach, A. L.; Jäckel, F.; Feldmann, J. Single Gold Nanostars Enhance Raman Scattering. *Appl. Phys. Lett.* **2009**, *94*, 153113.

132.   Doiron, B.; Mota, M.; Wells, M. P.; Bower, R.; Mihai, A.; Li, Y.; Cohen, L. F.; McN. Alford, N.; Petrov, P. K.; Oulton, R. F.; Maier, S. A. Quantifying Figures of Merit for Localized surface plasmon resonance applications: a materials survey, *ACS Photonics* **2019**, *6*, 240-259.

133.   Ding, S.-Y.; Yi, J.; Li, J.-F.; Ren, B.; Wu, D.-Y-; Panneerselvam, R.; Tian, Z.-Q. Nanostructure-Based Plasmon-Enhanced Raman Spectroscopy for Surface Analysis of Materials. *Nat. Rev. Mater.* **2016**, *1*, 16021.

134.   Haes, A. J.; Haynes, C. L.; McFarland, A. D.; Schatz, G. C.; Van Duyne, R. P.; Zou, S., Plasmonic Materials for Surface-Enhanced Sensing and Spectroscopy. *MRS Bull.* **2005**, *30*, 368-375.

135.   Xi, W.; Shrestha, B. K.; Haes, A. J. Promoting Intra- and Intermolecular Interactions in Surface-Enhanced Raman Scattering. *Anal. Chem.* **2018**, *90*, 128-143.

136.   Vincent, B.; Edwards, J.; Emmett, S.; Jones, A. Depletion Flocculation in Dispersions of Sterically-Stabilized Particles ("Soft Spheres"). *Colloid Surf.* **1986**, *18*, 261-281.

137.   Wijenayaka, L. A.; Ivanov, M. R.; Cheatum, C. M.; Haes, A. J. Improved Parametrization for Extended Derjaguin, Landau, Verwey, and Overbeek Predictions of Functionalized Gold Nanosphere Stability. *J. Phys. Chem. C* **2015**, *119*, 10064-10075.

138.   Suherman, A. L.; Zampardi, G.; Kuss, S.; Tanner, E. E. L.; Amin, H. M. A.; Young, N. P.; Compton, R. G.,Understanding Gold Nanoparticle Dissolution in Cyanide-Containing Solution *Via* Impact-Chemistry. *Phys. Chem. Chem. Phys.* **2018**, *20*, 28300-28307.

139.   Reidy, B.; Dawson Kenneth, A.; Lynch, I.; Haase, A.; Luch, A.; Lynch, I. Mechanisms of Silver Nanoparticle Release, Transformation and Toxicity: A Critical Review of Current Knowledge and Recommendations for Future Studies and Applications. *Materials* **2013**, *6*, 2295-2350.

140. Zook, J. M.; Long, S. E.; Cleveland, D.; Geronimo, C. L. A.; MacCuspie, R. I. Measuring Silver Nanoparticle Dissolution in Complex Biological and Environmental Matrices Using UV-Visible Absorbance. *Anal. Bioanal. Chem.* **2011**, *401*, 1993-2002.

141. Velzeboer, I.; Quik, J. T. K.; van de Meent, D.; Koelmans, A. A. Rapid Settling of Nanoparticles Due to Heteroaggregation with Suspended Sediment. *Environ. Toxicol. Chem.* **2014**, *33*, 1766-1773.

142. Liu, H. H.; Surawanvijit, S.; Rallo, R.; Orkoulas, G.; Cohen, Y. Analysis of Nanoparticle Agglomeration in Aqueous Suspensions *via* Constant-Number Monte Carlo Simulation. *Environ. Sci. Technol.* **2011**, *45*, 9284-9292.

143. Shen, C.; Li, B.; Huang, Y.; Jin, Y. Kinetics of Coupled Primary- and Secondary-Minimum Deposition of Colloids under Unfavorable Chemical Conditions. *Environ. Sci. Technol.* **2007**, *41*, 6976-6982.

144. Xi, W.; Phan, H. T.; Haes, A. J. How to Accurately Predict Solution-Phase Gold Nanostar Stability. *Anal. Bioanal. Chem.* **2018**, *410*, 6113-6123.

145. Jung, L. S.; Campbell, C. T. Sticking Probabilities in Adsorption of Alkanethiols from Liquid Ethanol Solution onto Gold. *J. Phys. Chem. B* **2000**, *104*, 11168-11178.

146. Gabor Arpad, S. *Introduction to Surface Chemistry and Catalysis*, 1994.

147. Phenrat, T.; Saleh, N.; Sirk, K.; Kim, H.-J.; Tilton, R.; Lowry, G. Stabilization of Aqueous Nanoscale Zerovalent Iron Dispersions by Anionic Polyelectrolytes: Adsorbed Anionic Polyelectrolyte Layer Properties and Their Effect on Aggregation and Sedimentation. *J. Nanopart. Res.* **2008**, *10*, 795-814.

148. Saunders, S. R.; Eden, M. R.; Roberts, C. B. Modeling the Precipitation of Polydisperse Nanoparticles Using a Total Interaction Energy Model. *J. Phys. Chem. C* **2011**, *115*, 4603-4610.

149. Skoglund, S.; Lowe, T. A.; Hedberg, J.; Blomberg, E.; Wallinder, I. O.; Wold, S.; Lundin, M. Effect of Laundry Surfactants on Surface Charge and Colloidal Stability of Silver Nanoparticles. *Langmuir* **2013**, *29*, 8882-8891.

150. Hotze, E. M.; Phenrat, T.; Lowry, G. V. Nanoparticle Aggregation: Challenges to Understanding Transport and Reactivity in the Environment. *J. Environ. Qual.* **2010**, *39*, 1909-1924.

151. Pinchuk, A. O. Size-Dependent Hamaker Constant for Silver Nanoparticles. *J. Phys. Chem. C* **2012**, *116*, 20099-20102.

152. Lu, G.; Forbes, T. Z.; Haes, A. J. SERS Detection of Uranyl Using Functionalized Gold Nanostars Promoted by Nanoparticle Shape and Size. *Analyst* **2016**, *141*, 5137-5143.

153. Romero, I.; Aizpurua, J.; Bryant, G. W.; Garcia de Abajo, F. J. Plasmons in Nearly Touching Metallic Nanoparticles: Singular Response in the Limit of Touching Dimers. *Los Alamos National Laboratory, Preprint Archive, Cond. Matt.* **2007**, 1-11.

154. Dick, L. A.; Haes, A. J.; Van Duyne, R. P. Distance and Orientation Dependence of Heterogeneous Electron Transfer: A Surface-Enhanced Resonance Raman Scattering

Study of Cytochrome C Bound to Carboxylic Acid Terminated Alkanethiols Adsorbed on Silver Electrodes. *J. Phys. Chem. B* **2000**, *104*, 11752-11762.

155.   Kennedy, B. J.; Spaeth, S.; Dickey, M.; Carron, K. T. Determination of the Distance Dependence and Experimental Effects for Modified Sers Substrates Based on Self-Assembled Monolayers Formed Using Alkanethiols. *J. Phys. Chem. B* **1999**, *103*, 3640-3646.

156.   Kumari, G.; Kandula, J.; Narayana, C. How Far Can We Probe by SERS? *J. Phys. Chem. C* **2015**, *119*, 20057-20064.

157.   Pierre, M. C. S.; Haes, A. J. Purification Implications on SERS Activity of Silica Coated Gold Nanospheres. *Anal. Chem.* **2012**, *84*, 7906-7911.

158.   Volkert, A. A.; Subramaniam, V.; Ivanov, M. R.; Goodman, A. M.; Haes, A. J. Salt-Mediated Self Assembly of Thioctic Acid on Gold Nanoparticles. *ACS Nano* **2011**, *5*, 4570-4580.

159.   Sau, T. K.; Murphy, C. J. Room Temperature, High-Yield Synthesis of Multiple Shapes of Gold Nanoparticles in Aqueous Solution. *J. Am. Chem. Soc*. **2004**, *126*, 8648-8649.

160.   Chen, S.; Wang, Z. L.; Ballato, J.; Foulger, S. H.; Carroll, D. L. Monopod, Bipod, Tripod, and Tetrapod Gold Nanocrystals *J. Am. Chem. Soc*. **2003**, *125*, 16186-16187.

161.   Nehl, C. L.; Liao, H.; Hafner, J. H. Optical Properties of Star-Shaped Gold Nanoparticles. *Nano Lett*. **2006**, *6*, 683-688.

162.   Kumar, P. S.; Pastoriza-Santos, I.; Rodríguez-González, B.; García de Abajo, F. J.; Liz-Marzán, L. M. High-Yield Synthesis and Optical Response of Gold Nanostars. *Nanotechnology* **2008**, *19*, 015606.

163.   Barbosa, S.; Agrawal, A.; Rodríguez-Lorenzo, L.; Pastoriza-Santos, I.; Alvarez-Puebla, R. A.; Kornowski, A.; Weller, H.; Liz-Marzán, L. M. Tuning Size and Sensing Properties in Colloidal Gold Nanostars. *Langmuir* **2010**, *26*, 14943–14950.

164.   Guerrero-Martínez, A.; Barbosa, S.; Pastoriza-Santos, I.; Liz-Marzán, L. M. Nanostars Shine Bright for You. Colloidal Synthesis, Properties and Applications Of Branched Metallic Nanoparticles. *Curr. Opin. Colloid Interface Sci.* **2011**, *16*, 118–127.

165.   Wang, Y.; Sentosun, K.; Li, A.; Coronado-Puchau, M.; Sánchez-Iglesias, A.; Li, S.; Su, X.; Bals, S.; and Liz-Marzán, L. M. Engineering Structural Diversity in Gold Nanocrystals by Ligand-Mediated Interface Control. *Chem. Mater.* **2015**, *27*, 8032−8040.

166.   Hao, F.; L. Nehl, C.; Hafner, J. H.; Nordlander, P. Plasmon Resonances of a Gold Nanostar. *Nano Lett.* **2007**, *7*, 729-732.

167.   Evcimen, N. I.; Coskun, S.; Kozanoglu, D.; Ertas, G.; Unalan, H. C.; Nalbant Esenturk, E. Growth of Branched Gold Nanoparticles on Solid Surfaces and their Use as Surface-Enhanced Raman Scattering Substrates. *RSC Adv.* **2015**, *5*, 101656.

168.   Yang, D. P.; Liu, X.; Teng, C. P.; Owh, C.; Win, K. Y.; Lin, M.; Loh, X. J.; Wu, Y.-L.; Li, Z.; Ye, E. Unexpected Formation of Gold Nanoflowers by a Green Synthesis

Method as Agents For a Safe and Effective Photothermal Therapy. *Nanoscale* **2017**, *9*, 15753-15759.

169.   Cai, J.; Raghavan, V.; Bai, Y. J.; Zhou, M. H.; Liu, X. L.; Liao, C. H.; Ma, P.; Shi, L.; Dockery, P.; Keogh, I.; Fan, H. M.; Olivo, M. Controllable Synthesis of Tetrapod Gold Nanocrystals with Precisely Tunable Near-Infrared Plasmon Resonance Towards Highly Efficient Surface Enhanced Raman Spectroscopy Bioimaging. *J. Mater. Chem. B* **2015**, *3*, 7377-7385.

170.   Kim, G. W.; Ha, J. W. Polarization-Sensitive Single Dipoles Generated from Multiple Sharp Branches on the Surfaces of Single Gold Nanourchins. *J. Phys. Chem. C* **2017**, *121*, 19975−19982.

171.   Cao, X.; Chen, S.; Li, W.; Li, J.; Bi, L.; Shi, H. One-Step Synthesis of Highly-Branched Gold Nanostructures and its Application in Fabrication of SERS-Active Substrates. *AIP Adv.* **2018**, *8*, 105133.

172.   Bhattacharya, M.; Mazov, V.; Satpati, B.; Jena, P.; Das Chakraborty, S.; Kumar, S.; Pathak, B.; Kuznetsov, D. V.; Senapati, D. Exploiting Le Chatelier's Principle for a One-Pot Synthesis of Nontoxic Hhoggnps with the Sharpest Nanoscopic Features Suitable for Tunable Plasmon Spectroscopy and High Throughput SERS Sensing. *Chem. Commun.* **2017**, *53*, 10402-10405.

173.   Li, A.; Li, S. Large-Volume Hot Spots in Gold Spiky Nanoparticle Dimers for High-Performance Surface-Enhanced Spectroscopy. *Nanoscale* **2014**, *6*, 12921-12928.

174.   Lee, S.; Song, Y. D.; Yang, Y. I.; Kim, G.-P.; Choi, I.; Yi, J. Solution Based, on Chip Direct Growth of Three-Dimensionally Wrinkled Gold Nanoparticles for a SERS Active Substrate. *Chem. Commun.* **2015**, *51*, 213-216.

175.   Jia, W.; Li, J.; Jiang, L. Synthesis of Highly Branched Gold Nanodendrites with a NarrowSize Distribution and Tunable NIR and SERS Using a Multiamin Surfactant. *ACS Appl. Mater. Interfaces* **2013**, *5*, 6886−6892.

176.   Xu, Q.; Guo, X.; Xu, L.; Ying, Y.; Wu, Y.; Wen, Y.; Yang, H. Template-Free Synthesis Of SERS-Active Gold Nanopopcorn for Rapid Detection of Chlorpyrifos Residues. *Sens. Actuators B* **2017**, *241*, 1008-1013.

177.   Li, S.; Zhang, L.; Wang, T.; Li, L.; Wang, C.; Su, Z. The Facile Synthesis of Hollow Au Nanoflowers for Synergistic Chemo-Photothermal Cancer Therapy. *Chem. Commun.,* **2015**, *51*, 14338-14341.

178.   Vijayaraghavan, P.; Liu, C.-H.; Hwang, K. C. Synthesis of Multibranched Gold Nanoechinus Using a Gemini Cationic Surfactant and Its Application for Surface Enhanced Raman Scattering. *ACS Appl. Mater. Interfaces* **2016**, *8*, 23909−23919.

179.   Wu, H.-L.; Chen, C.-H.; Huang, M.-H. Seed-Mediated Synthesis of Branched Gold Nanocrystals Derived from the Side Growth of Pentagonal Bipyramids and the Formation of Gold Nanostars. *Chem. Mater.* **2009**, *21*, 110–114.

180.   Niu, W.; Chua, Y. A. A.; Zhang, W.; Huang, H.; Lu, X. Highly Symmetric Gold Nanostars: Crystallographic Control and Surface-Enhanced Raman Scattering Property. *J. Am. Chem. Soc.* **2015**, *137*, 10460−10463.

181.   Maiorano, G.; Rizzello, L.; Malvindi, M. A.; Shankar, S. S.; Martiradonna, L.; Falqui, A.; Cingolani, R.; Pompa, P. P. Monodispersed and Size-Controlled Multibranched Gold Nanoparticles with Nanoscale Tuning of Surface Morphology. *Nanoscale* **2011**, *3*, 2227-2232.

182.   Chandra, K.; Culver, K. S. V.; Werner, S. E.; Lee, R. C.; Odom, T. W. Manipulating the Anisotropic Structure of Gold Nanostars using Good's Buffers. *Chem. Mater.* **2016**, *28*, 6763-6769.

183.   Yuan, H.; Khoury, C. J.; Hwang, H.; Wilson, C. M.; Grant, G. A.; Vo-Dinh, T. Gold Nanostars: Surfactant-Free Synthesis,3D Modelling, and Two-Photon Photoluminescence Imaging. *Nanotechnology* **2012**, *23*, 075102.

184.   Indrasekara, A. S. D.S.; Meyers, S.; Shubeita, S.; Feldman, L. C.; Gustafsson, T.; Fabris, L. Gold Nanostar Substrates for SERS Sensing in the Femtomolar Regime. *Nanoscale* **2014**, *6*, 8891-8899.

185.   Zapata-Urzúa, C.; Pérez-Ortiz, M.; Acosta, G. A.; Mendoza, J.; Yedra, L.; Estradé, S.; Álvarez-Lueje, A.; Núñez-Vergara, L. J.; Albericio, F.; Lavilla, R.; Kogan, M. J. Hantzsch dihydropyridines: Privileged Structures for the Formation of Well-Defined Gold Nanostars. *J. Colloid Interface Sci.* **2015**, *453*, 260–269.

186.   Moukarzel, W.; Fitremann, J.; Marty, J.-D.. Seed-less Amino-Sugar Mediated Synthesis of Gold Nanostars. *Nanoscale* **2011**, 3, 3285-3290.

187.   Sau, T. K.; Rogach, A. L.; Döblinger, M.; Feldmann, J. One-Step High-Yield Aqueous Synthesis of Size-Tunable Multispiked Gold Nanoparticles. *Small* **2011**, *7*, 2188–2194.

188.   Pallavicini, P.; Donà, A.; Casu,A.; Chirico, G.; Collini, M.; Dacarro, G.; Falqui, A.; Milanese, C.; Sironic, L.; Taglietti, A. Triton X-100 for Three-Plasmon Gold Nanostars with Two Photothermally Active NIR (Near IR) and SWIR (Short-Wavelength IR) Channels. *Chem. Commun.* **2013**,*49*, 6265-6267.

189.   Atta, S.; Beetz, M.; Fabris, L. Understanding the Role of $AgNO_3$ Concentration and Seed Morphology to Achieve Tunable Shape Control in Gold Nanostars. *Nanoscale* **2019**, *11*, 2946-2958.

190.   Wheeler, D. A.; Green, T. D.; Wang, H.; Fernández-López, C.; Liz-Marzán, L.; Zou, S.; Knappenberger, K. L.; Zhang, J. Z. Optical Properties and Coherent Vibrational Oscillations of Gold Nanostars. *Chem. Phys. Lett.* **2012**, *543*, 127–132.

191.   Sanchez-Gaytan, B. L.; Swanglap, P.; Lamkin, T. J.; Hickey, R. J.; Fakhraai, Z.; Link, S.; Park S.-J. Spiky Gold Nanoshells: Synthesis and Enhanced Scattering Properties. *J. Phys. Chem. C* **2012**, *116*, 10318−10324.

192.   Hrelescu, C.; Sau,T. K.; Rogach, A. L.; Jäckel,F.; Laurent, G.; Douillard, L.; Charra, F. Selective Excitation of Individual Plasmonic Hotspots at the Tipsof Single Gold Nanostars. *Nano Lett.* **2011**, *11*, 402–407.

193.   Liu, X. L.; Wang, J.-H.; Liang, S.; Yang, D.-J.; Nan, F.; Ding, S.-J.; Zhou, L.; Hao, Z.-H.; Wang, Q.-Q. Tuning Plasmon Resonance of Gold Nanostars for Enhancements

of Nonlinear Optical Response and Raman Scattering. *J. Phys. Chem. C* **2014**, *118*, 9659−9664.

194.   Shao, L.; Susha, A. S.; Cheung, L. S.; Sau, T. K.; Rogach, A. L.; Wang, J. Plasmonic Properties of Single Multispiked Gold Nanostars: Correlating Modeling with Experiments. *Langmuir* **2012**, *28*, 8979−8984.

195.   Giannini, V.; Rodríguez-Oliveros, R.; Sánchez-Gil, J. A. Surface Plasmon Resonances of Metallic Nanostars/Nanoflowers for Surface-Enhanced Raman Scattering. *Plasmonics* **2010**, *5*, 99–104.

196.   Silvestri, A.; Lay, L.; Psaro, R.; Polito, L.; Evangelisti, C. Fluidic Manufacture of Star-Shaped Gold Nanoparticles. *Chem. Eur. J.* **2017**, *23*, 973-9735

197.   Ahmad, N.; Wang, G.; Nelayah, J.; Ricolleau, C.; Alloyeau, D. Exploring the Formation of Symmetric Gold Nanostars by Liquid-Cell Transmission Electron Microscopy. *Nano Lett.* **2017**, *17*, 4194−4201.

198.   Chandra, K.; Kumar, V.; Werner, S. E.; Odom, T. W. Separation of Stabilized MOPS Gold Nanostars by Density Gradient Centrifugation. *ACS Omega* **2017**, *2*, 4878−4884.

199.   Tran, V.; Thiel, C.; Svejda, J. T.; Jalali, M.; Walkenfort, B.; Erni, D.; Schlücker, S. Probing the SERS Brightness of Individual Au Nanoparticles, Hollow Au/Ag Nanoshells, Au Nanostars and Au Core/Au Satellite Particles: Single-Particle Experiments And Computer Simulations. *Nanoscale* **2018**, *10*, 21721-21731.

200.   Indrasekara, A. S. D. S.; Johnson, S. F.; Odion, R. A.; Vo-Dinh, T. Manipulation of the Geometry and Modulation of the Optical Response of Surfactant-Free Gold Nanostars: A Systematic Bottom- Up Synthesis. *ACS Omega* **2018**, *3*, 2202−2210.

201.   Pu, Y.; Zhao, Y.; Zheng, P.; Li, M. Elucidating the Growth Mechanism of Plasmonic Gold Nanostars with Tunable Optical and Photothermal Properties. *Inorg. Chem.* **2018**, *57*, 8599−8607.

202.   Vanrompay, H.; Bladt, E.; Albrecht, W.; Béché, A.; Zakhozheva, M.; Sánchez-Iglesias, A.; Liz-Marzán, L. M.; Bals, S. 3D Characterization of Heat-Induced Morphological Changes of Au Nanostars by Fast *In Situ* Electron Tomography. *Nanoscale* **2018**, *10*, 22792-22801.

203.   Tsoulos, T. V.; Fabris, L. Interface and Bulk Standing Waves Drive the Coupling of Plasmonic Nanostar Antennas. *J. Phys. Chem. C* **2018**, *122*, 28949-28957.

204.   de Puig, H.; Tam, J. O.; Yen, C.-W.; Gehrke, L.; Hamad-Schifferli, K. Extinction Coefficient of Gold Nanostars. *J. Phys. Chem. C* **2015**, *119*, 17408−17415.

205.   Tsoulos, T. V.; Han, L.; Weir, J.; Xin, H. L.; Fabris, L. A Closer Look at the Physical and Optical Properties of Gold Nanostars: An Experimental and Computational Study. *Nanoscale* **2017**, *9*, 3766-3773.

206.   Prodan, E.; Radloff, C.; Halas, N. J.; Nordlander, P. A Hybridization Model for the Plasmon Response of Complex Nanostructures, *Science* **2003**, *302*, 419-422.

207. Hentschel, M.; Saliba, M.; Vogelgesang, R.; Giessen, H.; Alivisatos, A. P.; Liu, N. Transition from Isolated to Collective Modes in Plasmonic Oligomers. *Nano Lett*. **2010**, *10*, 2721-2726.

208. Lukyanchuk, B.; Zheludev, N. I.; Maier, S. A.; Halas, N. J.; Nordlander, P.; Giessen, H.; Cong, C. T. The Fano Resonance in Plasmonic Nanostructures and Metamaterials, *Nat. Mater.* **2010**, *9*, 707-715.

209. Jain P. K.; El-Sayed, M. A. Plasmonic Coupling in Noble Metal Nanostructures, *Chem. Phys. Lett.* **2010**, *487*, 153-164.

210. Lombardi, A.; Grzelczak, M. P.; Crut, A.; Maioli, P.; Pastoriza-Santos, I.; Liz-Marzán, L. M.; Del Fatti, N.; Vallée, F. Optical Response of Individual Au–Ag@SiO$_2$ Heterodimers. *ACS Nano* **2013**, *7*, 2522-2531.

211. Yanai, A.; Grajower, M.; Lerman, G. M.; Hentschel,; Giessen, H.; Levy, U. Near- and Far-Field Properties of Plasmonic Oligomers under Radially and Azimuthally Polarized Light Excitation. *ACS Nano* **2014**, *8*, 4969-4974.

212. Zohar, N.; Chuntonov, L.; Haran, G. The Simplest Plasmonic Molecules: Metal Nanoparticle Dimers. *J. Photochem. Photobiol.* C **2014**, *21*, 26-39.

213. Yorulmaz, M.; Hoggard, A.; Zhao, H.; Wen, F.; , W.-S.; Halas, N. J.; Nordlander, P.; Link, S. Absorption Spectroscopy of an Individual Fano Cluster. *Nano Lett.* **2016**, *16*, 6497-6503.

214. Kusch, P.; Mastel, S.; Mueller, N. S.; Morquillas-Azpiazu, N.; Heeg, S.; Gorbachev, R.; Schedin, F.; Hübner, U.; Pascual, J. I.; Reich, S.; Hillenbrand, R. Dual-Scattering Near-Field Microscope for Correlative Nanoimaging of SERS and Electromagnetic Hotspots. *Nano Lett.* **2017**, *17*, 2667-2673.

215. Heeg, S.; Oikonomou, A.; Fernandez-Garcia, R.; Oikonomou, A.; Schedin, F.; Narula, R.; Maier, S. A.; Vijayaraghavan, A.; Reich, S. Polarized Plasmonic Enhancement by Au Nanostructures Probed through Raman Scattering of Suspended Graphene. *Nano Lett.* **2013**, *13*, 301-308.

216. Wasserroth, S.; Bisswanger, T.; Mueller, N. S.; Kusch, P.; Heeg, S.; Clark, N.; Schedin, F.; Gorbachev, R.; Reich, S. Graphene as a Local Probe to Investigate Near-Field Properties of Plasmonic Nanostructures, *Phys. Rev. B* **2018**, *97*, 155417.

217. Narula, R. ; Panknin, R.; Reich, S. Absolute Raman Matrix Elements of Graphene and Graphite. *Phys. Rev. B* **2010**, *82*, 045418.

218. Chen, C.-F.; Park, C.-H.; Boudouris, P. W.; Horng, J.; Geng, B.; Girit, C.; Zettl, A.; Crommie, M. F.; Segalman, R. A.; Louie, S. G.; Wang, F. Controlling Inelastic Light Scattering Quantum Pathways in Graphene, *Nature* **2011**, *471*, 617-620.

219. Mueller, N. S.; Reich, S. Microscopic Theory of Optical Absorption in Graphene Enhanced by Lattices of Plasmonic Nanoparticles. *Phys. Rev. B* **2018**, *97*, 235417.

220. Mueller, N. S.; Heeg, S.; Pena Alvarez, M.; Kusch, P.; Wasserroth, P.; Clark, N.; Schedin, F.; Parthenios, J.; Papagelis, K.; Galiotis, C., Evaluating Arbitrary Strain Configurations and Doping in Graphene with Raman Spectroscopy. *2D Mater.* **2017**, *5*, 015016.

221. Zhu, W.; Crozier, K. B. Quantum Mechanical Limit to Plasmonic Enhancement as Observed by Surface-Enhanced Raman Scattering. *Nat. Commun*. **2014**, *5*, 5228.

222. Lim, D.-K.; Jeon, K.-S.; Hwang, J.-H.; Kim, H.; Kwon, S.; Suh, Y. D.; Nam, J.-M. Highly Uniform and Reproducible Surface-Enhanced Raman Scattering from DNA Tailorable Nanoparticles with 1-nm Interior Gap. *Nat. Nanotechnol.* **2011**, *6*, 452-460.

223.   Talaga, D.; Comesaña-Hermo, M.; Ravaine, S.; Vallee, R. A. L.; Bonhommeau, S. Colocalized Dark-Feld Scattering, Atomic Force and Surface-Enhanced Raman Scattering Microscopic Imaging of Single Gold Nanoparticles. *J. Opt.* **2015**, *17*, 114006.

224.   Mueller, N. S.; Heeg, S.; Kusch, P.; Gaufrès, E.; Tang, N. Y.-W.; Hübner, U.; Martel, R.; Vijayaraghavan, A.; Reich, S. Plasmonic Enhancement of SERS Measured on Molecules in Carbon Nanotubes. *Faraday Discuss.* **2017**, *205*, 85-103.

225.   Mueller, N. S.; Heeg, S.; Reich, S. Surface-Enhanced Raman Scattering as a Higher-Order Raman Process. *Phys. Rev. A* **2016**, *94*, 023813.

226.   Kockum, A. F.; Miranowicz, A.; de Liberato, S.; Savasta, S.; Nori, F. Ultrastrong Coupling Between Light and Matter. *Nat. Rev. Phys.* **2019**, *1*, 19.

227.   Gaufret, E.; Tang, N. Y.-W.; Favron, A.; Allard, C.; Lapointe, F.; Jourdain, V.; Tahir, S.; Brosseau, C.-N.; Leonelli, R.; Martel, R. Aggregation Control of α-Sexithiophene *via* Isothermal Encapsulation Inside Single-Walled Carbon Nanotubes, *ACS Nano* **2016**, *10*, 10220-10226.

228.   Ye, Z.; Li, C.; Xu, Y.; Bell, S. E. J. Exploiting the Chemical Differences Between Ag and Au Colloids Allows Dramatically Improved SERS Detection of "Non-Adsorbing" Molecules. *Analyst* **2019**, *144*, 448-453.

229.   Dick, S.; Bell, S. E. J.; Alexander, K. J.; O'Neil, I. A.; Cosstick, R. SERS and SERRS Detection of the DNA Lesion 8-Nitroguanine: A Self-Labeling Modification. *Chem. Eur. J.* **2017**, *23*, 10663-10669.

230.   Canrinus, T. R.; Lee, W. W. Y.; Feringa, B. L.; Bell, S. E. J.; Browne, W. R. Supramolecular Low-Molecular Weight Hydrogelator Stabilization of SERS-Active Aggregated Nanoparticles for Solution and Gas Sensing. *Langmuir* **2017**, *33*, 8805-8812.

231.   Lee, W. W. Y.; Silverson, V. A. D.; Jones, L. E.; Ho, Y. C.; Fletcher, N. C.; McNaul, M.; Peters, K. L.; Speers, S. J.; Bell, S. E. J. Surface-Enhanced Raman Spectroscopy of Novel Psychoactive Substances Using Polymer-Stabilized Ag Nanoparticle Sggregates. *Chem. Commun.* **2016**, *52*, 493-496.

232.   Konrad, M. P.; Doherty, A. P.; Bell, S. E. J. Stable and Uniform SERS Signals from Self-Assembled Two-Dimensional Interfacial Arrays of Optically Coupled Ag Nanoparticles. *Anal. Chem.* **2013**, *85*, 6783-6789.

233.   Duan, H.; Wang, D.; Kurth, D. G.; Möhwald, H. Directing Self-Assembly of Nanoparticles at Water/Oil Interfaces. *Angew. Chem. Int. Ed.* **2004**, *43*, 5639-5642.

234.   Andryszewski, T.; Iwan, M.; Hołdyński, M.; Fiałkowski, M. Synthesis of a Free-Standing Monolayer of Covalently Bonded Gold Nanoparticles. *Chem. Mater.* **2016**, *28*, 5304-5313.

235.   Xu, Y.; Konrad, M. P.; Lee, W. W. Y.; Ye, Z.; Bell, S. E. J. A Method for Promoting Assembly of Metallic and Nonmetallic Nanoparticles into Interfacial Monolayer Films. *Nano Lett.* **2016**, *16*, 5255-5260.

236.   Kelly, J.; Patrick, R.; Patrick, S.; Bell, S. E. J. Surface-Enhanced Raman Spectroscopy for the Detection of a Metabolic Product in the Headspace Above Live Bacterial Cultures. *Angew. Chem. Int. Ed.* **2018**, *57*, 15686-15690.

237.   Xu, Y.; Konrad, M. P.; Trotter, J. L.; McCoy, C. P.; Bell, S. E. J. Rapid One-Pot Preparation of Large Freestanding Nanoparticle-Polymer Films. *Small* **2016**, *13*, 1602163.

238. Li, C.; Ye, Z.; McCabe, H.; Kelly, J.; Xu, Y.; Bell, S. E. J. Dataset Demonstrating the Working-Principles of Surface-Exposed Nanoparticle Sheet Enhanced Raman Spectroscopy. *Data in Brief* **2019**, *23*, 103746.

239. Xu, Y.; Ye, Z.; Li, C.; McCabe, H.; Kelly, J.; Bell, S. E. J. Pressing Solids Directly into Sheets of Plasmonic Nanojunctions Enables Solvent-Free Surface-Enhanced Raman Spectroscopy. *Appl. Mater. Today* **2018**, *13*, 352-358.

240. Serrano-Montes, A. B.; Jimenez de Aberasturi, D.; Langer, J. Giner-Casares, J. J.; Scarabelli, L.; Herrero, A.; Liz-Marzán, L. M. A General Method for Solvent Exchange of Plasmonic Nanoparticles and Self-Assembly into SERS-Active Monolayers *Langmuir* **2015**, *31*, 9205-9213

241. Velleman, L.; Scarabelli, L.; Sikdar, D.; Kornyshev, A. A.; Liz-Marzán, L. M.; Edel, J. B. Monitoring Plasmon Coupling and SERS Enhancement Through *in situ* Nanoparticle Spacing Modulation. *Faraday Discuss.* **2017**, *205*, 67-83.

242. Schulz, F.; Tober, S.; Lange, H. Size-Dependent Phase Transfer Functionalization of Gold Nanoparticles To Promote Well-Ordered Self-Assembly. *Langmuir* **2017**, *33*, 14437-14444.

243. Mueller, N. S.; Vieira, B. G. d. M.; Schulz, F.; Kusch, P.; Oddone, V.; Barros, E. B.; Lange, H.; Reich, S. Dark Interlayer Plasmons in Colloidal Gold Nanoparticle Bi- and Few-Layers. *ACS Photonics* **2018**, *5*, 3962-3969.

244. Mueller, N. S.; Viera, B. G. M.; Höing, D. F. Schulz, D. F.; Barros, E. B.; Lange, H.; Reich, S. Direct Optical Excitation of Dark Plasmons for Hot Electron Generation, *Faraday Discuss.* **2019**. DOI: 10.1039/C8FD00149A.

245. Solís, D. M.; Taboada, J. M.; Obelleiro, F.; Liz-Marzán, L. M.; García de Abajo, F. J. Towards Ultimate Nanoplasmonics Modeling. *ACS Nano* **2014**, *8*, 7559-7570.

246. Udayabhaskararao, T.; Altantzis, T.; Houben, L.; Coronado-Puchau, M.; Langer, J.; Popovitz-Biro, R.; Liz-Marzán, L. M.; Vuković, L.; Král, P.; Bals, S.; Klajn, R. Tunable Porous Nanoallotropes Prepared by Post-Assembly Etching of Binary Nanoparticle Superlattices. *Science* **2017**, *358*, 514-518.

247. Tay, L.-L. *et al.*, *Unpublished results*.

248. Milliken, S.; Fraser, J.; Poirier, S.; Hulse, J.; Tay, L.-L. Self-Assembled Vertically Aligned Au Nanorod Arrays for Surface Enhanced Raman Scattering (SERS) Detection of Cannabinol. *Spectrochim. Acta Part A* **2018**, *196*, 222-228.

249. Alvarez-Puebla, R. A.; Agarwal, A.; Khanal, B. P.; Aldeanueva-Potel, P.; Carbó-Argibay, E.; Pazos-Pérez, N.; Zubarev, E. R.; Kotov, N. A.; Liz-Marzán, L. M.; Real-Time Detection of Scrambled Prions on 3D Supercrystals of Gold Nanorods. *Proc. Natl. Acad. Sci U.S.A.* **2011**, *108*, 8157-8161.

250. Hamon, C.; Novikov, S.; Scarabelli, L.; Solís, D. M.; Altantzis, T.; Bals, S.; Taboada, J. M.; Obelleiro, F.; Liz-Marzán, L. M. Collective Plasmonic Properties in Few-Layer Gold Nanorod Supercrystals. *ACS Photonics* **2015**, *2*, 1482-1488.

251. Thai, T.; Zheng, Y.; Ng, S. H.; Mudie, S.; Altissimo, M.; Bach, U. Self-Assembly of Vertically Aligned Gold Nanorod Arrays on Patterned Substrates. *Angew. Chem. Int. Ed.* **2012**, *51*, 8732-8735.

252. Hamon, C.; Novikov, S.; Scarabelli, L.; Basabe-Desmonts, L.; Liz-Marzán, L. M. Hierarchical Self-Assembly of Gold Nanoparticles into Patterned Plasmonic Nanostructures. *ACS Nano* **2014**, *8*, 10694-10703.

253. Hanske, C.; González-Rubio, G.; Hamon, C.; Formentín, P.; Modin, E.; Chuvilin, A.; Guerrero-Martínez, A.; Marsal, L. F.; Liz-Marzán, L. M. Large-Scale Plasmonic

Pyramidal Supercrystals *via* Templated Self-Assembly of Monodisperse Gold Nanospheres. *J. Phys. Chem. C* **2017**, *121*, 10899-10906.

254.   Matricardi, C.; Hanske, C.; García-Pomar, J. L.; Langer, J.; Mihi, A.; Liz-Marzán, L. M. Gold Nanoparticle Plasmonic Superlattices as Surface Enhanced Raman Spectroscopy Substrates. *ACS Nano* **2018**, *12*, 8531-8539.

255.   Hanske, C. Hill, E. H.; Vila-Liarte, D.; González-Rubio, G.; Matricardi, C.; Mihi, A.; Liz-Marzán, L. M. Solvent Assisted Self-Assembly of Gold Nanorods into Hierarchically Organized Plasmonic Mesostructures. *ACS Appl. Mater. Interfaces* **2019**, *11*, 11763-11771.

256.   Lee, C. H.; Tian, L.; Singamaneni, S. Paper-Based SERS Swab for Rapid Trace Detection on Real-World Surfaces. *ACS Appl. Mater. Interfaces* **2010**, *2*, 3429–3435.

257.   Lee, C. H.; Hankus, M. E.; Tian, L.; Pellegrino, P. M.; Singamaneni, S.

258.   Yua , W. W.; White, I. M. Inkjet-Printed Paper-Based SERS Dipsticks and Swabs for Trace Chemical Detection. *Analyst* **2013**, *138*, 1020-1025.

259.   Yu, W. W.; White, I. M. Inkjet Printed Surface Enhanced Raman Spectroscopy Array on Cellulose Paper. *Anal. Chem.* **2010**, *82*, 9626-9630.

260.   Qu, L.-L.; Li, D.-W.; Xue, J. Q.; Zhai, W.-L.; Fossey, J. S.; Long, Y.-T. Batch Fabrication of Disposable Screen Printed SERS Arrays. *Lab Chip* **2012**, *12*, 876-881.

261.   Polavarapu, L.; La Porta, A.; Novikov, S. M.; Coronado-Puchau, M.; Liz-Marzán, L. M. Pen-on-paper Approach Toward the Design of Universal Surface Enhanced Raman Scattering Substrates. *Small* **2014**, *10*, 3065-3071.

262.   Idone, A.; Gulmini, M.; Henry, A.-I.; Casadio, F.; Chang, L.; Appolonia, L.; Van Duyne, R. P.; Shah, N. C. Silver Colloidal Pastes for Dye Analysis of Reference and Historical Textile Fibers Using Direct, Extractionless, Non-Hydrolysis Surface-Enhanced Raman Spectroscopy. *Analyst* **2013**, *138*, 5895-5903.

263.   Lu, G.; Lia, H.; Zhang, H. Nanoparticle-Coated PDMS Elastomers for Enhancement of Raman Scattering. *Chem. Commun.* **2011**, *47*, 8560-8562.

264.   Guo, Y.; Yu, J.; Li, C.; Li, Z.; Pan, J.; Liu, A.; Man, B.; Wu, T.; Xiu, X.; Zhang C. SERS Substrate Based on the Flexible Hybrid of Polydimethylsiloxane and Silver Colloid Decorated with Silver Nanoparticles. *Opt Express.* **2018**, *26*, 21784-21796.

265.   Shiohara, A.; Langer, J.; Polavarapu, L.; Liz-Marzán, L. M. Solution Processed Polydimethylsiloxane/ Gold Nanostar Flexible Substrates for Plasmonic Sensing. *Nanoscale* **2014**, *6*, 9817-9823.

266.   Park, S.; Lee, J.; Ko, H. Transparent and Flexible Surface-Enhanced Raman Scattering (SERS) Sensors Based on Gold Nanostar Arrays Embedded in Silicon Rubber Film. *ACS Appl. Mater. Interfaces* **2017**, *9*, 44088-44095.

267.   Fortuni, B.; Fujita, Y.; Ricci, M.; Inose, T.; Aubert, R.; Lu, G.; Hutchison, J. A.; Hofkens, J.; Latterini, L.; Uji-I, H. A Novel Method for *In Situ* Synthesis of SERS-Active Gold Nanostars on Polydimethylsiloxane Film. *Chem. Commun.* **2017**, *53*, 5121-5124.

268.   Good, D. M.; Thongboonkerd, V.; Novak, J.; Bascands, J. L.; Schanstra, J. P.; Coon, J. J.; Dominiczak, A.; Mischak, H. Body Fluid Proteomics for Biomarker Discovery: Lessons from the Past Hold the Key to Success in the Future. *J. Proteome Res.* **2007**, *6*, 4549–4555.

269.   Kong, K.; Kendall, C.; Stone, N.; Notingher, I. Raman Spectroscopy for Medical Diagnostics — From In-Vitro Bio Fl Uid Assays to in-Vivo Cancer Detection. *Adv. Drug Delivery Rev.* **2015**, *89*, 121–134.

270.   Pfeiffer, C.; Rehbock, C.; Hühn, D.; Carrillo-Carrion, C.; de Aberasturi, D. J.; Merk, V.; Barcikowski, S.; Parak, W. J. Interaction of Colloidal Nanoparticles with Their Local Environment: The (Ionic) Nanoenvironment around Nanoparticles Is Different from Bulk and Determines the Physico-Chemical Properties of the Nanoparticles. *J. R. Soc. Interface* **2014**, *11*, 20130931.

271.   Jaworska, A.; Fornasaro, S.; Sergo, V.; Bonifacio, A. Potential of Surface Enhanced Raman Spectroscopy (SERS) in Therapeutic Drug Monitoring (TDM). A Critical Review. *Biosensors* **2016**, *6*, 47.

272.   Montjoy, D. G.; Bahng, J. H.; Eskafi, A.; Hou, H.; Kotov, N. A. Omnidispersible Hedgehog Particles with Multilayer Coatings for Multiplexed Biosensing. *J. Am. Chem. Soc.* **2018**, *140*, 7835–7845.

273.   Bahng, J. H.; Yeom, B.; Wang, Y.; Tung, S. O.; Hoff, J. D.; Kotov, N. Anomalous Dispersions of 'Hedgehog' Particles. *Nature* **2015**, *517*, 596–599.

274.   Kogasaka, R.; Sakuma, Y.; Chiba, S.; Akihara, M.; Horino, K.; Nakao, T. Small Round Virus-like Particles Associated with Acute Gastroenteritis in Japanese Children. *J. Med.Virol.* **1980**, *5*, 151–160.

275.   Mir-Simon, B.; Morla-Folch, J.; Gisbert-Quilis, P.; Pazos-Perez, N.; Xie, H.; Bastús, N. G.; Puntes, V.; Alvarez-Puebla, R. A.; Guerrini, L. SERS Efficiencies of Micrometric Polystyrene Beads Coated with Gold and Silver Nanoparticles: The Effect of Nanoparticle Size. *J. Opt.* **2015**, *17*, 114012.

276.   Abalde-Cela, S.; Ho, S.; Rodríguez-González, B.; Correa-Duarte, M. A.; Álvarez-Puebla, R. A.; Liz-Marzán, L. M.; Kotov, N. A. Loading of Exponentially Grown LBL Films with Silver Nanoparticles and Their Application to Generalized SERS Detection. *Angew. Chem. Int. Ed.* **2009**, *48*, 5326-5329.

277.   Hao, E.; Schatz, G. C. Electromagnetic Fields around Silver Nanoparticles and Dimers. *J. Chem. Phys.* **2004**, *120*, 357–366.

278.   Fredriksson, H.; Alaverdyan, Y.; Dmitriev, A.; Langhammer, C.; Sutherland, D. S.; Zäch, M.; Kasemo, B. Hole-Mask Colloidal Lithography. *Adv. Mater.* **2007**, 19, 4297−4302.

279.   Aizpurua, J.; Hanarp, P.; Sutherland, D. S.; Käll, M.; Bryant, G. W.; García de Abajo, F. J. Optical Properties of Gold Nanorings. *Phys. Rev. Lett.* **2003**, 90, e057401.

280.   Fang, Y. R.; Verre, R.; Shao, L.; Nordlander, P.; Käll, M. Hot Electron Generation and Cathodoluminescence Nanoscopy of Chiral Split Ring Resonators. *Nano Lett.* **2016**, 16, 5183-5190.

281.   Acimovic, S. S.; Sipova, H.; Emilsson, G.; Dahlin, A. B.; Antosiewics, T. J.; Käll, M. Superior LSPR Substrates Based on Electromagnetic Decoupling for On-a-Chip High-Throughput Label-Free Biosensing. *Light: Sci. Appl.* **2017**, 6, e17042.

282.   Hakonen, A.; Svedendahl, M.; Ogier, R.; Yang, Z.-J.; Lodewijks, K.; Verre, R.; Shegai, T.; Andersson, P.O.; Käll, M. Dimer-on-Mirror SERS Substrates with Attogram Sensitivity Fabricated by Colloidal Lithography. *Nanoscale* **2015**, 7, 9405-9410.

283.   Länk, N. O.; Verre, R.; Johansson, P.; Käll, M. Large-Scale Silicon Nanophotonic Metasurfaces with Polarization Independent Near-Perfect Absorption. *Nano Lett.* **2017**, 17, 3054-3060.

284.   Verre, R.; Shao, L.; Länk, N.O.; Karpinski, P.; Yankovich, A. B.; Antosiewics, T. J.; Olsson, E.; Käll, M. Metasurfaces and Colloidal Suspensions Composed of 3D Chiral Si Nanoresonators. *Adv. Mater.* **2017**, 29, 1701352.

285.   Verre, R.; Länk, N. O.; Andrén, D.; Sipova, H.; Käll, M. Large-Scale Fabrication of Shaped High-Index Dielectric Nanoparticles on a Substrate and in Solution. *Adv. Opt. Mater.* **2018**, 6, e1701253.

286.   Baranov, D.G.; Verre, R.; Karpinski, P.; Käll, M. Anapole-Enhanced Intrinsic Raman Scattering from Silicon Nanodisks. *ACS Photonics* **2018**, 5, 2730-2736.

287.   Enlow, P. D.; Buncick, M.; Warmack, R. J.; Vo Dinh, T. Detection of Nitro polynuclear Aromatic Compounds by Surface Enhanced Raman Spectroscopy. *Anal. Chem.* **1986**, *58*, 1119-1123.

288.   Schmidt, M. S.; Hübner, J.; Boisen, A. Large Area Fabrication of Leaning Silicon Nanopillars for Surface Enhanced Raman Spectroscopy. *Adv. Mater.* **2012**, *24*, OP11-OP18.

289.   Hu, M.; Ou, F. S.; Wu, W.; Naumov, I.; Li, X.; Bratkovsky, A. M.; Williams, R. S.; Li, Z. Gold Nanofingers for Molecule Trapping and Detection. *J. Am. Chem. Soc.* **2010**, *132*, 12820–12822.

290.   Chen, J.; Mårtensson, T.; Dick, K. A.; Deppert, K.; Xu, H. Q.; Samuelson, L.; Xu, H. Surface-Enhanced Raman Scattering of Rhodamine 6G on Nanowire Arrays Decorated with Gold Nanoparticles. *Nanotechnology* **2008**, *19*, 275712.

291.   Karadan, P.; Aggarwal, S.; Anappara, A. A.; Narayana, C.; Barshilia, H. C. Tailored Periodic Si Nanopillar Based Architectures as Highly Sensitive Universal SERS Biosensing Platform. *Sens. Actuators B* **2018**, *254*, 264–271.

292.   Li, T.; Wu, K.; Rindzevicius, T.; Wang, Z.; Schulte, L.; Schmidt, M. S.; Boisen, A.; Ndoni, S. Wafer-Scale Nanopillars Derived from Block Copolymer Lithography for Surface-Enhanced Raman Spectroscopy. *ACS Appl. Mater. Interfaces* **2016**, *8*, 15668–15675.

293.   Jeon, T. Y.; Park, S.-G.; Kim, D.-H.; Kim, S.-H. Standing-Wave-Assisted Creation of Nanopillar Arrays with Vertically Integrated Nanogaps for SERS-Active Substrates. *Adv. Funct. Mater.* **2015**, *25*, 4681–4688.

294.   Ou, F. S.; Hu, M.; Naumov, I.; Kim, A.; Wu, W.; Bratkovsky, A. M.; Li, X.; Williams, R. S.; Li, Z. Hot-Spot Engineering in Polygonal Nanofinger Assemblies for Surface Enhanced Raman Spectroscopy. *Nano Lett.* **2011**, *11*, 2538–2542.

295.   Kim, A.; Barcelo, S. J.; Williams, R. S.; Li, Z. Melamine Sensing in Milk Products by Using Surface Enhanced Raman Scattering. *Anal. Chem.* **2012**, *84*, 9303–9309.

296.   Viehrig, M.; Thilsted, A. H.; Matteucci, M.; Wu, K.; Catak, D.; Schmidt, M. S.; Zór, K.; Boisen, A. Injection Molded Microfluidic Device for SERS Sensing Using Embedded Au-Capped Polymer Nanocones. *ACS Appl. Mater. Interfaces* **2018**, *10*, 37417–37425.

297.   Barcelo, S. J.; Wu, W.; Li, X.; Li, Z.; Williams, R. S. Nanoimprint Lithography of Plasmonic Platforms for SERS Applications. *Appl. Phys. A* **2015**, *121*, 443–449.

298.   Zhao, W.; Liu, X.; Xu,, Y.; Wang,, S.; Sun, T.; Liu, S.; Wua, X.; Xu, Z. Polymer Nanopillar Array with Au Nanoparticle Inlays as a Flexible and Transparent SERS Substrate. *RSC Adv.* **2016**, *6*, 35527–35531.

299.   Park, S.-G.; Mun, C.; Xiao, X.; Braun, A.; Kim, S.; Giannini, V.; Maier, S. A.; Kim, D.-H. Surface Energy-Controlled SERS Substrates for Molecular Concentration at Plasmonic Nanogaps. *Adv. Funct. Mater.* **2017**, *27*, 1703376.

300.   Wu, K.; Rindzevicius, T.; Schmidt, M. S.; Thilsted, A. H.; Boisen, A. Optimizing Silver-Capped Silicon Nanopillars to Simultaneously Realize Macroscopic, Practical-

Level SERS Signal Reproducibility and High Enhancement at Low Costs. *J. Raman Spectrosc.* **2017**, *48*, 1808–1818.

301.   Wu, K.; Rindzevicius, T.; Schmidt, M. S.; Mogensen, K. B.; Xiao, S.; Boisen, A. Plasmon Resonances of Ag Capped Si Nanopillars Fabricated Using Mask-Less Lithography. *Opt. Express* **2015**, *23*, 12965-12978.

302.   Wu, K.; Rindzevicius, T.; Schmidt, M. S.; Mogensen, K. B.; Hakonen, A.; Boisen, A. Wafer-Scale Leaning Silver Nanopillars for Molecular Detection at Ultra-Low Concentrations. *J. Phys. Chem. C* **2015**, *119*, 2053–2062.

303.   Stadelmann, K.; Elizabeth, A.; Martín Sabanés, N.; Domke, K. F. The SERS Signature of PbS Quantum Dot Oxidation. *Vib. Spectrosc.* **2017**, *91*, 157–162.

304.   Gong, T.; Hong, Z. Y.; Chen, C. H.; Tsai, C. Y.; Liao, L. D.; Kong, K. V. Optical Interference-Free Surface-Enhanced Raman Scattering CO-Nanotags for Logical Multiplex Detection of Vascular Disease-Related Biomarkers. *ACS Nano* **2017**, *11*, 3365–3375.

305.   Ashley, J.; Wu, K.; Hansen; M. F.; Schmidt, M. S.; Boisen A.; Sun, Y. Quantitative Detection of Trace Level Cloxacillin in Food Samples Using Magnetic Molecularly Imprinted Polymer Extraction and Surface-Enhanced Raman Spectroscopy Nanopillars. *Anal. Chem.* **2017**, *89*, 11484-11490.

306.   Hakonen, A.; Wu, K.; Stenbæk Schmidt, M.; Andersson P. O.; Boisen, A.; Rindzevicius, T. Detecting Forensic Substances Using Commercially Available SERS Substrates and Handheld Raman Spectrometers. *Talanta* **2018**, *189*, 649–652.

307.   Hakonen, A.; Wang, F.; Andersson, P. O.; Wingfors, H.; Rindzevicius, T.; Schmidt, M. S.; Soma, V. R.; Xu, S.; Li, Y.; Boisen, A; Wu, H. Hand-Held Femtogram Detection of Hazardous Picric Acid with Hydrophobic Ag Nanopillar SERS Substrates and Mechanism of Elasto-Capillarity. *ACS Sens.* **2017**, *2*, 198– 202.

308.   Morelli, L.; Zór, K.; Jendresen, C. B.; Rindzevicius, T.; Schmidt, M. S; Nielsen, A. T.; Boisen, A. Surface Enhanced Raman Scattering for Quantification of p -Coumaric Acid Produced by *Escherichia Coli*. *Anal. Chem.* **2017**, *89*, 3981–3987.

309.   Yang, J.; Palla, M.; Bosco, F. G.; Rindzevicius, T.; Alstrøm, T. S.; Schmidt, M. S.; Boisen A.; Ju, J.; Lin, Q. Surface-Enhanced Raman Spectroscopy Based Quantitative Bioassay on Aptamer-Functionalized Nanopillars Using Large-Area Raman Mapping. *ACS Nano* **2013**, *7*, 5350-5359.

310.   Thilsted, A. H.; Pan, J. Y.; Wu, K.; Zór, K.; Rindzevicius, T.; Schmidt, M. S.; Boisen, A. Lithography-Free Fabrication of Silica Nanocylinders with Suspended Gold Nanorings for LSPR-Based Sensing. *Small* **2016**, *12*, 6745–6752.

311.   Sanger, K.; Durucan, O.; Wu, K.; Thilsted, A. H.; Heiskanen, A.; Rindzevicius, T.; Schmidt, M. S.; Zór, K.; Boisen, A. Large-Scale, Lithography-Free Production of Transparent Nanostructured Surface for Dual-Functional Electrochemical and SERS Sensing. *ACS Sens.* **2017**, *2*, 1869–1875.

312.   Wu, K.; Li, T.; Schmidt, M. S.; Rindzevicius, T.; Boisen, A.; Ndoni, S. Gold Nanoparticles Sliding on Recyclable Nanohoodoos—Engineered for Surface-Enhanced Raman Spectroscopy. *Adv. Funct. Mater.* **2018**, *28*, 1704818.

313.   Hayashi, S.; Koh, R.; Ichiyama, Y.; Yamamoto, K. Evidence for Surface-Enhanced Raman Scattering on Non-Metallic Surfaces: Copper Phthalocyanine Molecules on GaP Small Particles, *Phys. Rev. Lett.* **1988**, *60*, 1085.

314.   Lombardi, J. R.; Birke, R. L. Theory of Surface-Enhanced Raman Scattering in Semiconductors, *J. Phys. Chem. C* **2014**, *118*, 11120-11130.

315. Kuznetsov, A. I.; Miroshnichenko, A. E.; Brongersma, M. L.; Kivshar, Y. S.; Luk'yanchuk, B. Optically Resonant Dielectric Nanostructures, *Science* **2016**, *354*, 846.

316. Alessandri, I.; Lombardi, J. R. Enhanced Raman Scattering with Dielectrics, *Chem. Rev.* **2016**, *116*, 14921-14981.

317. Calderola, M.; Albella, P.; Cortés, E.; Rahmani, M.; Roschuk, T.; Grinblat, G.; Oulton, R. F.; Bragas, A. V.; Maier, S. A. Non-Plasmonic Nanoantennas for Surface Enhanced Spectroscopies with Ultra-Low Heat Conversion, *Nat. Commun.* **2015**, *6*, 7915.

318. Cambiasso, J.; König, M.; Cortés, E.; Schlücker, S.; Maier, S. A. Surface-Enhanced Spectroscopies of a Molecular Monolayer in an All-Dielectric Nanoantenna, *ACS Photonics* **2018**, *5*, 1546-1557.

319. Cong, S.; Yuan, Y.; Chen, Z.; Hou, J.; Yang, M.; Su, Y.; Zhang, Y.; Li, L.; Li, Q.; Geng, F.; Zhao, Z. Noble Metal-Comparable SERS Enhancement from Semiconducting Metal Oxides by Making Oxygen Vacancies, *Nat. Commun.* **2015**, *6*, 7800.

320. Zheng, X.; Ren, F.; Zhang, S.; Zhang, X.; Wu, H.; Zhang, X.; Xing, Z.; Qin, W.; Liu, Y.; Jiang, C. A General Method for Large-Scale Fabrication of Semiconducting Oxides with High SERS Sensitivity: *ACS Appl. Mater. Interfaces* **2017**, *9*, 14534-14544.

321. Ben-Jaber, S.; Peveler, W. J.; Quesada-Cabrera, R.; Cortés, E.; Sotelo-Vazquez, C.; Abdul-Karim, N.; Maier, S. A.; Parkin, I. P. Photo-Induced Enhanced Raman Spectroscopy for Universal Ultra-Trace Detection of Explosives, Pollutants and Biomolecules, *Nat. Commun.* **2016**, *7*, 12189.

322. Ruedas-Rama, M. J.; Walters, J. D.; Orte, A.; Hall, E. A. H. Fluorescent Nanoparticles for Intracellular Sensing: A Review. *Anal. Chim. Acta* **2012,** *751*, 1-23.

323. Schlücker, S. Surface-Enhanced Raman Spectroscopy: Concepts and Chemical Applications. *Angew. Chem. Int. Ed.* **2014,** *53*, 4756-4795.

324. Lane, L. A.; Qian, X.; Nie, S. SERS Nanoparticles in Medicine: From Label-Free Detection to Spectroscopic Tagging. *Chem. Rev.* **2015,** *115*, 10489-10529.

325. Schlücker, S. SERS Microscopy: Nanoparticle Probes and Biomedical Applications. *ChemPhysChem* **2009,** *10*, 1344-1354.

326. Wang, Y.; Yan, B.; Chen, L. SERS Tags: Novel Optical Nanoprobes for Bioanalysis. *Chem. Rev.* **2013,** *113*, 1391-1428.

327. Rodriguez-Lorenzo, L.; Fabris, L.; Alvarez-Puebla, R. A. Multiplex Optical Sensing with Surface-Enhanced Raman Scattering: A Critical Review. *Anal. Chim. Acta* **2012,** *745*, 10-23.

328. Schlücker, S. *Surface Enhanced Raman Spectroscopy: Analytical, Biophysical and Life Science Applications*. WILEY-VCH Verlag GmbH & Co. KGaA: Weinheim, 2011.

329. Fabris, L. Gold-based SERS tags for biomedical imaging. *J. Opt.* **2015,** *17*, 114002.

330. Chou, L. Y. T.; Ming, K.; Chan, W. C. W. Strategies for the Intracellular Delivery of Nanoparticles. *Chem. Soc. Rev.* **2011,** *40*, 233-245.

331. Steinigeweg, D.; Schütz, M.; Salehi, M.; Schlücker, S. Fast and Cost-Effective Purification of Gold Nanoparticles in the 20–250 nm Size Range by Continuous Density Gradient Centrifugation. *Small* **2011,** *7*, 2443-2448.

332. Salehi, M.; Schneider, L.; Ströbel, P.; Marx, A.; Packeisen, J.; Schlücker, S. Two-Color SERS Microscopy for Protein Co-localization in Prostate Tissue with Primary Antibody–Protein A/G–Gold Nanocluster Conjugates. *Nanoscale* **2014,** *6*, 2361-2367.

333. Küstner, B.; Gellner, M.; Schütz, M.; Schöppler, F.; Marx, A.; Ströbel, P.; Adam, P.; Schmuck, C.; Schlücker, S. SERS Labels for Red Laser Excitation: Silica-Encapsulated SAMs on Tunable Gold/Silver Nanoshells. *Angew. Chem. Int. Ed.* **2009,** *48*, 1950-1953.

334. Wang, Y. L.; Schlucker, S. Rational Design and Synthesis of SERS Labels. *Analyst* **2013,** *138*, 2224-2238.

335. McNay, G.; Eustace, D.; Smith, W. E.; Faulds, K.; Graham, D. Surface-Enhanced Raman Scattering (SERS) and Surface-Enhanced Resonance Raman Scattering (SERRS): A Review of Applications. *Appl. Spectrosc.* **2011,** *65*, 825-837.

336. McLintock, A.; Cunha-Matos, C. A.; Zagnoni, M.; Millington, O. R.; Wark, A. W. Universal Surface-Enhanced Raman Tags: Individual Nanorods for Measurements from the Visible to the Infrared (514-1064 nm). *ACS Nano* **2014,** *8*, 8600-8609.

337. Ni, J.; Lipert, R. J.; Dawson, G. B.; Porter, M. D. Immunoassay Readout Method Using Extrinsic Raman Labels Adsorbed on Immunogold Colloids. *Anal. Chem.* **1999,** *71*, 4903-4908.

338. Grubisha, D. S.; Lipert, R. J.; Park, H.-Y.; Driskell, J.; Porter, M. D. Femtomolar Detection of Prostate-Specific Antigen: An Immunoassay Based on Surface-Enhanced Raman Scattering and Immunogold Labels. *Anal. Chem.* **2003,** *75*, 5936-5943.

339. Porter, M. D.; Lipert, R. J.; Siperko, L. M.; Wang, G.; Narayanan, R. SERS as a Bioassay Platform: Fundamentals, Design, and Applications. *Chem. Soc. Rev.* **2008,** *37*, 1001-1011.

340. Jehn, C.; Küstner, B.; Adam, P.; Marx, A.; Ströbel, P.; Schmuck, C.; Schlücker, S. Water Soluble SERS Labels Comprising a SAM with Dual Spacers for Controlled Bioconjugation. *Phys. Chem. Chem. Phys.* **2009,** *11*, 7499-7504.

341. Schütz, M.; Küstner, B.; Bauer, M.; Schmuck, C.; Schlücker, S. Synthesis of Glass-Coated SERS Nanoparticle Probes *via* SAMs with Terminal SiO_2 Precursors. *Small* **2010,** *6*, 733-737.

342. Pallaoro, A.; Braun, G. B.; Moskovits, M. Biotags Based on Surface-Enhanced Raman Can Be as Bright as Fluorescence Tags. *Nano Lett.* **2015,** *15*, 6745-6750.

343. Woo, M.-A.; Lee, S.-M.; Kim, G.; Baek, J.; Noh, M. S.; Kim, J. E.; Park, S. J.; Minai-Tehrani, A.; Park, S.-C.; Seo, Y. T.; Kim, Y.-K.; Lee, Y.-S.; Jeong, D. H.; Cho, M.-H. Multiplex Immunoassay Using Fluorescent-Surface Enhanced Raman Spectroscopic Dots for the Detection of Bronchioalveolar Stem Cells in Murine Lung. *Anal. Chem.* **2009,** *81*, 1008-1015.

344.   von Maltzahn, G.; Centrone, A.; Park, J.-H.; Ramanathan, R.; Sailor, M. J.; Hatton, T. A.; Bhatia, S. N. SERS-Coded Gold Nanorods as a Multifunctional Platform for Densely Multiplexed Near-Infrared Imaging and Photothermal Heating. *Adv. Mater.* **2009,** *21*, 3175-3180.

345.   Schütz, M.; Schlücker, S. Towards Quantitative Multi-Color Nanodiagnostics: Spectral Multiplexing with Six Silica-Encapsulated SERS Labels. *J. Raman Spectrosc.* **2016,** *47*, 1012-1016.

346.   Samanta, A.; Maiti, K. K.; Soh, K.-S.; Liao, X.; Vendrell, M.; Dinish, U. S.; Yun, S.-W.; Bhuvaneswari, R.; Kim, H.; Rautela, S.; Chung, J.; Olivo, M.; Chang, Y.-T. Ultrasensitive Near-Infrared Raman Reporters for SERS-Based *In Vivo* Cancer Detection. *Angew. Chem. Int. Ed.* **2011,** *50*, 6089-6092.

347.   Maiti, K. K.; Dinish, U. S.; Fu, C. Y.; Lee, J.-J.; Soh, K.-S.; Yun, S.-W.; Bhuvaneswari, R.; Olivo, M.; Chang, Y.-T. Development of Biocompatible SERS Nanotag with Increased Stability by Chemisorption of Reporter Molecule for *In Vivo* Cancer Detection. *Biosens. Bioelectron.* **2010,** *26*, 398-403.

348.   Maiti, K. K.; Samanta, A.; Vendrell, M.; Soh, K.-S.; Olivo, M.; Chang, Y.-T. Multiplex Cancer Cell Detection by SERS Nanotags with Cyanine and Triphenylmethine Raman Reporters. *Chem. Commun.* **2011,** *47*, 3514-3516.

349.   Brem, S.; Schlücker, S. Surface-Enhanced Raman Spectroscopy and Density Functional Theory Calculations of a Rationally Designed Rhodamine with Thiol Groups at the Xanthene Ring. *J. Phys. Chem. C* **2017,** *121*, 15310-15317.

350.   Schütz, M.; Müller, C. I.; Salehi, M.; Lambert, C.; Schlücker, S. Design and Synthesis of Raman Reporter Molecules for Tissue Imaging by Immuno-SERS Microscopy. *J. Biophotonics* **2011,** *4*, 453-463.

351.   Su, X.; Zhang, J.; Sun, L.; Koo, T.-W.; Chan, S.; Sundararajan, N.; Yamakawa, M.; Berlin, A. A. Composite Organic−Inorganic Nanoparticles (COINs) with Chemically Encoded Optical Signatures. *Nano Lett.* **2005,** *5*, 49-54.

352.   Qian, X.; Peng, X.-H.; Ansari, D. O.; Yin-Goen, Q.; Chen, G. Z.; Shin, D. M.; Yang, L.; Young, A. N.; Wang, M. D.; Nie, S. *In Vivo* Tumor Targeting and Spectroscopic Detection with Surface-Enhanced Raman Nanoparticle Tags. *Nat. Biotechnol.* **2007,** *26*, 83-90.

353.   Cormack, P. A. G.; Hernandez-Santana, A.; Prasath, R. A.; McKenzie, F.; Graham, D.; Smith, W. E. Multidentate Macromolecules for Functionalisation, Passivation and Labelling of Metal Nanoparticles. *Chem. Commun.* **2008**, 2517-2519.

354.   McKenzie, F.; Ingram, A.; Stokes, R.; Graham, D. SERRS Coded Nanoparticles for Biomolecular Labelling with Wavelength-Tunable Discrimination. *Analyst* **2009,** *134*, 549-556.

355.   Wang, Y.; Salehi, M.; Schütz, M.; Rudi, K.; Schlücker, S. Microspectroscopic SERS Detection of Interleukin-6 with Rationally Designed Gold/Silver Nanoshells. *Analyst* **2013,** *138*, 1764-1771.

356.   Schütz, M.; Steinigeweg, D.; Salehi, M.; Kömpe, K.; Schlücker, S. Hydrophilically stabilized Gold Nanostars as SERS Labels for Tissue Imaging of The Tumor Suppressor P63 By Immuno-SERS Microscopy. *Chem. Commun.* **2011,** *47*, 4216-4218.

357.   Strozyk, M. S.; Jimenez de Aberasturi, D.; Liz-Marzan, L. M. Composite Polymer Colloids for SERS-Based Applications. *Chem. Rec.* **2018,** *18*, 807-818.

358.   Contreras-Caceres, R.; Sanchez-Iglesias, A.; Karg, M.; Pastoriza-Santos, I.; Perez-Juste, J.; Pacifico, J.; Hellweg, T.; Fernandez-Barbero, A.; Liz-Marzan, L. M. Encapsulation and Growth of Gold Nanoparticles in Thermoresponsive Microgels. *Adv. Mater.* **2008,** *20*, 1666-1670.

359.   Perez-Juste, J.; Pastoriza-Santos, I.; Liz-Marzan, L. M. Multifunctionality in Metal@Microgel Colloidal Nanocomposites. *J. Mater. Chem. A* **2013,** *1*, 20-26.

360.   Bodelon, G.; Montes-Garcia, V.; Fernandez-Lopez, C.; Pastoriza-Santos, I.; Perez-Juste, J.; Liz-Marzan, L. M. Au@pNIPAM SERRS Tags for Multiplex Immunophenotyping Cellular Receptors and Imaging Tumor Cells. *Small* **2015,** *11*, 4149-4157.

361.   Casado-Rodriguez, M. A.; Sanchez-Molina, M.; Lucena-Serrano, A.; Lucena-Serrano, C.; Rodriguez-Gonzalez, B.; Algarra, M.; Diaz, A.; Valpuesta, M.; Lopez-Romero, J. M.; Perez-Juste, J.; Contreras-Caceres, R. Synthesis of Vinyl-Terminated Au Nanoprisms and Nanooctahedra Mediated by 3-Butenoic Acid: Direct Au@PNIPAM Fabrication with Improved SERS Capabilities. *Nanoscale* **2016,** *8*, 4557-4564.

362.   Feng, Y. H.; Wang, Y.; Wang, H.; Chen, T.; Tay, Y. Y.; Yao, L.; Yan, Q. Y.; Li, S. Z.; Chen, H. Y. Engineering "Hot" Nanoparticles for Surface-Enhanced Raman Scattering by Embedding Reporter Molecules in Metal Layers. *Small* **2012,** *8*, 246-251.

363.   Jimenez de Aberasturi, D.; Serrano-Montes, A. B.; Langer, J.; Henriksen-Lacey, M.; Parak, W. J.; Liz-Marzan, L. M. Surface Enhanced Raman Scattering Encoded Gold Nanostars for Multiplexed Cell Discrimination. *Chem. Mater.* **2016,** *28*, 6779-6790.

364.   Tam, N. C. M.; Scott, B. M. T.; Voicu, D.; Wilson, B. C.; Zheng, G. Facile Synthesis of Raman Active Phospholipid Gold Nanoparticles. *Bioconjugate Chem.* **2010,** *21*, 2178-2182.

365.   Ip, S.; MacLaughlin, C. M.; Gunari, N.; Walker, G. C. Phospholipid Membrane Encapsulation of Nanoparticles for Surface-Enhanced Raman Scattering. *Langmuir* **2011,** *27*, 7024-7033.

366.   Tam, N. C. M.; McVeigh, P. Z.; MacDonald, T. D.; Farhadi, A.; Wilson, B. C.; Zheng, G. Porphyrin-Lipid Stabilized Gold Nanoparticles for Surface Enhanced Raman Scattering Based Imaging. *Bioconjugate Chem.* **2012,** *23*, 1726-1730.

367.   Alipour, E.; Halverson, D.; McWhirter, S.; Walker, G. C. Phospholipid Bilayers: Stability and Encapsulation of Nanoparticles. *Annu. Rev. Phys. Chem.* **2017,** *68*, 261-283.

368. Cheng, X. J.; Zhao, G.; Lu, Y.; Yan, M.; Wang, H.; Chen, H. Y. Controllable Oligomerization: Defying Step-Growth Kinetics in the Polymerization of Gold Nanoparticles. *Chem. Commun.* **2018,** *54*, 7746-7749.

369. Zheng, X. S.; Hu, P.; Cui, Y.; Zong, C.; Feng, J. M.; Wang, X.; Ren, B. BSA-Coated Nanoparticles for Improved SERS-Based Intracellular pH Sensing. *Anal. Chem.* **2014,** *86*, 12250-12257.

370. Yuan, H. K.; Liu, Y.; Fales, A. M.; Li, Y. L.; Liu, J.; Vo-Dinh, T. Quantitative Surface-Enhanced Resonant Raman Scattering Multiplexing of Biocompatible Gold Nanostars for *in Vitro* and *ex Vivo* Detection. *Anal. Chem.* **2013,** *85*, 208-212.

371. Dominguez-Medina, S.; McDonough, S.; Swanglap, P.; Landes, C. F.; Link, S. *In Situ* Measurement of Bovine Serum Albumin Interaction with Gold Nanospheres. *Langmuir* **2012,** *28*, 9131-9139.

372. Tsai, D. H.; DelRio, F. W.; Keene, A. M.; Tyner, K. M.; MacCuspie, R. I.; Cho, T. J.; Zachariah, M. R.; Hackley, V. A. Adsorption and Conformation of Serum Albumin Protein on Gold Nanoparticles Investigated Using Dimensional Measurements and *in Situ* Spectroscopic Methods. *Langmuir* **2011,** *27*, 2464-2477.

373. Blanco-Covian, L.; Montes-Garcia, V.; Girard, A.; Fernandez-Abedul, M. T.; Perez-Juste, J.; Pastoriza-Santos, I.; Faulds, K.; Graham, D.; Blanco-Lopez, M. C. Au@Ag SERRS Tags Coupled to a Lateral Flow Immunoassay for the Sensitive Detection of Pneumolysin. *Nanoscale* **2017,** *9*, 2051-2058.

374. Mulvaney, S. P.; Musick, M. D.; Keating, C. D.; Natan, M. J. Glass-Coated, Analyte-Tagged Nanoparticles: A New Tagging System Based on Detection with Surface-Enhanced Raman Scattering. *Langmuir* **2003,** *19*, 4784-4790.

375. Liz-Marzán, L. M.; Giersig, M.; Mulvaney, P. Synthesis of Nanosized Gold-Silica Core-Shell Particles. *Langmuir* **1996**, *12*, 4329-4335

376. Doering, W. E.; Nie, S. Spectroscopic Tags Using Dye-Embedded Nanoparticles and Surface-Enhanced Raman Scattering. *Anal. Chem.* **2003,** *75*, 6171-6176.

377. Schütz, M.; Salehi, M.; Schlücker, S. Direct Silica Encapsulation of Self-Assembled-Monolayer-Based Surface-Enhanced Raman Scattering Labels with Complete Surface Coverage of Raman Reporters by Noncovalently Bound Silane Precursors. *Chem. Asian J.* **2014,** *9*, 2219-2224.

378. Wang, C.; Chen, Y.; Wang, T.; Ma, Z.; Su, Z. Monodispersed Gold Nanorod-Embedded Silica Particles as Novel Raman Labels for Biosensing. *Adv. Funct. Mater.* **2008,** *18*, 355-361.

379. Rodríguez-Lorenzo, L.; Krpetic, Z.; Barbosa, S.; Alvarez-Puebla, R. A.; Liz-Marzán, L. M.; Prior, I. A.; Brust, M. Intracellular Mapping with SERS-Encoded Gold Nanostars. *Integr. Biol.* **2011**, *9*, 922-926.

380. Lee, S.; Chon, H.; Yoon, S.-Y.; Lee, E. K.; Chang, S.-I.; Lim, D. W.; Choo, J. Fabrication of SERS-Fluorescence Dual Modal Nanoprobes and Application to Multiplex Cancer Cell Imaging. *Nanoscale* **2012,** *4*, 124-129.

381. Gellner, M.; Steinigeweg, D.; Ichilmann, S.; Salehi, M.; Schütz, M.; Kömpe, K.; Haase, M.; Schlücker, S. 3D Self-Assembled Plasmonic Superstructures of Gold Nanospheres: Synthesis and Characterization at the Single-Particle Level. *Small* **2011,** *7*, 3445-3451.

382. Chung, T.-H.; Wu, S.-H.; Yao, M.; Lu, C.-W.; Lin, Y.-S.; Hung, Y.; Mou, C.-Y.; Chen, Y.-C.; Huang, D.-M. The Effect of Surface Charge on the Uptake and Biological Function of Mesoporous Silica Nanoparticles in 3T3-L1 Cells and Human Mesenchymal Stem Cells. *Biomaterials* **2007,** *28*, 2959-2966.

383. Rodríguez-Fernández, D.; Langer, J.; Henriksen-Lacey, M.; Liz-Marzán, L. M. Hybrid Au–SiO$_2$ Core–Satellite Colloids as Switchable SERS Tags. *Chem. Mater.* **2015,** *27*, 2540-2545.

384. Shanthil, M.; Thomas, R.; Swathi, R. S.; George Thomas, K.,Ag@SiO$_2$ Core–Shell Nanostructures: Distance-Dependent Plasmon Coupling and SERS Investigation. *J. Phys. Chem. Lett.* **2012,** *3*, 1459-1464.

385. T. Ung, L.M. Liz-Marzán, P. Mulvaney Optical Properties of Thin Films of Au@SiO$_2$ Particles. *J. Phys. Chem. B* **2001**, *105*, 3441-3452.

386. Li, S.; Pedano, M. L.; Chang, S.-H.; Mirkin, C. A.; Schatz, G. C. Gap Structure Effects on Surface-Enhanced Raman Scattering Intensities for Gold Gapped Rods. *Nano Lett.* **2010,** *10*, 1722-1727.

387. Hermanson, G. T. *Bioconjugate Techniques*, Elsevier, 2013.

388. Sapsford, K. E.; Algar, W. R.; Berti, L.; Gemmill, K. B.; Casey, B. J.; Oh, E.; Stewart, M. H.; Medintz, I. L. Functionalizing Nanoparticles with Biological Molecules: Developing Chemistries that Facilitate Nanotechnology. *Chem. Rev.* **2013,** *113*, 1904-2074.

389. Wang, C.; Yan, Q.; Liu, H. B.; Zhou, X. H.; Xiao, S. J. Different EDC/NHS Activation Mechanisms between PAA and PMAA Brushes and the Following Amidation Reactions. *Langmuir* **2011,** *27*, 12058-12068.

390. Sun, L.; Sung, K. B.; Dentinger, C.; Lutz, B.; Nguyen, L.; Zhang, J. W.; Qin, H. Y.; Yamakawa, M.; Cao, M. Q.; Lu, Y.; Chmura, A. J.; Zhu, J.; Su, X.; Berlin, A. A.; Chan, S.; Knudsen, B. Composite Organic-Inorganic Nanoparticles as Raman Labels for Tissue Analysis. *Nano Lett.* **2007,** *7*, 351-356.

391. Dugandžić, V., Drikermann, D., Ryabchykov, O., Undisz, A., Vilotijević, I., Lorkowski, S.; Bocklitz, T. W.; Matthäus, C; Weber, K.;Cialla-May, D.; Popp, J. Surface Enhanced Raman Spectroscopy-Detection of the Uptake of Mannose-Modified Nanoparticles by Macrophages *In Vitro*: A Model for Detection of Vulnerable Atherosclerotic Plaques. *J. Biophotonics* **2018**, e201800013.

392. Lee, J. H.; You, M. H.; Kim, G. H.; Nam, J. M. Plasmonic Nanosnowmen with a Conductive Junction as Highly Tunable Nanoantenna Structures and Sensitive, Quantitative and Multiplexable Surface-Enhanced Raman Scattering Probes. *Nano Lett.* **2014,** *14*, 6217-6225.

393.   Zhang, Y.; Walkenfort, B.; Yoon, J. H.; Schlücker, S.; Xie, W. Gold and Silver Nanoparticle Monomers are Non-SERS-Active: A Negative Experimental Study with Silica-Encapsulated Raman-Reporter-Coated Metal Colloids. *Phys. Chem. Chem. Phys.* **2015,** *17*, 21120-21126.

394.   Kleinman, S. L.; Frontiera, R. R.; Henry, A.-I.; Dieringer, J. A.; Van Duyne, R. P. Creating, Characterizing, and Controlling Chemistry with SERS Hot Spots. *Phys. Chem. Chem. Phys.* **2013,** *15*, 21-36.

395.   Steinigeweg, D.; Schütz, M.; Schlücker, S. Single Gold Trimers and 3D Superstructures Exhibit a Polarization-Independent SERS Response. *Nanoscale* **2013,** *5*, 110-113.

396.   Salehi, M.; Steinigeweg, D.; Ströbel, P.; Marx, A.; Packeisen, J.; Schlücker, S., Rapid Immuno-SERS Microscopy for Tissue Imaging with Single-Nanoparticle Sensitivity. *J. Biophotonics* **2013,** *6*, 785-792.

397.   Mulvihill, M. J.; Ling, X. Y.; Henzie, J.; Yang, P. Anisotropic Etching of Silver Nanoparticles for Plasmonic Structures Capable of Single-Particle SERS. *J. Am. Chem. Soc.* **2010,** *132*, 268-274.

398.   Wissler, J.; Wehmeyer, M.; Bäcker, S.; Knauer, S.; Schlücker, S. Simultaneous Rayleigh/Mie and Raman/Fluorescence Characterization of Molecularly Functionalized Colloids by Correlative Single-Particle Real-Time Imaging in Suspension. *Anal. Chem.* **2018,** *90*, 723-728.

399.   Park, J. E.; Jung, Y.; Kim, M.; Nam, J. M. Quantitative Nanoplasmonics. *ACS Cent. Sci.* **2018,** *4*, 1303-1314.

400.   Nam, J. M.; Oh, J. W.; Lee, H.; Suh, Y. D. Plasmonic Nanogap-Enhanced Raman Scattering with Nanoparticles. *Acc. Chem. Res.* **2016,** *49*, 2746-2755.

401.   Wang, Z.; Zong, S.; Wu, L.; Zhu, D.; Cui, Y. SERS-Activated Platforms for Immunoassay: Probes, Encoding Methods, and Applications. *Chem. Rev.* **2017,** *117*, 7910-7963.

402.   Shan, B.; Pu, Y.; Chen, Y.; Liao, M.; Li, M. Novel SERS Labels: Rational Design, Functional Integration and Biomedical Applications. *Coord. Chem. Rev.* **2018,** *371*, 11-37.

403.   Mao, L.; Li, Z.; Wu, B.; Xu, H. Effects of Quantum Tunneling in Metal Nanogap on Surface-Enhanced Raman Scattering. *Appl. Phys. Lett.* **2009**, *94*, 243102.

404.   Chen. W.; Zhang, S.; Kang, M.; Liu, W.; Ou, Z.; Li, Y.; Zhang, Y.; Guan, Z.; Xu, H.. Probing the Limits of Plasmonic Enhancement Using a Two-Dimensional Atomic Crystal Probe. *Light: Sci. Appl.* **2018**, *7*, 56.

405.   Dieringer, J. A.; Wustholz, K. L.; Masiello, D. J.; Camden J. P.; Kleinman, S. L.; Schatz G. C.; Van Duyne, R. P. Surface-Enhanced Raman Excitation Spectroscopy of a Single Rhodamine 6G Molecule. *J. Am. Chem. Soc.* **2009**, *131*, 849-854.

406.   Chu, Y.; Banaee, M. G.; Crozier, K. B. Double-Resonance Plasmon Substrates for Surface-Enhanced Raman Scattering with Enhancement at Excitation and Stokes Frequencies. *ACS Nano* **2010**, *4*, 2804-2810.

407. Shegai, T.; Li, Z.; Dadosh, T.; Zhang, Z.; Xu, H.; Haran, G. Managing Light Polarization *via* Plasmon–Molecule Interactions within an Asymmetric Metal Nanoparticle Trimer. *Proc. Natl. Acad. Sci. U. S. A.* **2008**, *105*, 16448-16453.

408. Wei, H.; Hao, F.; Huang, Y.; Wang, W.; Nordlander, P.; Xu, H. Polarization Dependence of Surface-Enhanced Raman Scattering in Gold Nanoparticle−Nanowire Systems. *Nano Lett.* **2008**, *8*, 2497-2502.

409. Li, Z.; Shegai, T.; Haran, G.; Xu, H. Multiple-Particle Nanoantennas for Enormous Enhancement and Polarization Control of Light Emission. *ACS Nano* **2009**, *3*, 637-642.

410. Mubeen, S.; Zhang, S.; Kim, N.; Lee, S.; Krämer, S.; Moskovits, M. Plasmonic Properties of Gold Nanoparticles Separated from a Gold Mirror by an Ultrathin Oxide. *Nano Lett.* **2012**, *12*, 2088-2094.

411. Tsoutsi, D.; Guerrini, L.; Hermida-Ramon, J. M.; Giannini, V.; Liz-Marzán, L. M.; Wei, A.; Alvarez-Puebla, R. A. Simultaneous SERS detection of Copper and Cobalt at Ultratrace Levels. *Nanoscale* **2013**, *5*, 4776-4784.

412. Chung, E.; Gao, R.; Ko, J.; Choi, N.; Lim, D. W.; Lee, E. K.; Chang, S.-I.; Choo, J. Trace Analysis of Mercury(II) Ions Using Aptamer-Modified Au/Ag Core–Shell Nanoparticles and SERS Spectroscopy in a Microdroplet Channel. *Lab Chip* **2013**,*13*, 260-266.

413. Yin, J.; Wu, T.; Song, J.; Zhang, Q.; Liu, S.; Xu, R.; Duan, H. SERS-Active Nanoparticles for Sensitive and Selective Detection of Cadmium Ion (Cd^{2+}). *Chem. Mater.* **2011**, *23*, 4756–4764.

414. Dugandžić, V.; Kupfer, S.; Jahn, M.; Henkel, T.; Weber, K.; Cialla-May, D.; Popp, J. A SERS-Based Molecular Sensor for Selective Detection and Quantification of Copper(II) Ions. *Sens. Actuators B* **2019**, *279*, 230–237.

415. Alvarez-Puebla, R. A. Liz-Marzán, L. M. SERS Detection of Small Inorganic Molecules and Ions. *Angew. Chem. Int. Ed.* **2012**, *51*, 11214-11223.

416. Cao, Y.; Li, D.-W.; Zhao, L.-J.; Liu, X.-Y.; Cao, X.-M.; Long, Y.-T. Highly Selective Detection of Carbon Monoxide in Living Cells by Palladacycle Carbonylation-Based Surface Enhanced Raman Spectroscopy Nanosensors. *Anal. Chem.* **2015**, *87*, 9696–9701.

417. Tang, H.; Zhu, C.; Meng, G.; Wu, N. Surface-Enhanced Raman Scattering Sensors for Food Safety and Environmental Monitoring. *J. Electrochem. Soc.* **2018**, *165*, B3098-B3118.

418. Cao, W. Y. C.; Jin, R.; Mirkin, C. A. Nanoparticles with Raman Spectroscopic Fingerprints for DNA and RNA Detection. *Science* **2002**, *297*, 1536-1540

419. Kim, W. H.; Lee, J. U.; Song, S.; Kim, S.; Choi, Y. J.; Sim, S. J. A Label-Free, Ultra-Highly Sensitive and Multiplexed SERS Nanoplasmonic Biosensor for miRNA Detection Using a Head-Flocked Gold Nanopillar. *Analyst* **2019**, *144*, 1768-1776.

420. Vo-Dinh T.; Allain L. R.; Stokes, D. L. Cancer Gene Detection Using Surface-Enhanced Raman Scattering (SERS). *J. Raman Spectrosc.* **2002**, *33*, 511-516.

421. Lee, S.; Kadam, U. S.; Craig, A. P.; Irudayaraj, J. *In vivo* Biodetection Using Surface-enhanced Raman spectroscopy in Biosensors Based on Nanomaterials and Nanodevices, eds. J. Li N. Wu, CRC Press, Taylor and Francis Group, Boca Raton (2014), p. 165-172

422. Hao, H. P.; Wang, G. J.; Sun, J. G. Enantioselective Pharmacokinetics of Ibuprofen and Involved Mechanisms. *Drug Metab. Rev.* **2005**, *37*, 215–234.

423. Brown, J. M.; Davies, S. G. Chemical Asymmetric Synthesis. *Nature* **1989**, *342*, 631–636.

424. Maier, N. M.; Franco, P.; Lindner, W. Separation of Enantiomers: Needs, Challenges, Perspectives. *J. Chromatogr. A* **2001**, *906*, 3-33.

425. Lee, S. J.; Lin, W. A Chiral Molecular Square with Metallo-Corners for Enantioselective Sensing. *J. Am. Chem. Soc.* **2002**, *124*, 4554–4555.

426. Tkachenko G.; Brasselet, E. Optofluidic Sorting of Material Chirality by Chiral Light. *Nat. Commun.* **2014**, *5*, 3577 (1-7).

427. Cameron, R. P.; Barnett, S. M.; Yao, A. M. Discriminatory Optical Force for Chiral Molecules. *New J. Phys.* **2014**, *16*, 013020 (1-18).

428. Wang, Y.; Yu, Z.; Ji, W.; Tanaka, Y.; Sui, H.; Zhao, B.; Ozaki, Y. Enantioselective Discrimination of Alcohols by Hydrogen Bonding: A SERS Study. *Angew. Chem. Int. Ed.* **2014**, *53*, 13866-13870.

429. Wang, Y.; Yu, Z.; Han, X.; Su, H.; Ji, W.; Cong Q.; Zhao, B.; Ozaki, Y. Charge-Transfer-Induced Enantiomer Selective Discrimination of Chiral Alcohols by SERS *J. Phys. Chem. C* **2016**, *120*, 29374-29381.

430. Tierney, H. L.; Murphy, C. J.; Sykes, E. C. H. Regular Scanning Tunneling Microscope Tips Can Be Intrinsically Chiral. *Phys. Rev. Lett.* **2011**, *106*, 010801.

431. Ozaki, Y. The 26th International Conference on Raman Spectroscopy, 2018, Jeju, Korea, ThPM1-01.

432. Sukmanee, T.; Wongravee, K.; Kitahama, Y.; Ekgasit, S.; Pienpinijtham, P.; Itoh, T.; Ozaki, Y. *Ms. submitted*.

433. Nurushima, T.; Okamoto, H. Strong Nanoscale Optical Activity Localized in Two-Dimensional Chiral Metal Nanostructures. *J. Phys. Chem. C* **2013**, *117*, 23964-23969.

434. Park, J.-E.; Lee, Y.; Nam, J.-M. Precisely Shaped, Uniformly Formed Gold Nanocubes with Ultrahigh Reproducibility in Single-Particle Scattering and Surface-Enhanced Raman Scattering. *Nano Lett.* **2018**, *18*, 6475-6482.

435. González-Rubio, G.; Díaz-Núñez, P.; Rivera, A.; Prada, A.; Tardajos, G.; González-Izquierdo, J.; Bañares, L.; Llombart, P.; Macdowell, L. G.; Alcolea-Palafox, M.; Liz-Marzán, L. M.; Peña-Rodríguez, O.; Guerrero-Martínez, A. Femtosecond Laser Reshaping Yields Gold Nanorods with Ultranarrow Surface Plasmon Resonances. *Science* **2017**, *358*, 640-644.

436. Lim, D. K.; Jeon, K. S.; Kim, H. M.; Nam, J. M.; Suh, Y. D. Nanogap-Engineerable Raman-Active Nanodumbbells for Single-Molecule Detection. *Nat. Mater.* **2010,** *9*, 60-67.

437.   Lee, J.-H.; Nam, J.-M.; Jeon, K.-S.; Lim, D.-K.; Kim, H.; Kwon, S.; Lee, H.; Suh, Y. D. Tuning and Maximizing the Single-Molecule Surface-Enhanced Raman Scattering from DNA-Tethered Nanodumbbells. *ACS Nano* **2012,** *6*, 9574-9584.

438.   Oh, J. W.; Lim, D. K.; Kim, G. H.; Suh, Y. D.; Nam, J. M. Thiolated DNA-Based Chemistry and Control in the Structure and Optical Properties of Plasmonic Nanoparticles with Ultrasmall Interior Nanogap. *J. Am. Chem. Soc.* **2014,** *136*, 14052-14059.

439.   Song, J.; Duan, B.; Wang, C.; Zhou, J.; Pu, L.; Fang, Z.; Wang, P.; Lim, T. T.; Duan, H. SERS-Encoded Nanogapped Plasmonic Nanoparticles: Growth of Metallic Nanoshell by Templating Redox-Active Polymer Brushes. *J. Am. Chem. Soc.* **2014,** *136*, 6838-6841.

440.   Kim, M.; Ko, S. M.; Kim, J. M.; Son, J.; Lee, C.; Rhim, W. K.; Nam, J. M. Dealloyed Intra-Nanogap Particles with Highly Robust, Quantifiable Surface-Enhanced Raman Scattering Signals for Biosensing and Bioimaging Applications. *ACS Cent. Sci.* **2018,** *4*, 277-287.

441.   Savage, K. J.; Hawkeye, M. M.; Esteban, R.; Borisov, A. G.; Aizpurua, J.; Baumberg, J. J. Revealing the Quantum Regime In Tunnelling Plasmonics. *Nature* **2012,** *491*, 574-577.

442.   Lin, L.; Zapata, M.; Xiong, M.; Liu, Z.; Wang, S.; Xu, H.; Borisov, A. G.; Gu, H.; Nordlander, P.; Aizpurua, J.; Ye, J. Nanooptics of Plasmonic Nanomatryoshkas: Shrinking the Size of a Core-Shell Junction to Subnanometer. *Nano Lett.* **2015,** *15*, 6419-6428.

443.   Marks, H.; Schechinger, M.; Garza, J.; Locke, A.; Coté, G. Surface Enhanced Raman Spectroscopy (SERS) for *In Vitro* Diagnostic Testing at the Point of Care. *Nanophotonics* **2017,** *6*, 681-701.

444.   Henry, A.-I.; Sharma, B.; Cardinal, M. F.; Kurouski. D.; Van Duyne, R. P. Surface-Enhanced Raman Spectroscopy Biosensing: *In Vivo* Diagnostics and Multimodal Imaging. *Anal. Chem.* **2016**, 88, 6638–6647.

445.   Xu, H.; Kall, M. Surface-Plasmon-Enhanced Optical Forces in Silver Nanoaggregates. *Phys. Rev. Lett.* **2002**, *89*, 246802.

446.   Juan M. L.; Righini, M.; Quidant R. Plasmon Nano-Optical Tweezers. *Nat. Photon.* **2011**, *5*, 349.

447.   Lim, D.-K.; Jeon, K.-S.; Kim, H. M.; Nam J.-M.; Suh, Y. D. Nanogap-Engineerable Raman-Active Nanodumbbells for Single-Molecule Detection. *Nat. Mater.* **2009**, *9*, 60-67.

448.   Thacker, V. V.; Herrmann, L. O.; Sigle, D. O.; Zhang, T.; Liedl, T.; Baumberg J. J.; Keyser, U. F. DNA Origami Based Assembly of Gold Nanoparticle Dimers for Surface-Enhanced Raman Scattering. *Nat. Commun.* **2014**, *5*, 3448.

449.   Taylor, R. W.; Lee T.-C.; Scherman, O. A.; Esteban, R.; Aizpurua, J.; Huang, F. M.; Baumberg, J. J.; Mahajan, S. Precise Subnanometer Plasmonic Junctions for SERS

within Gold Nanoparticle Assemblies Using Cucurbit[n]uril "Glue". *ACS Nano* **2011**, *5*, 3878-3887.

450.   Kim, N. H.; Hwang, W.; Baek, K.; Rohman, M. R.; Kim, J.; Kim, H. W.; Mun, J.; Lee, S. Y.; Yun, G.; Murray, J.; Ha, J. W.; Rho, J.; Moskovits, M.; Kim, K. Smart SERS Hot Spots: Single Molecules Can Be Positioned in a Plasmonic Nanojunction Using Host–Guest Chemistry. *J. Am. Chem. Soc.* **2018**, *140*, 4705-4711.

451.   Esteban, R.; Borisov, A. G.; Nordlander, P.; Aizpurua, J. Bridging Quantum and Classical Plasmonics with a Quantum-Corrected Model. *Nat. Commun.* **2012**, *3*, 825.

452.   Sigle, D. O.; Hugall, J. T.; Ithurria, S.; Dubertret, B.; Baumberg, J. J. Probing Confined Phonon Modes in Individual CdSe Nanoplatelets Using Surface-Enhanced Raman Scattering. *Phys. Rev. Lett.* **2014**, *113*, 087402.

453.   Takase, M.; Ajiki, H.; Mizumoto, Y.; Komeda, K.; Nara, M.; Nabika, H.; Yasuda, S.; Ishihara, H.; Murakoshi, K. Selection-Rule Breakdown in Plasmon-Induced Electronic Excitation of an Isolated Single-Walled Carbon Nanotube. *Nat. Photonics* **2013**, *7*, 550-554.

454.   Fang, Y. R.; Wei, H.; Hao, F.; Nordlander, P.; Xu, H. X. Remote-Excitation Surface-Enhanced Raman Scattering Using Propagating Ag Nanowire Plasmons. *Nano Lett.* **2009**, *9*, 2049-2053.

455.   Hutchison, J. A.; Centeno, S. P.; Odaka, H.; Fukumura, H.; Hofkens, J.; Uji-i, H. Subdiffraction Limited, Remote Excitation of Surface Enhanced Raman Scattering. *Nano Lett.* **2009**, *9*, 995-1001.

456.   Wei, H.; Pan, D.; Zhang, S.; Li, Z.; Li, Q.; Liu, N.; Wang, W.; Xu, H. Plasmon Waveguiding in Nanowires. *Chem. Rev.* **2018**, *118*, 2882-2926.

457.   Lu, G.; De Keersmaecker, H.; Su, L.; Kenens, B.; Rocha, S.; Fron, E.; Chen, C.; Van Dorpe, P.; Mizuno, H.; Hofkens, J.; Hutchison, J. A.; Uji-i, H. Live-Cell SERS Endoscopy Using Plasmonic Nanowire Waveguides. *Adv. Mater.* **2014**, *26*, 5124-5128.

458.   Ma, X.; Zhu, Y.; Yu, N.; Kim, S.; Liu, Q.; Apontti, L.; Xu, D.; Yan, R.; Liu, M. Toward High-Contrast Atomic Force Microscopy-Tip-Enhanced Raman Spectroscopy Imaging: Nanoantenna-Mediated Remote-Excitation on Sharp-Tip Silver Nanowire Probes. *Nano Lett.* **2019**, *19*, 100-107.

459.   Day, J. K.; Neumann, O.; Grady, N. K.; Halas, N. J. Nanostructure-Mediated Launching and Detection of 2D Surface Plasmons. *ACS Nano* **2010**, *4*, 7566-7572.

460.   Zong C.; Xu, M.; Xu, L. J.; Wei, T.; Ma, X.; Zheng, X.-S.; Hu, R.; Ren, B. Surface-Enhanced Raman Spectroscopy for Bioanalysis: Reliability and Challenges. *Chem. Rev.* **2018**, *118*, 4946-4980.

461.   Fang, Y.; Li, Y.; Xu, H.; Sun, M. Ascertaining p,p′-Dimercaptoazobenzene Produced from p-Aminothiophenol by Selective Catalytic Coupling Reaction on Silver Nanoparticles. *Langmuir* **2010**, *26*, 7737-7746.

462.   Sun, M.; Hou, Y.; Li, Z.; Liu, L.; Xu, H. Remote Excitation Polarization-Dependent Surface Photochemical Reaction by Plasmonic Waveguide. *Plasmonics* **2011**, *6*, 681-687.

463.   Sun, M.; Zhang, Z.; Zheng, H.; Xu, H. *In-situ* Plasmon-Driven Chemical Reactions Revealed by High Vacuum Tip-Enhanced Raman Spectroscopy. *Sci. Rep.* **2012**, *2*, 647.

464.   Gruenke, N. L.; Cardinal, M. F.; McAnally, M. O.; Frontiera R. R.; Schatz, G. C.; Van Duyne, R. P. Ultrafast and Nonlinear Surface-Enhanced Raman Spectroscopy. *Chem. Soc. Rev.* **2016**, *45*, 2263-2290.

465.   Li, J. F.; Huang, Y. F.; Ding, Y.; Yang, Z. L.; Li, S. B.; Zhou, X. S.; Fan, F. R.; Zhang, W.; Zhou, Z. Y.; Wu, D. Y.; Ren, B.; Wang, Z. L.; Tian, Z. Q. Shell-Isolated Nanoparticle-Enhanced Raman Spectroscopy. *Nature* **2010,** *464*, 392-395.

466.   Li, C. Y.; Meng, M.; Huang, S. C.; Li, L.; Huang, S. R.; Chen, S.; Meng, L. Y.; Panneerselvam, R.; Zhang, S. J.; Ren, B.; Yang, Z. L.; Li, J. F.; Tian, Z. Q. "Smart" Ag Nanostructures for Plasmon-Enhanced Spectroscopies. *J. Am. Chem. Soc.* **2015,** *137*, 13784-13787.

467.   Li, J. F.; Ding, S. Y.; Yang, Z. L.; Bai, M. L.; Anema, J. R.; Wang, X.; Wang, A.; Wu, D. Y.; Ren, B.; Hou, S. M.; Wandlowski, T.; Tian, Z. Q. Extraordinary Enhancement of Raman Scattering from Pyridine on Single Crystal Au and Pt Electrodes by Shell-Isolated Au Nanoparticles. *J. Am. Chem. Soc.* **2011,** *133*, 15922-15925.

468.   Li, J. F.; Zhang, Y. J.; Ding, S. Y.; Panneerselvam, R.; Tian, Z. Q. Core–Shell Nanoparticle-Enhanced Raman Spectroscopy. *Chem. Rev.* **2017,** *117*, 5002-5069.

469.   Wang, D.; Wan, L. J. Electrochemical Scanning Tunneling Microscopy: Adlayer Structure and Reaction at Solid/Liquid Interface. *J. Phys. Chem. C* **2007,** *111*, 16109-16130.

470.   Li, J. F.; Zhang, Y. J.; Rudnev, A. V.; Anema, J. R.; Li, S. B.; Hong, W. J.; Rajapandiyan, P.; Lipkowski, J.; Wandlowski, T.; Tian, Z. Q. Electrochemical Shell-Isolated Nanoparticle-Enhanced Raman Spectroscopy: Correlating Structural Information and Adsorption Processes of Pyridine at the Au(hkl) Single Crystal/Solution Interface. *J. Am. Chem. Soc.* **2015,** *137*, 2400-2408.

471.   Wang, Y. H.; Zhang, Y. J.; Liang, M. M.; Chen, S.; Radjenovic, P.; Zhang, H.; Yang, Z. L.; Zhou, X. S.; Tian, Z. Q.; Li, J. F. Probing Interfacial Electronic and Catalytic Properties on Well-Defined Surfaces Using *In Situ* Raman Spectroscopy. *Angew. Chem. Int. Ed.* **2018,** *57*, 11257-11261.

472.   Li, C. Y.; Dong, J. C.; Jin, X.; Chen, S.; Panneerselvam, R.; Rudnev, A. V.; Yang, Z. L.; Li, J. F.; Wandlowski, T.; Tian, Z. Q. *In Situ* Monitoring of Electrooxidation Processes at Gold Single Crystal Surfaces Using Shell-Isolated Nanoparticle-Enhanced Raman Spectroscopy. *J. Am. Chem. Soc.* **2015,** *137*, 7648-7651.

473.   Dong, J. C.; Zhang, X. G.; Briega-Martos, V.; Jin, X.; Yang, J.; Chen, S.; Yang, Z. L.; Wu, D. Y.; Feliu, J. M.; Williams, C. T.; Tian, Z. Q.; Li, J. F. *In Situ* Raman Spectroscopic Evidence for Oxygen Reduction Reaction Intermediates at Platinum Single-Crystal Surfaces. *Nat. Energy* **2019,** *4*, 60-67.

474.   Zhang, H.; Wang, C.; Sun, H. L.; Fu, G.; Chen, S.; Zhang, Y. J.; Chen, B. H.; Anema, J. R.; Yang, Z. L.; Li, J. F.; Tian, Z. Q. *In Situ* Dynamic Tracking of

Heterogeneous Nanocatalytic Processes by Shell-Isolated Nanoparticle-Enhanced Raman Spectroscopy. *Nat. Commun.* **2017,** *8*, 15447.

475. Guerrero, A. R.; Aroca, R. F. Surface-Enhanced Fluorescence with Shell-Isolated Nanoparticles (SHINEF). *Angew. Chem. Int. Ed.* **2011,** *50*, 665-668.

476. Li, C. Y.; Gao, J.; Yi, J.; Zhang, X. G.; Cao, X. D.; Meng, M.; Wang, C.; Huang, Y. P.; Zhang, S. J.; Wu, D. Y.; Wu, C. L.; Xu, J. H.; Tian, Z. Q.; Li, J. F. Plasmon-Enhanced Ultra-Sensitive Surface Analysis Using Ag Nanoantenna. *Anal. Chem.* **2018,** *90*, 2018-2022.

477. Yin, H.; Yi, J.; Yang, Z. W.; Xu, Z. Y.; Xie, S. J.; Li, L.; Li, C. Y.; Xu, J.; Zhang, H.; Zhang, S. J.; Li, J. F.; Tian, Z. Q. Plasmon Enhanced Quantum Dots Fluorescence and Energy Conversion in Water Splitting Using Shell-Isolated Nanoparticles. *Nano Energy* **2017,** *42*, 232-240.

478. Meng, M.; Zhang, F. L.; Yi, J.; Lin, L. H.; Zhang, C. L.; Bodappa, N.; Li, C. Y.; Zhang, S. J.; Aroca, R. F.; Tian, Z. Q.; Li, J. F. Shell-Isolated Nanoparticle-Enhanced Phosphorescence. *Anal. Chem.* **2018,** *90*, 10837-10842.

479. Huang, Y. P.; Huang, S. C.; Wang, X. J.; Bodappa, N.; Li, C. Y.; Yin, H.; Su, H.-S.; Meng, M.; Zhang, H.; Ren, B.; Yang, Z. L.; Zenobi, R.; Tian, Z. Q.; Li, J. F. Shell-Isolated Tip-Enhanced Raman and Fluorescence Spectroscopy. *Angew. Chem. Int. Ed.* **2018,** *57*, 7523-7527.

480. Liang, Z.; Zhang, S.; Li, X.; Wang, T.; Huang, Y.; Hang, W.; Yang, Z.; Li, J.; Tian, Z. Tip-Enhanced Ablation and Ionization Mass Spectrometry for Nanoscale Chemical Analysis. *Sci. Adv.* **2017,** *3,* eaaq1059.

481. Hong, K. Y.; de Albuquerque, C. D. L.; Poppi, R. J.; Brolo, A. G. Determination of Aqueous Antibiotic Solutions Using SERS Nanogratings. *Anal. Chim. Acta* **2017,** *982*, 148-155.

482. Shi, R. Y.; Liu, X. J.; Ying, Y. B. Facing Challenges in Real-Life Application of Surface-Enhanced Raman Scattering: Design and Nanofabrication of Surface-Enhanced Raman Scattering Substrates for Rapid Field Test of Food Contaminants. *J. Agric. Food Chem.* **2018,** *66*, 6525-6543.

483. Fan, M. K.; Andrade, G. F. S.; Brolo, A. G. A Review on the Fabrication of Substrates for Surface Enhanced Raman Spectroscopy and their Applications in Analytical Chemistry. *Anal. Chim. Acta* **2011,** *693*, 7-25.

484. Massarini, E.; Wasterby, P.; Landstrom, L.; Lejon, C.; Beck, O.; Andersson, P. O. Methodologies for Assessment of Limit of Detection and Limit of Identification Using Surface-Enhanced Raman Spectroscopy. *Sens. Actuators B* **2015,** *207*, 437-446.

485. Goodacre, R.; Graham, D.; Faulds, K. Recent Developments in Quantitative SERS Moving: Towards Absolute Quantification. *TrAC, Trends Anal. Chem.* **2018**, *102*, 359-368.

486. Subaihi, A.; Xu, Y.; Muhamadali, H.; Mutter, S. T.; Blanch, E. W.; Ellis, D. I.; Goodacre, R. Towards Improved Quantitative Analysis Using Surface-Enhanced

Raman Scattering Incorporating Internal Isotope Labelling. *Anal. Methods* **2017**, *9*, 6636-6644.

487.   Itoh, N.; Bell, S. E. J. High Dilution Surface-Enhanced Raman Spectroscopy for Rapid Determination of Nicotine in e-Liquids for Electronic Cigarettes. *Analyst* **2017**, *142*, 994-998.

488.   Subaihi, A.; Muhamadali, H.; Mutter, S. T.; Blanch, E.; Ellis, D. I.; Goodacre, R. Quantitative Detection of Codeine in Human Plasma Using Surface Enhance Raman Scattering *via* Adaptation of the Isotopic Labelling Principle. *Analyst* **2017**, *142*, 1099-1105.

489.   Zakel, S.; Rienitz, O.; Güttler, B.; Stosch, R. Double Isotope Dilution Surface-Enhanced Raman Scattering as a Reference Procedure for the Quantification of Biomarkers in Human Serum. *Analyst* **2011**, *136*, 3956-3961.

490.   Hidi, I. J.; Jahn, M.; Weber, K.; Bocklitz, T.; Pletz, M. W.; Cialla-May, D.; Popp, J. Lab-on-a-Chip-Surface Enhanced Raman Scattering Combined with the Standard Addition Method: Toward the Quantification of Nitroxoline in Spiked Human Urine Samples. *Anal. Chem.* **2016**, *88*, 9173-9180.

491.   Mamian-Lopez, M. B.; Poppi, R. J. Standard Addition Method Applied to the Urinary Quantification of Nicotine in the Presence of Cotinine and Anabasine Using Surface Enhanced Raman Spectroscopy and Multivariate Curve Resolution. *Anal. Chim. Acta* **2013***, 760*, 53-59.

492.   Westley, C.; Xu, Y.; Thilaganathan, B.; Carnell, A. J.; Turner, N. J.; Goodacre, R. Absolute Quantification Of Uric Acid In Human Urine Using Surface Enhanced Raman Scattering With The Standard Addition Method. *Anal. Chem.* **2017**, *89*, 2471-2477.

493.   Gromski, P. S.; Muhamadali, H.; Ellis, D. I.; Xu, Y.; Correa, E.; Turner, M. L.; Goodacre, R. A Tutorial Review: Metabolomics and Partial Least Squares-Discriminant Analysis – A Marriage of Convenience or a Shotgun Wedding. *Anal. Chim. Acta* **2015**, *879*, 10-23.

494.   Xu, Y.; Muhamadali, H.; Sayqal, A.; Dixon, N.; Goodacre, R. Partial Least Squares with Structured Output for Modelling the Metabolomics Data Obtained from Complex Experimental Designs: A Study into the Y-Block Coding. *Metabolites* **2016**, *6*, 38.

495.   Gracie, K.; Correa, E.; Mabbott, S.; Dougan, J. A.; Graham, D.; Goodacre, R.; Faulds, K. Simultaneous Detection and Quantification of Three Bacterial Meningitis Pathogens by SERS. *Chem. Sci.* **2014**, *5*, 1030-1040.

496.   Crawford, A. C.; Skuratovsky, A.; Porter, M. D. Sampling Error: Impact on the Quantitative Analysis of Nanoparticle-Based Surface-Enhanced Raman Scattering Immunoassays. *Anal. Chem.* **2016,** *88*, 6515-6522.

497.   Itoh, T.; Yamamoto, Y. S. Recent Topics on Single-Molecule Fluctuation Analysis Using Blinking in Surface-Enhanced Resonance Raman Scattering: Clarification by the Electromagnetic Mechanism. *Analyst* **2016,** *141*, 5000-5009.

498.   Fang, Y.; Seong, N. H.; Dlott, D. D. Measurement of the Distribution of Site Enhancements in Surface-Enhanced Raman Scattering. *Science* **2008,** *321*, 388-392.

499. Zrimsek, A. B.; Chiang, N. H.; Mattei, M.; Zaleski, S.; McAnally, M. O.; Chapman, C. T.; Henry, A. I.; Schatz, G. C.; Van Duyne, R. P. Single-Molecule Chemistry with Surface- and Tip-Enhanced Raman Spectroscopy. *Chem. Rev.* **2017,** *117*, 7583-7613.

500. Etchegoin, P. G.; Meyer, M.; Blackie, E.; Le Ru, E. C. Statistics of Single-Molecule Surface Enhanced Raman Scattering Signals: Fluctuation Analysis with Multiple Analyte Techniques. *Anal. Chem.* **2007,** *79*, 8411-8415.

501. dos Santos, D. P.; Andrade, G. F. S.; Temperini, M. L. A.; Brolo, A. G. Electrochemical Control of the Time-Dependent Intensity Fluctuations in Surface-Enhanced Raman Scattering (SERS). *J. Phys. Chem. C* **2009,** *113*, 17737-17744.

502. de Albuquerque, C. D. L.; Sobral, R. G.; Poppi, R. J.; Brolo, A. G. Digital Protocol for Chemical Analysis at Ultralow Concentrations by Surface-Enhanced Raman Scattering. *Anal. Chem.* **2018,** *90*, 1248-1254.

503. Tian, Y. F.; Wu, P.; Liu, Q.; Wu, X.; Hou, X. D. Mapping for Total Surface-Enhanced Raman Scattering to Improve its Quantification Analysis. *Talanta* **2016,** *161*, 151-156.

504. Darby, B. L.; Le Ru, E. C. Competition between Molecular Adsorption and Diffusion: Dramatic Consequences for SERS in Colloidal Solutions. *J. Am. Chem. Soc.* **2014,** *136*, 10965-10973.

505. Ameer, F. S.; Hu, W. F.; Ansar, S. M.; Siriwardana, K.; Collier, W. E.; Zou, S. L.; Zhang, D. M. Robust and Reproducible Quantification of SERS Enhancement Factors Using a Combination of Time-Resolved Raman Spectroscopy and Solvent Internal Reference Method. *J. Phys. Chem. C* **2013,** *117*, 3483-3488.

506. Feliu, N.; Hassan, M.; Rico, E. G.; Cui, D. X.; Parak, W.; Alvarez-Puebla, R. SERS Quantification and Characterization of Proteins and Other Biomolecules. *Langmuir* **2017,** *33*, 9711-9730.

507. Brule, T.; Bouhelier, A.; Yockell-Lelievre, H.; Clement, J. E.; Leray, A.; Dereux, A.; Finot, E. Statistical and Fourier Analysis for In-line Concentration Sensitivity in Single Molecule Dynamic-SERS. *ACS Photonics* **2015,** *2*, 1266-1271.

508. Fan, M. K.; Cheng, F. S.; Wang, C.; Gong, Z. J.; Tang, C. Y.; Man, C. Z.; Brolo, A. G. SERS Optrode as a "Fishing Rod" to Direct Preconcentrate Analytes from Superhydrophobic Surfaces. *Chem. Commun.* **2015,** *51*, 1965-1968.

509. De Angelis, F.; Gentile, F.; Mecarini, F.; Das, G.; Moretti, M.; Candeloro, P.; Coluccio, M. L.; Cojoc, G.; Accardo, A.; Liberale, C.; Zaccaria, R. P.; Perozziello, G.; Tirinato, L.; Toma, A.; Cuda, G.; Cingolani, R.; Di Fabrizio, E. Breaking the Diffusion Limit with Super-Hydrophobic Delivery of Molecules to Plasmonic Nanofocusing SERS Structures. *Nat. Photonics* **2011,** *5*, 683-688.

510. Bhowmik, D.; Mote, K. R.; MacLaughlin, C. M.; Biswas, N.; Chandra, B.; Basu, J. K.; Walker, G. C.; K. Madhu, P. K.; Maiti, S. Cell-Membrane-Mimicking Lipid-Coated Nanoparticles Confer Raman Enhancement to Membrane Proteins and Reveal Membrane-Attached Amyloid-β Conformation. *ACS Nano* **2015**, *9*, 9070–9077.

511. Shanmukh, S.; Jones, L.; Driskell, J.; Zhao, Y.; Dluhy, R.; Tripp, R. A. Rapid and Sensitive Detection of Respiratory Virus Molecular Signatures Using a Silver Nanorod Array SERS Substrate. *Nano Lett.* **2006**, *6*, 2630–2636.

512. Jarvis, R. M.; Brooker, A.; Goodacre, R. Surface-Enhanced Raman Spectroscopy for Bacterial Discrimination Utilizing a Scanning Electron Microscope with a Raman Spectroscopy Interface. *Anal. Chem.* **2004**, *76*, 5198–5202.

513. Dina, N. E.; Raluca Gherman, A. M.; Chiş, V.; Sârbu, C.; Wieser, A.; Bauer, D.; Haisch, C. Characterization of Clinically Relevant Fungi *via* SERS Fingerprinting Assisted by Novel Chemometric Models. *Anal. Chem.* **2018**, *90*, 2484–2492.

514. Garcia-Rico, E.; Alvarez-Puebla, R. A.; Guerrini, L. Direct Surface-Enhanced Raman Scattering (SERS) Spectroscopy of Nucleic Acids: From Fundamental Studies to Real-Life Applications. *Chem. Soc. Rev.* **2018**, *47*, 4909-4923

515. Morla-Folch , J.; Gisbert-Quilis , P.; Masetti , M.; Garcia-Rico , E.; Alvarez-Puebla, R. A.; Guerrini, L. Conformational SERS Classification of K-Ras Point Mutations for Cancer Diagnostics. *Angew. Chem. Int. Ed.* **2017**, *56*, 2381-2385.

516. Tsoutsi, D.; Montenegro, J. M.; Dommershausen, F.; Koert, U.; Liz-Marzán, L. M.; Parak, W. J.; Alvarez-Puebla, R. A. Quantitative SERS Ultradetection of Atomic Inorganic Ions: The Case of Chlorine. *ACS Nano* **2011**, *5*, 7539-7546.

517. Rivera-Gil, P.; Vazquez-Vazquez, C.; Giannini, V.; Callao, M. P.; Parak W. J.; Correa-Duarte, M. A.; Alvarez-Puebla, R. A. Plasmonic Nanoprobes for Real-Time Optical Monitoring of Nitric Oxide inside Living Cells. *Angew. Chem. Int. Ed.* **2013**, *52*, 13694-13698.

518. Guerrini, L.; Arenal, R.; Mannini, B.; Chiti, F.; Pini, R.; Matteini, P.; Alvarez-Puebla, R. A. SERS Detection of Amyloid Oligomers on Metallorganic-Decorated Plasmonic Beads. *ACS Appl. Mater. Interfaces* **2015**, *7*, 9420−9428.

519. Sanles-Sobrido, M.; Rodríguez-Lorenzo, L.; Lorenzo-Abalde, S.; González-Fernández, A.; Correa-Duarte, M. A.; Alvarez-Puebla, R. A.; Liz-Marzán, L. M. Label-Free SERS Detection of Relevant Bioanalytes on Silver-Coated Carbon Nanotubes: The Case of Cocaine. *Nanoscale* **2009**, *1*, 153-158.

520. He, L.; Tom Rodda, T.; Haynes, C. L.; Deschaines, T.; Strother, T.; Diez-Gonzalez, F.; Labuza, T. P. Detection of a Foreign Protein in Milk Using Surface-Enhanced Raman Spectroscopy Coupled with Antibody-Modified Silver Dendrites. *Anal. Chem.* **2011**, *83*, 1510–1513.

521. Yang, L.; Fu, C.; Wang, H.; Xu, S.; Xu, W. Aptamer-Based Surface-Enhanced Raman Scattering (SERS) Sensor for Thrombin Based on Supramolecular Recognition, Oriented Assembly, and Local Field Coupling. *Anal. Bioanal. Chem.* **2017**, *409*, 235–242.

522. Alvarez-Puebla, R. A.; Liz-Marzán, L. M. Traps and Cages for Universal SERS Detection. *Chem. Soc. Rev.* **2012**, *41*, 43-51.

523.   Moskovits, M.; Suh, J. S. Surface Selection Rules for Surface-Enhanced Raman Spectroscopy: Calculations and Application to the Surface-Enhanced Raman Spectrum of Phthalazine on Silver. *J. Phys. Chem.* **1984**, *88*, 5526–5530.

524.   Guerrini, L.; Pazos, E.; Penas, C.; Vázquez, M. E.; Mascareñas, J. L.; Alvarez-Puebla, R. A. Highly Sensitive SERS Quantification of the Oncogenic Protein c-Jun in Cellular Extracts. *J. Am. Chem. Soc.* **2013**, *135*, 10314–10317.

525.   Pazos, E.; Garcia-Algar, M.; Penas, C.; Nazarenus, M.; Torruella, A.; Pazos-Perez, N.; Guerrini, L.; Vázquez, M. E.; Garcia-Rico, E.; Mascareñas, J. L.; Alvarez-Puebla, R. A. Surface-Enhanced Raman Scattering Surface Selection Rules for the Proteomic Liquid Biopsy in Real Samples: Efficient Detection of the Oncoprotein c-MYC. *J. Am. Chem. Soc.* **2016**, *138*, 14206–14209.

526.   Marks, H. L.; Pishko, M. V.; Jackson, G. W.; Coté, G. L. Rational Design of a Bisphenol A Aptamer Selective Surface-Enhanced Raman Scattering Nanoprobe. *Anal. Chem.* **2014**, *86*, 11614–11619.

527.   Pang, S.; Labuza, T. P.; He, L. Development of a Single Aptamer-Based Surface Enhanced Raman Scattering Method for Rapid Detection Of Multiple Pesticides. *Analyst* **2014**, *139*, 1895-1901.

528.   Odion, R. A.; Strobbia, P.; Crawford, B. M.; Vo-Dinh, T. Inverse Surface-Enhanced Spatially Offset Raman Spectroscopy (SESORS) Through a Monkey Skull, *J. Raman Spectrosc.* **2018**, *49*, 1452-1460.

529.   Vo-Dinh, T.; Liu, Y.; Crawford, B. M.; Wang, H. N.; Yuan, H.; Register, J. K.; Khoury, C. G.; Shining Gold Nanostars: From Cancer Diagnostics to Photothermal Treatment and Immunotherapy, *J. Immunol. Sci.* **2018**, *2*, 1-8

530.   Alvarez-Puebla, R. A.; Liz-Marzán, L. M. SERS-Based Diagnosis and Biodetection. *Small* **2010**, *6*, 604-610.

531.   Lewin, J. S. Future Directions in Minimally Invasive Intervention. *Trans. Am. Clin. Climatol. Assoc.* **2017**, *128*, 346–352.

532.   Wang, H. N.; Crawford, B. M.; Fales, A. M.; Bowie, M. L.; Seewaldt, V. L.; Vo-Dinh, T. Multiplexed Detection of MicroRNA Biomarkers Using SERS-Based Inverse Molecular Sentinel (iMS) Nanoprobes. *J. Phys. Chem. C* **2016**, *120*, 21047-21050.

533.   Vo-Dinh, T.; Hiromoto, M. Y. K.; Begun, G. M.; Moody, R. L. Surface-Enhanced Raman Spectrometry for Trace Organic Analysis. *Anal. Chem.* **1984**, *56*, 1667–1670.

534.   Vo-Dinh, T. Surface-Enhanced Raman Spectroscopy Using Metallic Nanostructures. *TrAC, Trends Anal. Chem.* **1998**, *17*, 557-582.

535.   Khoury, C. G.; Vo-Dinh, T. Plasmonic Nanowave Substrates for SERS: Fabrication and Numerical Analysis. *J. Phys. Chem. C* **2012**, *116*, 7534–7545.

536.   Ngo, H. T.; Wang, H.-N-; Fales, A. M.; Vo-Dinh, T. Label-Free DNA Biosensor Based on SERS Molecular Sentinel on Nanowave Chip. *Anal. Chem.* **2013**, *85*, 6378–6383.

537.   Vo-Dinh, T.; Dhawan, A.; Norton, S. J.; Khoury, C. G.; Wang, H. N.; Veena Misra, V.; Gerhold, M. D. Plasmonic Nanoparticles and Nanowires: Design, Fabrication and Application in Sensing. *J. Phys. Chem. C* **2010**, *114*, 7480–7488.

538.   Ngo, H. T.; Wang, H.-N.; Fales, A. M.; Nicholson, B. P.; Woods, C. W.; Vo-Dinh, T. DNA Bioassay-on-Chip Using SERS Detection for Dengue Diagnosis. *Analyst* **2014**, *139*, 5655-5659.

539.   Ngo, H. T.; Freedman, E.; Odion, R. A.; Strobbia, P.; Indrasekara, A. S. D. S.; Vohra, P.; Taylor, S. M.; Vo-Dinh, T. Direct Detection of Unamplified Pathogen RNA in Blood Lysate using an Integrated Lab-in-a-Stick Device and Ultrabright SERS Nanorattles, *Sci. Rep.* **2018**, *8*, 4075.

540.   Ngo, H. T.; Gandra, N.; Fales, A. M.; Taylor, S. M.; Vo-Dinh, T. Sensitive DNA Detection and SNP Discrimination Using Ultrabright SERS Nanorattles and Magnetic Beads for Malaria Diagnostics. *Biosens. Bioelectr.* **2016**, *81*, 8-14.

541.   Vohra, P.; Strobbia, P.; Ngo, H. T.; Lee, W. T.; Vo-Dinh, T. Rapid Nanophotonics Assay for Head and Neck Cancer Diagnosis, *Sci. Rep.* **2018**, *8*, 12989.

542.   Wang, H. N.; Register, J. K.; Fales, A. M.; Gandra, N.; Cho, E. H.; Boico, A.; Palmer, G. M.; Klitzman, B.; Vo-Dinh, T. Surface-Enhanced Raman Scattering Nanosensors for *In Vivo* Detection of Nucleic Acid Targets in a Large Animal Model, *Nano Res.* **2018**, *11*, 4005-4016.

543.   Liu, Y.; Maccarini, P.; Palmer, G. M.; Etienne, W.; Zhao, Y.; Lee, C. T.; Ma, X.; Inman, B. A.; Vo-Dinh, T. Synergistic Immuno Photothermal Nanotherapy (SYMPHONY) for the Treatment of Unresectable and Metastatic Cancers, *Sci. Rep.* **2017**, *7*, 8606.

544.   Liu, Y.; Chang, Z.; Yuan, H.; Fales, A. M.; Vo-Dinh, T. Quintuple-Modality (SERS-MRI-CT-TPL-PTT) Plasmonic Nanoprobe for Theranostics, *Nanoscale* **2013**, *5*, 12126-12131.

545.   Cheng, Z.; Choi, N.; Wang, R.; Lee, S.; Moon, K. C.; Yoon, S. Y.; Chen, L.; Choo, J. Simultaneous Detection of Dual Prostate Specific Antigrns Using SERS-Based Immunoassay for Accurate Diagnosis of Prostate Cancer. *ACS Nano* **2017**, *11*, 4926-4933.

546.   Chrimes, A. F.; Khoshmanesh, K.; Stoddart, P. R.; Mitchell, A.; Kalantar-Zadeh, K. Microfluidics and Raman Microscopy: Current Applications and Future Challenges. *Chem. Soc. Rev.* **2013**, *42*, 5880-5906.

547.   Nayak, S.; Blumenfeld, N. R.; Laksanasopin, T.; Sia, S. K. Point of Care Diagnostics: Recent Developments in a Connected Age. *Anal. Chem.* **2017**, *89*, 102-123.

548.   Chon, H.; Lim, C.; Ha, S. M.; Ahn, Y.; Lee, E. K.; Chang, S. I.; Seong, G. H.; Choo, J. On-chip Immunoassay Using Surface-Enhanced Raman Scattering of Hollow Gold Nanospheres. *Anal. Chem.* **2010**, *82*, 5290-5295.

549.   Choi, N.; Lee, J.; Ko, J.; Jeon, J. H.; Rhie G.; deMello, A. J.; Choo, J. Integrated SERS-Based Microdroplet Platform for the Automated Immunoassay of F1 Antigens in *Yersinia Pestis*. *Anal. Chem.* **2017**, *89*, 8413-8420.

550.   Hidi, I. J.; Jahn, M.; Pletz, M. W.; Weber, K.; Cialla-May, D.; Popp, J. Toward Levofloxacin Monitoring in Human Urine Samples by Employing the LOC-SERS Technique. *J. Phys. Chem. C* **2016**, *120*, 20613-20623.

551.   Mühlig, A.; Bocklitz, T. W.; Labugger, I.; Dees, S.; Henk, S.; Richter, E.; Andres, S.; Merker, M.; Stöckel, S.; Weber, K.; Cialla-May, D.; Popp, J. LOC-SERS: A Promising Closed System for the Identification of Mycobacteria. *Anal. Chem.* **2016**, *88*, 7998-8004.

552.   Patze, S.; Huebner U.; Liebold, F.; Weber, K; Cialla-May, D.; Popp, J. SERS as an Analytical Tool in Environmental Science: The Detection of Sulfamethoxazole in Water in the Nanomolar Range by Applying a Microfluidic Cartridge Setup. *Anal. Chim. Acta* **2017**, *949*, 1-7.

553.   Hemmer, E.; Venkatachalam, N.; Hyodo, H.; Hattori, A.; Ebina, Y.; Kishimoto, H.; Soga, K. Upconverting and NIR Emitting Rare Earth Based Nanostructures for NIR-Bioimaging. *Nanoscale* **2013**, *5*, 11339-11361.

554.   Hemmer, E.; Benayas, A.; Légaré, F.; Vetrone, F. Exploiting the Biological Windows: Current Perspectives on Fluorescent Bioprobes Emitting above 1000 nm. *Nanoscale Horiz.* **2016**, *1*, 168–184.

555.   Tang, L.; Li, S.; Han, F.; Liu, L.; Xu, L.; Ma, W.; Kuang, H.; Li, A.; Wang, L.; Xu, C. SERS-Active Au@Ag Nanorod Dimers for Ultrasensitive Dopamine Detection. *Biosens. Bioelectron.* **2015**, *71*, 7-12.

556.   Gao, F.; Liu, L.; Cui, G.; Xu, L.; Wu, X.; Kuang, H.; Xu, C. Regioselective Plasmonic Nano-Assemblies for Bimodal Sub-Femtomolar Dopamine Detection. *Nanoscale* **2017**, *9*, 223-229.

557.   Wu, X.; Chen, X.; Gao, F.; Ma, W.; Xu, L.; Kuang, H.; Li, A.; Xu, C. SERS Encoded Nanoparticle Heterodimers for the Ultrasensitive Detection of Folic Acid. *Biosens. Bioelectron.* **2016**, *75*, 55-58.

558.   Zhu, Y.; Kuang, H.; Xu, L.; Ma, W.; Peng, C.; Hua, Y.; Wang, L.; Xu, C. Gold Nanorod Assembly Based Approach to Toxin Detection by SERS. *J. Mater. Chem.* **2012**, *22*, 2387-2391.

559.   Zhao, S.; Ma, W.; Xu, L.; Wu, X.; Kuang, H.; Wang, L.; Xu, C. Ultrasensitive SERS Detection of VEGF Based on a Self-Assembled Ag Ornamented–Au Pyramid Superstructure. *Biosens. Bioelectron.* **2015**, *68*, 593-597.

560.   Ma, W.; Yin, H.; Xu, L.; Wu, X.; Kuang, H.; Wang, L.; Xu, C. Ultrasensitive Aptamer-Based SERS Detection of PSAs by Heterogeneous Satellite Nanoassemblies. *Chem. Commun.* **2014**, *50*, 9737-9740.

561.   Wu, X.; Fu, P.; Ma, W.; Xu, L.; Kuang, H.; Xu, C. SERS-Active Silver Nanoparticle Trimers for Sub-Attomolar Detection of Alpha Fetoprotein. *RSC Adv.* **2015**, *5*, 73395-73398.

562.   Zhao, Y.; Liu, L.; Kuang, H.; Wang, L.; Xu, C. SERS-Active Ag@Au Core–Shell NP Assemblies for DNA Detection. *RSC Adv.* **2014,** *4*, 56052-56056.

563.   Chisanga, M.; Muhamadali, H.; Ellis, D. I.; Goodacre, R. Surface-Enhanced Raman Scattering (SERS) in Microbiology: Illumination and Enhancement of the Microbial World. *Appl. Spectrosc.* **2018,** *72*, 987-1000.

564.   Dina, N. E.; Zhou, H.; Colniță, A.; Leopold, N.; Szoke-Nagy, T.; Coman, C.; Haisch, C. Rapid Single-Cell Detection and Identification of Pathogens by Using Surface-Enhanced Raman Spectroscopy. *Analyst* **2017,** *142*, 1782-1789.

565.   Carmicheal, J.; Hayashi, C.; Huang, X.; Liu, L.; Lu, Y.; Krasnoslobodtsev, A.; Lushnikov, A.; Kshirsagar, P. G.; Patel, A.; Jain, M.; Lyubchenko, Y. L.; Lu, Y.; Batra, S. K.; Kaur, S., Label-Free Characterization of Exosome *via* Surface Enhanced Raman Spectroscopy for the Early Detection of Pancreatic Cancer. *Nanomedicine* **2019,** *16*, 88-96.

566.   Kneipp, J.; Kneipp, H.; McLaughlin, M.; Brown, D.; Kneipp, K. *In Vivo* Molecular Probing of Cellular Compartments with Gold Nanoparticles and Nanoaggregates. *Nano Lett.* **2006,** *6*, 2225-2231.

567.   Silwal, A. P.; Lu, H. P. Raman Spectroscopic Analysis of Signaling Molecules-Dopamine Receptors Interactions in Living Cells. *ACS Omega* **2018,** *3*, 14849-14857.

568.   Lussier, F.; Brulé, T.; Vishwakarma, M.; Das, T.; Spatz, J. P.; Masson, J.-F. Dynamic-SERS Optophysiology: A Nanosensor for Monitoring Cell Secretion Events. *Nano Lett.* **2016,** *16*, 3866-3871.

569.   Shiota, M.; Naya, M.; Yamamoto, T.; Hishiki, T.; Tani, T.; Takahashi, H.; Kubo, A.; Koike, D.; Itoh, M.; Ohmura, M.; Kabe, Y.; Sugiura, Y.; Hiraoka, N.; Morikawa, T.; Takubo, K.; Suina, K.; Nagashima, H.; Sampetrean, O.; Nagano, O.; Saya, H.; Yamazoe, S.; Watanabe, H.; Suematsu, M., Gold-Nanofève Surface-Enhanced Raman Spectroscopy Visualizes Hypotaurine as a Robust Anti-Oxidant Consumed in Cancer Survival. *Nat. Commun.* **2018,** *9*, 1561.

570.   Lussier, F.; Brulé, T.; Bourque, M.-J.; Ducrot, C.; Trudeau, L.-É.; Masson, J.-F. Dynamic SERS Nanosensor for Neurotransmitter Sensing near Neurons. *Faraday Discuss.* **2017,** *205*, 387-407.

571.   Kneipp, H.; Mobjerg, N.; Jorgensen, A.; Bohr, H. G.; Helix-Nielsen, C.; Kneipp, J.; Kneipp, K., Surface Enhanced Raman Scattering on Tardigrada Towards Monitoring and Imaging Molecular Structures in Live Cryptobiotic Organisms. *J. Biophotonics* **2013,** *6*, 759-764.

572.   Ando, J.; Fujita, K.; Smith, N. I.; Kawata, S. Dynamic SERS Imaging of Cellular Transport Pathways with Endocytosed Gold Nanoparticles. *Nano Lett.* **2011,** *11*, 5344-5348.

573.   Drescher, D.; Zeise, I.; Traub, H.; Guttmann, P.; Seifert, S.; Buchner, T.; Jakubowski, N.; Schneider, G.; Kneipp, J. *In situ* Characterization of SiO_2 Nanoparticle Biointeractions Using Bright Silica. *Adv. Funct. Mater.* **2014,** *24*, 3765-3775.

574. Huefner, A.; Kuan, W.-L.; Müller, K. H.; Skepper, J. N.; Barker, R. A.; Mahajan, S. Characterization and Visualization of Vesicles in the Endo-Lysosomal Pathway with Surface-Enhanced Raman Spectroscopy and Chemometrics. *ACS Nano* **2016,** *10*, 307-316.

575. Wang, M.; Cao, X.; Lu, W.; Tao, L.; Zhao, H.; Wang, Y.; Guo, M.; Dong, J.; Qian, W. Surface-Enhanced Raman Spectroscopic Detection and Differentiation of Lung Cancer Cell Lines (A549, H1229) and Normal cell Line (AT II) Based on Gold Nanostar Substrates. *RSC Adv.* **2014,** *4*, 64225-64234.

576. Zhang, Y. J.; Zeng, Q. Y.; Li, L. F.; Qi, M. N.; Qi, Q. C.; Li, S. X.; Xu, J. F. Label-Free Rapid Identification of Tumor Cells and Blood Cells with Silver Film SERS Substrate. *Opt. Express* **2018,** *26*, 33044-33056.

577. Caprettini, V.; Huang, J. A.; Moia, F.; Jacassi, A.; Gonano, C. A.; Maccaferri, N.; Capozza, R.; Dipalo, M.; De Angelis, F. Enhanced Raman Investigation of Cell Membrane and Intracellular Compounds by 3D Plasmonic Nanoelectrode Arrays. *Adv. Sci.* **2018,** *5*, 1800560.

578. Vitol, E. A.; Orynbayeva, Z.; Bouchard, M. J.; Azizkhan-Clifford, J.; Friedman, G.; Gogotsi, Y. *In Situ* Intracellular Spectroscopy with Surface Enhanced Raman Spectroscopy (SERS)-Enabled Nanopipettes. *ACS Nano* **2009,** *3*, 3529-3536.

579. Dong, J.; Chen, Q.; Rong, C.; Li, D.; Rao, Y. Minimally Invasive Surface-Enhanced Raman Scattering Detection with Depth Profiles Based on a Surface-Enhanced Raman Scattering-Active Acupuncture Needle. *Anal. Chem.* **2011,** *83*, 6191-6195.

580. Yuen, C.; Liu, Q. Towards *in Vivo* Intradermal Surface Enhanced Raman Scattering (SERS) Measurements: Silver Coated Microneedle Based SERS Probe. *J. Biophotonics* **2014,** *7*, 683-689.

581. Li, P.; Zhou, B.; Cao, X.; Tang, X.; Yang, L.; Hu, L.; Liu, J. Functionalized Acupuncture Needle as Surface-Enhanced Resonance Raman Spectroscopy Sensor for Rapid and Sensitive Detection of Dopamine in Serum and Cerebrospinal Fluid. *Chem. Eur. J.* **2017,** *23*, 14278-14285.

582. Ochsenkühn, M. A.; Jess, P. R. T.; Stoquert, H.; Dholakia, K.; Campbell, C. J. Nanoshells for Surface-Enhanced Raman Spectroscopy in Eukaryotic Cells: Cellular Response and Sensor Development. *ACS Nano* **2009,** *3*, 3613-3621.

583. Boca, S.; Rugina, D.; Pintea, A.; Barbu-Tudoran, L.; Astilean, S. Flower-Shaped Gold Nanoparticles: Synthesis, Characterization and their Application as SERS-Active Tags Inside Living Cells. *Nanotechnology* **2010,** *22*, 055702.

584. Panikkanvalappil, S. R.; Mackey, M. A.; El-Sayed, M. A. Probing the Unique Dehydration-Induced Structural Modifications in Cancer Cell DNA Using Surface Enhanced Raman Spectroscopy. *J. Am. Chem. Soc.* **2013,** *135*, 4815-4821.

585. Drescher, D.; Giesen, C.; Traub, H.; Panne, U.; Kneipp, J.; Jakubowski, N. Quantitative Imaging of Gold and Silver Nanoparticles in Single Eukaryotic Cells by Laser Ablation ICP-MS. *Anal. Chem.* **2012,** *84*, 9684-9688.

586. Buchner, T.; Drescher, D.; Traub, H.; Schrade, P.; Bachmann, S.; Jakubowski, N.; Kneipp, J. Relating Surface-Enhanced Raman Scattering Signals of Cells to Gold Nanoparticle Aggregation as Determined by LA-ICP-MS Micromapping. *Anal. Bioanal. Chem.* **2014**, *406*, 7003-7014.

587. Madzharova, F.; Heiner, Z.; Simke, J.; Selve, S.; Kneipp, J. Gold Nanostructures for Plasmonic Enhancement of Hyper-Raman Scattering. *J. Phys. Chem. C* **2018**, *122*, 2931-2940.

588. Tsoulos, T. V.; Atta, S.; Lagos. M. J.; Batson, P. E.; Tsilomelekis, G.; Fabris, L. Rational Design of Gold Nanostars with Tailorable Plasmonic Properties. *ChemRxiv* **2018**. DOI: 10.26434/chemrxiv.6552743.v1

589. Heck, C.; Kanehira, Y.; Kneipp, J.; Bald, I. Placement of Single Proteins within the SERS Hot Spots of Self-Assembled Silver Nanolenses. *Angew. Chem. Int. Ed.* **2018**, *57*, 7444-7447.

590. Kneipp, K.; Kneipp, H.; Kneipp, J. Probing Plasmonic Nanostructures by Photons and Electrons. *Chem. Sci.* **2015**, *6*, 2721-2726.

591. Živanović, V.; Kochovski, Z.; Arenz, C.; Lu, Y.; Kneipp, J. SERS and Cryo-EM Directly Reveal Different Liposome Structures during Interaction with Gold Nanoparticles. *J. Phys. Chem. Lett.* **2018**, *9*, 6767-6772.

592. Drescher, D.; Guttmann, P.; Buchner, T.; Werner, S.; Laube, G.; Hornemann, A.; Tarek, B.; Schneider, G.; Kneipp, J. Specific Biomolecule Corona Is Associated with Ring-Shaped Organization of Silver Nanoparticles in Cells. *Nanoscale* **2013**, *5*, 9193-9198.

593. Kneipp, J.; Kneipp, H.; Rice, W. L.; Kneipp, K. Optical Probes for Biological Applications Based on Surface Enhanced Raman Scattering from Indocyanine Green on Gold Nanoparticles. *Anal. Chem.* **2005**, *77*, 2381-2385.

594. Song, J.; Zhou, J.; Duan, H. Self-Assembled Plasmonic Vesicles of SERS-Encoded Amphiphilic Gold Nanoparticles for Cancer Cell Targeting and Traceable Intracellular Drug Delivery. *J. Am. Chem. Soc.* **2012**, *134*, 13458-13469.

595. Ali, M. R. K.; Panikkanvalappil, S. R.; El-Sayed, M. A. Enhancing the Efficiency of Gold Nanoparticles Treatment of Cancer by Increasing Their Rate of Endocytosis and Cell Accumulation Using Rifampicin. *J. Am. Chem. Soc.* **2014**, *136*, 4464-4467.

596. Suarasan, S.; Focsan, M.; Potara, M.; Soritau, O.; Florea, A.; Maniu, D.; Astilean, S. Doxorubicin-Incorporated Nanotherapeutic Delivery System Based on Gelatin-Coated Gold Nanoparticles: Formulation, Drug Release, and Multimodal Imaging of Cellular Internalization. *ACS Appl. Mater. Interfaces* **2016**, *8*, 22900-22913.

597. Deng, R.; Qu, H.; Liang, L.; Zhang, J.; Zhang, B.; Huang, D.; Xu, S.; Liang, C.; Xu, W. Tracing the Therapeutic Process of Targeted Aptamer/Drug Conjugate on Cancer Cells by Surface-Enhanced Raman Scattering Spectroscopy. *Anal. Chem.* **2017**, *89*, 2844-2851.

598.   Mackey, M. A.; Saira, F.; Mahmoud, M. A.; El-Sayed, M. A. Inducing Cancer Cell Death by Targeting Its Nucleus: Solid Gold Nanospheres *versus* Hollow Gold Nanocages. *Bioconjugate Chem.* **2013,** *24*, 897-906.

599.   Liu, Y.; Ashton, J. R.; Moding, E. J.; Yuan, H. K.; Register, J. K.; Fales, A. M.; Choi, J.; Whitley, M. J.; Zhao, X. G.; Qi, Y.; Ma, Y.; Vaidyanathan, G.; Zalutsky, M. R.; Kirsch, D. G.; Badea, C. T.; Vo-Dinh, T. A Plasmonic Gold Nanostar Theranostic Probe for *In Vivo* Tumor Imaging and Photothermal Therapy. *Theranostics* **2015,** *5*, 946-960.

600.   Ali, M. R. K.; Wu, Y.; Han, T.; Zang, X.; Xiao, H.; Tang, Y.; Wu, R.; Fernández, F. M.; El-Sayed, M. A. Simultaneous Time-Dependent Surface-Enhanced Raman Spectroscopy, Metabolomics, and Proteomics Reveal Cancer Cell Death Mechanisms Associated with Gold Nanorod Photothermal Therapy. *J. Am. Chem. Soc.* **2016,** *138*, 15434-15442.

601.   Aioub, M.; El-Sayed, M. A. A Real-Time Surface Enhanced Raman Spectroscopy Study of Plasmonic Photothermal Cell Death Using Targeted Gold Nanoparticles. *J. Am. Chem. Soc.* **2016,** *138*, 1258-1264.

602.   Narayanan, N.; Nair, L. V.; Karunakaran, V.; Joseph, M. M.; Nair, J. B.; Ramya, A. N.; Jayasree, R. S.; Maiti, K. K. Investigation of Apoptotic Events at Molecular Level Induced by SERS Guided Targeted Theranostic Nanoprobe. *Nanoscale* **2016,** *8*, 11392-11397.

603.   Espinosa, A.; Silva, A. K. A.; Sanchez-Iglesias, A.; Grzelczak, M.; Pechoux, C.; Desboeufs, K.; Liz-Marzan, L. M.; Wilhelm, C. Cancer Cell Internalization of Gold Nanostars Impacts Their Photothermal Efficiency *In Vitro* and *In Vivo*: Toward a Plasmonic Thermal Fingerprint in Tumoral Environment. *Adv. Healthcare Mater.* **2016,** *5*, 1040-1048.

604.   Zhan, Y.; Liu, Y.; Zu, H.; Guo, Y.; Wu, S.; Yang, H.; Liu, Z.; Lei, B.; Zhuang, J.; Zhang, X.; Huang, D.; Hu, C. Phase-Controlled Synthesis of Molybdenum Oxide Nanoparticles for Surface Enhanced Raman Scattering and Photothermal Therapy. *Nanoscale* **2018,** *10*, 5997-6004.

605.   Liu, Z.; Chen, H.; Jia, Y.; Zhang, W.; Zhao, H.; Fan, W.; Zhang, W.; Zhong, H.; Ni, Y.; Guo, Z. A Two-Dimensional Fingerprint Nanoprobe Based on Black Phosphorus for Bio-SERS Analysis and Chemo-Photothermal Therapy. *Nanoscale* **2018,** *10*, 18795-18804.

606.   Nergiz, S. Z.; Gandra, N.; Tadepalli, S.; Singamaneni, S. Multifunctional Hybrid Nanopatches of Graphene Oxide and Gold Nanostars for Ultraefficient Photothermal Cancer Therapy. *ACS Appl. Mater. Interfaces* **2014,** *6*, 16395-16402.

607.   Zhang, Y.; Zou, Y.; Liu, F.; Xu, Y.; Wang, X.; Li, Y.; Liang, H.; Chen, L.; Chen, Z.; Tan, W. Stable Graphene-Isolated-Au-Nanocrystal for Accurate and Rapid Surface Enhancement Raman Scattering Analysis. *Anal. Chem.* **2016,** *88*, 10611-10616.

608.   Haldavnekar, R.; Venkatakrishnan, K.; Tan, B. Non Plasmonic Semiconductor Quantum SERS Probe as a Pathway for *In Vitro* Cancer Detection. *Nat. Commun.* **2018,** *9*, 3065.

609.   Austin, L. A.; Kang, B.; Yen, C.-W.; El-Sayed, M. A. Plasmonic Imaging of Human Oral Cancer Cell Communities During Programmed Cell Death by Nuclear-Targeting Silver Nanoparticles. *J. Am. Chem. Soc.* **2011,** *133*, 17594-17597.

610.   Kneipp, J.; Kneipp, H.; Wittig, B.; Kneipp, K. One- and Two-Photon Excited Optical pH Probing for Cells Using Surface-Enhanced Raman and Hyper-Raman Nanosensors. *Nano Lett.* **2007,** *7*, 2819-2823.

611.   Wei, H. R.; Willner, M. R.; Marr, L. C.; Vikesland, P. J. Highly Stable SERS pH Nanoprobes Produced by Co-Solvent Controlled AuNP Aggregation. *Analyst* **2016,** *141*, 5159-5169.

612.   Peng, R. Y.; Si, Y. M.; Deng, T.; Zheng, J.; Li, J. S.; Yang, R. H.; Tan, W. H. A Novel SERS Nanoprobe for the Ratiometric Imaging of Hydrogen Peroxide in Living Cells. *Chem. Commun.* **2016,** *52*, 8553-8556.

613.   Wang, W. K.; Zhang, L. M.; Li, L.; Tian, Y. A Single Nanoprobe for Ratiometric Imaging and Biosensing of Hypochlorite and Glutathione in Live Cells Using Surface-Enhanced Raman Scattering. *Anal. Chem.* **2016,** *88*, 9518-9523.

614.   Han, S.; Sun, J.; Wang, J.; Qian, W.; Dong, J. A Built-In Surface-Enhanced Raman Scattering-Active Microneedle for Sampling *In Vivo* and Surface-Enhanced Raman Scattering Detection *Ex Vivo* of NO. *J. Raman Spectrosc.* **2018,** *49*, 1747-1755.

615.   Pozzi, E. A.; Zrimsek, A. B.; Lethiec, C. M.; Schatz, G. C.; Hersam, M. C.; Van Duyne, R. P. Evaluating Single-Molecule Stokes and Anti-Stokes SERS for Nanoscale Thermometry. *J. Phys. Chem. C* **2015,** *119*, 21116-21124.

616.   Gardner, B.; Stone, N.; Matousek, P. Non-Invasive Chemically Specific Measurement of Subsurface Temperature in Biological Tissues Using Surface-Enhanced Spatially Offset Raman Spectroscopy. *Faraday Discuss.* **2016,** *187*, 329-339.

617.   Kang, J. W.; So, P. T. C.; Dasari, R. R.; Lim, D.-K. High Resolution Live Cell Raman Imaging Using Subcellular Organelle-Targeting SERS-Sensitive Gold Nanoparticles with Highly Narrow Intra-Nanogap. *Nano Lett.* **2015,** *15*, 1766-1772.

618.   Qi, G.; Zhang, Y.; Xu, S.; Li, C.; Wang, D.; Li, H.; Jin, Y. Nucleus and Mitochondria Targeting Theranostic Plasmonic Surface-Enhanced Raman Spectroscopy Nanoprobes as a Means for Revealing Molecular Stress Response Differences in Hyperthermia Cell Death between Cancerous and Normal Cells. *Anal. Chem.* **2018,** *90*, 13356-13364.

619.   Shen, Y.; Liang, L.; Zhang, S.; Huang, D.; Deng, R.; Zhang, J.; Qu, H.; Xu, S.; Liang, C.; Xu, W. Organelle-Targeting Gold Nanorods for Macromolecular Profiling of Subcellular Organelles and Enhanced Cancer Cell Killing. *ACS Appl. Mater. Interfaces* **2018,** *10*, 7910-7918.

620. Driver, M.; Li, Y.; Zheng, J.; Decker, E.; Julian McClements, D.; He, L. Fabrication of Lipophilic Gold Nanoparticles for Studying Lipids by Surface Enhanced Raman Spectroscopy (SERS). *Analyst* **2014,** *139*, 3352-3355.

621. Matthews, J. R.; Payne, C. M.; Hafner, J. H. Analysis of Phospholipid Bilayers on Gold Nanorods by Plasmon Resonance Sensing and Surface-Enhanced Raman Scattering. *Langmuir* **2015,** *31*, 9893-9900.

622. Suga, K.; Yoshida, T.; Ishii, H.; Okamoto, Y.; Nagao, D.; Konno, M.; Umakoshi, H. Membrane Surface-Enhanced Raman Spectroscopy for Sensitive Detection of Molecular Behavior of Lipid Assemblies. *Anal. Chem.* **2015,** *87*, 4772-4780.

623. Taylor, R. W.; Benz, F.; Sigle, D. O.; Bowman, R. W.; Bao, P.; Roth, J. S.; Heath, G. R.; Evans, S. D.; Baumberg, J. J. Watching Individual Molecules Flex Within Lipid Membranes Using SERS. *Sci. Rep.* **2014,** *4*, 5940.

624. Kneipp, J.; Kneipp, H.; Rajaduraj, A.; Redmond, R. W.; Kneipp, K. Optical Probing and Imaging of Live Cells Using SERS Labels. *J. Raman Spectrosc.* **2009,** *40*, 1-5.

625. Panikkanvalappil, S. R.; Hira, S. M.; Mahmoud, M. A.; El-Sayed, M. A. Unraveling the Biomolecular Snapshots of Mitosis in Healthy and Cancer Cells Using Plasmonically-Enhanced Raman Spectroscopy. *J. Am. Chem. Soc.* **2014,** *136*, 15961-15968.

626. Moody, B.; Haslauer, C. M.; Kirk, E.; Kannan, A.; Loboa, E. G.; McCarty, G. S. *In Situ* Monitoring of Adipogenesis with Human-Adipose-Derived Stem Cells Using Surface-Enhanced Raman Spectroscopy. *Appl. Spectrosc.* **2010,** *64*, 1227-1233.

627. Živanović, V.; Semini, G.; Laue, M.; Drescher, D.; Aebischer, T.; Kneipp, J. Chemical Mapping of Leishmania Infection in Live Cells by SERS Microscopy. *Anal. Chem.* **2018,** *90*, 8154-8161.

628. Stremersch, S.; Marro, M.; Pinchasik, B. E.; Baatsen, P.; Hendrix, A.; De Smedt, S. C.; Loza-Alvarez, P.; Skirtach, A. G.; Raemdonck, K.; Braeckmans, K. Identification of Individual Exosome-Like Vesicles by Surface Enhanced Raman Spectroscopy. *Small* **2016,** *12*, 3292-3301.

629. Shin, H.; Jeong, H.; Park, J.; Hong, S.; Choi, Y. Correlation between Cancerous Exosomes and Protein Markers Based on Surface-Enhanced Raman Spectroscopy (SERS) and Principal Component Analysis (PCA). *ACS Sens.* **2018,** *3*, 2637-2643.

630. Park, J.; Hwang, M.; Choi, B.; Jeong, H.; Jung, J. H.; Kim, H. K.; Hong, S.; Park, J. H.; Choi, Y. Exosome Classification by Pattern Analysis of Surface-Enhanced Raman Spectroscopy Data for Lung Cancer Diagnosis. *Anal. Chem.* **2017,** *89*, 6695-6701.

631. Kuang, H.; Ma, W.; Xu, L.; Wang, L.; Xu, C. Nanoscale Superstructures Assembled by Polymerase Chain Reaction (PCR): Programmable Construction, Structural Diversity, and Emerging Applications. *Acc. Chem. Res.* **2013,** *46*, 2341-2354.

632. Ma, W.; Kuang, H.; Xu, L.; Ding, L.; Xu, C.; Wang, L.; Kotov, N. A. Attomolar DNA Detection with Chiral Nanorod Assemblies. *Nat. Commun.* **2013,** *4*, 2689.

633.   Ma, W.; Sun, M.; Fu, P.; Li, S.; Xu, L.; Kuang, H.; Xu, C. A Chiral-Nanoassemblies-Enabled Strategy for Simultaneously Profiling Surface Glycoprotein and MicroRNA in Living Cells. *Adv. Mater.* **2017,** *29*, 1703410.

634.   Xu, L.; Yan, W.; Ma, W.; Kuang, H.; Wu, X.; Liu, L.; Zhao, Y.; Wang, L.; Xu, C. SERS Encoded Silver Pyramids for Attomolar Detection of Multiplexed Disease Biomarkers. *Adv. Mater.* **2015,** *27*, 1706-1711.

635.   Ma, W.; Fu, P.; Sun, M.; Xu, L.; Kuang, H.; Xu, C. Dual Quantification of MicroRNAs and Telomerase in Living Cells. *J. Am. Chem. Soc.* **2017,** *139*, 11752-11759.

636.   Ma, W.; Xu, L.; de Moura, A. F.; Wu, X.; Kuang, H.; Xu, C.; Kotov, N. A. Chiral Inorganic Nanostructures. *Chem. Rev.* **2017,** *117*, 8041-8093.

637.   Xu, L.; Zhao, S.; Ma, W.; Wu, X.; Li, S.; Kuang, H.; Wang, L.; Xu, C. Multigaps Embedded Nanoassemblies Enhance *In Situ* Raman Spectroscopy for Intracellular Telomerase Activity Sensing. *Adv. Funct. Mater.* **2016,** *26*, 1602-1608.

638.   Xu, L.; Kuang, H.; Xu, C.; Ma, W.; Wang, L.; Kotov, N. A. Regiospecific Plasmonic Assemblies for *in Situ* Raman Spectroscopy in Live Cells. *J. Am. Chem. Soc.* **2012,** *134*, 1699-1709.

639.   Qu, A.; Wu, X.; Xu, L.; Liu, L.; Ma, W.; Kuang, H.; Xu, C. SERS- and Luminescence-Active Au-Au-UCNP Trimers for Attomolar Detection of Two Cancer Biomarkers. *Nanoscale* **2017,** *9*, 3865-3872.

640.   Radziuk, D.; Moehwald, H. Prospects for Plasmonic Hot Spots in Single Molecule SERS Towards the Chemical Imaging of Live Cells. *Phys. Chem. Chem. Phys.* **2015,** *17*, 21072-21093.

641.   Carroll, S.; Al-Rubeai, M.; ACSD Labelling and Magnetic Cell Separation: A Rapid Method of Separating Antibody Secreting Cells from Non-Secreting Cells. *J. Immunol. Meth.* **2005**, *296*, 171-178

642.   Pallaoro, A.; Hoonejani M. R.; Braun, G. B.; Meinhart, C. D.; Moskovits, M. Rapid Identification by Surface-Enhanced Raman Spectroscopy of Cancer Cells at Low Concentrations Flowing in a Microfluidic Channel. *ACS Nano* **2015**, *9*, 4328–4336.

643.   Wu, X.; Luo, L.; Yang, S.; Ma, X.; Li, Y.; Dong, C.; Tian, Y.; Zhang, L.; Shen, Z.; Wu, A. Improved SERS Nanoparticles for Direct Detection of Circulating Tumor Cells in the Blood. *ACS Appl. Mater. Interfaces* **2015**, *7*, 9965–9971.

644.   Garcia-Algar, M.; Fernandez-Carrascal, A.; Olano-Daza, A.; Guerrini, L.; Feliu, N.; Parak, W. J.; Guimera, R.; Garcia-Rico, E.; Alvarez-Puebla, R. A. Adaptive Metabolic Pattern Biomarker for Disease Monitoring and Staging of Lung Cancer with Liquid Biopsy. *npj Precis. Oncol.* **2018**, *2*, 16.

645.   Jarvis, R. M.; Goodacre, R. Rapid Discrimination of Bacteria Using surface Enhanced Raman Spectroscopy. *Anal. Chem.* **2004**, *76*, 40-47.

646.   Patel, I. S.; Premasiri, W. R.; Moir, D. T.; Ziegler, L. D. Barcoding Bacterial Cells: A SERS-Based Methodology for Pathogen Identification. *J. Raman Spectrosc.* **2008**, *39*, 1660-1672.

647.   Muhamadali, H.; Chisanga, M.; Subaihi, A.; Goodacre, R. Combining Raman and FT-IR Spectroscopy with Quantitative Isotopic Labelling for Differentiation of *E. Coli* Cells at Community and Single Cell Levels. *Anal. Chem.* **2015**, *87*, 4578-4586.

648.   Premasiri, W. R.; Lee, J. C.; Sauer-Budge, A.; Théberge, R.; Costello, C. E.; Ziegler, L. D. The Biochemical Origins of the Surface-Enhanced Raman Spectra of Bacteria: A Metabolomics Profiling by SERS. *Anal. Bioanal. Chem.* **2016**, *408*, 4631-4647.

649.   Kubryk, P.; Niessner, R.; Ivleva, N. P. The Origin of the Band at Around 730 cm^{-1} in the SERS Spectra of Bacteria: A Stable Isotope Approach. *Analyst* **2016**, *141*, 2874-2878.

650.   Cui, L.; Yang, K.; Zhou, G. W.; Huang, W. E.; Zhu, Y.G. Surface-Enhanced Raman Spectroscopy Combined with Stable Isotope Probing to Monitor Nitrogen Assimilation at Both Bulk and Single-Cell Level. *Anal. Chem.* **2017**, *89*, 5793–5800.

651.   Chisanga, M.; Muhamadali, H.; Kimber R.; Goodacre, R. Quantitative Detection of Isotopically Enriched *E. Coli* Cells by SERS. *Faraday Discuss.* **2017**, *205*, 331-343.

652.   Premasiri, W. R.; Chen, Y.; Williamson, P. M.; Bandarage, D. C.; Pyles, C.; Ziegler, L. D. Rapid Urinary Tract Infection Diagnostics by Surface-Enhanced Raman Spectroscopy (SERS): Identification and Antibiotic Susceptibilities. *Anal. Bioanal. Chem.* **2017**, *409*, 3043-3054.

653.   Kelly, J.; Patrick, R.; Patrick, S.; Bell, S. E. J. Surface-Enhanced Raman Spectroscopy for the Detection of a Metabolic Product in the Headspace Above Live Bacterial Cultures. *Angew. Chem. Int. Ed.* **2018**, *130*, 15912-15916.

654.   Bodelon, G.; Montes-Garcia, V.; Lopez-Puente, V.; Hill, E. H.; Hamon, C.; Sanz-Ortiz, M. N.; Rodal-Cedeira, S.; Costas, C.; Celiksoy, S.; Perez-Juste, I.; Scarabelli, L.; La Porta, A.; Perez-Juste, J.; Pastoriza-Santos, I.; Liz-Marzan, L. M. Detection and Imaging of Quorum Sensing in *Pseudomonas Aeruginosa* Biofilm Communities by Surface-Enhanced Resonance Raman Scattering. *Nat. Mater.* **2016**, *15*, 1203-1210.

655.   Lopez-Puente, V.; Abalde-Cela, S.; Angelome, P. C.; Alvarez-Puebla, R. A.; Liz-Marzan, L. M. Plasmonic Mesoporous Composites as Molecular Sieves for SERS Detection. *J. Phys. Chem. Lett.* **2013**, *4*, 2715-2720.

656.   Bodelón, G.; Montes-García, V.; Costas, C.; Pérez-Juste, I.; Pérez-Juste, J.; Pastoriza-Santos, I.; Liz-Marzán, L. M. Imaging Bacterial Inter-Species Chemical Interactions by Surface Enhanced Raman Scattering. *ACS Nano* **2017**, *11*, 4631-4640.

657.   De Marchi, S.; Bodelón, G.; Vázquez-Iglesias, L.; Liz-Marzán, L. M.; Pérez-Juste, J.; Pastoriza-Santos, I.. Surface-Enhanced Raman Scattering (SERS) Imaging of Bioactive Metabolites in Mixed Bacterial Populations. *Appl. Mater. Today* **2019**, *14*, 207-215.

658.   Walter, A.; März, A.; Schumacher, W.; Röscha, P.; Popp, J. Towards a Fast, High Specific and Reliable Discrimination of Bacteria on Strain Level by Means of SERS in a Microfluidic Device. *Lab Chip* **2011**, *11*, 1013-1021.

659.   Pethig, R. Dielectrophoresis: Status of the Theory, Technology, and Applications. *Biomicrofluidics* **2010**, *4*, 022811.

660.   Cheng, I.-F. Chang, H.-C-; Chen, T.-Y.; Hu, C.; Yang, F.-L. Rapid (<5 min) Identification of Pathogen in Human Blood by Electrokinetic Concentration and Surface-Enhanced Raman Spectroscopy. *Sci. Rep.* **2013**, *3*, 2365.

661.   Pazos-Perez, N.; Pazos, E.; Catala, C.; Mir-Simon, B.; Gómez-de Pedro, S.; Sagales, J.; Villanueva, C.; Vila, J.; Soriano, A.; García de Abajo, F. J. Alvarez-Puebla, R. A. Ultrasensitive Multiplex Optical Quantification of Bacteria in Large Samples of Biofluids. *Sci. Rep.* **2016**, *6*, 29014.

662.   Xie, W.; Schlücker, S. Medical Applications of Surface-Enhanced Raman Scattering. *Phys. Chem. Chem. Phys.* **2013,** *15*, 5329-5344.

663.   Zhang, Y.; Schlücker, S., iSERS Microscopy for Tissue-Based Cancer Diagnostics with SERS Nanotags. In *Confocal Raman Microscopy* Thomas Dieing, O. H., Jan Toporski, Ed. Springer International Publishing AG 2018: Switzerland, 2018; Vol. 66.

664.   Schlücker, S.; Schaeberle, M. D.; Huffman, S. W.; Levin, I. W. Raman Microspectroscopy: A Comparison of Point, Line, and Wide-Field Imaging Methodologies. *Anal. Chem.* **2003,** *75*, 4312-4318.

665.   Schlücker, S.; Küstner, B.; Punge, A.; Bonfig, R.; Marx, A.; Ströbel, P., Immuno-Raman Microspectroscopy: *In Situ* Detection of Antigens in Tissue Specimens by Surface-Enhanced Raman Scattering. *J. Raman Spectrosc.* **2006,** *37*, 719-721.

666.   Schlücker, S.; Salehi, M.; Bergner, G.; Schütz, M.; Ströbel, P.; Marx, A.; Petersen, I.; Dietzek, B.; Popp, J. Immuno-Surface-Enhanced Coherent Anti-Stokes Raman Scattering Microscopy: Immunohistochemistry with Target-Specific Metallic Nanoprobes and Nonlinear Raman Microscopy. *Anal. Chem.* **2011,** *83*, 7081-7085.

667.   Hewitt, S. M.; Baskin, D. G.; Frevert, C. W.; Stahl, W. L.; Rosa-Molinar, E. Controls for Immunohistochemistry: The Histochemical Society's Standards of Practice for Validation of Immunohistochemical Assays. *J. Histochem. Cytochem.* **2014,** *62*, 693-697.

668.   Wang, X.-P.; Walkenfort, B.; König, M.; König, L.; Kasimir-Bauer, S.; Schlücker, S. Fast and Reproducible iSERS Microscopy of Single HER2-Positive Breast Cancer Cells Using Gold Nanostars as SERS Nanotags. *Faraday Discuss.* **2017,** *205*, 377-386.

669.   MacLaughlin, C. M.; Mullaithilaga, N.; Yang, G.; Ip, S. Y.; Wang, C.; Walker, G. C. Surface-Enhanced Raman Scattering Dye-Labeled Au Nanoparticles for Triplexed Detection of Leukemia and Lymphoma Cells and SERS Flow Cytometry. *Langmuir* **2013,** *29*, 1908-1919.

670.   Zhang, Y.; Wang, X.-P.; Perner, S.; Bankfalvi, A.; Schlücker, S. Effect of Antigen Retrieval Methods on Nonspecific Binding of Antibody–Metal Nanoparticle Conjugates on Formalin-Fixed Paraffin-Embedded Tissue. *Anal. Chem.* **2018,** *90*, 760-768.

671. Lutz, B. R.; Dentinger, C. E.; Nguyen, L. N.; Sun, L.; Zhang, J.; Allen, A. N.; Chan, S.; Knudsen, B. S. Spectral Analysis of Multiplex Raman Probe Signatures. *ACS Nano* **2008,** *2*, 2306-2314.

672. Kahraman, M.; Mullen, E. R.; Korkmaz, A.; Wachsmann-Hogiu, S. Fundamentals and Applications of SERS-Based Bioanalytical Sensing. *Nanophotonics* **2017**, *6*, 831–852.

673. Indrasekara, A. S. D. S.; Fabris, L. SERS-based Approaches toward Genetic Profiling. *Bioanalysis* **2015**, *7*, 263-278.

674. Fabris, L. SERS Tags: The Next Promising Tool for Personalized Cancer Detection? *ChemNanoMat.* **2016**, *2*, 249-258.

675. Keren S.; Zavaleta C.; Cheng, Z.; de la Zerda, A.; Gheysens, O.; Gambhir, S. S. Noninvasive Molecular Imaging of Small Living Subjects Using Raman Spectroscopy. *Proc. Natl. Acad. Sci. U. S. A.* **2008**, *105*, 5844–5849.

676. Qian, X.; Peng, X.-H.; Ansari, D. O.; Yin-Goen, Q.; Chen, G. Z.; Shin, D. M.; Yang, L.; Young, A. N.; Wang, M. D.; Nie, S. *In Vivo* Tumor Targeting and Spectroscopic Detection with Surface-Enhanced Raman Nanoparticle Tags. *Nat. Biotechnol.* **2008**, *26*, 83–90.

677. Asiala, S. M.; Shand, N. C.; Faulds, K.; Graham, D. Surface-Enhanced, Spatially Offset Raman Spectroscopy (SESORS) in Tissue Analogues. *ACS Appl. Mater. Interfaces* **2017**, *9*, 25488-25494.

678. Pal, S.; Harmsen, S.; Oselechyk, A.; Hsu, H.-T.; Kircher, M. F. MUC1 Aptamer Targeted SERS Nanoprobes. *Adv. Funct. Mater.* **2017**, *27*, 1606632.

679. Indrasekara, A. S. D. S.; Paladini, B. J.; Naczynski, D. J.; Starovoytov, V.; Moghe, P. V.; Fabris, L. Dimeric Gold Nanoparticle Assemblies as Tags for SERS- Based Cancer Detection. *Adv. Healthcare Mater.* **2013**, *2*, 1370-1376.

680. Narod, S. A. Disappearing Breast Cancers. *Curr. Oncol.* **2012**, *19*, 59-60.

681. Vendrell, M.; Maiti, K. K.; Dhaliwal, K.; Chang, Y.-T. Surface-Enhanced Raman Scattering in Cancer Detection and Imaging. *Trends Biotechnol.* **2013**, *31*, 249-257.

682. Karabeber, H.; Huang, R.; Iacono, P.; Samii, J. M.; Pitter, K.; Holland, E. C.; Kircher, M. F. Guiding Brain Tumor Resection Using Surface-Enhanced Raman Scattering Nanoparticles and a Hand-Held Raman Scanner. *ACS Nano* **2014**, *8*, 9755–9766.

683. Wang, Y. W.; Kang, S.; Khan, A.; Bao, P. Q.; Liu, J. T. C. *In Vivo* Multiplexed Molecular Imaging of Esophageal Cancer *via* Spectral Endoscopy of Topically Applied SERS Nanoparticles. *Biomed. Opt. Exp.* **2015**, *6*, 3714-3723.

684. Zhang, Y.; Mi, X.; Tan, X.; Xiang, R. Recent Progress on Liquid Biopsy Analysis using Surface-Enhanced Raman Spectroscopy. *Theranostics* **2019**, *9*, 491-525.

685. Lauridsen, R. K.; Sommer, L. M.; Johansen, H. K.; Rindzevicius, T.; Molin, S.; Jelsbak, L.; Engelsen, S. B.; Boisen, A. SERS Detection of The Biomarker Hydrogen Cyanide from *Pseudomonas Aeruginosa* Cultures Isolated from Cystic Fibrosis Patients. *Sci. Rep.* **2017**, *7*, 45264.

686.   Bhamidipati, M.; Cho, H. Y.; Lee, K.-B.; Fabris, L. SERS-based Quantification of Biomarker Expression at the Single Cell Level Enabled by Gold Nanostars and Truncated Aptamers. *Bioconjugate Chem.* **2018**, *29*, 2970-2981.

687.   Zong, S.; Wang, Z.; Chen, H.; Cui, Y. Ultrasensitive Telomerase Activity Detection by Telomeric Elongation Controlled Surface Enhanced Raman Scattering. *Small* **2013**, *9*, 4215–4220.

688.   Ngo, H. T.; Wang, H. N.; Burke, T.; Ginsburg, G. S.; Vo-Dinh, T. Multiplex Detection of Disease Biomarkers Using SERS Molecular Sentinel-On-Chip. *Anal. Bioanal. Chem.* **2014**, *406*, 3335-3344.

689.   Lowe, A. J.; Huh, Y. S.; Strickland, A. D.; Erickson, D.; Batt, C. A. Multiplex Single Nucleotide Polymorphism Genotyping Utilizing Ligase Detection Reaction Coupled Surface Enhanced Raman Spectroscopy. *Anal. Chem.* **2010**, *82*, 5810–5814.

690.   Zhou, W.; Tian, W. F.; Yin, B.-C.; Ye, B. C. Simultaneous Surface-Enhanced Raman Spectroscopy Detection of Multiplexed MicroRNA Biomarkers. *Anal. Chem.* **2017**, *89*, 6120–6128.

691.   Nima, Z. A.; Mahmood, M.; Xu, Y.; Mustafa, T.; Watanabe, F.; Nedosekin, D. A.; Juratli, M. A.; Fahmi, T.; Galanzha, E. I.; Nolan, J. P.; Basnakian, A. G.; Zharov, V. P.; Biris, A. Circulating Tumor Cell Identification by Functionalized Silver-Gold Nanorods with Multicolor, Super-Enhanced SERS And Photothermal Resonances. *Sci. Rep.* **2014**, *4*, 4752.

692.   Wang, Z.; Zong, S.; Wang, Y.; Li, N.; Li, L.; Lu, J.; Wang, Z.; Chen, B.; Cui, Y. Screening and Multiple Detection of Cancer Exosomes Using a SERS-Based Method. *Nanoscale* **2018**, *10*, 9053-9062.

693.   Harmsen, S.; Huang, R.; Wall, M. A.; Karabeber, H.; Samii, J. M.; Spaliviero, M.; White, J. R.; Monette, S.; O'connor, R.; Pitter, K. L.; Sastra, S. A.; Saborowski, M.; Holland, E. C.; Singer, S.; Olive, K. P.; Lowe, S. W.; Blasberg, R. G.; Kircher, M. F. Surface-Enhanced Resonance Raman Scattering Nanostars for High-Precision Cancer Imaging. *Science Transl. Med.* **2015**, *7*, 271ra7.

694.   Oseledchyk, A.; Andreou, C.; Wall, M. A.; Kircher, M. F. Folate-Targeted Surface-Enhanced Resonance Raman Scattering Nanoprobe Ratiometry for Detection of Microscopic Ovarian Cancer. *ACS Nano* **2017**, *11*, 1488-1497.

695.   Andreou, C.; Neuschmelting, V.; Tschaharganeh, D.-F.; Huang, C.-H.; Oseledchyk, A.; Iacono, P.; Karabeber, H.; Colen, R. R.; Mannelli, L.; Lowe, S. W.; Kircher, M. F. Imaging of Liver Tumors Using Surface-Enhanced Raman Scattering Nanoparticles. *ACS Nano* **2016**, *10*, 5015-5026.

696.   Ke, P. C.; Lin, S.; Parak, W. J.; Davis, T. P.; Caruso, F. A Decade of Protein Corona. *ACS Nano* **2017**, *11*, 11773−11776.

697.   Saraiva, C.; Praça, C.; Ferreira, R.; Santos, T.; Ferreira, L.; Bernardino, L. Nanoparticle-Mediated Brain Drug Delivery: Overcoming Blood–Brain Barrier to Treat Neurodegenerative Diseases. *J. Controlled Release* **2016**, 235, 34-47.

698.   Yuan, H.; Wilson, C. M.; Xia, J.; Doyle, S. L.; Li, S.; Fales, A. M.; Liu, Y.; Ozaki, E.; Mulfaul, K.; Hanna, G.; Palmer, G. M.; Wang, L. V.; Grant, G. A.; Vo-Dinh, T. Plasmonics-Enhanced and Optically Modulated Delivery of Gold Nanostars into Brain Tumor, *Nanoscale* **2014**, *6*, 4078-4082.

699.   Zavaleta, C. L.; Garai, E.; Liu, J. T. C.; Sensarn, S.; Mandella, M. J.; Van de Sompel, D.; Friedland, S.; Van Dam, J.; Contag, C. H.; Gambhir, S. S. A Raman-Based Endoscopic Strategy for Multiplexed Molecular Imaging. *Proc. Nat. Acad. Sci. U. S. A.* **2013**, *110*, E2288-E2297

700.   Sharma, N.; Takeshita, N.; Ho, K. Y. Raman Spectroscopy for the Endoscopic Diagnosis of Esophageal, Gastric, and Colonic Diseases. *Clin. Endosc.* **2016**, *49*, 404–407.

701.   Garai, E.; Sensarn, S.; Zavaleta, C. L.; Loewke, N. O.; Rogalla, S.; Mandella, M. J.; Felt, S. A.; Friedland, S.; Liu, J. T.; Gambhir, S. S.; Contag, C. H. A Real-Time Clinical Endoscopic System for Intraluminal, Multiplexed Imaging of Surface-Enhanced Raman Scattering Nanoparticles. *PLoS ONE* **2015**, *10*, e0123185.

702.   Li, T. D.; Zhang, R.; Chen, H.; Huang, Z.-P.; Ye, X.; Wang, H.; Deng, A.-M.; Kong, J.-L. An Ultrasensitive Polydopamine Bi-functionalized SERS Immunoassay for Exosome-Based Diagnosis and Classification of Pancreatic Cancer. *Chem. Sci.* **2018**, *9*, 5372-5382.

703.   Feng, J.; Xu, L.; Cui, G.; Wu, X.; Ma, W.; Kuang, H.; Xu, C. Building SERS-Active Heteroassemblies for Ultrasensitive Bisphenol A Detection. *Biosens. Bioelectron.* **2016,** *81*, 138-142.

704.   Li, A.; Tang, L.; Song, D.; Song, S.; Ma, W.; Xu, L.; Kuang, H.; Wu, X.; Liu, L.; Chen, X.; Xu, C. A SERS-Active Sensor Based on Heterogeneous Gold Nanostar Core-Silver Nanoparticle Satellite Assemblies for Ultrasensitive Detection of Aflatoxinb1. *Nanoscale* **2016,** *8*, 1873-1878.

705.   Schmit, V. L.; Martoglio, R.; Scott, B.; Strickland, A. D.; Carron, K. T. Lab-on-a-Bubble: Synthesis, Characterization, and Evaluation of Buoyant Gold Nanoparticle-Coated Silica Spheres. *J. Am. Chem. Soc.* **2012,** *134*, 59-62.

706.   Xu, L.; Yin, H.; Ma, W.; Kuang, H.; Wang, L.; Xu, C. Ultrasensitive SERS Detection of Mercury Based on the Assembled Gold Nanochains. *Biosens. Bioelectron.* **2015,** *67*, 472-476.

707.   Wu, X.; Tang, L.; Ma, W.; Xu, L.; Liu, L.; Kuang, H.; Xu, C. SERS-Active Au NR Oligomer Sensor for Ultrasensitive Detection of Mercury Ions. *RSC Adv.* **2015,** *5*, 81802-81807.

708.   Ma, W.; Sun, M.; Xu, L.; Wang, L.; Kuang, H.; Xu, C. A SERS Active Gold Nanostar Dimer for Mercury Ion Detection. *Chem. Commun.* **2013,** *49*, 4989-4991.

709.   Zhao, Y.; Xu, L.; Liz-Marzán, L. M.; Kuang, H.; Ma, W.; Asenjo-García, A.; García de Abajo, F. J.; Kotov, N. A.; Wang, L.; Xu, C. Alternating Plasmonic Nanoparticle Heterochains Made by Polymerase Chain Reaction and Their Optical Properties. *J. Phys. Chem. Let.* **2013,** *4*, 641-647.

710.	Lin, E.-C.; Fang, J.; Park, S.-C.; Stauden, T.; Pezoldt, J.; Jacobs, H. O. Effective Collection and Detection of Airborne Species Using SERS-Based Detection and Localized Electrodynamic Precipitation. *Adv. Mater.* **2013,** *25*, 3554-3559.

711.	Huang, Z.; Meng, G.; Huang, Q.; Yang, Y.; Zhu, C.; Tang, C. Improved SERS Performance from Au Nanopillar Arrays by Abridging the Pillar Tip Spacing by Ag Sputtering. *Adv. Mater.* **2010,** *22*, 4136-4139.

712.	Zhao, Y.; Sun, M.; Ma, W.; Kuang, H.; Xu, C. Biological Molecules-Governed Plasmonic Nanoparticle Dimers with Tailored Optical Behaviors. *J. Phys. Chem. Let.* **2017,** *8*, 5633-5642.

713.	Wang, X.; Shi, W.; Jin, Z.; Huang, W.; Lin, J.; Ma, G.; Li, S.; Guo, L. Remarkable SERS Activity Observed from Amorphous ZnO Nanocages. *Angew. Chem. Int. Ed.* **2017,** *129*, 9983-9987.

714.	Tao, L.; Chen, K.; Chen, Z.; Cong, C.; Qiu, C.; Chen, J.; Wang, X.; Chen, H.; Yu, T.; Xie, W.; Deng, S.; Xu, J.-B. 1T′ Transition Metal Telluride Atomic Layers for Plasmon-Free SERS at Femtomolar Levels. *J. Am. Chem. Soc.* **2018,** *140*, 8696-8704.

715.	Zhao, Y.; Kornienko, N.; Liu, Z.; Zhu, C.; Asahina, S.; Kuo, T.-R.; Bao, W.; Xie, C.; Hexemer, A.; Terasaki, O.; Yang, P.; Yaghi, O. M. Mesoscopic Constructs of Ordered and Oriented Metal–Organic Frameworks on Plasmonic Silver Nanocrystals. *J. Am. Chem. Soc.* **2015,** *137*, 2199-2202.

716.	Xu, L.; Ma, W.; Wang, L.; Xu, C.; Kuang, H.; Kotov, N. A. Nanoparticle assemblies: dimensional transformation of nanomaterials and scalability. *Chem. Soc. Rev.* **2013,** *42*, 3114-3126.

717.	Kearns, H.; Goodacre, R.; Jamieson, L. E.; Graham, D.; Faulds, K. SERS Detection of Multiple Antimicrobial-Resistant Pathogens Using Nanosensors. *Anal. Chem.* **2017**, *89*, 12666−12673.

718.	Szlag, V. M.; Styles, M. J.; Madison, L. R.; Campos, A. R.; Wagh, B.; Sprouse, D.; Schatz, G. C.; Reineke, T. M.; Haynes, C. L. SERS Detection of Ricin B-Chain *via* N-Acetyl-Galactosamine Glycopolymers. *ACS Sens.* **2016**, *1*, 842–846.

719.	Szlag, V. M.; Jung, S.; Rodriguez, R. S.; Bourgeois, M.; Bryson, S.; Schatz, G. C.; Reineke, T. M.; Haynes, C. L. Isothermal Titration Calorimetry for the Screening of Aflatoxin B1 Surface-Enhanced Raman Scattering Sensor Affinity Agents. *Anal. Chem.* **2018**, *90*, 13409–13418.

720.	Cheung, M.; Lee, W. W. Y.; Cowcher, D. P.; Goodacre, R.; Bell, S. E. J. SERS of Meso-Droplets Supported on Superhydrophobic Wires Allows Exquisitely Sensitive Detection of Dipicolinic Acid, an Anthrax Biomarker, Considerably Below the Infective Dose. *Chem. Commun.* **2016**, *52*, 9925-9928.

721.	Zhang, X.; Young, M. A.; Lyandres, O.; Van Duyne, R. P. Rapid Detection of an Anthrax Biomarker by Surface-Enhanced Raman Spectroscopy. *J. Am. Chem. Soc.* **2005**, *127*, 4484-4489.

722.	Szlag, V. M.; Rodriguez, R. S.; He, J.; Hudson-Smith, N.; Kang, H.; Le, N.; Reineke, T. M.; Haynes, C. L. Molecular Affinity Agents for Intrinsic Surface-

Enhanced Raman Scattering (SERS) Sensors. *ACS Appl. Mater. Interfaces* **2018**, *10*, 31825–31844.

723.   Granger, J. H.; Porter, M. D. The Case for Human Serum as a Highly Preferable Sample Matrix for Detection of Anthrax Toxins. *ACS Sens.* **2018**, *3*, 2303−2310.

724.   Lim, C. Y.; Granger, J. H.; Porter, M. D. SERS Detection of Clostridium Botulinum Neurotoxin Serotypes A and B in Buffer and Serum: Towards the Development of a Biodefense Test Platform. *Anal. Chim. Acta X* **2019**, *1*, 100002.

725.   Hwang, J.; Lee, S.; Choo, J. Application of a SERS-Based Lateral Flow Immunoassay Strip for the Rapid and Sensitive Detection of Staphylococcal Enterotoxin B. *Nanoscale* **2016**, *8*, 11418-11425.

726.   Gao, F.; Feng, S.; Chen, Z.; Li-Chan, E.C.; Grant, E.; Lu, X. Detection and Quantification of Chloramphenicol in Milk and Honey Using Molecularly Imprinted Polymers: Canadian Penny-Based SERS Nano-Biosensor. *J. Food Sci.* **2014**, *79*, N2542-N2549.

727.   Gao, F.; Hu, Y.; Chen, D.; Li-Chan, E. C. Y.; Grant, E.; Lu, X. Determination of Sudan I in Paprika Powder by Molecularly Imprinted Polymers-Thin Layer Chromatography-Surface Enhanced Raman Spectroscopic Biosensor. *Talanta* **2015**, *143*, 344-352.

728.   Lamont, E. A.; He, L.; Warriner, K.; Labuza, T. P.; Sreevatsan, S. A Single DNA Aptamer Functions as a Biosensor for Ricin. *Analyst* **2011**, *136*, 3884-3895.

729.   He, L.; Lamont, E.; Veeregowda, B.; Sreevatsan, S.; Haynes, C. L.; Diez-Gonzalez, F.; Labuza, T. P. Aptamer-Based Surface-Enhanced Raman Scattering Detection of Ricin in Liquid Foods. *Chem. Sci.* **2011**, *2*, 1579-1582.

730.   Zengin, A.; Tamer, U.; Caykara, T. Fabrication of a SERS Based Aptasensor for Detection of Ricin B Toxin. *J. Mater. Chem. B* **2015**, *3*, 306-315.

731.   Campos, A. R.; Gao, Z.; Blaber, M. G.; Huang, R.; Schatz, G. C.; Van Duyne, R. P.; Haynes, C. L. Surface-Enhanced Raman Spectroscopy Detection of Ricin B Chain in Human Blood. *J. Phys. Chem. C* **2016**, *120*, 20961–20969.

732.   Lyandres, O.; Shah, N. C.; Yonzon, C. R.; Walsh Jr., J. T.; Glucksberg, M. R.; Van Duyne, R. P. Real-Time Glucose Sensing by Surface-Enhanced Raman Spectroscopy in Bovine Plasma Facilitated by a Mixed Decanethiol/Mercaptohexanol Partition Layer. *Anal. Chem.* **2005,** 77, 6134-6139.

733.   Yonzon, C. R.; Haynes, C. L.; Zhang, X.; Walsh, Jr., J. T.; Van Duyne, R. P. A Glucose Biosensor Based on Surface-Enhanced Raman Scattering: Improved Partition Layer, Temporal Stability, Reversibility, and Resistance to Serum Protein Interference. *Anal. Chem.* **2004,** 76, 78-85 .

734.   Zheng, J.; Zhao, C.; Tian, G.; He, L. Rapid Screening for Ricin Toxin on Letter Papers Using Surface Enhanced Raman Spectroscopy. *Talanta* **2017**, *162*, 552-557.

735.   Radu, A. I.; Ryabchykov, O.; Bocklitz, T. W.; Huebner, U.; Weber, K.; Cialla-May, D.; Popp, J. Toward Food Analytics: Fast Estimation of Lycopene and B-Carotene

Content in Tomatoes Based on Surface Enhanced Raman Spectroscopy (SERS). *Analyst* **2016**, *141*, 4447-4455.

736. Zhu, C. H.; Meng, G. W.; Huang, Q.; Huang, Z. L. Vertically Aligned Ag Nanoplate-Assembled Film as a Sensitive and Reproducible SERS Substrate for the Detection of PCB-77. *J. Hazard. Mater.* **2012,** *211*, 389-395.

737. Bantz, K. C.; Haynes, C. L. Surface-Enhanced Raman Scattering Detection and Discrimination of Polychlorinated Biphenyls. *Vibr. Spectrosc.* **2009,** *50*, 29-35.

738. Jones, C. L.; Bantz, K. C.; Haynes, C. L. Partition Layer-Modified Substrates for Reversible Surface-Enhanced Raman Scattering Detection of Polycyclic Aromatic Hydrocarbons. *Anal. Bioanal. Chem.* **2009,** *394*, 303-311.

739. Bantz, K. C.; Nelson, H. D.; Haynes, C. L. Plasmon-Enabled Study of Self-Assembled Alkanethiol Ordering on Roughened Ag Substrates. *J. Phys. Chem. C* **2012,** *116*, 3585-3593.

740. Xiao, L. L.; Zhang, M.; Liu, Z.; Bian, W. W.; Zhang, X. L.; Zhan, J. H. Hydrophobic Silver Nanowire Membrane for Swabbing Extraction and *In Situ* SERS Detection of Polycyclic Aromatic Hydrocarbons on Toys. *Anal. Methods* **2017,** *9*, 1816-1824.

741. Alvarez-Puebla, R. A.; Contreras-Caceres, R.; Pastoriza-Santos, I.; Perez-Juste, J.; Liz-Marzan, L. M. Au@pNIPAM Colloids as Molecular Traps for Surface-Enhanced, Spectroscopic, Ultra-Sensitive Analysis. *Angew. Chem. Int. Ed.* **2009,** *48*, 138-143.

742. Contreras-Caceres, R.; Abade-Cela, S.; Guardia-Giros, P.; Fernandez-Barbero, A.; Perez-Juste, J.; Alvarez-Puebla, R. A.; Liz-Marzan, L. M. Multifunctional Microgel Magnetic/Optical Traps for SERS Ultradetection. *Langmuir* **2011,** *27*, 4520-4525.

743. Mueller, M.; Tebbe, M.; Andreeva, D. V.; Karg, M.; Alvarez-Puebla, R. A.; Pazos-Perez, N.; Fery, A. Large-Area Organization of pNIPAM-Coated Nanostars as SERS Platforms for Polycyclic Aromatic Hydrocarbons Sensing in Gas Phase. *Langmuir* **2012,** *28*, 9168-9173.

744. Leyton, P.; Sanchez-Cortes, S.; Garcia-Ramos, J. V.; Domingo, C.; Campos-Vallette, M.; Saitz, C.; Clavijo, R. E. Selective Molecular Recognition of Polycyclic Aromatic Hydrocarbons (PAHs) on Calix[4]arene-Functionalized Ag Nanoparticles by Surface-Enhanced Raman Scattering. *J. Phys. Chem. B* **2004,** *108*, 17484-17490.

745. Guerrini, L.; Garcia-Ramos, J. V.; Domingo, C.; Sanchez-Cortes, S. Functionalization of Ag Nanoparticles with Dithiocarbamate Calix[4]arene as an Effective Supramolecular Host for the Surface-Enhanced Raman Scattering Detection of Polycyclic Aromatic Hydrocarbons. *Langmuir* **2006,** *22*, 10924-10926.

746. Guerrini, L.; Garcia-Ramos, J. V.; Domingo, C.; Sanchez-Cortes, S. Sensing Polycyclic Aromatic Hydrocarbons with Dithiocarbamate-Functionalized Ag Nanoparticles by Surface-Enhanced Raman Scattering. *Anal. Chem.* **2009,** *81*, 953-960.

747. Zhu, C. H.; Meng, G. W.; Huang, Q.; Li, Z. B.; Huang, Z. L.; Wang, M. L.; Yuan, J. P. Large-Scale Well-Separated Ag Nanosheet-Assembled Micro-Hemispheres Modified

with HS-beta-CD as Effective SERS Substrates for Trace Detection of PCBs. *J. Mater. Chem.* **2012,** *22*, 2271-2278.

748.   Montes-Garcia, V.; Fernandez-Lopez, C.; Gomez, B.; Perez-Juste, I.; Garcia-Rio, L.; Liz-Marzan, L. M.; Perez-Juste, J.; Pastoriza-Santos, I. Pillar[5] arene-Mediated Synthesis of Gold Nanoparticles: Size Control and Sensing Capabilities. *Chem. Eur. J.* **2014,** *20*, 8404-8409.

749.   Montes-Garcia, V.; Gomez-Gonzalez, B.; Martinez-Solis, D.; Taboada, J. M.; Jimenez-Otero, N.; de Una-Alvarez, J.; Obelleiro, F.; Garcia-Rio, L.; Perez-Juste, J.; Pastoriza-Santos, I. Pillar[5]arene-Based Supramolecular Plasmonic Thin Films for Label-Free, Quantitative and Multiplex SERS Detection. *ACS Appl. Mater. Interfaces* **2017,** *9*, 26372-26382.

750.   Xie, Y. F.; Wang, X.; Han, X. X.; Xue, X. X.; Ji, W.; Qi, Z. H.; Liu, J. Q.; Zhao, B.; Ozaki, Y. Sensing of Polycyclic Aromatic Hydrocarbons with Cyclodextrin Inclusion Complexes on Silver Nanoparticles by Surface-Enhanced Raman Scattering. *Analyst* **2010,** *135*, 1389-1394.

751.   Pfannkuche, J.; Lubecki, L.; Schmidt, H.; Kowalewska, G.; Kronfeldt, H. D. The Use of Surface-Enhanced Raman Scattering (SERS) for Detection of PAHs in the Gulf of Gdansk (Baltic Sea). *Mar. Pollut. Bull.* **2012,** *64*, 614-626.

752.   Kreno, L. E.; Hupp, J. T.; Van Duyne, R. P. Metal-Organic Framework Thin Film for Enhanced Localized Surface Plasmon Resonance Gas Sensing. *Anal. Chem.* **2010,** *82*, 8042-8046.

753.   Cao, X. L.; Hong, S. H.; Jiang, Z. J.; She, Y. X.; Wang, S. S.; Zhang, C.; Li, H.; Jin, F.; Jin, M. J.; Wang, J. SERS-Active Metal-Organic Frameworks with Embedded Gold Nanoparticles. *Analyst* **2017,** *142*, 2640-2647.

754.   He, L. C.; Liu, Y.; Liu, J. Z.; Xiong, Y. S.; Zheng, J. Z.; Liu, Y. L.; Tang, Z. Y. CoreShell Noble-Metal@Metal-Organic-Framework Nanoparticles with Highly Selective Sensing Property. *Angew. Chem. Int. Ed.* **2013,** *52*, 3741-3745.

755.   Cai, Y. Z.; Wu, Y. P.; Xuan, T.; Guo, X. Y.; Wen, Y.; Yang, H. F. Core-Shell Au@Metal-Organic Frameworks for Promoting Raman Detection Sensitivity of Methenamine. *ACS Appl. Mater. Interfaces* **2018,** *10*, 15412-15417.

756.   Kreno, L. E.; Greeneltch, N. G.; Farha, O. K.; Hupp, J. T.; Van Duyne, R. P. SERS of Molecules that Do Not Adsorb on Ag Surfaces: A Metal-Organic Framework-Based Functionalization Strategy. *Analyst* **2014,** *139*, 4073-4080.

757.   Hu, Y. L.; Liao, J.; Wang, D. M.; Li, G. K. Fabrication of Gold Nanoparticle-Embedded Metal-Organic Framework for Highly Sensitive Surface-Enhanced Raman Scattering Detection. *Anal. Chem.* **2014,** *86*, 3955-3963.

758.   Sun, H.; Cong, S.; Zheng, Z.; Wang, Z.; Chen, Z.; Zhao, Z. Metal–Organic Frameworks as Surface Enhanced Raman Scattering Substrates with High Tailorability. *J. Am. Chem. Soc.* **2019,** *141*, 870−878.

759.   Nicolson, F.; Jamieson, L. E.; Mabbott, S.; Shand, N. C.; Graham, D.; Faulds, K. Through Barrier Detection of Ethanol Using Handheld Raman Spectroscopy -

Conventional Raman *versus* Spatially Offset Raman Spectroscopy (SORS). *J. Raman Spectrosc.* **2017,** *48*, 1828-1838.

760.   Nicolson, F.; Jamieson, L. E.; Mabbott, S.; Plakas, K.; Shand, N. C.; Detty, M. R.; Graham, D.; Faulds, K. Through Tissue Imaging of a Live Breast Cancer Tumour Model Using Handheld Surface Enhanced Spatially Offset Resonance Raman Spectroscopy (SESORRS). *Chem. Sci.* **2018,** *9*, 3788-3792.

761.   Nicolson, F.; Jamieson, L. E.; Mabbott, S.; Plakas, K.; Shand, N. C.; Detty, M. R.; Graham, D.; Faulds, K. Surface Enhanced Resonance Raman Spectroscopy (SERRS) for Probing Through Plastic and Tissue Barriers Using a Handheld Spectrometer. *Analyst* **2018,** *143*, 5965-5973.

762.   Nicolson, F.; Jamieson, L. E.; Mabbott, S.; Plakas, K.; Shand, N. C.; Detty, M. R.; Graham, D.; Faulds, K. Multiplex Imaging of Live Breast Cancer Tumour Models Through Tissue Using Handheld Surface Enhanced Spatially Offset Resonance Raman Spectroscopy (SESORRS). *Chem. Commun.* **2018,** *54*, 8530-8533.

763.   Nicolson, F.; Jamieson, L. E.; Mabbott, S.; Plakas, K.; Shand, N. C.; Detty, M. R.; Graham, D.; Faulds, K. Towards Establishing a Minimal Nanoparticle Concentration for Applications Involving Surface Enhanced Spatially Offset Resonance Raman Spectroscopy (SESORRS) *In Vivo*. *Analyst* **2018,** *143*, 5358-5363.

764.   Odion, R. A.; Strobbia, P.; Crawford, B. M.; Vo-Dinh, T. Inverse Surface-Enhanced Spatially Offset Raman Spectroscopy (SESORS) Through a Monkey Skull. *J. Raman Spectrosc.* **2018**, *49*, 1452-1460.

765.   Noonan, J.; Asiala, S. M.; Grassia, G.; MacRitchie, N.; Gracie, K.; Carson, J.; Moores, M.; Girolami, M.; Bradshaw, A. C.; Guzik, T. J.; Meehan, G. R.; Scales, H. E.; Brewer, J. M.; McInnes, I. B.; Sattar, N.; Faulds, K.; Garside, P.; Graham, D.; Maffia, P. *In Vivo* Multiplex Molecular Imaging of Vascular Inflammation Using Surface-Enhanced Raman Spectroscopy. *Theranostics* **2018,** *8*, 6195-6209.

766.   Burstein, E.; Lundqvist, S.; Mills, D. L. In *Surface enhanced Raman Scattering*; Chang, R. K.; Furtak, T. E., Eds.; Plenum Press: New York, 1982; pp. 51–66.

767.   Lombardi, J. R.; Birke, R. L. A Unified View of Surface-Enhanced Raman Scattering. *Acc. Chem. Res.* **2009**, *42*, 734–742.

768.   Lombardi, J. R.; Birke, R. L.; Lu, T.; Xu, J. Charge-Transfer Theory of Surface Enhanced Raman Spectroscopy: Herzberg–Teller Contributions. *J. Chem. Phys.* **1986**, *84*, 4174–4180.

769.   Lombardi, J. R.; Birke, R. L. A Unified Approach to Surface-Enhanced Raman Spectroscopy. *J. Phys. Chem. C* **2008**, *112*, 5605–5617.

770.   Gale, R. J. *Spectroelectrochemistry : Theory and Practice*; Springer US, 1988.

771.   Konishi, T.; Kiguchi, M.; Takase, M.; Nagasawa, F.; Nabika, H.; Ikeda, K.; Uosaki, K.; Ueno, K.; Misawa, H.; Murakoshi, K. Single Molecule Dynamics at a Mechanically Controllable Break Junction in Solution at Room Temperature. *J. Am. Chem. Soc.* **2013**, *135*, 1009–1014.

772. Tian, Z. Q.; Lian, Y. Z.; Lin, T. Q. SERS Studies on Interfacial Water in Concentrated NaClO$_4$ Solutions. *J. Electroanal. Chem.* **1989**, *265*, 277–282.

773. Chen, Y. X.; Tian, Z. Q. Dependence of Surface Enhanced Raman Scattering of Water on the Hydrogen Evolution Reaction. *Chem. Phys. Lett.* **1997**, *281*, 379–383.

774. Kedziora, G. S.; Schatz, G. C. Calculating Dipole and Quadrupole Polarizabilities Relevant to Surface Enhanced Raman Spectroscopy. *Spectrochim. Acta A* **1999**, *55*, 625–638.

775. Polubotko, A. M. Some Anomalies of the SER Spectra of Symmetrical Molecules Adsorbed on Transition Metal Substrates: Consideration by the Dipole–Quadrupole SERS Theory. *J. Raman Spectrosc.* **2005**, *36*, 522–532.

776. Johansson, P.; Xu, H.; Käll, M. Surface-Enhanced Raman Scattering and Fluorescence Near Metal Nanoparticles. *Phys. Rev. B* **2005**, *72*, 035427.

777. Nabika, H.; Takase, M.; Nagasawa, F.; Murakoshi, K. Toward Plasmon-Induced Photoexcitation of Molecules. *J. Phys. Chem. Lett.* **2010**, *1*, 2470–2487.

778. Mulvaney, P. Surface Plasmon Spectroscopy of Nanosized Metal Particles. *Langmuir* **1996**, *12*, 788–800.

779. Brown, A. M.; Sheldon, M. T.; Atwater, H. A. Electrochemical Tuning of the Dielectric Function of Au Nanoparticles. *ACS Photonics* **2015**, *2*, 459–464.

780. Zapata Herrera, M.; Aizpurua, J.; Kazansky, A. K.; Borisov, A. G. Plasmon Response and Electron Dynamics in Charged Metallic Nanoparticles. *Langmuir* **2016**, *32*, 2829–2840.

781. Iida, T.; Ishihara, H. Unconventional Control of Excited States of a Dimer Molecule by a Localized Light Field Between Metal Nanostructures. *Phys. Status Solidi A* **2009**, *206*, 980–984.

782. Iida, T.; Aiba, Y.; Ishihara, H. Anomalous Optical Selection Rule of an Organic Molecule Controlled by Extremely Localized Light Field. *Appl. Phys. Lett.* **2011**, *98*, 053108.

783. Jain, P. K.; Ghosh, D.; Baer, R.; Rabani, E.; Alivisatos, A. Near-Field Manipulation of Spectroscopic Selection Rules on the Nanoscale. Proc. *Proc. Natl. Acad. Sci. U. S. A.* **2012**, *109*, 8016–8019.

784. Lidzey, D. G.; Bradley, D. D. C.; Skolnick, M. S.; Virgili, T.; Walker, S.; Whittaker, D. M. Strong Exciton-Photon Coupling in an Organic Semiconductor Microcavity. *Nature* **1998**, *395*, 53–55.

785. Bellessa, J.; Bonnand, C.; Plenet, J. C.; Mugnier, J. Strong Coupling between Surface Plasmons and Excitons in an Organic Semiconductor. *Phys. Rev. Lett.* **2004**, *93*, 036404.

786. Hutchison, J. A.; Schwartz, T.; Genet, C.; Devaux, E.; Ebbesen, T. W. Modifying Chemical Landscapes by Coupling to Vacuum Fields. *Angew. Chem. Int. Ed.* **2012**, *51*, 1592–1596.

787.   Nagasawa, F.; Takase, M.; Murakoshi, K. Raman Enhancement *via* Polariton States Produced by Strong Coupling between a Localized Surface Plasmon and Dye Excitons at Metal Nanogaps. *J. Phys. Chem. Lett.* **2014**, *5*, 14–19.

788.   Kato, F.; Minamimoto, H.; Nagasawa, F.; Yamamoto, Y. S.; Itoh, T.; Murakoshi, K. Active Tuning of Strong Coupling States between Dye Excitons and Localized Surface Plasmons via Electrochemical Potential Control. *ACS Photonics* **2018**, *5*, 788–796.

789.   Minamimoto, H.; Kato, F.; Nagasawa, F.; Takase, M.; Murakoshi, K. Electrochemical Control of Strong Coupling States Between Localized Surface Plasmons and Molecule Excitons for Raman Enhancement. *Faraday Discuss.* **2017**, *205*, 261–269.

790.   Rivera, N.; Kaminer, I.; Zhen, B.; Joannopoulos, J. D.; Soljačić, M. Shrinking Light to Allow Forbidden Transitions on the Atomic Scale. *Science* **2016**, *353*, 263–269.

791.   Baranov, A. V.; Bobovich, Y. S. Super-Enhanced Hyper-Raman Scattering From Dyes Adsorbed on Colloidal Silver Particles. *JETP Lett.* **1982,** *36*, 339-343.

792.   Murphy, D. V.; Vonraben, K. U.; Chang, R. K.; Dorain, P. B. Surface-Enhanced Hyper-Raman Scattering from SO_3^{2-} Adsorbed on Ag Powder. *Chem. Phys. Lett.* **1982,** *85*, 43-47.

793.   Simmons, P. D.; Turley, H. K.; Silverstein, D. W.; Jensen, L.; Camden, J. P. Surface-Enhanced Spectroscopy for Higher-Order Light Scattering: A Combined Experimental and Theoretical Study of Second Hyper-Raman Scattering. *J. Phys. Chem. Lett.* **2015,** *6*, 5067-5071.

794.   Denisov, V. N.; Mavrin, B. N.; Podobedov, V. B. Hyper-Raman Scattering by Vibrational Excitations in Crystals, Glasses and Liquids. *Phys. Rep.* **1987,** *151*, 1-92.

795.   Madzharova, F.; Heiner, Z.; Kneipp, J. Surface Enhanced Hyper Raman Scattering (SEHRS) and its Applications. *Chem. Soc. Rev.* **2017,** *46*, 3980-3999.

796.   Kneipp, K.; Kneipp, H.; Itzkan, I.; Dasari, R. R.; Feld, M. S. Surface-Enhanced Non-Linear Raman Scattering at the Single-Molecule Level. *Chem. Phys.* **1999,** *247*, 155-162.

797.   Kneipp, J.; Kneipp, H.; Kneipp, K. Two-Photon Vibrational Spectroscopy for Biosciences Based on Surface-Enhanced Hyper-Raman Scattering. *Proc. Nat. Acad. Sci. U. S. A.* **2006,** *103*, 17149-17153.

798.   Yoshikawa, H.; Adachi, T.; Sazaki, G.; Matsui, T.; Nakajima, K.; Masuhara, H. Surface-Enhanced Hyper-Raman Spectroscopy Using Optical Trapping of Silver Nanoparticles for Molecular Detection in Solution. *J. Opt. A: Pure Appl. Opt.* **2007,** *9*, S164.

799.   Milojevich, C. B.; Mandrell, B. K.; Turley, H. K.; Iberi, V.; Best, M. D.; Camden, J. P. Surface-Enhanced Hyper-Raman Scattering from Single Molecules. *J. Phys. Chem. Lett.* **2013,** *4*, 3420-3423.

800.   Nie, S.; Lipscomb, L. A.; Yu, N.-T. Surface-Enhanced Hyper-Raman Spectroscopy. *Appl. Spectrosc. Rev.* **1991,** *26*, 203-276.

801. Golab, J. T.; Sprague, J. R.; Carron, K. T.; Schatz, G. C.; Van Duyne, R. P. A Surface Enhanced Hyper-Raman Scattering Study of Pyridine Adsorbed Onto Silver: Experiment and Theory. *J. Chem. Phys.* **1988,** *88* , 7942-7951.

802. Yang, W. H.; Schatz, G. C. *Ab Initio* and Semiempirical Molecular Orbital Studies of Surface Enhanced and Bulk Hyper-Raman Scattering from Pyridine. *J. Chem. Phys.* **1992,** *97*, 3831-3845.

803. Valley, N.; Jensen, L.; Autschbach, J.; Schatz, G. C. Theoretical Studies of Surface Enhanced Hyper-Raman Spectroscopy: The Chemical Enhancement Mechanism. *J. Chem. Phys.* **2010,** *133*, 054103.

804. Mullin, J.; Valley, N.; Blaber, M. G.; Schatz, G. C. Combined Quantum Mechanics (TDDFT) and Classical Electrodynamics (Mie Theory) Methods for Calculating Surface Enhanced Raman and Hyper-Raman Spectra. *J. Phys. Chem. A* **2012,** *116*, 9574-9581.

805. Christie, J. H.; Lockwood, D. J., Selection Rules for Three- and Four-Photon Raman Interactions. *J. Chem. Phys.* **1971,** *54*, 1141-1154.

806. Živanović, V.; Madzharova, F.; Heiner, Z.; Arenz, C.; Kneipp, J. Specific Interaction of Tricyclic Antidepressants with Gold and Silver Nanostructures as Revealed by Combined One- and Two-Photon Vibrational Spectroscopy. *J. Phys. Chem. C* **2017,** *121*, 22958-22968.

807. Turley, H. K.; Camden, J. P. A Nonlinear Approach to Surface-Enhanced Sensing in the Short-Wave Infrared. *Chem. Commun.* **2014,** *50*, 1472-1474.

808. Gühlke, M.; Heiner, Z.; Kneipp, J. Combined Near-Infrared Excited SEHRS and SERS Spectra of pH Sensors Using Silver Nanostructures. *Phys. Chem. Chem. Phys.* **2015,** *17*, 26093-26100.

809. Trujillo, M. J.; Camden, J. P. Utilizing Molecular Hyperpolarizability for Trace Analysis: A Surface-Enhanced Hyper-Raman Scattering Study of Uranyl Ion. *ACS Omega* **2018,** *3*, 6660-6664.

810. Gühlke, M.; Heiner, Z.; Kneipp, J. Surface-Enhanced Hyper-Raman and Raman Hyperspectral Mapping. *Phys. Chem. Chem. Phys.* **2016,** *18*, 14228-14233.

811. Heiner, Z.; Gühlke, M.; Živanović, V.; Madzharova, F.; Kneipp, J. Surface-Enhanced Hyper Raman Hyperspectral Imaging and Probing in Animal Cells. *Nanoscale* **2017,** *9*, 8024-8032.

812. Li, W.-H.; Li, X.-Y.; Yu, N.-T. Surface-Enhanced Hyper-Raman Spectroscopy (SEHRS) and Surface-Enhanced Raman Spectroscopy (SERS) Studies of Pyrazine and Pyridine Adsorbed on Silver Electrodes. *Chem. Phys. Lett.* **1999,** *305*, 303-310.

813. Li, X.-Y.; Huang, Q.-J.; Petrov, V. I.; Xie, Y.-T.; Luo, Q.; Yu, X.; Yan, Y.-J. Surface-Enhanced Hyper-Raman and Surface-Enhanced Raman Scattering from Molecules Adsorbed on Nanoparticles-on-Smooth-Electrode (NOSE) Substrate I. Pyridine, Pyrazine and Benzene. *J. Raman Spectrosc.* **2005,** *36*, 555-573.

814.	Hulteen, J. C.; Young, M. A.; Van Duyne, R. P. Surface-Enhanced Hyper-Raman Scattering (SEHRS) on Ag Film over Nanosphere (FON) Electrodes: Surface Symmetry of Centrosymmetric Adsorbates. *Langmuir* **2006,** *22*, 10354-10364.

815.	Kneipp, H.; Kneipp, K. Surface-Enhanced Hyper Raman Scattering in Silver Colloidal Solutions. *J. Raman Spectrosc.* **2005,** *36*, 551-554.

816.	Madzharova, F.; Heiner, Z.; Gühlke, M.; Kneipp, J. Surface-Enhanced Hyper-Raman Spectra of Adenine, Guanine, Cytosine, Thymine, and Uracil. *J. Phys. Chem. C* **2016,** *120*, 15415-15423.

817.	Madzharova, F.; Heiner, Z.; Kneipp, J. Surface Enhanced Hyper-Raman Scattering of the Amino Acids Tryptophan, Histidine, Phenylalanine, and Tyrosine. *J. Phys. Chem. C* **2017,** *121*, 1235-1242.

818.	Shimada, R.; Hamaguchi, H. O. Solute-Solvent Intermolecular Vibronic Coupling as Manifested by the Molecular Near-Field Effect in Resonance Hyper-Raman Scattering. *J. Chem. Phys.* **2011,** *134*, 034516.

819.	Gühlke, M.; Heiner, Z.; Kneipp, J. Surface-Enhanced Raman and Surface-Enhanced Hyper-Raman Scattering of Thiol-Functionalized Carotene. *J. Phys. Chem. C* **2016,** *120*, 20702-20709.

820.	Milojevich, C. B.; Silverstein, D. W.; Jensen, L.; Camden, J. P. Probing Two-Photon Properties of Molecules: Large Non-Condon Effects Dominate the Resonance Hyper-Raman Scattering of Rhodamine 6G. *J. Am. Chem. Soc.* **2011,** *133*, 14590-14592.

821.	Milojevich, C. B.; Silverstein, D. W.; Jensen, L.; Camden, J. P. Probing One-Photon Inaccessible Electronic States with High Sensitivity: Wavelength Scanned Surface Enhanced Hyper-Raman Scattering. *ChemPhysChem* **2011,** *12*, 101-103.

822.	Espina Palanco, M.; Bo Mogensen, K.; Gühlke, M.; Heiner, Z.; Kneipp, J.; Kneipp, K. Templated Green Synthesis of Plasmonic Silver Nanoparticles in Onion Epidermal Cells Suitable for Surface-Enhanced Raman and Hyper-Raman Scattering. *Beilstein J. Nanotechnol.* **2016,** *7*, 834-840.

823.	Itoh, T.; Ozaki, Y.; Yoshikawa, H.; Ihama, T.; Masuhara, H. Hyper-Rayleigh Scattering and Hyper-Raman Scattering of Dye-Adsorbed Silver Nanoparticles Induced by a Focused Continuous-Wave Near-Infrared Laser. *Appl. Phys. Lett.* **2006,** *88*, 084102.

824.	Leng, W.; Yasseri, A. A.; Sharma, S.; Li, Z.; Woo, H. Y.; Vak, D.; Bazan, G. C.; Kelley, A. M. Silver Nanocrystal-Modified Silicon Nanowires as Substrates for Surface-Enhanced Raman and Hyper-Raman Scattering. *Anal. Chem.* **2006,** *78*, 6279-6282.

825.	Kitahama, Y.; Hayashi, H.; Itoh, T.; Ozaki, Y. Measurement of pH-Dependent Surface-Enhanced Hyper-Raman Scattering at Desired Positions on Yeast Cells *via* Optical Trapping. *Analyst* **2017,** *142*, 3967-3974.

826.	Stockle, R.; Suh, Y.; Deckert, V.; Zenobi, R. Nanoscale Chemical Analysis by Tip-Enhanced Raman Spectroscopy. *Chem. Phys. Lett.* **2000**, *318*, 131–136.

827. Anderson, M. Locally Enhanced Raman Spectroscopy with an Atomic Force Microscope. *Appl. Phys. Lett.* **2000**, *76*, 3130–3132.

828. Hayazawa, N.; Inouye, Y.; Sekkat, Z.; Kawata, S. Metallized Tip Amplification of Near-Field Raman Scattering. *Opt. Commun.* **2000**, *183*, 333–336.

829. Deckert-Gaudig, T.; Taguchi, A.; Kawata, S.; Deckert, V. Tip-Enhanced Raman Spectroscopy – From Early Developments to Recent Advances. *Chem. Soc. Rev.* **2017**, *46*, 4077-4110

830. Wang, X.; Huang, S. C.; Huang, T. X.; Su, H. S.; Zhong, J. H.; Zeng, Z. C.; Li, M. H.; Ren, B. Tip-Enhanced Raman Spectroscopy for Surfaces and Interfaces. *Chem. Soc. Rev.* **2017**, *46*, 4020-4041.

831. Shao, F.; Zenobi, R. Tip-enhanced Raman Spectroscopy: Principles, Practice, and Applications to Nanospectroscopic Imaging of 2D Materials. *Anal. Bioanal. Chem.* **2019**, *411*, 37-61.

832. Pozzi, E.A.; Goubert, G.; Chiang, N.; Jiang, N.; Chapman, C. T.; McAnally, M. O.; Henry, A. I.; Seideman, T.; Schatz, G. C.; Hersam, M. C.; Van Duyne, R. P. Ultrahigh-Vacuum Tip-Enhanced Raman Spectroscopy. *Chem. Rev.* **2017**, *117*, 4961-4982.

833. Lee, J. H.; Crampton, K. T.; Tallarida, N.; Apkarian, A. V. Visualizing Vibrational Normal Modes of a Single Molecule with Atomically Confined Light. *Nature* **2019**, *568*, 78–82.

834. Steidtner, J.; Pettinger, B. Tip-Enhanced Raman Spectroscopy and Microscopy on Single Dye Molecules with 15nm Resolution. *Phys. Rev. Lett.* **2008**, *100*, 4.

835. Jiang, N.; Chiang, N.; Madison, L. R.; Pozzi, E. A.; Wasielewski, M. R.; Seideman, T.; Ratner, M. A.; Hersam, M. C.; Schatz, G. C.; Van Duyne, R. P. Nanoscale Chemical Imaging of a Dynamic Molecular Phase Boundary with Ultrahigh Vacuum Tip-Enhanced Raman Spectroscopy. *Nano Lett.* **2016**, *16*, 3898-3904.

836. Schmid, T.; Yeo, B. S.; Leong, G.; Stadler, J.; Zenobi, R. Performing Tip-Enhanced Raman Spectroscopy in Liquids. *J. Raman Spectrosc.* **2009**, *40*, 1392-1399.

837. Zeng, Z. C.; Huang, S. C.; Wu, D. Y. Meng, L. Y.; Li, M. H.; Huang, T. X.; Zhong, J. H.; Wang, X.; Yang, Z. L. Ren, B. Electrochemical Tip-Enhanced Raman Spectroscopy. *J. Am. Chem. Soc.* **2015**, *137,* 11928-11931.

838. Kurouski, D.; Mattei, M.; Van Duyne, R. P. Probing Redox Reactions at the Nanoscale with Electrochemical Tip-Enhanced Raman Spectroscopy. *Nano Lett.* **2015**, *15*, 7956-7962.

839. Sabanes, N. M.; Ohto, T.; Andrienko, D.; Nagata, Y. Domke, K. F. Electrochemical TERS Elucidates Potential-Induced Molecular Reorientation of Adenine/Au(111). *Angew. Chem. Int. Ed.* **2017**, *5*, 9796-9801.

840. Huang, T. X.; Huang, S. C.; Li, M. H.; Zeng, Z. C.; Wang, X. Ren, B. Tip-Enhanced Raman Spectroscopy: Tip-Related Issues. *Anal. Bioanal. Chem.* **2015**, *407*, 8177-8195.

841. Ren, B.; Picardi, G.; Pettinger, B. Preparation of Gold Tips Suitable for Tip-Enhanced Raman Spectroscopy and Light Emission by Electrochemical Etching. *Rev. Sci. Instrum.* **2004**, *75*, 837-841.

842. Dickmann, K.; Demming, F.; Jersch, J. New Etching Procedure for Silver Scanning Tunneling Microscopy Tips. *Rev. Sci. Instrum.* **1996**, *67*, 845.

843. Taguchi, A.; Yu, J.; Verma, P.; Kawata, S. Optical Antennas with Multiple Plasmonic Nanoparticles for Tip-Enhanced Raman Microscopy. *Nanoscale* **2015**, *7*, 17424–17433.

844. Trautmann, S.; Richard-Lacroix, M.; Dathe, A.; Schneidewind, H.; Dellith, J.; Fritzsche, W.; Deckert, V. Plasmon Response Evaluation Based on Image-Derived Arbitrary Nanostructures. *Nanoscale* **2018**, *106*, 874–9839.

845. Yang, L. K.; Huang, T. X.; Zeng, Z. C. Li, M. H.; Wang, X.; Yang, F. Z.; Ren, B. Rational Fabrication of a Gold-Coated AFM TERS Tip by Pulsed Electrodeposition. *Nanoscale* **2015**, *7*, 18225-18231.

846. Huang, T. X.; Li, C. W.; Yang, L. K.; Zhu, J. F.; Yao, X.; Liu, C.; Lin, K. Q.; Zeng, Z. C.; Wu, S. S.; Wang, X.; Yang, F. Z.; Ren, B. Rational Fabrication of Silver-Coated AFM TERS Tips with a High Enhancement and Long Lifetime. *Nanoscale* **2018**, *10*, 4398-4405.

847. Ichimura, T.; Fujii, S.; Verma, P.; Yano, T.; Inouye, Y.; Kawata, S. Subnanometric Near-Field Raman Investigation in the Vicinity of a Metallic Nanostructure. *Phys. Rev. Lett.* **2009**, *102*, 186101.

848. Deckert-Gaudig, T.; Kämmer, E.; Deckert, V. Tracking of Nanoscale Structural Variations on a Single Amyloid Fibril with Tip-Enhanced Raman Scattering. *J. Biophotoics.* **2012**, *5*, 215–219.

849. Pettinger, B.; Ren, B.; Picardi, G.; Schuster,. R.; Ertl, G. Nanoscale probing of adsorbed species by tip-enhanced Raman spectroscopy. *Phys. Rev. Lett.* **2004**, *92*, 096101.

850. Ren, B.; Picardi, G.; Pettinger, B.; Schuster,. R.; Ertl, G. Tip-Enhanced Raman Spectroscopy of Benzenethiol Adsorbed on Au and Pt Single-Crystal Surfaces. *Angew. Chem. Int. Ed.* **2005**, *44*, 139 –142.

851. Singh, P.; Deckert, V. Local Protonation Control Using Plasmonic Activation. *Chem. Commun.* **2014**, *50*, 11204–11207.

852. van Schrojenstein Lantman, E. M.; Deckert-Gaudig, T.; Mank, A. J. G.; Deckert, V.; Weckhuysen, B. M. Catalytic Processes Monitored at the Nanoscale with Tip-Enhanced Raman Spectroscopy. *Nat. Nanotechnol.* **2012**, *7*, 583–586.

853. Zhang, Z.; Richard-Lacroix, M.; Deckert, V. Plasmon Induced Polymerization Using a TERS Approach: a Platform for Nanostructured 2D/1D Material Production. *Faraday Discuss.* **2017**, *205*, 213-216.

854. Zhong, J. H.; Jin, X.; Meng, L.; Wang, X.; Su, H. S.; Yang, Z. L; Williams, C. T.; Ren, B. Probing the Electronic and Catalytic Properties of a Bimetallic Surface with 3 nm Resolution. *Nat. Nanotechnol.* **2017**, *12*, 132–136.

855. Su, H. S.; Zhang, X. G.; Sun, J. J.; Jin, X.; Wu, D. Y.; Lian, X. B.; Zhong, J. H.; Ren, B. Real-Space Observation of Atomic Site-Specific Electronic Properties of a Pt Nanoisland/Au(111) Bimetallic Surface by Tip-Enhanced Raman Spectroscopy. *Angew. Chem. Int. Ed.* **2018**, *57*, 13177-13181.

856. Chen, X.; Brasiliense, V.; Van Duyne, R. P. Operando Observation of Molecular-Scale Manipulation Using Electrochemical Tip-Enhanced Raman Spectroscopy. *J. Phys. Chem. C.* **2018**, *122*, 24329-24333.

857. Nguyen, D.; Kang, G.; Chiang, N.; Chen, X.; Seideman T.; Hersam, M. C.; Schatz,G. C.; Van Duyne, R. P. Probing Molecular-Scale Catalytic Interactions between Oxygen and Cobalt Phthalocyanine Using Tip-Enhanced Raman Spectroscopy. *J. Am. Chem. Soc.* **2018**, *140*, 5948−5954.

858. Jiang, S.; Zhang, Y.; Zhang, R.; Hu, C. R.; Liao, M. H.; Luo, Y.; Yang, J. L.; Dong, Z. C.; Hou, J. G. Distinguishing Adjacent Molecules on a Surface Using Plasmon-Enhanced Raman Scattering. *Nat. Nanotechnol.* **2015**, *10*, 865–869.

859. Yano, T.; Ichimura, T.; Kuwahara, S.; H'Dhili, F.; Uetsuki, K.; Okuno, Y.; Verma, P.; Kawata, S. Tip-Enhanced Nano-Raman Analytical Imaging of Locally Induced Strain Distribution in Carbon Nanotubes. *Nat. Commun.* **2013**, *4*, 2592.

860. Deckert-Gaudig, T.; Kämmer, E.; Deckert, V. Tracking of Nanoscale Structural Variations on a Single Amyloid Fibril with Tip-Enhanced Raman Scattering. *J. Biophotonics* **2012**, *5*, 215–219.

861. Sheng, S.; Wu, J.-B.; Cong, X.; Li, W.; Gou, J.; Zhong, Q.; Cheng, P.; Tan, P.-H.; Chen, L.; Wu, K. Vibrational Properties of a Monolayer Silicene Sheet Studied by Tip-Enhanced Raman Spectroscopy. *Phys. Rev. Lett.* **2017**, *119*, 196803.

862. Su, W.; Kumar, N.; Mignuzzi, S.; Crain, J.; Roy, D. Nanoscale Mapping of Excitonic Processes in Single-Layer MoS_2 Using Tip-Enhanced Photoluminescence Microscopy. *Nanoscale* **2016**, *8*, 10564–10569.

863. Milekhin, A. G.; Rahaman, M.; Rodyakina, E. E.; Latyshev, A. V.; Dzhagan, V. M.; Zahn D. R. T. Giant Gap-Plasmon Tip-Enhanced Raman Scattering of MoS_2 Monolayers on Au Nanocluster Arrays. *Nanoscale* **2018**, *10*, 2755–2763.

864. Schmid, T.; Burkhard, J.; Yeo, B.-S.; Zhang, W.; Zenobi, R. Towards Chemical Analysis of Nanostructures in Biofilms I: Imaging of Biological Nanostructures. *Anal. Bioanal. Chem.* **2008**, *391*, 1899–1905.

865. Neugebauer, U.; Rösch, P.; Schmitt, M.; Popp, J.; Julien, C.; Rasmussen, A.; Budich, C.; Deckert, V. On the Way to Nanometer-Sized Information of the Bacterial Surface by Tip-Enhanced Raman Spectroscopy. *ChemPhysChem* **2006**, *7*, 1428–1430.

866. Richter, M.; Hedegaard, M.; Deckert-Gaudig, T.; Lampen, P.; Deckert, V. Laterally Resolved and Direct Spectroscopic Evidence of Nanometer-Sized Lipid and Protein Domains on a Single Cell. *Small* **2011**, *7*, 209–214.

867. He, Z.; Han, Z.; Kizer, M.; Linhardt, R. J.; Wang, X.; Sinyukov, A. M.; Wang, J.; Deckert, V.; Sokolov, A. V.; Hu, J.; Scully, M. Tip-Enhanced Raman Imaging of

Single-Stranded DNA with Single Base Resolution. *J. Am. Chem. Soc.* **2019**, *141*, 753–757.

868.   Lin, X.-M.; Deckert-Gaudig, T.; Singh, P.; Siegmann, M.; Kupfer, S.; Zhang, Z.; Gräfe, S.; Deckert, V. Direct Base-to-Base Transitions in ssDNA Revealed by Tip-Enhanced Raman Scattering, 2016, arXiv:1604.06598.

869.   Kurouski, D.; Deckert-Gaudig, T.; Deckert, V.; Lednev, I. K. Structure and Composition of Insulin Fibril Surfaces Probed by TERS. *J. Am. Chem. Soc.* **2012**, *134*, 13323–13329.

870.   Treffer, R.; Lin, X.; Bailo, E.; Deckert-Gaudig, T.; Deckert, V. Distinction of Nucleobases - a Tip-Enhanced Raman Approach. *Beilstein J. Nanotechnol.* **2011**, *2*, 628–637.

871.   Bailo, E.; Deckert, V. Tip-Enhanced Raman Spectroscopy of Single RNA Strands: Towards a Novel Direct-Sequencing Method. *Angew. Chem. Int. Ed.* **2008**, *47*, 1658–1661.

872.   Hayazawa, N.; Watanabe, H.; Saito, Y.; Kawata, S. Towards Atomic Site-Selective Sensitivity in Tip-Enhanced Raman Spectroscopy. *J. Chem. Phys.* **2006**, *125*, 244706-244707.

873.   Domke, K. F.; Zhang, D.; Pettinger, B. Tip-Enhanced Raman Spectra of Picomole Quantities of DNA Nucleobases at Au(111). *J. Am. Chem. Soc.* **2007**, *129*, 6708–6709.

874.   Lipiec, E.; Sekine, R.; Bielecki, J.; Kwiatek, W. M.; Wood, B. R. Molecular Characterization of DNA Double Strand Breaks with Tip-Enhanced Raman Scattering. *Angew. Chem. Int. Ed.* **2014**, *53*, 169–172.

875.   Olschewski, K.; Kämmer, E.; Stöckel, S.; Bocklitz, T.; Deckert-Gaudig, T.; Zell, R.; Cialla-May, D.; Weber, K.; Deckert, V.; Popp, J. A Manual and an Automatic TERS Based Virus Discrimination. *Nanoscale* **2015**, *7*, 4545–4552.

876.   Cialla, D.; Deckert-Gaudig, T.; Budich, C.; Laue, M.; Moeller, R.; Naumann, D.; Deckert, V.; Popp, J. Raman to the Limit: Tip-Enhanced Raman Spectroscopic Investigations of a Single Tobacco Mosaic Virus. *J Raman Spectrosc.* **2009**, *40*, 240–243.

877.   Zhang, C.; Chen, B. Q.; Li, Z. Y. Optical Origin of Subnanometer Resolution in Tip-Enhanced Raman Mapping. *J. Phys. Chem. C* **2015**, *119*, 11858-11871

878.   Meng, LY; Yang, Z. L. Directional Surface Plasmon-Coupled Emission of Tilted-Tip Enhanced Spectroscopy. *Nanophotonics* **2018**, *7*, 1325-1332.

879.   Ichimura, T.; Hayazawa, N.; Hashimoto, M.; Inouye, Y.; Kawata, S. Tip-Enhanced Coherent Anti-Stokes Raman Scattering for Vibrational Nanoimaging. *Phys. Rev. Lett.* **2004**, *92*, 220801.

880.   Wickramasinghe, H. K.; Chaigneau, M.; Yasukuni, R.; Picardi, G.; Ossikovski, R. Billion-Fold Increase in Tip-Enhanced Raman Signal. *ACS Nano* **2014**, *8*, 3421–3426.

881.   Mueller, N. S.; Juergensen, S.; Höflich, K.; Reich, S.; Kusch, P. Excitation-Tunable Tip-Enhanced Raman Spectroscopy, *J. Phys. Chem. C* **2018**, *122*, 28273-28279.

882. Neubrech, F.; Pucci, A.; Cornelius, T. W.; Karim, S.; García-Etxarri, A.; Aizpurua, J. Resonant Plasmonic and Vibrational Coupling in a Tailored Nanoantenna for Infrared Detection. *Phys. Rev. Lett.* **2008**, *101*, 157403.

883. Neubrech, F.; Pucci, A. Plasmonic Enhancement of Vibrational Excitations in the Infrared. *IEEE J. Sel. Top. Quantum Electron.* **2013**, *19*, 4600809.

884. Neubrech, F.; Huck, C.; Weber, K.; Pucci, A.; Giessen, H. Surface-Enhanced Infrared Spectroscopy Using Resonant Nanoantennas. *Chem. Rev.* **2017**, *117*, 5110–5145.

885. Vogt, J.; Huck, C.; Neubrech, F.; Pucci, A. Plasmonic Light Scattering and Infrared Vibrational Signal Enhancement. In *Frontiers of Plasmon Enhanced Spectroscopy Volume 2*; Ozaki, Y., Schatz, G. C., Graham, D., Itoh, T., Eds.; 2016; pp 1–19.

886. Wu, C.; Khanikaev, A. B.; Adato, R.; Arju, N.; Yanik, A. A.; Altug, H.; Shvets, G. Fano-Resonant Asymmetric Metamaterials for Ultrasensitive Spectroscopy and Identification of Molecular Monolayers. *Nat. Mater.* **2012**, *11*, 69–75.

887. Neubrech, F.; Beck, S.; Glaser, T.; Hentschel, M.; Giessen, H.; Pucci, A. Spatial Extent of Plasmonic Enhancement of Vibrational Signals in the Infrared. *ACS Nano* **2014**, *8*, 6250–6258.

888. Neuman, T.; Huck, C.; Vogt, J.; Neubrech, F.; Hillenbrand, R.; Aizpurua, J.; Pucci, A. Importance of Plasmonic Scattering for an Optimal Enhancement of Vibrational Absorption in SEIRA with Linear Metallic Antennas. *J. Phys. Chem. C* **2015**, *119*, 26652–26662.

889. Siemes, C.; Bruckbauer, A.; Goussev, A.; Otto, A.; Sinther, M.; Pucci, A. SERS-Active Sites on Various Copper Substrates. *J. Raman Spectrosc.* **2001**, *32*, 231–239.

890. Sinther, M.; Pucci, A.; Otto, A.; Priebe, A.; Diez, S.; Fahsold, G. Enhanced Infrared Absorption of SERS-Active Lines of Ethylene on Cu. *Phys. Status Solidi* **2001**, *188*, 1471–1476.

891. Vogt, J.; Huck, C.; Neubrech, F.; Toma, A.; Gerbert, D.; Pucci, A. Impact of the Plasmonic Near- and Far-Field Resonance-Energy Shift on the Enhancement of Infrared Vibrational Signals. *Phys. Chem. Chem. Phys.* **2015**, *17*, 21169–21175.

892. Huck, C.; Vogt, J.; Neuman, T.; Nagao, T.; Hillenbrand, R.; Aizpurua, J.; Pucci, A.; Neubrech, F. Strong Coupling between Phonon-Polaritons and Plasmonic Nanorods. *Opt. Express* **2016**, *24*, 25528.

893.   Seok, T. J.; Jamshidi, A.; Kim, M.; Dhuey, S.; Lakhani, A.; Choo, H.; Schuck, P. J.; Cabrini, S.; Schwartzberg, A. M.; Bokor, J.; Yablonovitch, E.; Wu, M. C. Radiation Engineering of Optical Antennas for Maximum Field Enhancement. *Nano Lett.* **2011**, *11*, 2606–2610.

894.   Tzschoppe, M.; Huck, C.; Vogt, J.; Neubrech, F.; Pucci, A. Impact of Metal-Optical Properties on Surface-Enhanced Infrared Absorption. *J. Phys. Chem. C* **2018**, *122*, 15678–15687.

895.   Bohren, C. F.; Clothiaux, E. E.; Huffman, D. R. *Absorption and Scattering of Light by Small Particles*, 2nd ed.; Wiley-VCH: Weinheim, Germany, 2009.

896.   Meng, F.; Pucci, A. Growth of Silver on MgO(001) and Infrared Optical Properties. *Phys. Status Solidi* **2007**, *244*, 3739–3749.

897.   Lust, M.; Priebe, A.; Fahsold, G.; Pucci, A. Infrared Spectroscopic Study of the CO-Mediated Decrease of the Percolation Threshold during the Growth of Ultrathin Metal Films on MgO(001). *Surf. Interface Anal.* **2002**, *33*, 487–490.

898.   Griffiths, P. R. Surface-enhanced Infrared Absorption Spectroscopy: Principles and Applications. In *Spectroscopic Properties of Inorganic and Organometallic Compounds: Techniques, Materials and Applications, Volume 44*; Yarwood, J., Douthwaite, R., Duckett, S., Eds.; The Royal Society of Chemistry, 2013; pp 95–122.

899.   Enders, D.; Nagao, T.; Pucci, A.; Nakayama, T.; Aono, M. Surface-Enhanced ATR-IR Spectroscopy with Interface-Grown Plasmonic Gold-Island Films near the Percolation Threshold. *Phys. Chem. Chem. Phys.* **2011**, *13*, 4935-4941.

900.   Priebe, A.; Sinther, M.; Fahsold, G.; Pucci, A. The Correlation between Film Thickness and Adsorbate Line Shape in Surface Enhanced Infrared Absorption. *J. Chem. Phys.* **2003**, *119*, 4887–4890.

901.   Cetin, A. E.; Aksu, S.; Turkmen, M.; Etezadi, D.; Altug, H. Theoretical and Experimental Analysis of Subwavelength Bowtie-Shaped Antennas. *J. Electromagn. Waves Appl.* **2015**, *29*, 1686–1698.

902.   Huck, C.; Vogt, J.; Sendner, M.; Hengstler, D.; Neubrech, F.; Pucci, A. Plasmonic Enhancement of Infrared Vibrational Signals: Nanoslits *versus* Nanorods. *ACS Photonics* **2015**, *2*, 1489–1497.

903. Vogt, J.; Zimmermann, S.; Huck, C.; Tzschoppe, M.; Neubrech, F.; Fatikow, S.; Pucci, A. Chemical Identification of Individual Fine Dust Particles with Resonant Plasmonic Enhancement of Nanoslits in the Infrared. *ACS Photonics* **2017**, *4*, 560–566.

904. Huck, C.; Tzschoppe, M.; Semenyshyn, R.; Neubrech, F.; Pucci, A. Chemical Identification of Single Ultrafine Particles Using Surface-Enhanced Infrared Absorption. *Phys. Rev. Applied* **2019**, *11*, 014036.

905. Mayerhöfer, T. G.; Knipper, R.; Hübner, U.; Cialla-May, D.; Weber, K.; Meyer, H.-G.; Popp, J. Ultra Sensing by Combining Extraordinary Optical Transmission with Perfect Absorption. *ACS Photonics* **2015,** *2*, 1567-1575.

906. Knipper, R.; Mayerhöfer, T. G.; Kopecký, V.; Huebner, U.; Popp, J. Observation of Giant Infrared Circular Dichroism in Plasmonic 2D-Metamaterial Arrays. *ACS Photonics* **2018**, *5*, 1176-1180.

907. Knipper, R.; Kopecký, V.; Huebner, U.; Popp, J.; Mayerhöfer, T. G. Slit-Enhanced Chiral- and Broadband Infrared Ultra-Sensing. *ACS Photonics* **2018,** *5*, 3238-3245.

908. Mayerhöfer, T. G.; Popp, J. Electric Field Standing Wave Effects in Internal Reflection and ATR Spectroscopy. *Spectrochim. Acta A* **2018,** *191*, 165-171.

909. Pahlow, S.; Mayerhöfer, T.; van der Loh, M.; Hubner, U.; Dellith, J.; Weber, K.; Popp, J. Interference-Enhanced Raman Spectroscopy as a Promising Tool for the Detection of Biomolecules on Raman-Compatible Surfaces. *Anal. Chem.* **2018,** *90*, 9025-9032.

910. Carr, G. L.; Chubar, O.; Dumas, P. Multichannel Detection with a Synchrotron Light Source: Design and Potential. In *Spectrochemical Analysis Using Infrared Multichannel Detectors*; Bhargava, R., Levin, I. W., Eds.; Blackwell Publishing Ltd: Oxford, UK, 2007; pp 56–84.

911. Dong, L.; Yang, X.; Zhang, C.; Cerjan, B.; Zhou, L.; Tseng, M. L.; Zhang, Y.; Alabastri, A.; Nordlander, P.; Halas, N. J. Nanogapped Au Antennas for Ultrasensitive Surface-Enhanced Infrared Absorption Spectroscopy. *Nano Lett.* **2017**, *17*, 5768–5774.

912. Linic, S.; Aslam, U.; Boerigter, C.; Morabito, M. Photochemical Transformations on Plasmonic Metal Nanoparticles. *Nat. Mater.* **2015**, *14*, 567-576.

913. Brongersma, M. L.; Halas, N. J.; Nordlander, P. Plasmon-Induced Hot Carrier Science and Technology. *Nat. Nanotechnol.* **2015**, *10*, 25-34.

914.   Baffou, G.; Quidant, R. Nanoplasmonics for Chemistry. *Chem. Soc. Rev.* **2014**, *43*, 3898-3907.

915.   Christopher, P.; Moskovits, M. Hot Charge Carrier Transmission from Plasmonic Nanostructures. *Annu. Rev. Phys. Chem.* **2017**, *68*, 379-398.

916.   Aslam, U.; Rao, V. G.; Chavez, S.; Linic, S. Catalytic Conversion of Solar to Chemical Energy on Plasmonic Metal Nanostructures. *Nat. Catal.* **2018**, *1*, 656-665.

917.   Zhan, C.; Chen, X.-J.; Yi, J.; Li, J.-F.; Wu, D.-Y.; Tian, Z.-Q. From Plasmon-Enhanced Molecular Spectroscopy to Plasmon-Mediated Chemical Reactions. *Nat. Rev. Chem.* **2018**, *2*, 216-230.

918.   Nitzan, A.; Brus, L. E. Theoretical Model for Enhanced Photochemistry on Rough Surfaces. *J. Chem. Phys.* **1981**, *75*, 2205-2214.

919.   Chen, C. J.; Osgood, R. M. Direct Observation of the Local-Field-Enhanced Surface Photochemical Reactions. *Phys. Rev. Lett.* **1983**, *50*, 1705-1708.

920.   Mubeen, S.; Lee, J.; Singh, N.; Kramer, S.; Stucky, G. D.; Moskovits, M. An Autonomous Photosynthetic Device in Which All Charge Carriers Derive From Surface Plasmons. *Nat. Nanotech.* **2013**, *8*, 247-251.

921.   Christopher, P.; Xin, H.; Linic, S. Visible-Light-Enhanced Catalytic Oxidation Reactions on Plasmonic Silver Nanostructures. *Nat. Chem.* **2011**, *3*, 467-472.

922.   Kim, Y.; Smith, J. G.; Jain, P. K. Harvesting Multiple Electron–Hole Pairs Generated Through Plasmonic Excitation of Au Nanoparticles. *Nat. Chem.* **2018**, 10, 763-769.

923.   Zhou, L.; Swearer, D. F.; Zhang, C.; Robatjazi, H.; Zhao, H.; Henderson, L.; Dong, L.; Christopher, P.; Carter, E. A.; Nordlander, P.; Halas, N. J. Quantifying Hot Carrier and Thermal Vontributions in Plasmonic Photocatalysis. *Science* **2018**, *362*, 69-72.

924.   Oshikiri, T.; Ueno, K.; Misawa, H. Plasmon-Induced Ammonia Synthesis through Nitrogen Photofixation with Visible Light Irradiation. *Angew. Chem. Int. Ed.* **2014**, 53, 9802-9805.

925.   Huang, Y.-F.; Zhu, H.-P.; Liu, G.-K.; Wu, D.-Y.; Ren, B.; Tian, Z.-Q. When the Signal Is Not from the Original Molecule To Be Detected: Chemical Transformation of para-Aminothiophenol on Ag during the SERS Measurement. *J. Am. Chem. Soc.* **2010**, *132*, 9244-9246.

926.   Hartman, T.; Wondergem, C. S.; Kumar, N.; van den Berg, A.; Weckhuysen, B. M. Surface- and Tip-Enhanced Raman Spectroscopy in Catalysis. *J. Phys. Chem. Lett.* **2016,** *7*, 1570-1584.

927.   Zhang, Y.; He, S.; Guo, W.; Hu, Y.; Huang, J.; Mulcahy, J. R.; Wei, W. D. Surface-Plasmon-Driven Hot Electron Photochemistry. *Chem. Rev.* **2018,** *118*, 2927-2954

928.   Cortés, E. Efficiency and Bond Selectivity in Plasmon-Induced Photochemistry. *Adv. Opt. Mater.* **2017,** *5*, 1700191.

929.   Gieseking, R. L.; Ratner, M. A.; Schatz, G. C. Review of Plasmon-Induced Hot-Electron Dynamics and Related SERS Chemical Effects. In *Frontiers of Plasmon Enhanced Spectroscopy Volume 1*, American Chemical Society: 2016; Vol. 1245, pp 1-22.

930.   Ren, X.; Cao, E.; Lin, W.; Song, Y.; Liang, W.; Wang, J. Recent Advances in Surface Plasmon-Driven Catalytic Reactions. *RSC Adv.* **2017,** *7*, 31189-31203

931.   Sun, M.; Huang, Y.; Xia, L.; Chen, X.; Xu, H. The pH-Controlled Plasmon-Assisted Surface Photocatalysis Reaction of 4-Aminothiophenol to p,p′-Dimercaptoazobenzene on Au, Ag, and Cu Colloids. *J. Phys. Chem. C* **2011,** *115*, 9629-9636

932.   Choi, H.-K.; Park, W.-H.; Park, C.-G.; Shin, H.-H.; Lee, K. S.; Kim, Z. H. Metal-Catalyzed Chemical Reaction of Single Molecules Directly Probed by Vibrational Spectroscopy. *J. Am. Chem. Soc.* **2016,** *138*, 4673-4684.

933.   Brandt, N. C.; Keller, E. L.; Frontiera, R. R. Ultrafast Surface-Enhanced Raman Probing of the Role of Hot Electrons in Plasmon-Driven Chemistry. *J. Phys. Chem. Lett.* **2016,** *7*, 3179-3185.

934.   Dong, B.; Fang, Y.; Chen, X.; Xu, H.; Sun, M. Substrate-, Wavelength-, and Time-Dependent Plasmon-Assisted Surface Catalysis Reaction of 4-Nitrobenzenethiol Dimerizing to p,p′-Dimercaptoazobenzene on Au, Ag, and Cu Films. *Langmuir* **2011,** *27*, 10677-10682.

935.   Choi, H.-K.; Lee, K. S.; Shin, H.-H.; Kim, Z. H. Identification of the First Elementary Step in the Photocatalytic Reduction of Nitrobenzenethiols on a Metallic Surface. *J. Phys. Chem. Lett.* **2016,** *7*, 4099-4104.

936. Zhang, Z.; Merk, V.; Hermanns, A.; Unger, W. E. S.; Kneipp, J. Role of Metal Cations in Plasmon-Catalyzed Oxidation: A Case Study of p-Aminothiophenol Dimerization. *ACS Catal.* **2017,** *7*, 7803-7809

937.	Zhang, Z.; Kneipp, J. Mapping the Inhomogeneity in Plasmonic Catalysis on Supported Gold Nanoparticles Using Surface-Enhanced Raman Scattering Microspectroscopy. *Anal. Chem.* **2018,** *90*, 9199-9205.

938.	Xu, P.; Kang, L.; Mack, N. H.; Schanze, K. S.; Han, X.; Wang, H.-L. Mechanistic Understanding of Surface Plasmon Assisted Catalysis on a Single Particle: Cyclic Redox of 4-Aminothiophenol. *Sci. Rep.* **2013,** *3*, 2997.

939.	Keller, E. L.; Frontiera, R. R. Ultrafast Nanoscale Raman Thermometry Proves Heating Is Not a Primary Mechanism for Plasmon-Driven Photocatalysis. *ACS Nano* **2018,** *12*, 5848-5855.

940.	Kim, N. H.; Meinhart, C. D.; Moskovits, M. Plasmon-Mediated Reduction of Aqueous Platinum Ions: The Competing Roles of Field Enhancement and Hot Charge Carriers. *J. Phys. Chem. C* **2016,** *120*, 6750-6755.

941.	Kim, K.; Lee, S. H.; Choi, J.-Y.; Shin, K. S. Fe^{3+} to Fe^{2+} Conversion by Plasmonically Generated Hot Electrons from Ag Nanoparticles: Surface-Enhanced Raman Scattering Evidence. *J. Phys. Chem. C* **2014,** *118*, 3359-3365.

942.	Szczerbiński, J.; Gyr, L.; Kaeslin, J.; Zenobi, R. Plasmon-Driven Photocatalysis Leads to Products Known from E-beam and X-ray-Induced Surface Chemistry. *Nano Lett.* **2018,** *18*, 6740-6749.

943.	Willets, K. A. Probing Nanoscale Interfaces with Electrochemical Surface-Wnhanced Raman Scattering. *Curr. Opin. Electrochem.* **2019,** *13*, 18-24.

944.	Zaleski, S.; Wilson, A. J.; Mattei, M.; Chen, X.; Goubert, G.; Cardinal, M. F.; Willets, K. A.; Van Duyne, R. P. Investigating Nanoscale Electrochemistry with Surface- and Tip-Enhanced Raman Spectroscopy. *Acc. Chem. Res.* **2016,** *49*, 2023-2030.

945.	Cortés, E.; Etchegoin, P. G.; Le Ru, E. C.; Fainstein, A.; Vela, M. E.; Salvarezza, R. C. Monitoring the Electrochemistry of Single Molecules by Surface-Enhanced Raman Spectroscopy. *J. Am. Chem. Soc.* **2010,** *132*, 18034-18037.

946. Cortés, E.; Etchegoin, P. G.; Le Ru, E. C.; Fainstein, A.; Vela, M. E.; Salvarezza, R. C. Strong Correlation between Molecular Configurations and Charge-Transfer Processes Probed at the Single-Molecule Level by Surface-Enhanced Raman Scattering. *J. Am. Chem. Soc.* **2013,** *135*, 2809-2815.

947. Zong, C.; Chen, C.-J.; Zhang, M.; Wu, D.-Y.; Ren, B. Transient Electrochemical Surface-Enhanced Raman Spectroscopy: A Millisecond Time-Resolved Study of an Electrochemical Redox Process. *J. Am. Chem. Soc.* **2015,** *137*, 11768-11774.

948. Zaleski, S.; Cardinal, M. F.; Klingsporn, J. M.; Van Duyne, R. P. Observing Single, Heterogeneous, One-Electron Transfer Reactions. *J. Phys. Chem. C* **2015,** *119*, 28226-28234.

949. Zaleski, S.; Cardinal, M. F.; Chulhai, D. V.; Wilson, A. J.; Willets, K. A.; Jensen, L.; Van Duyne, R. P. Toward Monitoring Electrochemical Reactions with Dual-Wavelength SERS: Characterization of Rhodamine 6G (R6G) Neutral Radical Species and Covalent Tethering of R6G to Silver Nanoparticles. *J. Phys. Chem. C* **2016,** *120*, 24982-24991.

950. Wilson, A. J.; Molina, N. Y.; Willets, K. A. Modification of the Electrochemical Properties of Nile Blue through Covalent Attachment to Gold As Revealed by Electrochemistry and SERS. *J. Phys. Chem. C* **2016,** *120*, 21091-21098.

951. Wilson, A. J.; Willets, K. A. Unforeseen Distance-Dependent SERS Spectroelectrochemistry From Surface-Tethered Nile Blue: The Role of Molecular Orientation. *Analyst* **2016,** *141*, 5144-5151.

952. Wilson, A. J.; Willets, K. A. Visualizing Site-Specific Redox Potentials on the Surface of Plasmonic Nanoparticle Aggregates with Superlocalization SERS Microscopy. *Nano Lett.* **2014,** *14*, 939-945.

953. Weber, M. L.; Wilson, A. J.; Willets, K. A. Characterizing the Spatial Dependence of Redox Chemistry on Plasmonic Nanoparticle Electrodes Using Correlated Super-Resolution Surface-Enhanced Raman Scattering Imaging and Electron Microscopy. *J. Phys. Chem. C* **2015,** *119*, 18591-18601.

954. Willets, K. A. Super-Resolution Imaging of SERS Hot Spots. *Chem. Soc. Rev.* **2014,** *43*, 3854-3864.

955.   Manjavacas, A.; Liu, J. G.; Kulkarni, V.; Nordlander, P. Plasmon-Induced Hot Carriers in Metallic Nanoparticles. *ACS Nano* **2014,** *8*, 7630-7638.

956.   Han, X.; Lee, H. K.; Lee, Y. H.; Hao, W.; Liu, Y.; Phang, I. Y.; Li, S.; Ling, X. Y. Identifying Enclosed Chemical Reaction and Dynamics at the Molecular Level Using Shell-Isolated Miniaturized Plasmonic Liquid Marble. *J. Phys. Chem. Lett.* **2016**, *7*, 1501-1506.

957.   Han, X.; Koh, C. S. L.; Lee, H. K.; Chew, W. S.; Ling, X. Y. Microchemical Plant in a Liquid Droplet: Plasmonic Liquid Marble for Sequential Reactions and Attomole Detection of Toxin at Microliter Scale. *ACS Appl. Mater. Interfaces* **2017**, *9*, 39635-39640.

958.   Phan-Quang, G. C.; Lee, H. K.; Ling, X. Y. Isolating Reactions at the Picoliter Scale: Parallel Control of Reaction Kinetics at the Liquid–Liquid Interface. *Angew. Chem. Int. Ed.* **2016**, *55*, 8304-8308.

959.   Koh, C. S. L.; Lee, H. K.; Phan-Quang, G. C.; Han, X.; Lee, M. R.; Yang, Z.; Ling, X. Y. SERS- and Electrochemically Active 3D Plasmonic Liquid Marbles for Molecular-Level Spectroelectrochemical Investigation of Microliter Reactions. *Angew. Chem. Int. Ed.* **2017**, *56*, 8813-8817.

960.   Lee, H. K.; Lee, Y. H.; Morabito, J. V.; Liu, Y.; Koh, C. S. L.; Phang, I. Y.; Pedireddy, S.; Han, X.; Chou, L.-Y.; Tsung, C.-K.; Ling, X. Y. Driving CO_2 to a Quasi-Condensed Phase at the Interface between a Nanoparticle Surface and a Metal–Organic Framework at 1 bar and 298 K. *J. Am. Chem. Soc.* **2017**, *139*, 11513-11518.

961.   Sim, H. Y. F.; Lee, H. K.; Han, X.; Koh, C. S. L.; Phan-Quang, G. C.; Lay, C. L.; Kao, Y.-C.; Phang, I. Y.; Yeow, E. K. L.; Ling, X. Y. Concentrating Immiscible Molecules at Solid@MOF Interfacial Nanocavities to Drive an Inert Gas–Liquid Reaction at Ambient Conditions. *Angew. Chem. Int. Ed.* **2018**, *57*, 17058-17062.